Coupling and decoupling of biogeochemical cycles in marine ecosystems

Dissertation
zur Erlangung des akademischen Grades eines
Doktors der Naturwissenschaften
- Dr. rer. nat. -
am Fachbereich 2 (Biologie/Chemie)
der Universität Bremen

vorgelegt von **Sönke Hohn**

Erstgutachter: Prof. Dr. Dieter Wolf-Gladrow
Zweitgutachter: Prof. Dr. Andreas Oschlies

Bremen, January 22, 2009

Contents

Preface

The global cycles of biologically important elements in the ocean are coupled to each other via the production of biomass (Fig. 1). Once incorporated into organic molecules and compartimented in cellular structures, the fate of biogeochemical elements is linked until bacterial breakdown of organic molecules, remineralization, releases the elements again as dissolved inorganic or, to a smaller amount, organic nutrients. Remineralization processes thus again decouple the fluxes of different biogeochemical elements from each other (Fig. 1).

The elemental composition (stoichiometry) of biomass appears to be relatively uniform in marine ecosystems (Redfield et al., 1963). The average ratios of C:N:P in marine biomass is found to be 106:16:1, respectively (Redfield et al., 1963). This ratio can be explained by a combination of different organic molecules that have characteristic C:N:P ratios (Geider and La Roche, 2002). Neutral lipids and carbohydrates do not contain nitrogen or phosphorus but only carbon, oxygen and hydrogen. Phospholipids additionally contain a phosphate group associated to the glycerol. Proteins are rich in nitrogen and also contain carbon, oxygen, hydrogen and small amounts of sulfur. Enzymes, belonging to the functional group of proteins, can also contain small amounts of metal ions in their reaction centres. DNA is a combination of saccharides, nitrogen rich organic bases and phosphates. And ribosomes that are needed for DNA transcription are especially rich in phosphorus. Many other different structural and functional molecules are combined in biomass, making organisms a combination of different chemical elements that perform complex chemical reactions called life. The common cellular structure underlying all organisms causes the similarity of the biochemical composition of the biomass of different organisms.

However, different species have evolved different physiological requirements for chemical elements due to different realized metabolic pathways (Fig. 1). Cyanobacteria for example are capable of splitting the triple bond between two nitrogen atoms and thus transform gaseous nitrogen into reactive nitrogen. Cyanobacteria have also developed high requirements for iron because the enzyme nitrogenase, that performs the splitting of gaseous nitrogen, contains large amounts of iron. Other phytoplankton organisms require less iron but depend on the availability of reactive nitrogen. Diatoms take up dissolved silicon in the form of silicic acid and build cell walls of amorphous hydrated silica. Diatoms are thus also dependent on the availability of silicon to perform cell division. Coccolithophores produce small plates of calcite that are attached to the cell surface and thus couple calcium to the fluxes of carbon. The biominerals silica and calcite, which are the most important biominerals in phytoplankton, can have high geological importance due to sedimentation and accumulation at the sea floor.

From the perspective of biogeochemistry, species can be combined to so called phytoplankton functional types (PFT) of calcifiers, nitrogen fixers, silicifiers, DMS producers, and various others, depending on similarities in their physiological properties. The combination of different species or functional groups in the plankton community of different ocean regions leads to differences in the average stoichiometric composition of the produced biomass. The chemical composition of biomass

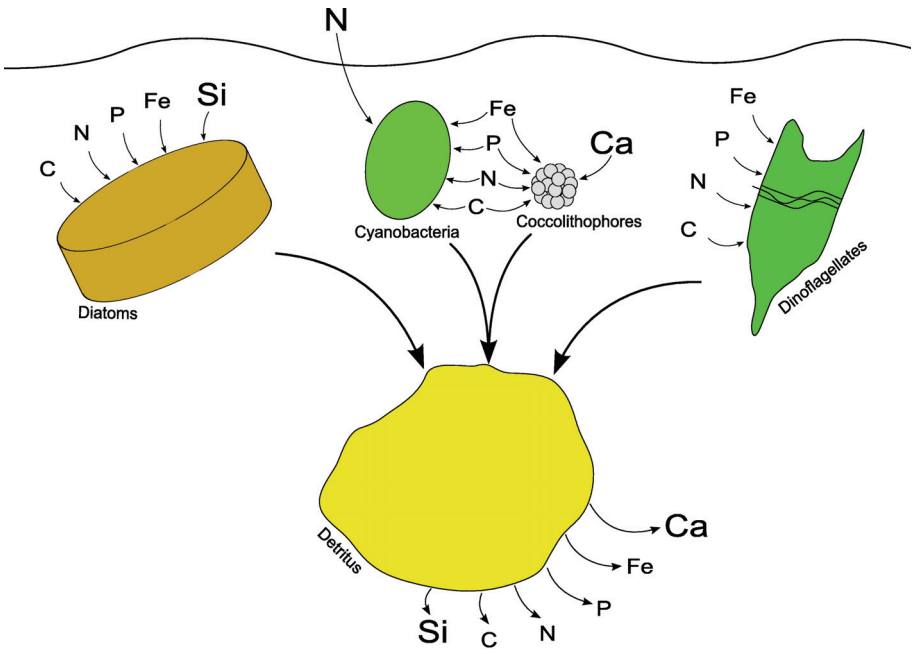

Figure 1: *The elemental cycles of carbon, nitrogen, phosphorous, silicon and iron, and many other biologically important elements, are coupled to each other via the formation of biomass. Different organisms may have different requirements for nutrition. When organisms die, they add to the pool of dead organic material, detritus. Decomposition of detritus releases the elements from being incorporated into organic molecules and particles and again decouples the fate of elements from each other.*

is thus only uniform in a statistical sense and the coupling of biogeochemical elements varies on the level of species compositions.

Environmental conditions also determine the chemical composition of phytoplankton organisms as nutrient uptake is strongly dependent on nutrient availability. Even though the fluxes of different elements are coupled via formation of organic molecules, the combination of molecules in the cell can vary due to physiological responses to the environment. For example, when algae grow under nitrogen-limiting conditions, nitrogen uptake is reduced and cellular nitrogen, protein, and chlorophyll contents decline, raising the intracellular C:N ratio. The cellular content of protein strongly affects metabolic activity as most metabolic reactions are catalized by enzymes. At low irradiance levels, photosynthetic carbon fixation is inhibited and the intracellular C:N ratio decreases. As most metabolic reactions also require energy in form of ATP or NADH, which are provided via photosynthesis or respiration of starch or lipids, carbon deficiency due to light-limitation also reduces cellular activity. The coupling of biogeochemical elements may thus also vary on the species or individual level.

Iron is only needed in small amounts in phytoplankton cells but iron deficiency has various effects on cellular stoichiometry. Iron is involved in the assimilation of nitrogen because it occurs in the reaction centre of the enzyme nitrate reductase. Iron is also involved in photosynthesis as it is part of the electron transport chain and the photosystems. Different roles of iron in the cellular metabolism of different elements induce different regulations of elemental composition under iron-limitation. In diatoms, increased Si:N and Si:C ratios are observed when diatoms grow in iron deficient medium (Hutchins and Bruland, 1998; Takeda, 1998).

Uptake of nutrients does not only affect intracellular nutrient concentrations but also changes the

environmental surrounding. Depth profiles of nutrient concentrations show a decline of nutrient concentrations towards the ocean surface, which is caused by biological nutrient consumption. Productive ocean regions usually exhibit stronger seasonal variability of surface nutrient concentrations than less productive regions. Observed concentrations of biogeochemical elements are therefore strongly determined by biological activity. However, the distribution of elements in ocean waters, is not only affected by the formation of biomass. The breakdown of organic matter, mostly by bacterial activity, releases nutrients that were incorporated into organic molecules. Remineralization of detritus is thus a source of nutrients to the water column and nutrient concentrations in ocean waters have to be understood as a dynamic state between source fluxes and sinks of the respective compound. The supply of fresh nutrients via remineralization also depends on the stoichiometric composition of the decomposed biomass. The covariation of N:P in the deep ocean, for example, is mainly the result of the average N:P ratio in biomass. Furthermore, different remineralization time scales of different elements lead to a vertical fractionation in the remineralization of organic matter while it vertically sinks through the water column, affecting the vertical stoichiometry of nutrient concentrations.

The aim of this thesis is to investigate how the coupling and decoupling of biogeochemical cycles is affected under different environmental conditions and how this feeds back to the fluxes and concentrations of elements in the global ocean. Ecosystem models have proven to be valuable tools to synthesize knowledge and to simulate complex dynamical systems. Complex interactions in nature can often be simulated by relatively simple mathematical models that focus on a few key processes that have been defined as the focus of the scientific investigation. This thesis concentrates on two ocean regions, the Southern Ocean and a tidal basin in the European Wadden Sea, whose phytoplankton communities are dominated by diatoms. The model approach therefore considers only one group of phytoplankton, namely diatoms, and ecological effects of different community structures and physiological adaptations of more than one phytoplankton species are not regarded in this study.

Thesis outline

The thesis is divided into four studies that concentrate on different aspects of marine ecosystem modelling.

Study 1 investigates the biogeochemistry in a shallow coastal tidal basin in the Danish-German Wadden Sea. The applied ecosystem model allows for variable C:N stoichiometry in phytoplankton biomass and is analysed for carbon and nitrogen fluxes within and between the tidal basin and the adjacent North Sea.

In the second study, the parameterization of phytoplankton physiology is extended by inclusion of the elements silicon and iron. For model validation, the results are compared to literature data of laboratory experiments.

Study 3 investigates the performance of the new parameterization of Si:N:C:Chl ratios in diatoms in a global biogeochemical ocean general circulation model (BOGCM). The analysis of the model results focuses on the silicon cycle in the Southern Ocean and its connections to carbon and nitrogen cycling.

In study 4, the BOGCM is run at high resolution on a cubed sphere model grid. Simulations are performed on the JUMP supercomputer at the Helmholtz Research Centre Jülich and the model is analysed for its computational costs and scalability on the new architecture.

The general outcome of this thesis is summarized and discussed in a general discussion at the end of this thesis.

Declaration on the contribution to multi-author sections

Study 1 - Modelling primary productivity in a shallow coastal tidal basin

The basic model idea came from Markus Schartau. I have implemented the hydrological environment and the pelagic biogeochemical state variables in both water boxes. Then I added a benthic component and the impact of benthic filterfeeders on pelagic tracers to the pelagic model. Data for model validation has been provided by Justus van Beusekom. All model simulations, optimizations, and analyses were carried out by me. The manuscript has been written by me with the help of the coauthors.

Study 2 - A model of the carbon:nitrogen:silicon stoichiometry of diatoms based on metabolic processes

The parameterization was developed by me and all simulations were done by myself. The manuscript has been written by me with the help of the coauthors.

Study 3 - Coupling and decoupling of silicon and nitrogen cycles in the Southern Ocean

The coupling of the physical and biogeochemical model has mostly been done by Martin Losch. Model simulations that are relevant for this study were performed by me and Christoph Völker. The analyses were carried out with the help of Christoph Völker and the writing of the manuscript was done by me with the help of the coauthors.

Study 4 - High resolution modelling

Model runs and analyses have been performed by Martin Losch, Michael Schröder and Christoph Völker. The manuscript was mainly written by Christoph Völker with the help of all coauthors. My coauthorship is justified by provision of the applied biological parameterization and my contributions to discussions about model results.

Chapter 1

General Introduction

Fossil fuels are the remainder of biomass that was not oxidized to carbon dioxide under anoxic conditions several million years ago. Burning of fossil fuels is a source of carbon dioxide to the atmosphere. Land use changes have decreased the amount of terrestrial biomass and soils that store large amounts of carbon. Carbon emissions and land use changes together cause an overall increase in atmospheric CO_2 concentrations. Increasing atmospheric concentrations of CO_2 increase the absorption of long wave radiation in the atmosphere and thus induce a heating of the atmosphere (IPCC, 2007). One of the major tasks of environmental science is currently to improve the understanding of the climate system and the effects of anthropogenic carbon emissions on the global climate and the ocean.

The ocean is an important part in the climate system. Heat exchange with the ocean is a major driver of the atmospheric circulation, but the ocean itself is driven by the atmosphere due to precipitation and evaporation, wind stress, heat fluxes, and salinity and temperature effects on seawater density. The ocean is the major reservoir of carbon and dissolution of CO_2 in seawater has a buffering effect on rising atmospheric CO_2 concentrations (Watson and Orr, 2003). But dissolution of CO_2 in seawater also leads to a decrease in pH, as CO_2 and H_2O form carbonic acid.

Currently the ocean is taking up about 48% of the anthropogenic carbon emissions (Takahashi, 2004). However, it is uncertain, how oceanic carbon uptake will change in an acidifying and warming ocean. One of the most important tasks in marine science is therefore to improve our understanding of the global ocean carbon cycle and to identify and quantify possible feedback mechanisms between the marine carbon cycle and atmospheric CO_2 concentrations. This knowledge is especially needed to make model predictions of future changes of the climate system and its response to the anthropogenically caused rise in atmospheric CO_2 concentrations due to the burning of fossil fuels.

The biological fluxes of carbon in the marine carbon cycle are coupled to the fluxes of other elements, like N, P, Si, Fe and S, via the production of biomass. Primary production by phytoplankton depends on the availability of these elements as nutrients. The purpose of this modelling study is to investigate how the biogeochemical fluxes of C, N, and Si are coupled in marine ecosystems. This study also addresses the role of iron in the coupling of C, N, and Si in diatom physiology and investigates which effects stoichiometric variations in phytoplankton biomass can have on large scale biogeochemical fluxes. This thesis considers physiological variations in biomass stoichiometry of one phytoplankton group only and no variations in the species composition of the plankton community.

1.1 Ecological stoichiometry

The word stoichiometry originates from the greek language and stands for measuring of elements. In chemical reactions, different elements or molecules, the reactants, are transformed into reaction products. Molecules consist of a fixed number of atoms of one or more elements. Elements thus react in a fixed numerical proportion. The numerical proportions that balance chemical reactions are called stoichiometry (Sterner and Elser, 2002).

The most famous example of introducing stoichiometry into ecology is most probably the work by Alfred C. Redfield (1934, 1942, 1958, 1963). Based on the data set of R. H. Fleming, Redfield (1958) found the stoichiometric composition of C:N:P in plankton biomass to be 106:16:1 on average (Geider and La Roche, 2002). These ratios, the Redfield ratios, seem to be uniformly distributed in the global ocean and also the concentrations of dissolved inorganic carbon, nitrate, and phosphate covary with similar ratios of 105:15:1 in deep sea waters (Broecker and Peng, 1982). Redfield (1958) concluded the covariation in deep ocean concentrations of C:N:P to be mainly the result of production and remineralization of biomass with a constant ratio of C:N:P.

Assigning biomass a fixed stoichiometric composition is like regarding biomass as a large molecule with a fixed contribution of different elements. Cells are made of a number of different organic molecules, like amino acids, fatty acids, saccharides, and many more, and each molecule has a fixed stoichiometry. Macromolecules, like proteins, lipids, carbohydrates, DNA, and RNA, may vary for a certain degree in their stoichiometric composition, as they consist of a variable combination of smaller molecules as monomeric sub-units. Despite possible variations in the numerical proportions of different elements in the respective molecule classes, the combination of elements is always the same. Neutral lipids and carbohydrates are made of carbon, oxygen, and hydrogen, amino acids also contain nitrogen and small amounts of sulfur, and phospholipids, DNA, RNA, and especially ribosomes also contain phosphorous. Different cells resemble each other in their general molecular composition. All cells have membranes that consist of lipid bilayers. All cells have DNA, RNA and ribosomes. All cells contain functional and structural proteins. It is therefore very likely that cells of different organisms are very similar in their stoichiometric composition.

However, some important stoichiometric differences between different types of organisms exist, mainly caused by different body structures. The cell wall of diatoms is made of amorphous hydrated silica, resulting in a physiological requirement of diatoms for dissolved silica as an important nutrient for cell growth and cell division (Martin-Jézéquel et al., 2000). Coccolithophores excrete small plates of calcium carbonate, the coccoliths, that remain attached to the cell surface. Coccolithophores thus exhibit elevated cellular contents of carbon, caused by the coccoliths. The production of biominerals like SiO_2 or $CaCO_3$ strongly increases the stability of the cell walls and is therefore assumed to act as a defense mechanism against zooplankton grazing (Hamm et al., 2003).

Besides involving additional elements like Si or Ca in biomass production, the intracellular C:N:P ratio of a single algal species can also vary under certain environmental conditions. The uptake of different dissolved inorganic nutrients is not directly coupled in autotrophic organisms whereas the metabolic incorporation into organic molecules is. Dissolved nutrients do not necessarily occur in ratios that meet the physiological requirements of the algae and the nutrient availability thus influences the elemental composition of algal cells.

The intracellular C:N ratio in phytoplankton organisms varies between 3 and 17 mol mol^{-1} under nitrogen replete conditions and can reach up to 20 under nitrogen-limitation (Geider and La Roche, 2002). Carbon is the most abundant element in biomass (dry weight) and makes up about 24 to 80 % of all macromolecules (dry weight). Variations in the cellular carbon content are mainly caused by varying lipid and carbohydrate pools for energy storage (Turpin, 1991). The residual carbon is bound

to cellular structures. The major pools of nitrogen are proteins (structural and functional) and nucleic acids. Nitrogen is also included in chlorophyll and can be stored as nitrate in large vacuoles (Geider and La Roche, 2002). Highest variations in cellular nitrogen contents are caused by differences in concentrations of functional proteins (enzymes) or inorganic nitrogen storage.

When extracellular dissolved inorganic nitrogen (DIN) concentrations are depleted due to algal growth or dilution, cellular uptake of nitrogen is also reduced. Uptake of other nutrients can still continue as long as these nutrients are available. Decreasing cellular nitrogen uptake reduces the concentrations of protein and also chlorophyll. With a reduction of enzyme and chlorophyll contents, also photosynthetic uptake of carbon is affected by nitrogen-limitation. The uptake of nitrate and assimilation into amino acids requires carbon skeletons and energy. Energy is either provided by production of ATP and NADPH in the light-dependent electron transport chain or via respiration of previously fixed carbon compounds. Carbon skeletons are provided via respiratory pathways and the assimilation of nitrate stimulates the respiratory carbon flow. At very low irradiance levels, photosynthetic fixation of carbon is reduced and the cellular carbon content decreases due to continuous respiratory losses. Decreasing provision of cellular energy and carbon skeletons thus also reduces cellular uptake of nitrogen and incorporation into amino acids (Turpin, 1991).

The N:P ratio in marine biomass can vary between 5 and 19 mol mol^{-1} under nutrient replete conditions with an average value of about 16. Under nitrogen limiting conditions, the N:P ratio can even exceed values of 50. The relative contribution of protein and phospholipids to the cellular biomass partly accounts for the variability in the cellular N:P ratio. But also the ability of phytoplankton to store surplus phosphorus and nitrogen causes high variability of intracellular N:P ratios and a direct influence of N:P ratios in the provided growth medium (Geider and La Roche, 2002).

The NO_3^-:PO_4^{3-} ratio in the deep ocean shows an average value of 15:1 mol mol^{-1} (Lenton and Watson, 2000). The lower N:P ratio in deep ocean waters indicates a loss of nitrogen from the surface to the deep. Some bacteria perform a special pathway of anaerobic degradation of organic matter, which uses nitrate instead of oxygen as an acceptor of hydrogen and reduces NO_3^- to N_2. This pathway, denitrification, reduces the amounts of reactive nitrogen under anoxic conditions. Upwelling, nutrient rich waters are thus depleted in nitrogen relative to phosphorus, making nitrogen the most limiting nutrient in the surface ocean (Tyrrell, 1999). Nitrogen fixation by cyanobacteria again transforms N_2 into reactive nitrogen and maintains N:P ratios in the surface ocean close to the Redfield ratio of 16:1 (Falkowski, 2000).

Silicon and nitrogen are usually incorporated into diatom biomass at a molar ratio of about 1 under nutrient replete conditions (Brzezinski, 1985). Hutchins and Bruland (1998) and Takeda (1998) found that in iron-limited waters diatoms exhibit increased molar Si:N ratios of up to 3. Silicon is required by diatoms to build cell walls of amorphous hydrated silica, the frustules. Silicon is thus mainly of structural relevance in the diatom metabolism. Increasing Si:N ratios in iron-limited diatoms may either be caused by increased cellular silicon contents and thus stronger silicified frustules (Leynaert et al., 2004) or decreased cellular pools of nitrogen at unchanged silicon content (Marchetti and Harrison, 2007).

Iron availability is critical for the algal nitrogen metabolism. As already described above, the uptake of nitrate by algae is directly coupled to the assimilation of nitrogen into amino acids (Michal, 1999), and for this, nitrate has to be reduced to nitrite and then to ammonia. This reduction is catalysed by the enzymes nitrate reductase and nitrite reductase, which both contain iron in their reaction centres. Low iron availability thus reduces intracellular amounts of nitrate and nitrite reductase and consequently the assimilation of nitrate decreases. Even though silicon uptake has been shown to decrease under iron limitation too (Leynaert et al., 2004), iron is not known to be directly involved in the silicon metabolism of diatoms. Iron is an important part of the electron transport chain in the

light dependent reactions of photosysnthesis (Geider and La Roche, 2002) and the decrease of silicon uptake is most probably the result of reduced metabolic rates, as the cellular content of protein and photosynthetically fixed metabolic energy decreases at iron limitation. Iron limitation thus affects the coupling of silicon with carbon and nitrogen in the diatom metabolism.

The different variations in the stoichiometric composition of plankton organisms mentioned above indicate that the chemical composition of seawater can change the stoichiometric signal which is observed in plankton biomass. When phytoplankton grows, it depletes dissolved nutrients in the growth medium due to nutrient uptake into the cells. Phytoplankton growth thus actively changes the chemical composition of seawater. The stoichiometric composition of phytoplankton biomass mirrors the uptake ratios of different nutrients into algal cells and as nutrient uptake depends on the ambient nutrient concentrations, the chemical environment again influences phytoplankton stoichiometry. There is a direct bio-chemical feedback between nutrient uptake, cellular stoichiometry and nutrient concentrations in the growth medium.

As the distribution of nutrient concentrations affects phytoplankton physiology, it also affects the fluxes of carbon and other elements through the ecological foodweb structure. Via the feedback of phytoplankton stoichiometry to global nutrient distributions, there is also an impact of physiological variations in plankton stoichiometry on the global carbon cycle.

If we want to understand the global ocean carbon cycle, we also have to understand the physiological reactions of primary producers to variable nutrient compositions. Hence, we cannot model the global ocean carbon cycle without modelling the cycles of other elements and the connection of these via the production of biomass. In order to make future predictions of recent climate change with coupled biogeochemical ocean atmosphere general circulation models, we have to correctly implement how nutrient distributions will change during the climate change model scenarios. Understanding the variations in the stoichiometric ratios of elemental fluxes and nutrient distributions in the ocean may help us to improve model simulations of the global ocean carbon cycle.

1.2 Ecological modelling

Mathematical models have proven to be valuable tools to investigate complex dynamic systems. Models help us to improve our understanding in many different fields of environmental science, like meteorology and oceanography, but also in nuclear physics and chemistry. Mathematical models are also applied to understand complex interactions in ecology.

A large range of temporal and spatial scales are considered in the science of ecology. Depending on the processes of interest, the model design is chosen from a variety of different possible model architectures and setups to investigate the scientific question at hand. We roughly differentiate between individual based models (IBMs), distribution based models, and state variable or compartment models that will be coarsely reviewed in the following.

State variable models in ecology usually describe the average behaviour and properties of a population while implicitly assuming equality of different individuals of the considered population. Often these models are formulated in terms of densities or concentrations, rather than numbers of individuals. The nutrient-phytoplankton-zooplankton (NPZ) food chain model by Steele (1958) simulates predator-prey interactions between phytoplankton and zooplankton, and also includes a bottom-up control of phytoplankton growth rates via nutrient availability. This NPZ model was first applied in a two-layer ocean system, where all three compartments were uniformly distributed over the euphotic surface mixed layer (Gentleman, 2002). Phytoplankton grow in the surface layer and deplete nutrients that have to be resupplied via mixing of the surface layer with a nutrient rich deep layer. The

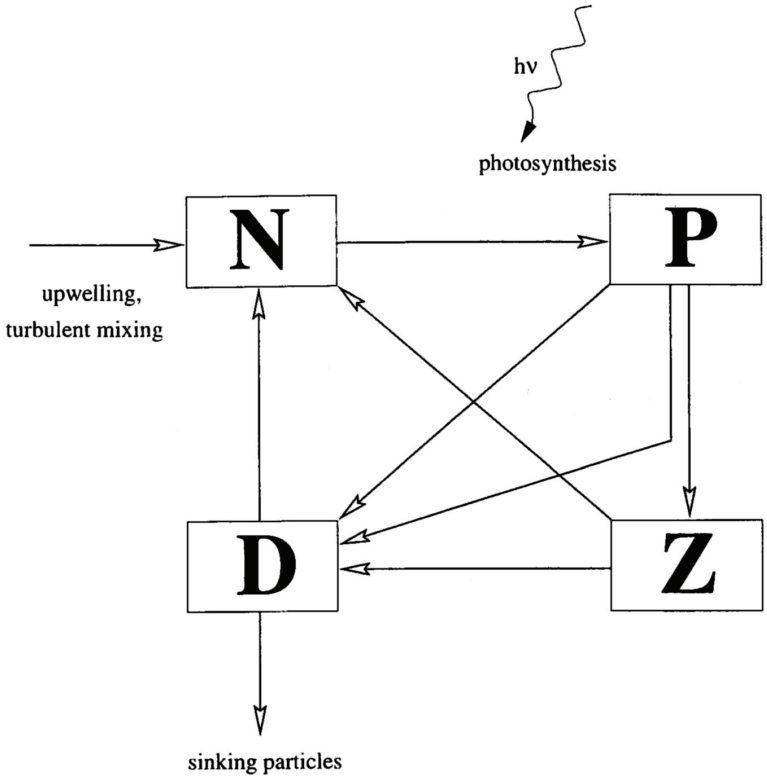

Figure 1.1: *Schematic of a typical NPZD-model. N=nutrients, P=Phytoplankton, Z=zooplankton, D=detritus. Arrows indicate fluxes between model compartments. Modified after Oschlies and Garcon (1999).*

phytoplankton biomass supports growth of the zooplankton population and the produced biomass, both by zooplankton and phytoplankton, is lost to the deep layer, where it is transformed into nutrients again. NPZ-models have been applied in biological oceanographic research for several decades by now and have mostly been used as theoretical investigation tools to improve our understanding of plankton dynamics and their dependencies on physical changes in the plankton environment or changes of parameter values and model equations (Franks, 2002). However, up to now NPZ-models have evolved to rather complex model systems by several extensions and inclusions of new processes and functional compartments.

Often only one nutrient is considered in NPZ-models, that is chosen to be represented by the most limiting nutrient, e.g. nitrogen, in the pelagic ecosystem. As different nutrients may become limiting in different ocean regions or for different phytoplankton organisms, the inclusion of additional pools of nutrients, like phosphorus, silicon, or iron, can strongly improve model simulations of global chlorophyll distribution fields (Aumont et al., 2003). The consideration of more than one nutrient allows for colimitation by different nutrients and for the modelling of multi-nutrient interactions in phytoplankton physiology (Flynn, 2003). Limitation by different nutrients can be modelled by applying Liebig's law of the minimum, which assumes that only one nutrient, the most limiting nutrient, actually limits photosynthesis and thus plankton growth (De Baar, 1994), or with a multiplicative approach, that uses the product of two limitation terms for growth limitation.

Consideration of more than one element in phytoplankton biomass may lead to variations in cellular quotas of different elements and thus cellular stoichiometry. In these models (quota models),

the variation in cell quotas is assumed to affect the metabolic condition and to regulate the metabolic rates (Geider et al., 1998). Unfortunately, not much is known about the regulation mechanisms and the mathematical form of the regulation functions is highly speculative.

Inclusion of detritus (NPZD-models) improves the description of remineralization processes and the fate of exported biomass (Six and Maier-Reimer, 1996). Consideration of bacteria introduces the representation of the microbial loop and improves the microbial food web structure (Fasham et al., 1990; Sarmiento et al., 1993). Also the inclusion of transparent exopolymer particles, TEP, in ecosystem models can improve our understanding of the aggregation process of phytoplankton and improve simulations of primary production and export of organic carbon (Engel et al., 2004).

The simple food web structure of an NPZ-model can also be extended by inclusion of additional groups of phytoplankton and zooplankton. Phytoplankton, for instance, can be divided into small picoplankton and large phytoplankton which represents fast growing diatoms (Denman and Peña, 2002; Denman, 2003). Zooplankton can then also be splitted into microzooplankton and mesozooplankton, which differ in the size spectrum of their preferred prey. One approach in introducing more complexity into ecosystem models and making the models more realistic is dividing plankton organisms into so called plankton functional types, PFTs, that are grouped according to differences in their biogeochemical traits (Le Quéré et al., 2005). Here, phytoplankton can be divided into silicifiers, calcifiers, DMS producers, nano- and picoplankton, and N_2-fixers. Zooplankton can be divided into carnivorous, herbivorous and detritivorous zooplankton, also of different size classes.

The European Regional Seas Ecosystem Model (ERSEM) is an attempt to include as much complexity as possible in the ecological food web structure by adding more and more state variables of different groups of organisms or even species to the model (Baretta et al., 1995). However, field data are often only available as bulk parameters like concentrations of chlorophyll or particulate organic carbon and nitrogen, so that many state variables in complex models again have to be combined to bulk parameters for model validation. Reducing complexity of nature to a few state variables makes model analysis much more feasible.

The implicit assumption of equality of all individuals of the population compartment in a state variable model does not account for the emergence of ecological patterns by individual behaviour, which may be important in some cases (Grimm et al., 1996; Woods et al., 2005). An alternative approach to state variable models are so called individual based models (IBMs). The smallest entity in this sort of models are single individuals. The entire population is thus described by the distribution of single individuals and population dynamics result from prognostic intra- and interspecific interactions on an individual basis. IBMs are often used to investigate the development of size structures in populations or stage specific responses to perturbations (Grimm, 1999). However, the simulation of single individuals is connected to large computational costs, especially in large populations like in the plankton community. Increasing the number of individuals in an IBM increases the memory requirements of the computing machine and also computing time. In order to reduce computational costs, very large populations can be modelled on an individual basis with the help of introducing super-individuals that represent a group of individuals which are combined assuming equality of individual properties and behaviour (Scheffer et al., 1995). Super-individuals can thus be regarded as hybrids between IBMs and classical state variable models.

One example of a plankton IBM is the Lagrangian Ensemble (LE) metamodel by Woods and Barkmann (1994). Here, several plankton individuals are combined to agents that follow different trajectories and thus experience different environmental conditions over time. Population densities and demographic patterns emerge from interactions that occur on an individual basis. The LE metamodel can be used to create virtual ecosystems to study plankton population dynamics under controlled environmental conditions. But, due to the large computational costs, these virtual ecosys-

tems are usually modelled in 1D as a vertical line or as a moored or free floating mesocosm of a restricted volume (Woods, 2005).

As a consequence of individual differences, ecological properties, such as growth rates, nutrient affinities, or size, are usually not equal for all individuals of a population but show variations over the population. The distribution of these properties can be represented by, for instance, log-normal (Bricaud and Morel, 1986) or gamma distributions (Risovic, 1993). Assuming distributed property values over the population can thus simulate individual variability in a statistical sense without the large requirements of computational power as for an IBM. Distribution based models are applied, for example, to model size based effects on particle aggregation in the parameterization of the export flux of organic carbon into the ocean interior (Kriest and Oschlies, 2008), differences in nutrient uptake kinetics due to surface to volume ratios in different size classes of phytoplankton cells, as has been shown by Pasciak and Gavis (1974), or grazing efficiency of a consumer on a ressource that consists of particles of different size classes (Armstrong, 1999).

The purpose of this study is to investigate the coupling of biogeochemical cycles and the implications of variable stoichiometry in phytoplankton organisms on the coupling of different biogeochemical elements. The consideration of population dynamics and intraspecific variability is not necessarily required for the modelling of ocean biogeochemistry. IBMs would also require too much computational power and are thus not suitable for the application in large scale ecosystems or the global ocean. In this thesis an NPZD-model is developed andapplied that considers different pools of elements and thus allows for variable stoichiometry in phytoplankton biomass. The model by Geider et al. (1998) for variable C:N:Chl ratios in phytoplankton biomass is chosen as the basis for further model development.

NPZ-models, or derived model versions, can easily be coupled to ocean general circulation models, OGCMs, by inclusion of the ecological state variables and additional advection-diffusion equations, that distribute the state variables as passive tracers in the ocean current system. These coupled biogeochemical ocean general circulation models, BOGCMs, can then be used to investigate the regional or global cycles of important biogeochemical elements.

1.3 Study regions

This thesis includes four studies that investigate state variable models on different spatial scales, from phytoplankton batch cultures over regional ecosystems to plankton communities in the global ocean.

The first study in this thesis is about the biogeochemical coupling of carbon and nitrogen in a shallow coastal tidal basin in the Danish-German Wadden Sea, the Sylt-Rømø tidal basin, that is connected to the North Sea via tidal currents. The North Sea is a temperate sea on the European continental shelf. The Wadden Sea is the adjacient transition zone between the sea and the continent. In the Wadden Sea, the terrestrial margin has a very gentle slope that falls dry during ebb and is flooded again twice a day. The tidal currents lead to a strong exchange of pelagic biogeochemical tracers between the North Sea and the Wadden Sea.

The study investigates the implications of variable C:N ratios in phytoplankton biomass on the transport fluxes of carbon and nitrogen between the North Sea and the Sylt-Rømø tidal basin. Modelling of transport fluxes requires good reproduction of tracer concentrations in the considered water masses and therefore a good representation of important biological processes in the model. The low water depth on the continental shelf leads to a very intense bentho-pelagic coupling, which is very different to the open ocean. The bentho-pelagic coupling causes fast cycling of nutrients in coastal

Figure 1.2: *Scales considered in this thesis: A) the Sylt-Rømø tidal basin; B) lab experiments with phytoplankton cultures; C) the Southern Ocean.*

waters and also influences physical properties of the water column via resuspension of sediments caused by strong tidal currents. The proximity of the North Sea and the Wadden Sea to the land makes sampling relatively easy and long time series of data and large data sets have been gathered in these waters. Continental shelf regions are usually very rich in nutrients due to riverine runoff and show very high productivity. Shelf seas are a source of alkalinity to the global ocean and play an important role in the global ocean carbon cycle (Thomas et al., 2004).

In the second study, the time development of batch cultures with a single diatom species is simulated. The laboratory experiments are interpreted to derive parameterizations of diatom physiology that can be applied in large scale ecosystem models.

In laboratory experiments, one can easily control the environmental conditions and identify physiological reactions to changes in different environmental factors. Bottle experiments usually investigate the reaction of one species only or a predator-prey system of only two species. Introduction of additional species or variations in more environmental parameters increases the degree of freedom in the reaction system and the more complex the analysis of the observations will get. In field studies, changes of an observed biological or chemical property may occur due to changes of a combination of different environmental parameters and the interpretation of the observations may become very difficult.

The batch experiments simulated in this study all investigate variations of the Si:N ratios in diatom biomass as a response to varying nutrient concentrations. Modelling of laboratory experiments can provide additional process understanding of the revealed physiological response to the environmental changes.

The third study concentrates on the Southern Ocean, here defined as the region south of 45°S. It encompasses about $7.6 \cdot 10^7$ km^2 or 22% of the world ocean. The Southern Ocean extends from subtropical over temperate to polar waters and is divided into different ecosystems by fronts (Orsi et al., 1995), including the Antarctic Circumpolar Current, ACC, that flows eastwards around Antarctica. The average depth of the Southern Ocean is about 4000 m so that benthic processes are in general negligible for the biogeochemistry of the pelagic. Low biomass concentrations are observed in the Southern Ocean despite relatively high concentrations of macronutrients like nitrate, silicic acid and phosphate (Banse, 1996). Deep vertical mixing due to strong winds causes low irradiance levels in the surface mixed layer of the Southern Ocean, but the major reason for growth limitation of phytoplankton is thought to be very low concentrations of the micronutrient iron (Martin et al., 1990;

De Baar et al., 1999).

Iron-limitation affects the coupling of Si to C and N in the diatom metabolism (Leynaert et al., 2004) and leads to increased Si:N ratios in diatom biomass (Hutchins and Bruland, 1998; Takeda, 1998). The third study of this thesis applies the parameterization of variable Si:N:C stoichiometry in diatoms, as developed in study 2, to a global biogeochemical ocean general circulation model. The model is then analysed for the biogeochemical implications of Si:N decoupling in iron-limited waters of the Southern Ocean.

The remoteness to most landmasses and the harsh weather conditions make the Southern Ocean one of the less investigated ocean regions. The size of the Southern Ocean, storms and the ice cover during austral winter make it difficult to collect data on a fair spatial and temporal resolution. However, during the Joint Global Ocean Flux Study, JGOFS, time series data has been collected at three stations in the Southern Ocean: one station at the Kerguelen plateau, KERFIX, a transect in the Antarctic Polar Frontal Zone, APFZ, and a station in the Ross Sea. The use of satellite based earth observation systems provides us with global maps of back scattered radiation from the sea surface, whose irradiance spectra are used to estimate pigment concentrations and sea surface temperature with high spatial and temporal resolution. But the maximum north-south extension of the satellites orbit, the cloud cover and the polar night limit the data coverage by remote sensing, especially in high latitudes. Also, the penetration depth of the remotely sensed signal into the water column is not always known, resulting in relatively large uncertainties of the remotely sensed data.

The fourth study investigates an eddy permitting biogeochemical model for the global domain. The model is set up on a cubed sphere model grid with a resolution of 510×510 grid points on each side of the cube, giving a maximum resolution of about 19 km. The global ocean includes many different biogeochemical regimes and ecosystems (Longhurst, 1998). Global ocean biogeochemical models are usually not capable of simulating the large variability in the remotely sensed chlorophyll signal and are thus usually compared to climatological data. In this study, the model is mainly analysed for its technical performance on the JUMP supercomputer at the Helmholtz Research Centre Jülich.

Chapter 2

Modelling primary productivity in a shallow coastal tidal basin

S. Hohn, C. Völker, J.E.E. van Beusekom, M. Schartau

2.1 Introduction

The 450 km coastline between Den Helder in the Netherlands and Blåvandshuk in Denmark encompasses with about 8000 km^2 the largest Wadden Sea area of the world (Reise, 2005). The Wadden Sea is used for aquaculturing and fisheries and the human influence on this unique ecosystem is very intense. Therefore, a good understanding of the system is needed to improve coastal management and to react to critical changes due to anthropogenic impact.

High nutrient concentrations and high irradiance levels in the shallow coastal waters make the Wadden Sea a very productive part of the North Sea (Asmus et al., 1998*b*). High chlorophyll concentrations are observed in the water column (Loebl et al., 2007; van Beusekom et al., 2008*a*) and in the sediments (Hedtkamp, 2005) and the algal biomass produced in the Wadden Sea supports a large and diverse food web (Baird et al., 2004). The high nutrient concentrations are caused by remineralization of particulate organic matter and by riverine runoff (Asmus et al., 1998*a*).

Increased riverine nutrient loads have lead to a five-fold increase in primary production compared to pre-industrial conditions (van Beusekom, 2005). The relative importance of benthic processes increases with decreasing water depth (Heip et al., 1995). In the Wadden Sea, pelagic end benthic processes contribute equally to the turnover of organic matter (van Beusekom et al., 1999). Settling of particles (Postma, 1981), trapping of particles in permeable sediments (Rusch and Huettel, 2000), and filter-feeding activity (Asmus and Asmus, 1998*b*), all contribute to an effective bentho-pelagic coupling in the Wadden Sea.

How biogeochemical processes in the Wadden Sea influence biogeochemistry in the North Sea, and vice versa, has been adressed by an interdisciplinary research project (SWAP) that concentrated on the tidal basin between the islands of Sylt and Rømø in the years 1990 to 1995 (Gätje and Reise, 1998). Carbon budgets suggest that the Wadden Sea imports organic matter from the North Sea (van Beusekom et al., 1999) and acts as a source for dissolved nutrients. This would declare the Wadden Sea a net heterotrophic system as it is supported by a net import of biomass that is remineralized in the saprophagous food web and cannot be maintained by its primary producers alone. The development of this heterotrophy may be caused by differences in the hydrodynamic forces that influence sinking and resuspension of particles during a tidal cycle (Postma, 1981) or simply by differences in the

water depth that affect the residence time of sinking detritus in the water column (Burchard et al., 2008).

In order to analyse the functioning of the ecosystem, i.e. to estimate how much biomass can be accumulated, how nutrients are recycled and what regulates the abundance of organisms, one has to understand what regulates and limits primary production, both, in the North Sea and in the Wadden Sea, as this is the key process generating the energy and biomass that maintains the entire ecosystem. During a seasonal cycle, primary production in the Wadden Sea is either limited by light or by nutrients (Colijn and Cadée, 2003). The intensity of either limitation and the timing of the transition will decide which factor outweighs the other. Besides light and nutrients, grazing and remineralization may have significant effects on primary production, too. Grazing of zooplankton or mussels can either promote or limit primary productivity (Asmus and Asmus, 1991). High grazing pressure will decrease the phytoplankton standing stock and thus the amount of carbon fixing biomass. But the release of nutrients by grazers may also support primary productivity. Grazing on phytoplankton distributes the produced biomass over an additional population, and may increase the amount of total biomass that can be accumulated in the system (Loreau, 1995). Asmus and Asmus (1991) proposed that the supporting effect of filterfeeding organisms on primary production exceeds their limiting effect in the tidal basin between Sylt and Rømø.

Mathematical ecosystem models have proven to be valuable tools to improve our understanding of the functioning of ecosystems and to test hypotheses. Several ecosystem models have been developed for the North Sea (Radach and Pätsch, 1997; Moll, 1998; Skogen and Moll, 2000). In this study, the shallow tidal basin between the german island of Sylt and the danish island of Rømø, the Sylt-Rømø bight or List tidal basin, has been chosen as study area because a huge amount of data and information is available for this system (Gätje and Reise, 1998). The bight is located between the two islands in the west and the mainland in the east and is bordered by two connections of the islands with the mainland in the north and in the south. So, there is only one tidal inlet between Sylt and Rømø, the Lyster Dyb, making the bight a suitable study area.

Fast et al. (1999) have already developed an ecosystem model for the Sylt-Rømø bight, the Sylt-Rømø Bight Ecosystem Model (SRB Model). The SRB Model is relatively complex. It divides the bight into seven different boxes with different geographical properties and contains a rather complex description of the benthic system with five benthic layers. It also includes many biological state variables for different organisms.

The approach of this study is to use an ecosystem model for the pelagic, that was developed to simulate mesocosm experiments (Schartau et al., 2007), and apply it to the shallow coastal system. The model describes the cycling of carbon and nitrogen but lacks the consideration of phosphorus and silicon. Although the foodweb structure in the model is relatively simple, it contains a rather complex description of algal physiology that decouples the uptake of carbon and nitrogen. The model is used to investigate the biogeochemical impact of the Wadden Sea and the role of different processes that affect primary production in the SRB.

2.2 Model description

2.2.1 Physical setup

The Sylt-Rømø bight (SRB) covers an area of $404.6 \cdot 10^6\ \mathrm{m}^2$ and includes $570 \cdot 10^6\ \mathrm{m}^3$ of water at low tide (Backhaus et al., 1998). The inflowing North Sea water almost doubles the water volume inside the bight twice a day during flood. Ebb flow removes the water again. The tidal range is about $1.8\ \mathrm{m}$ on average and the water level changes between $1\ \mathrm{m}$ below NN at low tide and $0.8\ \mathrm{m}$ above

NN at high tide. Maxumium values range between $3.5\ \mathrm{m}$ below and $4.0\ \mathrm{m}$ above NN (Backhaus et al., 1998).

We approximate the bight as a homogeneously mixed box that is coupled to a second box for the North Sea (NS). Processes and state variables in the two boxes are marked by subscripts, $_{srb}$ and $_{ns}$ respectively. The North Sea box has an area of $1.407 \cdot 10^{10}\ \mathrm{m}^2$ which corresponds to the area between 55.5°N and 7.4°E and the coastline. The volume is about $2.172 \cdot 10^{11}\ \mathrm{m}^3$, the average water depth is $15.44\ \mathrm{m}$, calculated from the ETOPO5 database (NOAA, 1988).

The water level in the SRB, P, shows a semidiurnal cycle caused by the frequency of the gravitational forcing of the sun and the moon (Eq. 2.1). The shift of the two different frequencies leads to a spring and neap tide cycle. The constants a_0, a_1 and a_2 have been chosen to reproduce the observed tidal pattern in the bight relative to NN.

$$P(t) = a_0 + a_1 \cdot sin(\omega_{moon} \cdot t) + a_2 \cdot sin(\omega_{sun} \cdot t) \tag{2.1}$$

$$\omega_{moon} = \frac{2\pi}{12.41\mathrm{h}} \tag{2.2}$$

$$\omega_{sun} = \frac{2\pi}{12.00\mathrm{h}} \tag{2.3}$$

Where t is measured in hours.

The absolute volume of water inside the SRB, Vol_{srb}, and the water transport through the Lister Dyb, δVol, can be determined using the hypsometric approximation of Backhaus et al. (1998) (Eq. 2.4).

$$Vol_{srb}(t) = b_0 + b_1 \cdot P(t) + b_2 \cdot P(t)^2 + b_3 \cdot P(t)^3 \tag{2.4}$$

The difference of the water volume between two time steps equals the water transport through the Lister Dyb, δVol. The water flowing into the bight is subtracted from the North Sea water volume, Vol_{ns}, and added again when leaving the bight.

$$\delta Vol(t) = Vol_{srb}(t) - Vol_{srb}(t - \Delta t) \tag{2.5}$$

$$Vol_{ns}(t) = Vol_{ns}(t - \Delta t) - \delta Vol(t) \tag{2.6}$$

The average water depth, z, is given by the water volume divided by the area of the box, A.

$$z_{ns} = \frac{Vol_{ns}(t)}{A_{ns}} \tag{2.7}$$

$$z_{srb} = \frac{Vol_{srb}(t)}{A_{srb}} \tag{2.8}$$

Doubling the water volume of the bight twice a day would lead to a very strong exchange of SRB water if the whole tidal prism would mix with the SRB water. This is not observed in reality. Most of the inflowing water leaves the bight without any influence on SRB water characteristics and only a small percentage of the tidal prism, p_{ex}, mixes with SRB water. The exchange efficiency, p_{ex}, was calculated by Fast et al. (1999) to be 8 to 12 % of the tidal prism. To account for this property, two different water bodies have to be assumed to occur in the SRB. One is the actual amount of water in the bight, Vol_{srb}, and the other is the amount of water showing the biogeochemical characteristics of the Wadden Sea, V_{srb}. For consistency, the same has to be carried out in the North Sea.

$$V_{ns}(t) = V_{ns}(t - \Delta t) - p_{ex} \cdot \delta Vol \tag{2.9}$$

$$V_{srb}(t) = V_{srb}(t - \Delta t) + p_{ex} \cdot \delta Vol \tag{2.10}$$

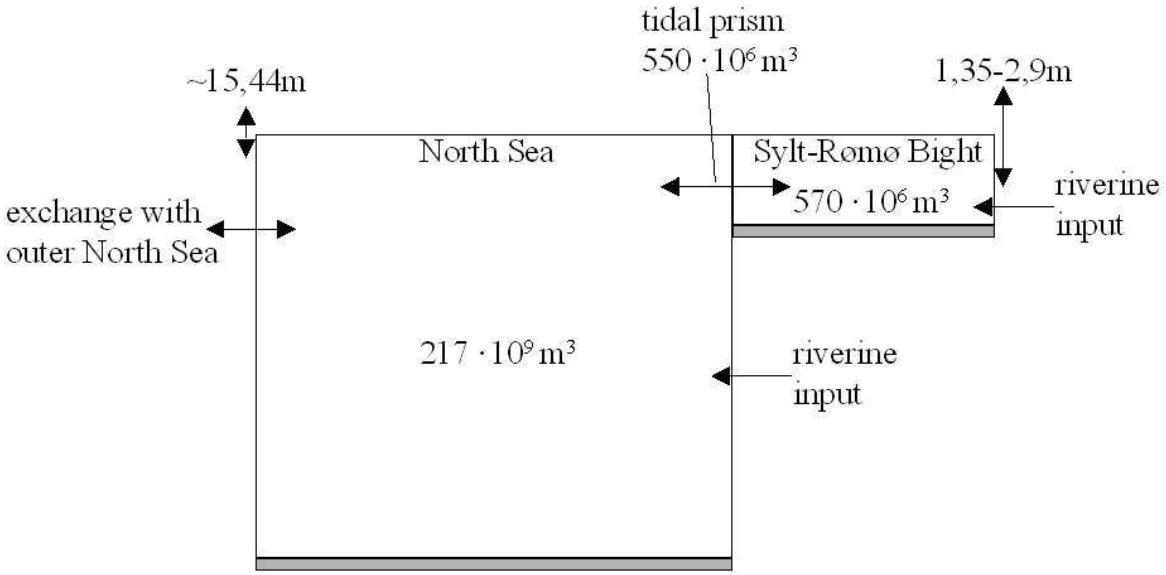

Figure 2.1: *The physical setup consists of two homogeneously mixed boxes for the pelagic that are connected via tidal transport. Shallow benthic boxes are associated to each pelagic box.*

The tidal flow leads to an exchange of pelagic biogeochemical tracers between NS and SRB. This exchange can be written as a rate of change of tracer concentration, C, that is proportional to $\Psi \cdot C$ (see equations in appendix).

$$\Psi_{ns}(t) = -\frac{p_{ex}}{V_{ns}} \cdot min\left[\, \delta Vol(t),\, 0 \,\right] \tag{2.11}$$

$$\Psi_{srb}(t) = \frac{p_{ex}}{V_{srb}} \cdot max\left[\, \delta Vol(t),\, 0 \,\right] \tag{2.12}$$

In this expression, only inflowing water leads to a change in tracer concentrations, outflow does not affect tracer concentrations.
In the North Sea box, the two large rivers Elbe and Weser import freshwater and dissolved nutrients into the system. In the Sylt-Rømø bight, riverine runoff occurs via two very small rivers, the Vidå and the Brede Å. Although the absolute freshwater discharge into the bight may be negligible small (Asmus et al., 1998*a*; Hickel, 1980), the observed DIN concentrations in the riverine runoff may reach up to 336 $\mu\mathrm{mol\,l^{-1}}$ (Claussen, pers. comm.). The freshwater transport itself is ignored in the ecosystem model, the amount of discharged nitrogen, N^{in} $(\mathrm{mmol\,d^{-1}})$, that enters the boxes, is

diluted in the water column and causes a change of DIN concentrations, N^{src} ($\mathrm{mmol\ m^{-3}\ d^{-1}}$).

$$\mathrm{N}^{src}_{srb} = \frac{\mathrm{N}^{in}_{riv}(t)}{V_{srb}(t)} \tag{2.13}$$

$$\mathrm{N}^{src}_{ns} = \frac{\mathrm{N}^{in}_{WE}(t)}{V_{ns}(t)} \tag{2.14}$$

To avoid unreasonable accumulation of nutrients in the system, a constant amount of water is assumed to exchange between the North Sea box and the outer North Sea, V^{ex}_{NS} ($\mathrm{m^3\ d^{-1}}$), that restores nutrient concentrations to normal values, Π_{ns} ($\mathrm{d^{-1}}$).

$$\Pi_{ns} = \frac{V^{ex}_{NS}}{V_{ns}} \tag{2.15}$$

A benthic box with a thickness of 10 cm, z_{ben}, is associated to each pelagic water box. The porewater of the sediments exchanges with the water column assuming a constant mixing rate, mr. As sediments in the North Sea are expected to have larger grain sizes and thus higher porosity, a higher mixing rate is assumed in the NS compared to the SRB. The effect of porewater exchange with the water column is defined by a constant exchange rate for the NS and another for the SRB divided by the thickness of the regarded box.

$$\Omega_{ns} = \frac{mr_{ns}}{z_{ns}} \tag{2.16}$$

$$\Omega_{srb} = \frac{mr_{srb}}{z_{srb}} \tag{2.17}$$

$$\Omega^{ben}_{ns} = \frac{mr_{ns}}{z_{ben}} \tag{2.18}$$

$$\Omega^{ben}_{srb} = \frac{mr_{srb}}{z_{ben}} \tag{2.19}$$

2.2.2 Salinity model

The salinity signals of the SRB and the NS, S_{srb} and S_{ns}, are calculated in a separate model to test whether the assumptions allow a reasonable reproduction of the hydrological framework of the SRB. Both watermasses are interconnected by the exchange of water, Ψ, due to tidal transport. To avoid continuous freshening of the system by riverine runoff, W^{dil}, the influence of an outer NS box with constant salinity, S_{NS}, and a constant exchange between the NS box and the outer NS, Π_{ns}, is implemented that restores North Sea salinity, S_{ns}, to normal concentrations.

The salinity model contains three parameters that have to be defined: the exchange efficiency of the tidal transport, p_{ex}, the salinity concentration in the outer North Sea, S_{NS}, and the exchange volume of the NS box with the outer North Sea, V^{ex}_{NS}. Water volumina and salinity concentrations are calculated by the model.

$$\frac{\mathrm{d}}{\mathrm{d}t} S_{ns} = -\ W^{dil}_{ns} \cdot S_{ns} \ +\ \Psi_{ns} \cdot (S_{srb} - S_{ns}) \ -\ \Pi_{ns} \cdot (S_{NS} - S_{ns}) \tag{2.20}$$

$$\frac{\mathrm{d}}{\mathrm{d}t} S_{srb} = -\ W^{dil}_{srb} \cdot S_{srb} \ +\ \Psi_{srb} \cdot (S_{ns} - S_{srb}) \tag{2.21}$$

The dilution factor of the effect of riverine freshwater input on salinity concentrations, W^{dil}, is given by the amount of freshwater discharge, V^{in} ($\mathrm{m^3\ d^{-1}}$), divided by the absolute box volume.

As freshwater salinity is assumed to be zero, the concentration gradient equals the salinity in the respective box.

$$W_{srb}^{dil} = \frac{V_{riv}^{in}(t)}{V_{srb}(t)} \tag{2.22}$$

$$W_{ns}^{dil} = \frac{V_{WE}^{in}(t)}{V_{ns}(t)} \tag{2.23}$$

The unknown model parameters were estimated by a least-squares fit to the data. The parameter values are compiled in Table 2.1.

Table 2.1: Physical parameters of the model.

Fixed parameters		
Symbol	Value and Unit	Description
a_0	-0.075 m	background sea level heigth
a_1	0.89 m	lunar amplitude
a_2	0.085 m	solar amplitude
b_0	$8.5135 \cdot 10^8$ m^3	fitting parameter
b_1	$3.3809 \cdot 10^8$ m^2	fitting parameter
b_2	$3.86 \cdot 10^7$ m	fitting parameter
b_3	$-9.36 \cdot 10^6$	fitting parameter
A_{srb}	$404.6 \cdot 10^6$ m^2	Area SRB
A_{ns}	$14.07 \cdot 10^9$ m^2	Area NS box

Parameters for variation		
Symbol	Value and Unit	Description
p_{ex}	0.013	exchange efficiency tidal transport
S_{NS}	33.3	salinity outer NS
V_{NS}^{ex}	$2 \cdot 10^9$ m^3 d^{-1}	exchange volume NS with outer NS

2.2.3 Ecosystem model

The ecosystem model calculates the concentrations of phytoplankton, zooplankton, detritus, dissolved organic matter and dissolved inorganic nutrients in the water column of the North Sea and the Sylt-Rømø bight (Fig. 2.2). Sinking detritus accumulates in the benthic layer where it is remineralized. Dissolved inorganic nutrients exchange between the porewater of the sediments and the water column. Dissolved oxygen is supplied to the porewater where it regulates benthic remineralization. In the SRB, microphytobenthos is included in the model as a second group of primary producers. Zoobenthos is implemented to regulate microphytobenthos biomass production. Filterfeeders in the SRB are not implemented as an own state variable but the effect of filterfeeding on phytoplankton and detritus concentrations is parameterized as described below. All components are divided into carbon and nitrogen pools. Phytoplankton and microphytobenthos biomass are also described in chlorophyll units. Total alkalinity, ALK, is included in the model to resolve carbonate chemistry and to calculate the air-sea gas-exchange of CO_2. The ordinary differential equations describing the

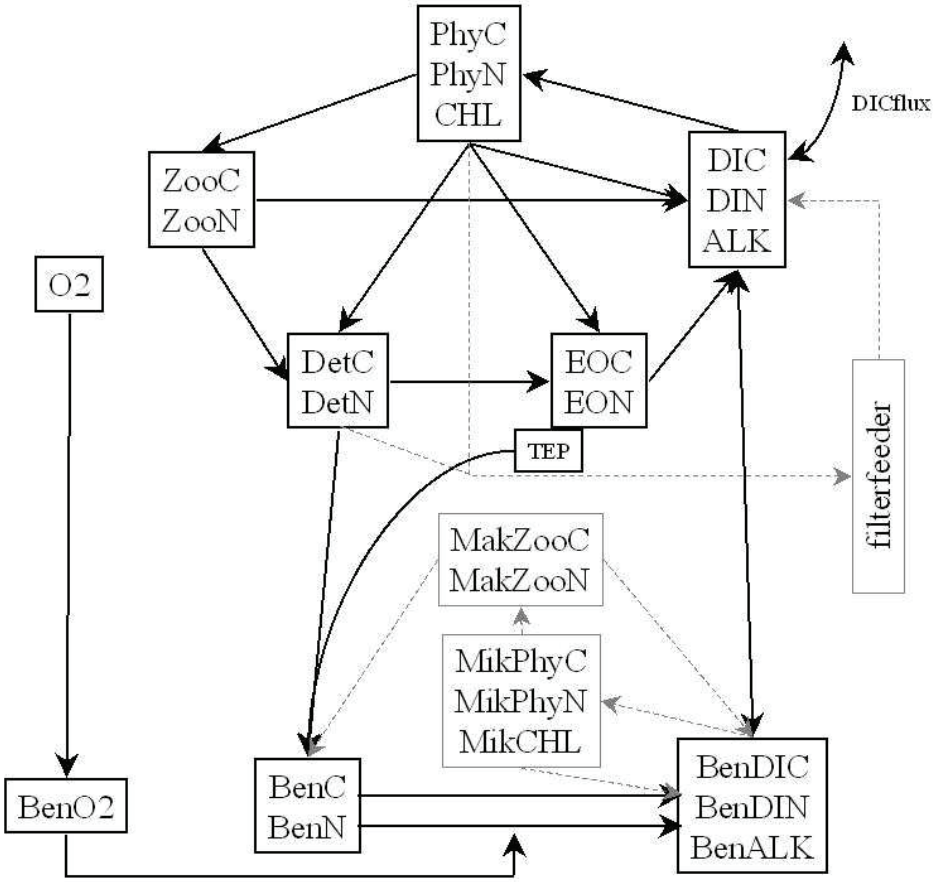

Figure 2.2: *Flowchart. State variables are displayed in boxes. Arrows indicate fluxes between state variables. State variables and fluxes are drawn in black when they occur in the NS and the SRB and in grey if they occur in the SRB only. The effect of filterfeeders on phytoplankton and detritus concentrations is parameterized and no additional state variable is implemented for filterfeeders.*

temporal changes of the state variables are given in the appendix. The processes leading to these changes are described in the following.

Seawater chemistry

As nutrients that are needed for the production of phytoplankton biomass only dissolved inorganic nitrogen and carbon, DIN and DIC, are considered in this model. DIN comprises nitrate, nitrite, and ammonia and is chemically treated as nitrate. Nitrification and denitrification are assumed to play only minor roles in the nitrogen cycle of the bight (Bruns and Meyer-Reil, 1998) and are therefore not included in the model, even though recent evaluation of winter nitrate concentrations suggest that denitrification may previously have been underestimated (van Beusekom et al., 2008*b*). The only natural source of nitrogen to the system is nitrogen discharge via continental runoff, N^{src}. Data of nitrogen input into the SRB via the two small rivers Vidå and Brede Å have been gathered by the Sønderjyllandsamt, Denmark (Claussen, pers. comm.). Nitrogen discharge of the rivers Weser and Elbe into the NS box, N^{in}_{WE}, are taken from Pätsch and Lenhart (2004). To avoid unreasonable accumulation of nitrogen in the system, an exchange with the outer NS, Π_{ns}, is implemented as already described above. The seasonal variation of DIN concentrations in the outer NS were calculated from

the ICES database (http://www.ices.dk).

DIC includes carbonate, bicarbonate and carbonic acid or dissolved CO_2. Depending on the difference of CO_2 concentrations, $d\mathrm{CO}_2^\star$, between the seawater and the atmosphere, air-sea gas-exchange of CO_2, $\mathcal{F}^\mathrm{C}$, is either a source or a sink of CO_2 to the water column. The gas transfer velocity, k_{av}, is calculated after Wanninkhof (1992). The carbonate chemistry is resolved after Millero (1995) using data of Mehrbach et al. (1973). The solubility of CO_2 in seawater, ff, is determined after Weiss and Price (1980).

$$\mathcal{F}^\mathrm{C} = d\mathrm{CO}_2^\star \cdot k_{av} \tag{2.24}$$

$$d\mathrm{CO}_2^\star = \mathrm{CO}_2^\star air - \mathrm{CO}_2^\star sea \tag{2.25}$$

$$\mathrm{CO}_2^\star air = p\mathrm{CO}_2^{air} \cdot ff \tag{2.26}$$

$$\mathrm{CO}_2^\star sea = \frac{DIC \cdot [\mathrm{H}]^2}{[\mathrm{H}]^2 + k_1 \cdot [\mathrm{H}] + k_1 \cdot k_2} \tag{2.27}$$

A decrease of nitrate or phosphate concentrations increases alkalinity by $1\ \mathrm{mol}\,\mathrm{mol}^{-1}$ nitrate or phosphate (Wolf-Gladrow et al., 2007). In the model, a constant molar N:P ratio of 16 is assumed (Redfield et al., 1963) that increases modelled alkalinity by $1\frac{1}{16}$ mol for each mol of DIN that is consumed, and vice versa.

The water column is assumed to be always 100% saturated with oxygen due to waves and strong tidal currents. Oxygen solubility in seawater is calculated after Garcia and Gordon (1992).

Phytoplankton

The biological model of phytoplankton growth and exudation is adopted from Schartau et al. (2007), whose equations for physiological acclimations are based on Geider et al. (1996, 1998). Carbon fixation, C^μ, follows the PI-curve from Webb et al. 1972 (Jassby and Platt, 1976). This asymptotic function is characterised by an initial slope, α_{chl}, and an apparent maximum carbon fixation rate, μ_C, (Eq. 2.27). The initial slope is regulated by the intracellular Chl:C ratio, θ^C, where a higher chlorophyll content of the cell raises photosynthetic yield (increases the slope). The maximum carbon fixation rate, μ_C^{max}, is regulated by the metabolic state of the cell, $\mathcal{R}_{phot}$, and an Arrhenius function for temperature dependence, T_{func}, to derive the apparent maximum carbon fixation rate, μ_C. The metabolic state of the cell is assumed to be represented by the intracellular N:C ratio, q. Carbon fixation increases to maximum rates with increasing N:C ratio and decreases with low N:C ratios, e.g. at nitrogen limitation.

$$\mathrm{C}^\mu = \mu_\mathrm{C} \cdot \left(1 - e^{-\frac{\theta^\mathrm{C} \cdot \alpha_{chl} \cdot \mathcal{I}}{\mu_\mathrm{C}}}\right) \tag{2.28}$$

$$\mu_\mathrm{C} = \mu_\mathrm{C}^{max} \cdot \mathcal{R}_{phot} \cdot T_{func} \tag{2.29}$$

$$\mathcal{R}_{phot} = 1 - e^{\sigma_{phot} \cdot (|q_{min} - q| - (q_{min} - q))^2} \tag{2.30}$$

$$T_{func} = e^{A_E\left(\frac{1}{T} - \frac{1}{T_{ref}}\right)} \tag{2.31}$$

Phytoplankton respiration, r_{phy}, is implemented as a temperature dependent background loss of carbon, r_C, with additional metabolic costs, ζ, for nitrogen assimilation, N^μ. The metabolic costs of nitrogen assimilation increase the feedback on the intracellular N:C ratio because the cellular uptake of nitrogen is directly coupled to a loss of carbon.

$$r_{phy} = r_\mathrm{C} \cdot T_{func} + \zeta \cdot \mathrm{N}^\mu \tag{2.32}$$

The assimilation of nitrogen is assumed to follow Michaelis-Menten kinetics, where the maximum

nitrogen uptake rate, V_{C}^{max}, is regulated by the intracellular N:C ratio, $\mathcal{R}_{chl}$. The temperature dependence already occurs in the calculation of μ_{C}. Downregulation of nitrogen uptake only occurs at very high N:C ratios, e.g. when light limitation prevents photosynthesis and intracellular energetic carbon compounds are depleted.

$$\mathrm{N}^{\mu} = V_{\mathrm{C}}^{max} \cdot \frac{DIN}{DIN + K_{\mathrm{N}}} \tag{2.33}$$

$$V_{\mathrm{C}}^{max} = V_{fact} \cdot \mu_{\mathrm{C}} \cdot q_{max} \cdot \mathcal{R}_{\mathrm{C}}^{\mathrm{N}} \tag{2.34}$$

$$\mathcal{R}_{\mathrm{C}}^{\mathrm{N}} = 1 - e^{\sigma_{\mathrm{C}}^{\mathrm{N}} \cdot (|q - q_{max}| - (q - q_{max}))^2} \tag{2.35}$$

Synthesis of chlorophyll, S^{chl}, is directly coupled to the assimilation of nitrogen in the model. The linear slope of the relationship between chlorophyll synthesis and nitrogen assimilation increases at low light conditions and allows for variable Chl:C and Chl:N ratios.

$$S^{chl} = \frac{\mathrm{N}^{\mu}}{\theta^{\mathrm{C}}} \cdot \mathcal{R}_{chl} \tag{2.36}$$

$$\mathcal{R}_{chl} = min\left[\theta_{max}^{\mathrm{N}}, \theta_{max}^{\mathrm{N}}\left(\frac{\mathrm{C}^{\mu}}{\theta^{\mathrm{C}} \cdot \alpha_{chl} \cdot \mathcal{I}}\right)\right] \tag{2.37}$$

Zooplankton

Zooplankton grazing, gr, is implemented as a sigmoid Holling type 3 function (Gentleman et al., 2003). Phytoplankton carbon and nitrogen are removed by grazing and fuel zooplankton biomass. Besides respiration, r_{zoo}, heterotrophs lose biomass quadratically proportional to their standing stock to simulate predation of higher trophic levels like fish. Lost zooplankton biomass enters the detritus pool (see appendix).

$$gr = g_{max} \cdot \frac{Phy\mathrm{N}^2}{\epsilon^2 + Phy\mathrm{N}^2} \tag{2.38}$$

$$\tag{2.39}$$

Detritus

Phytoplankton cells enter the detritus pool via aggregation. Aggregation, agg, is regarded as the product of phytoplankton biomass, detritus and an aggregation parameter, Φ_P. Detritus sinks out of the water column assuming a constant sinking velocity, v_{det}.

$$agg = \Phi_P \cdot Phy\mathrm{N} \cdot Det\mathrm{N} \tag{2.40}$$

Extracellular organic matter

Remineralization of detritus in the water column is divided into two steps. First, detritus is broken up into dissolved or extracellular organic carbon and nitrogen, EOC and EON, and second, the more labile EOC and EON is remineralized into dissolved inorganic carbon and nitrogen, DIC and

DIN. Both degradation processes are assumed to be linearly proportional to their substrates with a temperature dependent degradation rate. Excretion of labile components by phytoplankton also produces EOC and EON, whereas, a part of EOC is assumed to form transparent exopolymeric particles, TEP, that cannot be remineralized as fast as the labile EOC and sink out of the water column (Schartau et al., 2007).

Benthos

Sinking detritus that is not remineralized during the passage through the water column accumulates in the benthic layer, $Ben\mathrm{N}$ and $Ben\mathrm{C}$. Remineralization of dead organic material in the benthic layer is divided into the oxygen-dependent aerobic remineralization, $\mathcal{OXIC}$, and the oxygen-independent fermentation, $\mathcal{ANOX}$. The anaerobic remineralization is assumed to be linearly proportional to the amount of benthic detritus with a temperature dependent remineralization rate. The aerobic remineralization rate is also temperature dependent but faster than anaerobic degradation. The parameter p_{ox} determines the proportionate contribution of the two remineralization processes to total benthic remineralization, ω_{ben}. The aerobic remineralization of carbon is assumed to consume oxygen at a molar ratio of 1 and is limited by the supply of oxygen to the porewaters due to porewater mixing. Remineralization of benthic organic nitrogen is treated equally to carbon, except in case of oxygen limitation where the aerobic remineralization rate of nitrogen is multiplied by a regulation factor, $\mathcal{R}_{rem}$. Benthic remineralization release DIN and DIC to the porewater.

$$\mathcal{ANOX}^{Ben\mathrm{C}} = \omega_{ben\mathrm{C}}(T) \cdot (1 - p_{ox}) \cdot Ben\mathrm{C} \tag{2.41}$$

$$\mathcal{OXIC}^{Ben\mathrm{C}} = min\left[\, \omega_{ben\mathrm{C}}(T) \cdot p_{ox} \cdot Ben\mathrm{C}, BenO_2 \,\right] \tag{2.42}$$

$$\mathcal{ANOX}^{Ben\mathrm{N}} = \omega_{ben\mathrm{N}}(T) \cdot (1 - p_{ox}) \cdot Ben\mathrm{N} \tag{2.43}$$

$$\mathcal{OXIC}^{Ben\mathrm{N}} = \mathcal{R}_{rem} \cdot \omega_{ben\mathrm{N}}(T) \cdot p_{ox} \cdot Ben\mathrm{N} \tag{2.44}$$

$$\mathcal{R}_{rem} = \frac{min\left[\, \omega_{ben\mathrm{C}}(T) \cdot p_{ox} \cdot Ben\mathrm{C}, BenO_2 \,\right]}{\omega_{ben\mathrm{C}}(T) \cdot p_{ox} \cdot Ben\mathrm{C}} \tag{2.45}$$

Porewater

A constant amount of water per time exchanges between the porewater and the water column, mr. This exchange provides new oxygen to the benthic layer and transports DIN and DIC either into or out of the sediments, depending on the concentration gradient. To account for different porosities of NS and SRB sediments, different mixing rates are assumed for both boxes (Eqs. 2.16-2.19).

Microphytobenthos

Even at very shallow water depths, shading by phytoplankton and suspended sediments may cause very low irradiance levels at the seafloor. Benthic algae are known to be highly adapted to low-light conditions. When exposed to light, microbenthic algae immediately start to photosynthesize and hardly show any signs of photoinhibition at high irradiance levels (Hedtkamp pers. comm.). In the model, microphytobenthos represents a second group of primary producers and a competitor for nutrients to the phytoplankton. Photosynthetic carbon fixation of microphytobenthos, C^{μ}_{mic}, is assumed to increase linearly with irradiance levels at the seafloor, $\mathcal{I}_{mic}$. The extremely efficient light-harvesting mechanism is simulated by assuming a higher value for the linear slope, α_{mic}, than for phytoplankton. Assimilation of nutrients, respiration, chlorophyll synthesis and metabolic regulations are parameterized in the same way as already described for phytoplankton, whereas microphytobenthos is assumed to use DIN and DIC from the porewater and not from the water column.

$$\mathrm{C}^{\mu}_{mic} = \alpha_{mic} \cdot \mathcal{I}_{mic} \tag{2.46}$$

Mixotrophy of benthic diatoms (Nixdorf et al., 2001) is not considered in the model.

Macrozoobenthos

Many different macrozoobenthic species exist in the SRB that feed on phytoplankton, microphytobenthos or detritus and produce large amounts of biomass (Baird et al., 2004). In the model, a set of state variables is added for macrozoobenthos in order to delay the resupply of nutrients from the sediments to the water column. Macrozoobenthos feeds on microphytobenthos and builds up biomass. A temperature dependent mortality is assumed that transferres macrozoobenthos biomass into benthic detritus when temperature decreases in winter. Please note that macrozoobenthos does not feed on benthic detritus in our model although detritus is known to be an important food source for most macrozoobenthic organisms in nature. Macrozoobenthos, calculated in the model, is only needed to control microphytobenthos biomass and is assumed to represent benthic herbivores such as *Hydrobia ulvae*. Macrozoobenthos grazing is assumed to increase linearly with microphytobenthos and macrozoobenthos biomass. The slope of this increase is the grazing rate, g_{mic}. Very cold temperatures may cause increased mortality of macrobenthic organisms. The mortality of macrozoobenthos, M_{mac}, is assumed to increase strongly at temperatures lower than a reference temperature, T_m (Eq. 2.48). Filterfeeding organisms like bivalves and polychaetes are summarized as filterfeeders and described below.

$$gr_{mic} = g_{mic} \cdot Mic\mathrm{N} \cdot Macro\mathrm{N} \tag{2.47}$$

$$M_{mac} = \left(1 + max\left[0, \left(\frac{T_m - T_{srb}}{scale}\right)\right]^2\right) \cdot mort \tag{2.48}$$

Filterfeeders

The biomass of macrozoobenthic filterfeeders in the SRB is not calculated as a state variable of its own. The influence of filterfeeders on the ecosystem is implemented as a sink of particulate organic matter and a source of dissolved inorganic nutrients to the water column. The removal of particulate organic carbon, POC, from the water column by mussel beds and *Arenicola* flats in the bight has been determined by Asmus and Asmus (1998*b*). In the model, this uptake of POC is represented as a constant need for nutrition of these communities, FC_{max}. POC and PON are calculated as the sum of phytoplankton and detritus carbon and nitrogen. The POC and PON removed from the water column is immediately converted into DIC and DIN to represent respiration and excretion of filterfeeders and to close the budgets.

As mussels are known to adapt their filtration rates to ambient POC concentrations (Winter, 1973), the clearance rate, χ_{srb}, is calculated by dividing the POC demand of the filterfeeders, FC, by POC concentrations. With the clearance of a defined volume of water also phytoplankton nitrogen and detritus nitrogen are removed from the water column. As mussels are also able to reduce their filtration rate at very low POC concentrations (e.g. in winter) a Holling type 2 function is assumed to reduce carbon uptake and thus filtration at very low POC concentrations (Eq. 2.49). The degree of the reduction is given by a half saturation constant, K_h. The effect of filterfeeders is only implemented in the SRB and not in the NS. Temperature dependence of feeding activity is not considered.

$$FC = \frac{FC_{max} \cdot POC_{srb}}{K_h + POC_{srb}} \tag{2.49}$$

$$POC_{srb} = Phy\mathrm{C}_{srb} + Det\mathrm{C}_{srb} \tag{2.50}$$

$$\chi_{srb} = \frac{FC}{POC_{srb} \cdot V_{srb}} \tag{2.51}$$

2.2.4 Model runs

In a standard model run, the model is integrated for a total of seven years. Three years are spinup phase, using climatological forcing. The latter four years are considered for analysis and are forced by data of the years 2000 to 2003, if available. If no forcing data is available for one of the years, climatological forcing is applied.

Salinity model

The forcing of the salinity model is given by data of freshwater input into the SRB (Claussen, pers. comm.) and freshwater discharge of the rivers Weser and Elbe (Pätsch and Lenhart, 2004). As no forcing data of freshwater discharge into the SRB is available in the year 2003, a climatology is used for 2003 that has been calculated from the data of 2000 to 2002. Several runs are performed with the salinity model processing a threedimensional matrix of the unknown model parameters. The exchange efficiency, p_{ex}, is varied from 0.001 to 0.15, the salinity in the outer North Sea, S_{NS}, is varied from 31.1 to 37.0, and the exchange volume with the outer North Sea, V_{NS}^{ex}, is varied from $4 \cdot 10^8$ to $1.2 \cdot 10^{10}$ m^3 d^{-1}. Salinity concentrations of each model run are compared to salinity data of the years 2000 to 2003, both, in the NS and the SRB and the sum of the deviations squared is calculated to determine the optimal set of model parameters to explain the data.

Ecosystem model

The ecosystem model is forced by data of riverine nitrogen discharge (Claussen, pers. comm., Pätsch and Lenhart, 2004) as described for the salinity model. The annual cycle for daylength, maximum irradiance at noon, and inclination angle, is given by astronomical equations (Brock, 1981; Reed, 1977; Cooper, 1969; Milankovitch, 1930). The daily light cycle for surface irradiance, $\mathcal{I}_{surf}$ is calculated using the maximum irradiance at noon and the daylength for the particular day of the year. Water itself, chlorophyll and suspended particulate matter, SPM, cause extinction of light while it passes through the water column (Baker and Smith, 1982). The effect of SPM concentrations on light conditions is only implemented in the SRB and omitted in the NS box. Chlorophyll concentrations in the water column are calculated by the model, SPM concentrations in the bight are taken from measured data. The first three years are forced with a climatological cycle of SPM concentrations, the latter four years are forced by data of the years 2000 to 2003.

The average photosynthetic available radiation, $\mathcal{I}$, is given by the integral of irradiance over water depth. The extinction coefficient is assumed to depend linearly on SPM and chlorophyll concentrations in the water column with a constant extinction coefficient, κ_{spm}.

$$\mathcal{I} = \frac{-\mathcal{I}_{surf}}{\frac{\kappa \cdot z}{\beta}} \cdot \left(e^{\frac{\kappa \cdot z}{\beta}} - 1 \right) \tag{2.52}$$

$$\kappa = \kappa_w + \kappa_{chl} \cdot CHL + \kappa_{spm} \cdot SPM \tag{2.53}$$

Temperature data of the SRB and the NS are used as external forcing and influence metabolic rates. Salinity only influences air-sea gas-exchange of CO_2 and O_2. Salinity concentrations in the

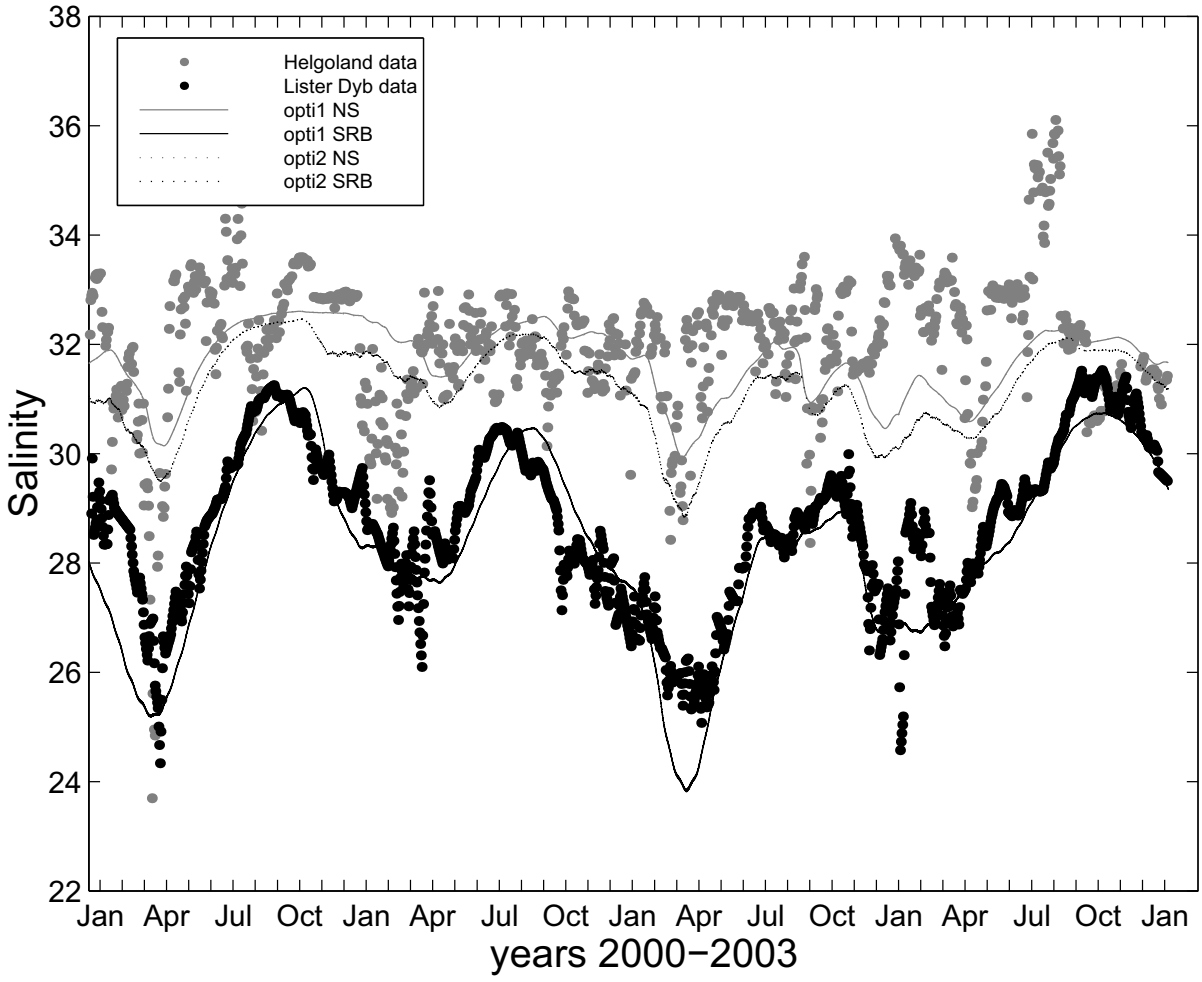

Figure 2.3: *Salinity model. Salinity data of the NS (grey) and the SRB (black) are shown as dots. The solid line (opti1) represents the optimized model solution to the data. The dotted line (opti2) shows an optimized model solution with fixed exchange efficiency ($p_{ex} = 0.1$).*

ecosystem model are kept constant at mean values that were calculated from the data, 28.7 in the SRB and 32.7 in the NS.

Parameter values of the standard model run are compiled in Tables 2.1 and 2.2.

2.3 Results

2.3.1 Salinity model

The optimization of the salinity model to measured salinity data results in an exchange efficiency of the tidal prism of 1.3%, a salinity of the outer North Sea box of 33.3, and a constant exchange of the North Sea box with the outer NS of $2 \cdot 10^9$ m^3 d^{-1} (Tab. 2.1). The salinity pattern produced with the optimized model parameters shows good agreement with measured data, in particular in the SRB (Fig. 2.3). In autumn and winter when precipitation over the continent increases, freshwater

Table 2.2: Table of model parameters.

Symbol	Value and Unit	Description
α_{chl}	0.21 mmol C m^2 (mg Chl W d)$^{-1}$	initial slope P-$\mathcal{I}$-curve
μ_{C}	13.0 d^{-1}	maximum photosynthetic rate
σ_{phot}	50 (mmol N)^2 (mmol C)$^{-2}$	regulation slope for photosynthesis
q_{min}	0.05	minimum N:C ratio
A_E	4500.0 K	slope for Arrhenius function
$Tref$	288.15 K	reference temperature
r_{C}	0.025 d^{-1}	background respiration rate phytoplankton
ζ	2.0 mmol C (mmol N)$^{-1}$	biosynthetic costs chlorophyll production
K_{N}	1.0 mmol N m^{-3}	half saturation constant nitrogen uptake
V_{fact}	0.5	scaling factor nitrogen uptake
q_{max}	0.20	maximum N:C ratio
$\sigma_{\mathrm{C}}^{\mathrm{N}}$	1000 (mmol N)^2 (mmol C)$^{-2}$	regulation slope nitrogen assimilation
$\theta_{\mathrm{N}}^{max}$	6.00	maximum Chl:N ratio
g_{max}	0.35 d^{-1}	maximum grazing rate
ϵ	0.95 mmol N m^{-3}	half saturation constant of grazing
FC_{max}	$2.4 \cdot 10^9$ mmol C d^{-1}	maximum POC uptake of filterfeeders
K_h	64.0 mmol C m^{-3}	half saturation constant filterfeeder grazing
$\omega_{ben\mathrm{C}}$	0.07 d^{-1}	benthic remineralization rate C
$\omega_{ben\mathrm{N}}$	0.07 d^{-1}	benthic remineralization rate N
p_{ox}	0.96	percentage oxic remineralization
mr_{ns}	0.22 m d^{-1}	porewater mixing rate NS
mr_{srb}	0.13 m d^{-1}	porewater mixing rate SRB
ρ_{C}	0.07 d^{-1}	EOC remineralization rate
ρ_{N}	0.07 d^{-1}	EON remineralization rate
f_{TEP}	0.495	TEP fraction of EOC
x	0.015	fraction of free floating TEP
r_{zoo}	0.02 d^{-1}	zooplankton respiration rate
γ_{C}	0.25 d^{-1}	excretion rate of EOC
γ_{N}	0.2 d^{-1}	excretion rate of EON
γ_{Chl}	0.35 d^{-1}	degradation rate of chlorophyll
Φ_P	0.05 (mmol N d)$^{-1}$	aggregation parameter
γ_{zoo}	0.3 m^3 (mmol N d)$^{-1}$	mortality rate of zooplankton
ω_{C}	0.07 d^{-1}	detritus remineralization rate C
ω_{N}	0.07 d^{-1}	detritus remineralization rate N
v_{det}	0.9 m d^{-1}	detritus sinking velocity
κ_w	0.04 m^{-1}	attenuation coefficient water
κ_{Chl}	0.064 m^2 (mg Chl)$^{-1}$	attenuation coefficient chlorophyll
κ_{SPM}	0.17 m^2 (g SPM)$^{-1}$	attenuation coefficient SPM
α_{mic}	1.8	initial slope P-$\mathcal{I}$-curve
μ_{mic}^{C}	100.0	maximum photosynthetic rate
$height$	1.3	adjusting sea level height
g_{mic}	0.5	maximum grazing rate

enters the SRB and the NS as riverine runoff and the salinity concentrations in the SRB and the NS decrease. In the dry season of the year salinity increases again. In the NS, the model produces a relatively weak seasonal signal. The dataset from Helgoland Reede shows much stronger variability

in salinity concentrations. The weaker signal in the North Sea box is a consequence of the assumption of instantaneous mixing within each box.

The exchange efficiency of the tidal prism is a crucial parameter in the model and as the modelled North Sea salinity does not match the data too well (see Fig. 2.3), a second optimization of the exchange efficiency is performed. In this optimization, North Sea salinity is prescribed using the Helgoland Reede dataset and the exchange efficiency is the only unknown parameter. The second optimization also results in an exchange efficiency of the tidal prism of 1.3%.

This exchange efficency of 1.3% appears to contradict the 8 to 12 % assumed by Fast et al. (1999) and the modelled mixing rates reported by Dick and Schönfeld (1996) for the North Frisian Wadden Sea just below the Sylt-Rømø Bight. However, an exchange efficiency of about 10% does not reproduce the salinity concentrations in the bight in our model. Figure 2.3 also shows the best fit of the salinity model with a fixed exchange efficiency of 10% (opti2). In this optimization, only the salinity of the outer NS and the exchange with the outer NS are varied. The salinity of the outer NS as well as the exchange volume with the outer NS result in the same parameter values as for the optimization with an exchange efficiency of 1.3%. The modelled North Sea salinity shows the same signal in both model runs.

2.3.2 Reference run

The reference run of the ecosystem model shows good reproduction of chlorophyll and DIN concentrations in the SRB. Especially the modelled DIN concentrations match the observed data in the bight very well. In the NS, the time development of the annual cycle slightly deviates from the observed pattern while the amplitude is in good agreement with the data (Fig. 2.4).

Winter DIN concentrations in the SRB reach maximum values between 40 and 72 $\mathrm{mmol\ m^{-3}}$. In summer, modelled DIN concentrations are depleted to almost zero. The drawdown of DIN occurs at the end of March at the same time as chlorophyll concentrations begin to rise, to form the spring bloom. The timing of the modelled spring bloom in the SRB is in good agreement with the data and appears at about the beginning of april. Maximum chlorophyll concentrations in the model are lower than in the data and reach only 20 $\mathrm{mg\ Chl\ m^{-3}}$. Besides underestimating the phytoplankton bloom, the model seems to overestimate phytoplankton concentrations in summer. In winter, chlorophyll concentrations are almost zero, although small amounts of chlorophyll can be found in the data. The observed winter chlorophyll concentrations will most probably be caused by resuspended algae.

In the North Sea, maximum winter concentrations of DIN do not exceed 50 $\mathrm{mmol\ m^{-3}}$. Depletion of DIN occurs too early in the model compared to the data. In summer, DIN is depleted to almost zero which is not observed in the data. The rise of DIN concentrations in the NS is well represented in autumn. A destinctive feature of the DIN signal in the NS is a pronounced increase of DIN that occurs at the end of winter and starts about the end of february to march.

In a model run with p_{ex} = 10%, the tracer concentrations of the ecosystem model do not show the observed patterns (data not shown). The transport of DIN from the NS into the bight leads to very pronounced phytoplankton growth in the bight and thus very high chlorophyll concentrations in summer and autumn. Winter concentrations of DIN never reach measured maximum values because the high nutrient loads of the two small rivers Vidå and Brede Å are washed out of the bight relatively fast, due to the strong exchange with the NS. We suppose the exchange efficiency of 8-12% of the tidal prism assumed by Fast et al. (1999) appears to be much too high for the physical setup used in this model.

The biogeochemistry of the SRB shows a strong interannual variability. Modelled winter DIN concentrations at the beginning of the year 2000 show strong deviations from the measured signal

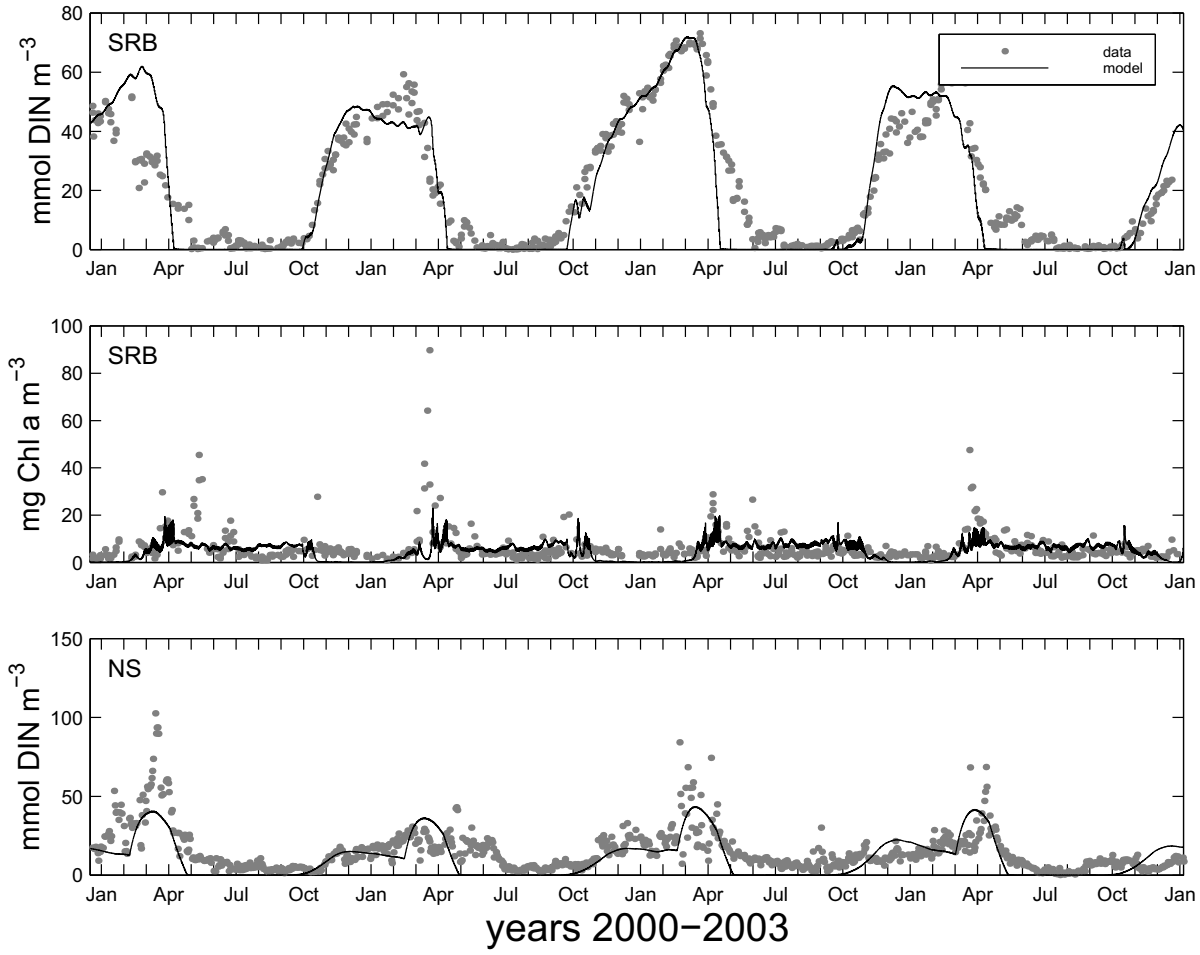

Figure 2.4: *Reference run. The model solution for a refence parameter set is shown together with measured data. The upper two graphs show DIN and chlorophyll concentrations in the SRB. The lower graph shows DIN concentrations in the NS.*

that are caused by the model spinup. During the first year of the model run the model approximates the measured DIN concentrations in the SRB. In the following years the maximum DIN concentrations reach 48, 72 and 55 $mmol\ m^{-3}$, respectively. The variation of winter DIN concentrations in the SRB is mainly caused by differences in riverine nutrient input. Slight deviations from DIN signals in winter are caused by using monthly averages for riverine runoff in the model and no daily measurements. Plankton concentrations do not seem to vary too intensively in the model. The interannual variability in plankton abundances is mainly caused by differences in SPM concentrations and temperatures and is also influenced by the ambient nutrient concentrations. The effect of different weather conditions such as cloudiness is not regarded in the model.

To understand what exactly causes the observed patterns in the model one has to analyse all state variables and the connecting fluxes. The time development of all state variables is shown in Figure 2.5.

In winter, light limitation diminishes phytoplankton growth rates despite very high DIN concentrations. When SPM concentrations decrease in spring and light conditions improve, phytoplankton

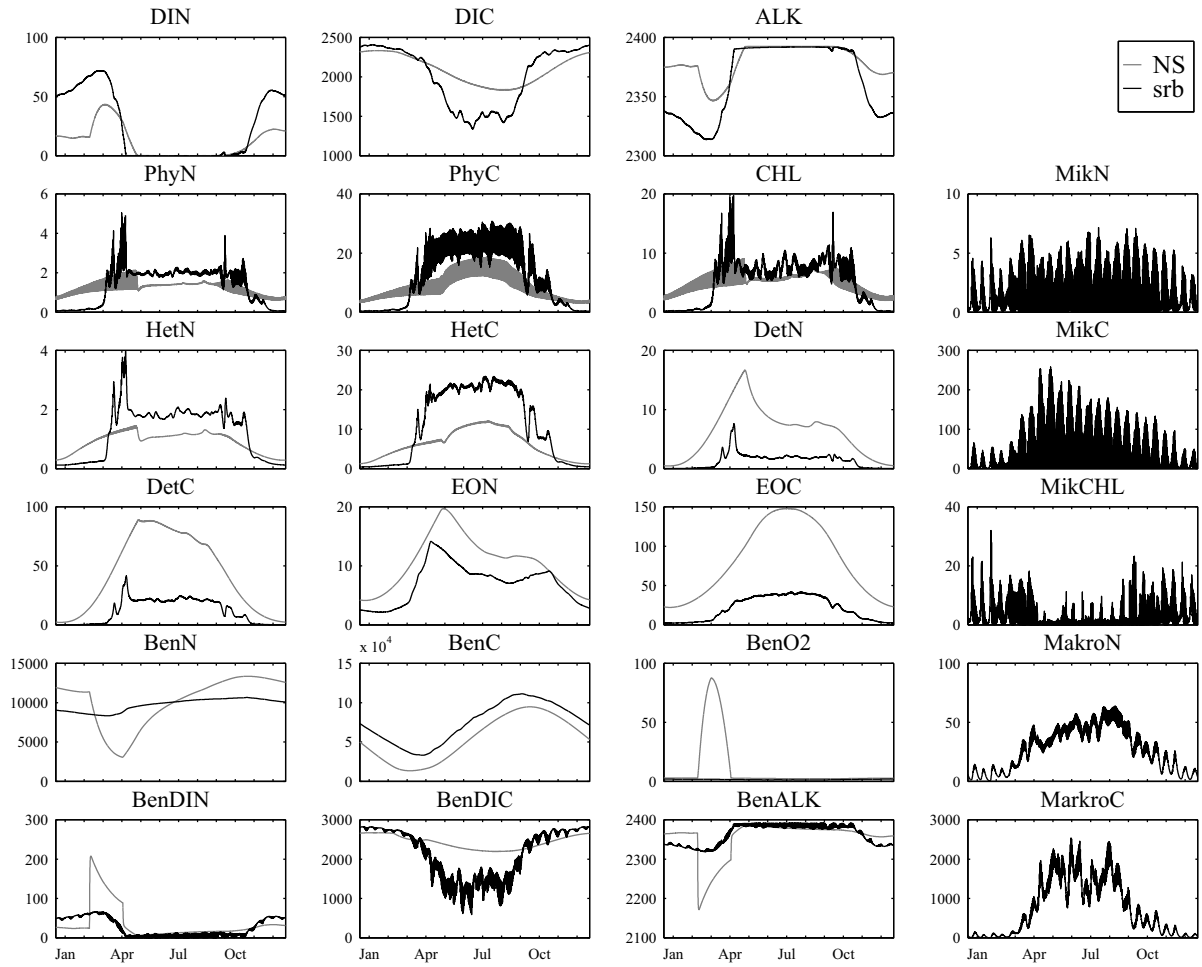

Figure 2.5: *Time development of all state variables for the year 2002. NS is coloured grey, SRB black. All concentrations in* $\mathrm{mmol\ m^{-3}}$*, except chlorophyll concentrations in* $\mathrm{mg\ m^{-3}}$.

begins to grow and a bloom develops. Phytoplankton growth depletes DIN and the bloom ends when DIN is depleted. Phytoplankton biomass decreases when zooplankton grazing and aggregation exceed phytoplankton growth rates. In summer, primary production shows highest rates (not shown) despite relatively low chlorophyll concentrations and growth is limited by the resupply of nutrients due to remineralization processes (Fig. 2.8). In autumn, storms raise SPM concentrations, light conditions worsen and phytoplankton growth decreases. At the same time as DIN depletion is reduced in autumn, precipitation elevates the amount of DIN that is imported by riverine runoff and DIN concentrations rise. Remineralization of nutrients that were captured in the benthic system also fuels DIN concentrations in the water column but as DIN concentrations are higher in the water column than in the porewater of the sediments, the net flux of DIN is directed into the sediments in winter (Fig. 2.8). During winter, phytoplankton growth is suppressed by low temperatures and low-light conditions. Mortality of macrozoobenthos increases when the temperature lowers and carbon and nitrogen, that were bound to macrozoobenthos biomass, enter the detritus pool of the benthic layer and are remineralized again.

In the North Sea, DIN depletion and production of phytoplankton biomass is much slower than in

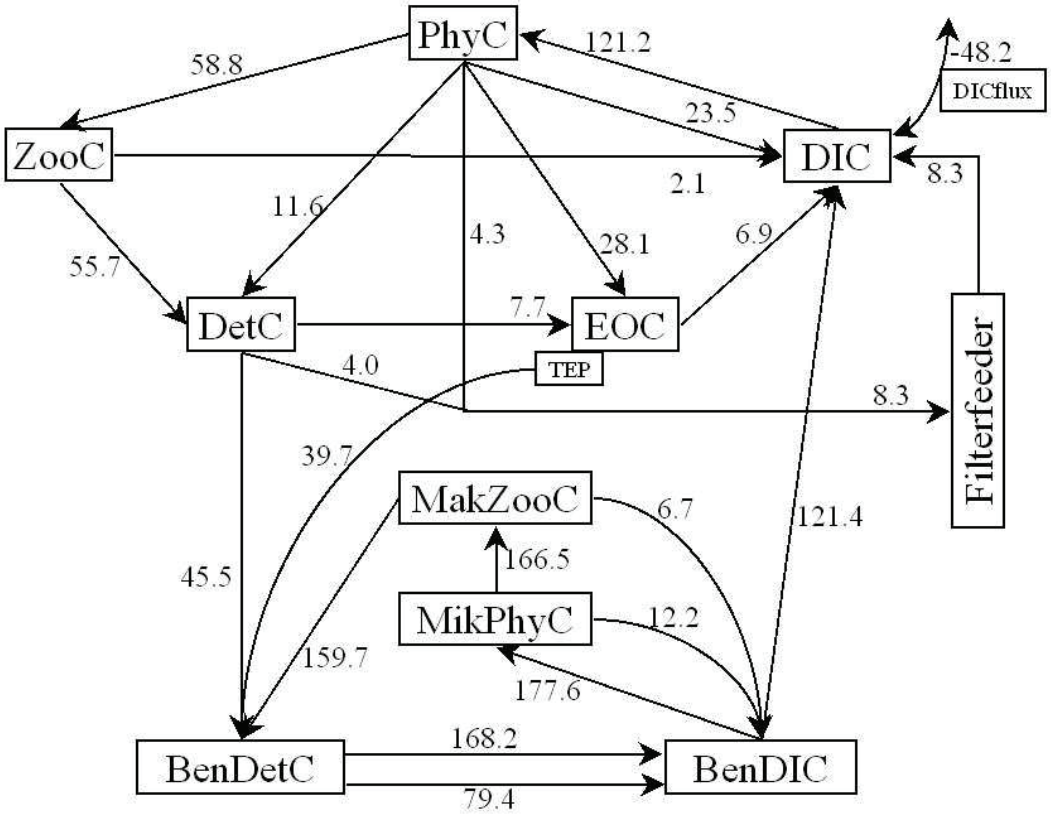

Figure 2.6: *Flux budget. The annual carbon fluxes in the SRB (in* $\mathrm{g\,C\,m^{-2}\,a^{-1}}$*) for the year 2002 are compiled in this graph.*

the SRB which can be explained by the lower average irradiance levels in the deeper NS box, even though the effect of suspended matter on light conditions is ignored in the model. The deeper water column in the NS also causes stronger accumulation of detritus in the water column than in SRB waters. Higher detritus concentrations lead to stronger influence of aggregation on phytoplankton biomass. The main differences between the North Sea and the Sylt-Rømø Bight are therefore a slower increase of phytoplankton biomass and lower maximum phytoplankton concentrations in the NS, as well as higher concentrations of detritus in the water column of the NS. At the end of winter, a pulse of DIN is released from the sediments in the North Sea, that is not produced in the Sylt-Rømø Bight. This pulse occurs after large amounts of benthic detritus have been decomposed and sediments leave anoxic conditions. The oxic remineralization then increases and adds to the anoxic remineralization. The sediments with larger grain sizes and higher porosity in the North Sea show higher resupply of oxygen and faster remineralization of benthic detritus.

A budget of the annual carbon fluxes in the SRB for the year 2002 is compiled in Figure 2.6. Gross primary production of phytoplankton is about 120 $\mathrm{g\,C\,m^{-2}\,a^{-1}}$, net primary production is about 100 $\mathrm{g\,C\,m^{-2}\,a^{-1}}$, due to phytoplankton respiration of about 20 $\mathrm{g\,C\,m^{-2}\,a^{-1}}$. Net primary production of microphytobenthos is about 165 $\mathrm{g\,C\,m^{-2}\,a^{-1}}$. The flux budget further indicates a net outgassing of CO_2 to the atmosphere of about 50 $\mathrm{g\,C\,m^{-2}\,a^{-1}}$ in the SRB. The annual flux budget

Table 2.3: Transport budgets of carbon and nitrogen between the North Sea and the Sylt-Rømø-Bight. The values are related to the area of the bight and show export minus import. A negative sign therefore describes a flux into the bight, whereas a positive value stands for an export out of the SRB into the NS.

Transport fluxes of carbon in [$\mathrm{g\ m^{-2}\ a^{-1}}$]				
for the year	2000	2001	2002	2003
DIC	-15.8	-58.4	-12.7	-56.5
PhyC	0.4	0.5	0.6	0.8
ZooC	0.6	0.6	0.8	0.9
DetC	-5.3	-5.2	-5.2	-5.1
EOC	-9.6	-9.7	-9.7	-9.5
Transport fluxes of nitrogen in [$\mathrm{mmol\ m^{-2}\ a^{-1}}$]				
for the year	2000	2001	2002	2003
DIN	154.3	133.2	173.5	69.0
PhyN	-0.3	0.2	1.3	2.5
ZooN	2.5	2.7	4.3	4.6
DetN	-64.2	-63.7	-65.1	-64.9
EON	-50.2	-46.0	-47.3	-42.1

in the SRB (Fig. 2.6) is not closed. Deviations in the budget are caused by the tidal transport that connects the SRB with the NS. The transport budget between the North Sea and the Sylt-Rømø Bight for carbon and nitrogen shows strong interannual variability (Tab. 2.3). In general, the SRB is a source of dissolved inorganic nitrogen to the NS. On average more than 100 $\mathrm{mmol\ DIN\ m^{-2}\ a^{-1}}$ is exported into the NS. High nutrient concentrations and irradiance levels in the bight support high productivity. Phytoplankton and zooplankton concentrations during the productive phase of the year are usually higher in the SRB than in the NS (Fig. 2.5) and cause a net export of live biomass into the NS. Concentrations of detritus and extracellular organic matter are higher in the NS than in the SRB due to the deeper water column. This concentration gradient leads to a steady import of detritus and extracellular organic matter into the bight. More dead organic material is imported into the bight than is exported as live biomass. The modelled carbon import is much lower than the proposed 100 $\mathrm{g\ C\ m^{-2}\ a^{-1}}$ (van Beusekom et al., 1999). The underestimation of the modelled carbon import into the bight may be caused by the low exchange efficiency of 1.3%, that is a result of the optimization of the salinity model. The excess nitrogen, that is imported into the bight, is released to the NS as DIN, together with the riverine nutrient input that is not converted into biomass. The excess carbon is released to the atmosphere (Fig. 2.6). Additionally to the import of organically bound carbon, inorganically dissolved carbon is imported into the bight, too. This import is mainly induced in summer when the concentration gradient of DIC leads to an import of DIC into the bight.

In the year 2000, phytoplankton carbon is exported into the NS whereas phytoplankton nitrogen

is imported into the bight. This can be explained by the decoupling of carbon and nitrogen pools in phytoplankton biomass. In the SRB, the phytoplankton C:N ratio changes between 5 in winter and 14 in summer, due to irradiance levels and nutrient availability. In the NS, the C:N ratios in phytoplankton range between 5 in winter and 8.5 in summer. The switching of the concentration gradient determines the sign of the transport flux and affects the net annual transport flux that can be observed in the model. With this timing also the C:N ratio of the annual flux changes.

2.3.3 Impact of filterfeeders

In order to analyse the influence of benthic filterfeeders on primary production in the SRB, the amount of maximum particulate organic carbon uptake of the filterfeeders, FC_{max}, was changed from 0.5 to 25 times the standard value (see Tab. 2.2). A plot of modelled primary production in the SRB over POC uptake results in an optimum curve (Fig. 2.7). On the left side of the maximum, increasing POC uptake of filterfeeders enhances primary production. On the right side of the maximum, the limiting effect of filterfeeders on primary production increases with increasing POC uptake and exceeds the supporting effect.

If the filterfeeders consume too much phytoplankton biomass, they deprive themselves of their own food ressource, if they consume too little, the system is not working efficiently. Only at the optimum POC uptake rate of the filterfeeders, growth of their own food source, i.e. primary production, is maximized. This reminds of the principle of maximum sustainable yield for the exploitation of a growing resource known from the fisheries biology, that is also applicable to natural communities (Beddington and May, 1977).

2.4 Discussion

2.4.1 Hydrodynamics

For a good reproduction of the annual salinity and DIN signals, the model requires a very low exchange efficiency of 1.3% . This value is much lower than the estimates of Fast et al. (1999) for the SRB and Dick and Schönfeld (1996) for the southern part of the North Frisian Wadden Sea. Such a low exchange efficiency also appears contradictory to the strong influence of the rivers Weser and Elbe on the SRB that was proposed by Hickel (1980). However, model runs with stronger influence of the NS on the bight ($p_{ex} = 8$ to 12%) do not reproduce the observed tracer signals in the SRB, as can be seen in Figure 2.3.

The exchange efficiency is a crucial model parameter, since it strongly affects tracer budgets and the coupling of NS and SRB. The low exchange efficiency obtained from optimizing the modelled salinity signal represents rather low influence of the NS and higher influence of the two small rivers on the tracer signals in the bight. The discrepancy between the low exchange efficiency of 1.3% and the results by Dick and Schönfeld (1996) and Fast et al. (1999) can be explained by assuming homogeneously mixed boxes in our model. Homogeneity implies that the annual runoff signal is instantaneously mixed within the waterboxes, leading to a relatively weak seasonal variability in salinity and DIN in the NS and strong variability in the small SRB. It is very likely that in reality the North Sea water in front of the Lister Dyb is affected much more strongly by riverine runoff, especially by the freshwater input from Elbe and Weser, than the average North Sea (Hickel, 1980). Less salty seawater between the Sylt-Rømø bight and the open North Sea would lead to a higher estimate of the exchange efficiency of the tidal prism to close the salt balance of the SRB. In principle this could be modelled by introducing a third model box that represents the North Sea along the North

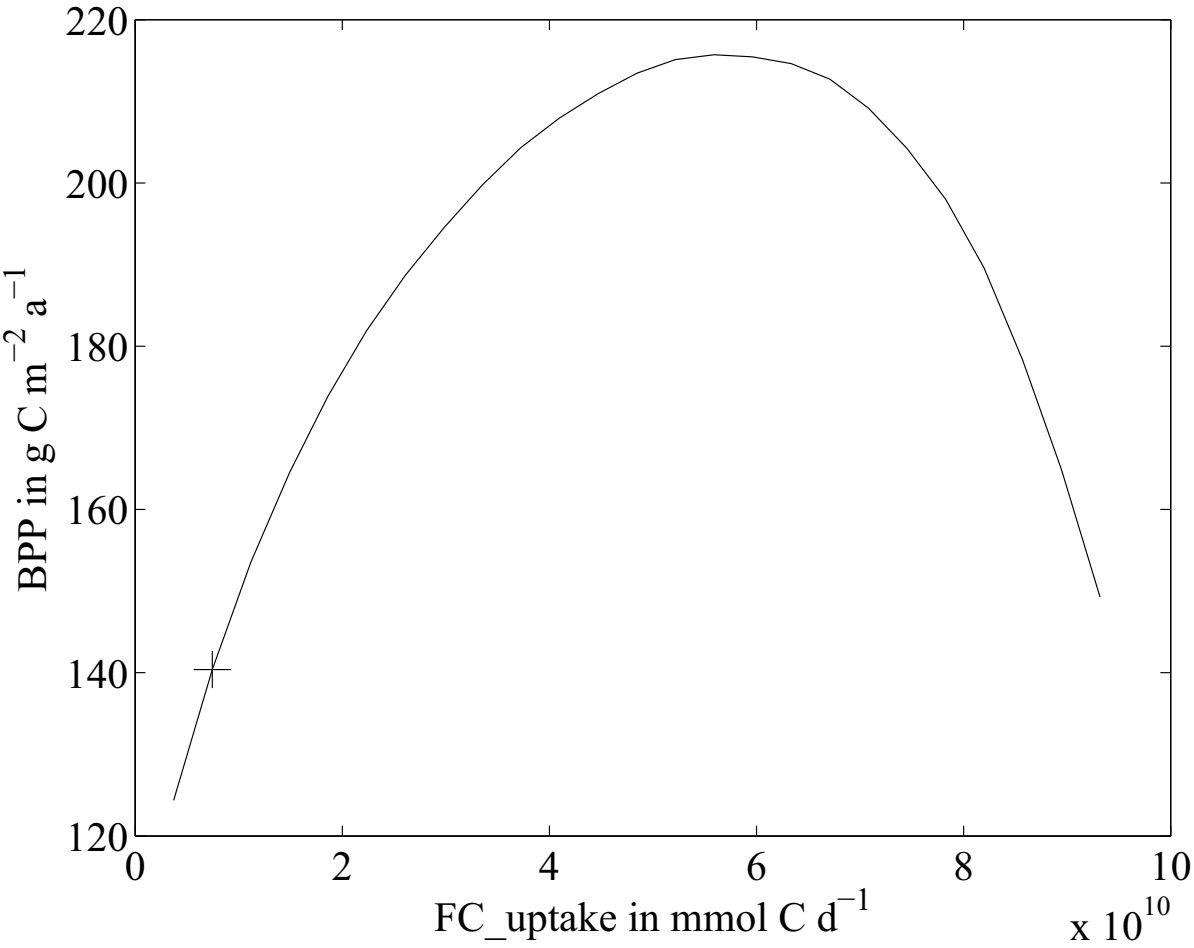

Figure 2.7: *Annual primary production, BPP, against carbon uptake of filterfeeders, FC. The cross marks the present situation (Asmus and Asmus, 1998a).*

Frisian coast. However, this would require measured salinity and nutrient data within this box at a sufficiently high temporal resolution to constrain the exchange rates.

We would consider our low exchange efficiency of 1.3% as an estimate of the exchange with the average North Sea, as represented by the salinity and nutrient signal at Helgoland, rather than as a true exchange efficiency across the Lister Dyb, which may be higher. A higher exchange efficiency, together with a stronger influence of Elbe water (with its high winter DIN concentrations) on the watermass outside the SRB, may in principle explain the observed DIN peak inside the SRB (Hickel, 1980). However, while the absolute amount of water entering the SRB directly from inland is rather small, the DIN concentration is quite high, so that it is unlikely that its contribution is completely unimportant.

2.4.2 Riverine runoff

Despite its simplified hydrological setup, the model reproduces the major observed patterns of DIN and chlorophyll in the SRB. The interannual variability in the DIN signal is mainly determined

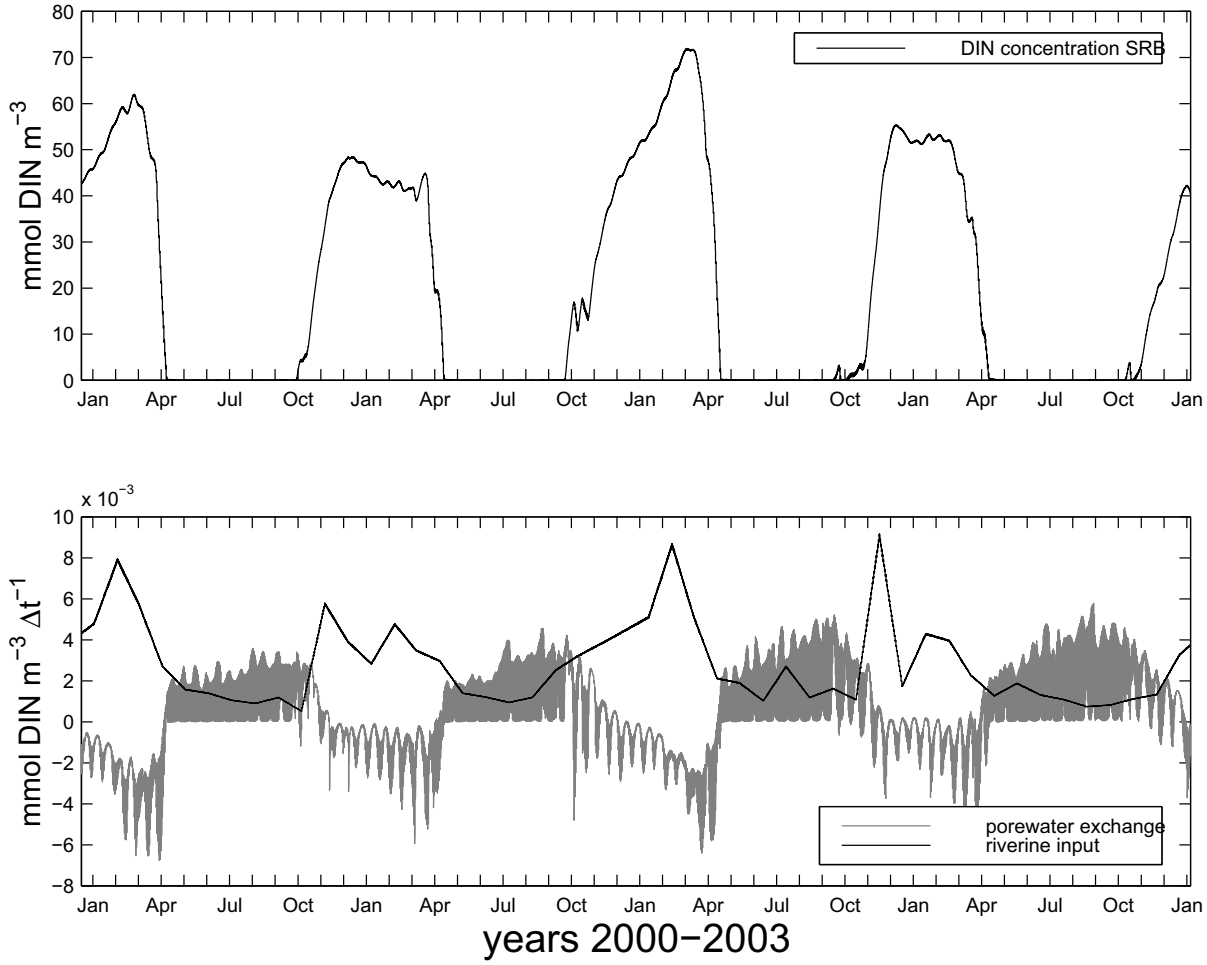

Figure 2.8: *Nutrient sources. The upper panel shows DIN concentrations in the SRB. The lower graph shows the impact of riverine input (black) and porewater exchange (grey) on ambient DIN concentrations in the bight. ($\Delta t = 6min$)*

by differences in nitrogen discharge due to riverine runoff (Fig. 2.8). Remineralization of benthic detritus is an additional source of nitrogen to the pelagic. However, a comparison of the nitrogen sources from porewater exchange and rivers in the SRB shows that the transport of DIN is directed into the sediments in winter (Fig. 2.8) and the major source of DIN is river discharge. In summer, benthic remineralization resupplies DIN to the pelagic thus maintaining phytoplankton growth. In winter, the major source of DIN to the water column of the SRB is riverine nitrogen discharge. These findings are contradictory to assuming the influence of the two rivers entering the bight to be negligible small (Asmus et al., 1998*a*; Asmus and Asmus, 1998*b*).

Model simulations without riverine nitrogen discharge lack an important source of DIN in the SRB that is needed to achieve high DIN concentrations in winter. Benthic remineralization cannot explain winter DIN concentrations as the porewater exchange of DIN is directed into the sediments in winter (Fig. 2.8). The inclusion of measured data as an external source of nitrogen supplies the amount of nitrogen to reproduce winter DIN concentrations in the bight.

2.4.3 Transport budget

The modelled carbon and nitrogen budgets (Tab. 2.3) agree with the notion that the SRB is a net heterotrophic system. The heterotrophy can be explained by differences in the water depths between both regarded systems. Detritus produced in the water column sinks down and accumulates in the sediments. In the shallow water of the SRB, detritus is removed relatively fast. In the NS, the higher sinking distance leads to a longer residence time of detritus in the pelagic and thus to higher detritus concentrations. The concentration gradient between SRB and NS causes a continuous import of detritus into the bight and thus an accumulation of detritus in the benthic layer of the SRB. The high productivity rates in the SRB and the export of living biomass into the NS do not balance the import of detritus carbon and nitrogen. The excess carbon is released to the atmosphere and the excess nitrogen is exported to the NS as DIN.

Postma (1981) proposed the asymmetry of the tidal currents to cause the trapping of particles in the sediments of the Wadden Sea, the scour effect. This study shows that differences in the topography alone, i.e. water depth, and a constant sinking velocity of detritus already leads to the trapping of detritus in the sediments of the Wadden Sea. Both effects together may have caused the development of a net heterotrophy in the Wadden Sea.

The decoupling of carbon and nitrogen fluxes in the model leads to an interesting response in the transport fluxes between the NS and the SRB. The budget for phytoplankton biomass in the year 2000 shows an import of phytoplankton nitrogen and an export of phytoplankton carbon (Tab. 2.3). This can be explained by the varying carbon to nitrogen ratio in phytoplankton, that depends on the growth situation. Table 2.3 shows net transport fluxes over the whole year and the direction of the transport flux differs in different times of the year as it depends on the direction of the concentration gradient. In summer the C:N ratio of phytoplankton biomass in the Sylt-Rømø-Bight is as high as 14 and much more carbon is exported with respect to nitrogen. In the darker season of the year where DIN concentrations are high, the C:N ratio lowers to about 5. The timing of this shift differs between the shallow bight and the profound North Sea and the period with this difference determines the C:N ratio and also the sign of the budget.

2.4.4 Bentho-pelagic coupling

The shallower the water column, the more important becomes the bentho-pelagic coupling (Heip et al., 1995). The benthic compartment acts as a second loop of the elemental cycles that removes nutrients from the pelagic during the growth season and releases them in winter when pelagic production is low due to light limitation.

Microphytobenthos is assumed to take up nutrients from the porewater and thus decreases the resupply of nutrients to the water column. Microphytobenthos as a competitor for nutrients causes a lack of nutrients in the pelagic and prevents strong phytoplankton growth. Without microphytobenthos, chlorophyll concentrations in the water column are much too high during summer and an autumn bloom of phytoplankton can be observed in the model that has no correspondence in field data (not shown). The autumn bloom cannot be prevented by only adding microphytobenthos to the model. When fall storms raise SPM concentrations in the bight light conditions worsen and growth of microphytobenthos decreases. Microphytobenthos biomass is then transferred to benthic detritus which is remineralized again. Irradiance levels in the water column are much higher than at the sediment surface. Therefore, the freshly remineralized nutrients cannot be used by microphytobenthos and an autumn bloom of phytoplankton is formed in the model that can even be markedly higher than

the spring bloom (data not shown). This autumn bloom is prevented by adding a macrozoobenthos compartment to the model that removes microphytobenthos biomass and stores the nutrients in a separate biomass pool. The mortality of macrozoobenthos is assumed to be relatively low throughout the year and to increase when temperatures become very low in winter. The biomass that is built up in the benthic compartment may also be exported out of the system by higher trophic levels like seabirds and fish that are not considered in this model approach. The release of nutrients via benthic remineralization of deceased biomass might be overestimated in the model due to the missing export but is negligibly small compared to the high nutrient concentrations produced by continental runoff.

The inclusion of microphytobenthos and macrozoobenthos is necessary to reproduce pelagic chlorophyll concentrations in the SRB although the parameterization may be regarded as provisional. Depending on the growth parameterization of microphytobenthos the distribution between pelagic and benthic primary production varies.

The comparison of benthic chlorophyll concentrations between the model and measured data is difficult. Measured chlorophyll concentrations in the sediments are relatively high to a depth of up to 15cm, but only the upper few millimeters can contribute to benthic primary production (MacIntyre et al., 1996). The microalgae in the deeper layers of the sediment seem to live heterotrophically but immediately start photosynthesis when they are exposed to light (Hedtkamp, pers. comm.). In order to deal with this mixotrophy in the model, the resolution of the benthic system will need to be improved by dividing the sediment into a higher number of benthic layers.

2.4.5 Impact of filterfeeders

The activity of filterfeeders as well as zooplankton grazers has a strong impact on the phytoplankton standing stock. Grazing of filterfeeders is a sink for phytoplankton biomass and therefore causes a negative feedback on primary production. On the other hand, the release of DIN and DIC by filterfeeders supports phytoplankton growth and causes a positive feedback on primary production (Asmus and Asmus, 1998*a*). In order to analyse which of these effects dominates in the SRB, a sensitivity study has been performed that results in an optimum curve for primary production over filterfeeder carbon uptake. The observed POC uptake measured by Asmus and Asmus (1998*a*), that is used in the standard model run, lies on the left side of the maximum of the optimum curve (Fig. 2.7). This might indicate that the filterfeeders themselves are a strongly exploited ressource. If not, an increase in filterfeeder biomass, and thus POC uptake, would lead to stronger primary production and would improve growth conditions for filterfeeders. Biomass of filterfeeders would grow until the maximum of the optimum curve is reached. Filterfeeders are not only exploited by mussel fisheries but also and in a great extend by birds, especially in spring and autumn when birds of passage visit the bight on their way north or south. In reality, the interannual dynamics of filterfeeders strongly depends on the recruitment success and this success is mostly influenced by climatic factors like temperature (Diederich et al., 2005; Thieltges et al., 2004) or other factors like predation (Beukema and Dekker, 2005).

Based on our model results, we suggest that the List tidal basin still has a large potential to accomodate more filterfeeders. Newly invading species like the rapidly spreading pacific oyster *Crassostrea gigas* (Büttger et al., 2008), that are not exploited naturally, may support primary production levels until the maximum of the optimum curve is reached and might outgrow naturally occurring species until they are discovered as a new food source themselves.

2.4.6 Limitations

The model is designed to simulate growth of one algal species only. It also only concerns the fluxes of carbon and nitrogen throughout the system and is therefore unable to limit algal growth due to depletion of either phosphorus or silicon in the water column. Silicon and phosphate are depleted about one month earlier than DIN (Loebl et al., 2007; van Beusekom et al., 2008*b*). The spring bloom ends simultaneously to the depletion of either phosphorus or silicon when DIN is still available in the water column. The lack of physiological dependencies on P and Si in the proposed model leads to the deviations between data and the model at the timing of the strong DIN drawdown.

A bloom of *Phaeocystis globosa* is frequently observed after the diatom spring bloom has ended (Loebl et al., 2007). The succession of these two algal groups will probably depend on concentrations of phosphorus and silicon and the stoichiometric elemental ratios of N, P, and Si in the water column. *Phaeocystis* is not depending on silicon and is known to possess alkaline phosphatase, an enzyme that allows *Phaeocystis* to use dissolved organic phosphorus as an additional source for P (van Boeckel, 1991). *Phaeocystis* may still find favourable growth conditions when silicon has been depleted by diatoms and dissolved organic nutrients are released to the water column. The succession of diatoms and *Phaeocystis* can simply not be reproduced with the chosen model design. But even if the proposed ecosystem model cannot reproduce the complete biogeochemistry in the Sylt-Rømø Bight without further improvement, it may already be regarded as a valuable tool to investigate several important questions concerning the biogeochemistry of the Wadden Sea.

2.5 Appendix

2.5.1 State variables

Subscripts refer to states, processes or rates in the SRB, $_{srb}$, the NS, $_{ns}$, or the outer NS, $_{NS}$. All pelagic state variables are exchanged between NS and SRB by tidal transport, Ψ.

Dissolved inorganic components

Dissolved inorganic components like DIN, DIC and alkalinity (ALK) exchange with the porewater of the respective benthic layer (Ω). DIN is consumed by nitrogen assimilation of phytoplankton (where q refers to the N:C ratio in phytoplankton) and released by remineralization of EON. Riverine nutrient input provides additional DIN to both boxes. In the SRB, filtration of filterfeeders removes phytoplankton and detritus from the water column and releases the carbon and nitrogen as DIC and DIN, respectively. In the NS, the exchange with the outer NS box restores DIN concentrations to normal conditions.

$$\begin{aligned}
\frac{\mathrm{d}}{\mathrm{d}t} DIN_{ns} &= -\left(\frac{\mathrm{N}^{\mu}_{ns}}{q_{ns}}\right) \cdot Phy\mathrm{N}_{ns} \;+\; \rho_{\mathrm{N}}(T_{ns}) \cdot EO\mathrm{N}_{ns} \\
&+ \;\Omega_{ns} \cdot (BenDIN_{ns} - DIN_{ns}) \;+\; \mathrm{N}^{src}_{ns} \\
&+ \;\Psi_{ns} \cdot (DIN_{srb} - DIN_{ns}) \\
&- \;\Pi_{ns} \cdot (DIN_{NS} - DIN_{ns}) \qquad (2.54) \\
\frac{\mathrm{d}}{\mathrm{d}t} DIN_{srb} &= -\left(\frac{\mathrm{N}^{\mu}_{srb}}{q_{srb}}\right) \cdot Phy\mathrm{N}_{srb} \;+\; \rho_{\mathrm{N}}(T_{srb}) \cdot EO\mathrm{N}_{srb} \\
&+ \;\Omega_{srb} \cdot (BenDIN_{srb} - DIN_{srb}) \;+\; \mathrm{N}^{src}_{srb} \\
&+ \;\Psi_{srb} \cdot (DIN_{ns} - DIN_{srb}) \\
&+ \;\chi_{srb} \cdot (Phy\mathrm{N}_{srb} + Det\mathrm{N}_{srb}) \qquad (2.55)
\end{aligned}$$

Respiration of phytoplankton and zooplankton releases DIC to the water column, photosynthetic carbon fixa-

tion of phytoplankton removes DIC. Remineralization of EOC adds to pelagic respiration and the gas exchange with the atmosphere tries to reestablish equilibrium conditions for the carbonate system in the water column.

$$\begin{aligned}
\frac{\mathrm{d}}{\mathrm{d}t}\, DIC_{ns} &= (r_{phy}(T_{ns}) \;+\; \zeta \cdot \mathrm{N}^{\mu}_{ns} - \mathrm{C}^{\mu}_{ns}) \cdot Phy\mathrm{C}_{ns} \\
&+ \rho_{\mathrm{C}}(T_{ns}) \cdot (1 - f_{TEP}) EO\mathrm{C}_{ns} \;+\; \mathcal{F}^{\mathrm{C}}_{ns} \\
&+ r_{zoo}(T_{ns}) \cdot Zoo\mathrm{C}_{ns} \\
&+ \Omega_{ns} \cdot (Ben DIC_{ns} - DIC_{ns}) \\
&+ \Psi_{ns} \cdot (DIC_{srb} - DIC_{ns}) \qquad (2.56) \\
\frac{\mathrm{d}}{\mathrm{d}t}\, DIC_{srb} &= (r_{phy}(T_{srb}) \;+\; \zeta \cdot \mathrm{N}^{\mu}_{srb} - \mathrm{C}^{\mu}_{srb}) \cdot Phy\mathrm{C}_{srb} \\
&+ \rho_{\mathrm{C}}(T_{srb}) \cdot (1 - f_{TEP}) EO\mathrm{C}_{srb} \;+\; \mathcal{F}^{\mathrm{C}}_{srb} \\
&+ r_{zoo}(T_{srb}) \cdot Zoo\mathrm{C}_{srb} \\
&+ \Omega_{srb} \cdot (Ben DIC_{srb} - DIC_{srb}) \\
&+ \Psi_{srb} \cdot (DIC_{ns} - DIC_{srb}) \\
&+ \chi_{srb} \cdot (Phy\mathrm{C}_{srb} + Det\mathrm{C}_{srb}) \qquad (2.57)
\end{aligned}$$

The consumption of nitrate and phosphate increases alkalinity and the release decreases alkalinity. Although phosphorus is not regarded in the model the effect of phosphorus uptake on alkalinity has to be included. The model assumes a fixed Redfield ratio for uptake and degradation of N and P that changes alkalinity by 1.0625 mol per mol nitrogen.

$$\begin{aligned}
\frac{\mathrm{d}}{\mathrm{d}t}\, ALK_{ns} &= \left(1 + \frac{1}{16}\right) \cdot \left(\frac{\mathrm{N}^{\mu}_{ns}}{q_{ns}}\right) \cdot Phy\mathrm{N}_{ns} \\
&- \left(1 + \frac{1}{16}\right) \cdot \rho_{\mathrm{N}}(T_{ns}) \cdot EO\mathrm{N}_{ns} \\
&- \Omega_{ns} \cdot (Ben ALK_{ns} - ALK_{ns}) \\
&+ \Psi_{ns} \cdot (ALK_{srb} - ALK_{ns}) \qquad (2.58) \\
\frac{\mathrm{d}}{\mathrm{d}t}\, ALK_{srb} &= \left(1 + \frac{1}{16}\right) \cdot \left(\frac{\mathrm{N}^{\mu}_{srb}}{q_{srb}}\right) \cdot Phy\mathrm{N}_{srb} \\
&- \left(1 + \frac{1}{16}\right) \cdot \rho_{\mathrm{N}}(T_{srb}) \cdot EO\mathrm{N}_{srb} \\
&- \Omega_{srb} \cdot (Ben ALK_{srb} - ALK_{srb}) \\
&+ \Psi_{srb} \cdot (ALK_{ns} - ALK_{srb}) \qquad (2.59)
\end{aligned}$$

Phytoplankton

Phytoplankton biomass in nitrogen units is produced by assimilation of DIN. Excretion of organically bound nitrogen reduces phytoplankton nitrogen, but the more important sinks for phytoplankton biomass are produced by grazing and aggregation. In the SRB, phytoplankton biomass is also reduced by filtration of filter-

feeders (χ).

$$\begin{aligned}
\frac{\mathrm{d}}{\mathrm{d}t}\,Phy\mathrm{N}_{ns} &= \left(\frac{\mathrm{N}^{\mu}_{ns}}{q_{ns}} - \gamma_{\mathrm{N}}\right)\cdot Phy\mathrm{N}_{ns} - \Phi_P \cdot Phy\mathrm{N}_{ns}\cdot Det\mathrm{N}_{ns} \\
&- gr_{ns}\cdot Zoo\mathrm{N}_{ns} + \Psi_{ns}\cdot(Phy\mathrm{N}_{srb} - Phy\mathrm{N}_{ns}) \qquad (2.60)\\
\frac{\mathrm{d}}{\mathrm{d}t}\,Phy\mathrm{N}_{srb} &= \left(\frac{\mathrm{N}^{\mu}_{srb}}{q_{srb}} - \gamma_{\mathrm{N}}\right)\cdot Phy\mathrm{N}_{srb} - \Phi_P \cdot Phy\mathrm{N}_{srb}\cdot Det\mathrm{N}_{srb} \\
&- gr_{srb}\cdot Zoo\mathrm{N}_{srb} + \Psi_{srb}\cdot(Phy\mathrm{N}_{ns} - Phy\mathrm{N}_{srb}) \\
&- \chi_{srb}\cdot Phy\mathrm{N}_{srb} \qquad (2.61)
\end{aligned}$$

Photosynthetic carbon fixation produces phytoplankton biomass that is reduced by respiration and secretion of organic carbon compounds.

$$\begin{aligned}
\frac{\mathrm{d}}{\mathrm{d}t}\,Phy\mathrm{C}_{ns} &= (\mathrm{C}^{\mu}_{ns} - r_{phy}(T_{ns}) - \zeta\cdot\mathrm{N}^{\mu}_{ns} - \gamma_{\mathrm{C}})\cdot Phy\mathrm{C}_{ns} \\
&- \frac{1}{q_{ns}}\cdot(\Phi_P\cdot Phy\mathrm{N}_{ns}\cdot Det\mathrm{N}_{ns}) - \frac{gr_{ns}}{q_{ns}}\cdot Zoo\mathrm{N}_{ns} \\
&+ \Psi_{ns}\cdot(Phy\mathrm{C}_{srb} - Phy\mathrm{C}_{ns}) \qquad (2.62)\\
\frac{\mathrm{d}}{\mathrm{d}t}\,Phy\mathrm{C}_{srb} &= (\mathrm{C}^{\mu}_{srb} - r_{phy}(T_{srb}) - \zeta\cdot\mathrm{N}^{\mu}_{srb} - \gamma_{\mathrm{C}})\cdot Phy\mathrm{C}_{srb} \\
&- \frac{1}{q_{srb}}\cdot(\Phi_P\cdot Phy\mathrm{N}_{srb}\cdot Det\mathrm{N}_{srb}) - \frac{gr_{srb}}{q_{srb}}\cdot Zoo\mathrm{N}_{srb} \\
&+ \Psi_{srb}\cdot(Phy\mathrm{C}_{ns} - Phy\mathrm{C}_{srb}) \\
&- \chi_{srb}\cdot Phy\mathrm{C}_{srb} \qquad (2.63)
\end{aligned}$$

Phytoplankton chlorophyll is synthesized as described above. Degradation of chlorophyll steadily reduces chlorophyll concentrations.

$$\begin{aligned}
\frac{\mathrm{d}}{\mathrm{d}t}\,CHL_{ns} &= \left(\mathcal{S}^{chl} - \gamma_{chl}\right)\cdot CHL_{ns} - gr_{ns}\cdot\theta^{\mathrm{N}}_{ns}\cdot Zoo\mathrm{N}_{ns} \\
&- \frac{\theta^{\mathrm{C}}_{ns}}{q_{ns}}\cdot(\Phi_P\cdot Phy\mathrm{N}_{ns}\cdot Det\mathrm{N}_{ns}) \\
&+ \Psi_{ns}\cdot(CHL_{srb} - CHL_{ns}) \qquad (2.64)\\
\frac{\mathrm{d}}{\mathrm{d}t}\,CHL_{srb} &= \left(\mathcal{S}^{chl} - \gamma_{chl}\right)\cdot CHL_{srb} - gr_{srb}\cdot\theta^{\mathrm{N}}_{srb}\cdot Zoo\mathrm{N}_{srb} \\
&- \frac{\theta^{\mathrm{C}}_{srb}}{q_{srb}}\cdot(\Phi_P\cdot Phy\mathrm{N}_{srb}\cdot Det\mathrm{N}_{srb}) \\
&+ \Psi_{srb}\cdot(CHL_{ns} - CHL_{srb}) \\
&- \chi_{srb}\cdot CHL_{srb} \qquad (2.65)
\end{aligned}$$

Zooplankton

Zooplankton biomass is fueled by zooplankton grazing. A quadratical loss term simulates grazing of higher trophic levels on zooplankton.

$$\begin{aligned}
\frac{\mathrm{d}}{\mathrm{d}t}\, Zoo\mathrm{N}_{ns} &= gr_{ns} \cdot Zoo\mathrm{N}_{ns} \;-\; \gamma_{zoo} \cdot {Zoo\mathrm{N}_{ns}}^2 \\
&+ \Psi_{ns} \cdot (Zoo\mathrm{N}_{srb} - CHL_{ns}) \qquad (2.66)\\
\frac{\mathrm{d}}{\mathrm{d}t}\, Zoo\mathrm{N}_{srb} &= gr_{srb} \cdot Zoo\mathrm{N}_{srb} \;-\; \gamma_{zoo} \cdot {Zoo\mathrm{N}_{srb}}^2 \\
&+ \Psi_{srb} \cdot (Zoo\mathrm{N}_{ns} - Zoo\mathrm{N}_{srb}) \qquad (2.67)
\end{aligned}$$

Zooplankton carbon is additionally reduced by zooplankton respiration.

$$\begin{aligned}
\frac{\mathrm{d}}{\mathrm{d}t}\, Zoo\mathrm{C}_{ns} &= \frac{gr_{ns}}{q_{ns}} \cdot Zoo\mathrm{N}_{ns} \;-\; \frac{\gamma_{zoo}}{q_{ns}^{zoo}} \cdot {Zoo\mathrm{N}_{ns}}^2 \;-\; r_{zoo}(T_{ns}) \cdot Zoo\mathrm{C}_{ns} \\
&+ \Psi_{ns} \cdot (Zoo\mathrm{C}_{srb} - Zoo\mathrm{C}_{ns}) \qquad (2.68)\\
\frac{\mathrm{d}}{\mathrm{d}t}\, Zoo\mathrm{C}_{srb} &= \frac{gr_{srb}}{q_{srb}} \cdot Zoo\mathrm{N}_{srb} \;-\; \frac{\gamma_{zoo}}{q_{srb}^{zoo}} \cdot {Zoo\mathrm{N}_{srb}}^2 \;-\; r_{zoo}(T_{srb}) \cdot Zoo\mathrm{C}_{srb} \\
&+ \Psi_{srb} \cdot (Zoo\mathrm{C}_{ns} - Zoo\mathrm{C}_{srb}) \qquad (2.69)
\end{aligned}$$

Detritus

Aggregation and the quadratic loss term for zooplankton produce new detritus. Remineralization as well as sinking reduces detritus concentrations. In the SRB, detritus is also consumed by filterfeeders.

$$\begin{aligned}
\frac{\mathrm{d}}{\mathrm{d}t}\, Det\mathrm{N}_{ns} &= \Phi_P \cdot Phy\mathrm{N}_{ns} \cdot Det\mathrm{N}_{ns} \;-\; \omega_{\mathrm{N}}(T_{ns}) \cdot Det\mathrm{N}_{ns} \\
&+ \gamma_{zoo} \cdot {Zoo\mathrm{N}_{ns}}^2 \;-\; \frac{v_{det}}{z_{ns}} \cdot Det\mathrm{N}_{ns} \\
&+ \Psi_{ns} \cdot (Det\mathrm{N}_{srb} - Det\mathrm{N}_{ns}) \qquad (2.70)\\
\frac{\mathrm{d}}{\mathrm{d}t}\, Det\mathrm{N}_{srb} &= \Phi_P \cdot Phy\mathrm{N}_{srb} \cdot Det\mathrm{N}_{srb} \;-\; \omega_{\mathrm{N}}(T_{srb}) \cdot Det\mathrm{N}_{srb} \\
&+ \gamma_{zoo} \cdot {Zoo\mathrm{N}_{srb}}^2 \;-\; \frac{v_{det}}{z_{srb}} \cdot Det\mathrm{N}_{srb} \\
&+ \Psi_{srb} \cdot (Det\mathrm{N}_{ns} - Det\mathrm{N}_{srb}) \\
&- \chi_{srb} \cdot Det\mathrm{N}_{srb} \qquad (2.71)
\end{aligned}$$

Detritus carbon and nitrogen are treated equally.

$$\begin{aligned}
\frac{\mathrm{d}}{\mathrm{d}t}\, Det\mathrm{C}_{ns} &= \frac{1}{q_{ns}} \cdot (\Phi_P \cdot Phy\mathrm{N}_{ns} \cdot Det\mathrm{N}_{ns}) - \omega_{\mathrm{C}}(T_{ns}) \cdot Det\mathrm{C}_{ns} \\
&+ \frac{\gamma_{zoo}}{q_{ns}^{zoo}} \cdot {Zoo\mathrm{N}_{ns}}^2 \;-\; \frac{v_{det}}{z_{ns}} \cdot Det\mathrm{C}_{ns} \\
&+ \Psi_{ns} \cdot (Det\mathrm{C}_{srb} - Det\mathrm{C}_{ns}) \qquad (2.72)\\
\frac{\mathrm{d}}{\mathrm{d}t}\, Det\mathrm{C}_{srb} &= \frac{1}{q_{srb}} \cdot (\Phi_P \cdot Phy\mathrm{N}_{srb} \cdot Det\mathrm{N}_{srb}) - \omega_{\mathrm{C}}(T_{srb}) \cdot Det\mathrm{C}_{srb} \\
&+ \frac{\gamma_{zoo}}{q_{srb}^{zoo}} \cdot {Zoo\mathrm{N}_{srb}}^2 \;-\; \frac{v_{det}}{z_{srb}} \cdot Det\mathrm{C}_{srb} \\
&+ \Psi_{srb} \cdot (Det\mathrm{C}_{ns} - Det\mathrm{C}_{srb}) \\
&- \chi_{srb} \cdot Det\mathrm{C}_{srb} \qquad (2.73)
\end{aligned}$$

Extracellular organic matter

Extracellular organic matter (EOM) is produced by degradation of detritus and also by secretion of organic molecules by algae. Remineralization to dissolved inorganic carbon and nitrogen removes EOM.

$$\begin{aligned}
\frac{\mathrm{d}}{\mathrm{d}t} EON_{ns} &= \gamma_{\mathrm{N}} \cdot Phy\mathrm{N}_{ns} + \omega_{\mathrm{N}}(T_{ns}) \cdot Det\mathrm{N}_{ns} \\
&- \rho_{\mathrm{N}}(T_{ns}) \cdot EON_{ns} \\
&+ \Psi_{ns} \cdot (EON_{srb} - EON_{ns}) \qquad (2.74) \\
\frac{\mathrm{d}}{\mathrm{d}t} EON_{srb} &= \gamma_{\mathrm{N}} \cdot Phy\mathrm{N}_{srb} + \omega_{\mathrm{N}}(T_{srb}) \cdot Det\mathrm{N}_{srb} \\
&- \rho_{\mathrm{N}}(T_{srb}) \cdot EON_{srb} \\
&+ \Psi_{srb} \cdot (EON_{ns} - EON_{srb}) \qquad (2.75)
\end{aligned}$$

A fraction of the extracellular organic carbon forms TEP that may also sink out of the water column and is remineralized much slower than other EOC.

$$\begin{aligned}
\frac{\mathrm{d}}{\mathrm{d}t} EOC_{ns} &= \gamma_{\mathrm{C}} \cdot Phy\mathrm{C}_{ns} + \omega_{\mathrm{C}}(T_{ns}) \cdot Det\mathrm{C}_{ns} \\
&- \rho_{\mathrm{C}}(T_{ns}) \cdot (1 - f_{TEP}) EOC_{ns} - \frac{v_{det}}{z_{ns}} \cdot (f_{TEP} - x) EOC_{ns} \\
&+ \Psi_{ns} \cdot (EOC_{srb} - EOC_{ns}) \qquad (2.76) \\
\frac{\mathrm{d}}{\mathrm{d}t} EOC_{srb} &= \gamma_{\mathrm{C}} \cdot Phy\mathrm{C}_{srb} + \omega_{\mathrm{C}}(T_{srb}) \cdot Det\mathrm{C}_{srb} \\
&- \rho_{\mathrm{C}}(T_{srb}) \cdot (1 - f_{TEP}) EOC_{srb} - \frac{v_{det}}{z_{srb}} \cdot (f_{TEP} - x) EOC_{srb} \\
&+ \Psi_{srb} \cdot (EOC_{ns} - EOC_{srb}) \qquad (2.77)
\end{aligned}$$

Benthos

Detritus carbon and nitrogen, that sinks out of the water column, accumulates in the benthic layer and is remineralized there by either oxic or anoxic remineralization. In the SRB, mortality of macrozoobenthos adds to the benthic detritus pool.

$$\begin{aligned}
\frac{\mathrm{d}}{\mathrm{d}t} Ben\mathrm{N}_{ns} &= \frac{v_{det}}{z_{ben}} \cdot Det\mathrm{N}_{ns} - \mathcal{OXIC}_{ns}^{Ben\mathrm{N}} - \mathcal{ANOX}_{ns}^{Ben\mathrm{N}} \qquad (2.78) \\
\frac{\mathrm{d}}{\mathrm{d}t} Ben\mathrm{N}_{srb} &= \frac{v_{det}}{z_{ben}} \cdot Det\mathrm{N}_{srb} - \mathcal{OXIC}_{srb}^{Ben\mathrm{N}} - \mathcal{ANOX}_{srb}^{Ben\mathrm{N}} \\
&+ M_{mac} \cdot Macro\mathrm{N} \qquad (2.79)
\end{aligned}$$

$$\begin{aligned}
\frac{\mathrm{d}}{\mathrm{d}t} Ben\mathrm{C}_{ns} &= \frac{v_{det}}{z_{ben}} \cdot (Det\mathrm{C}_{ns} + (f_{TEP} - x) \cdot EOC_{ns}) \\
&- \mathcal{OXIC}_{ns}^{Ben\mathrm{C}} - \mathcal{ANOX}_{ns}^{Ben\mathrm{C}} \qquad (2.80) \\
\frac{\mathrm{d}}{\mathrm{d}t} Ben\mathrm{C}_{srb} &= \frac{v_{det}}{z_{ben}} \cdot (Det\mathrm{C}_{srb} + (f_{TEP} - x) \cdot EOC_{srb}) \\
&- \mathcal{OXIC}_{srb}^{Ben\mathrm{C}} - \mathcal{ANOX}_{srb}^{Ben\mathrm{C}} \\
&+ M_{mac} \cdot Macro\mathrm{C} \qquad (2.81)
\end{aligned}$$

Benthic DIN and DIC are taken up by microphytobenthos in the SRB. Respiration of microphytobenthos and macrozoobenthos increases DIC concentrations in the porewaters.

$$\begin{aligned}
\frac{\mathrm{d}}{\mathrm{d}t}\, BenDIN_{ns} &= \mathcal{OXIC}_{ns}^{Ben\mathrm{N}} + \mathcal{ANOX}_{ns}^{Ben\mathrm{N}} \\
&- \Omega_{ben} \cdot (BenDIN_{ns} - DIN_{ns}) \qquad (2.82) \\
\frac{\mathrm{d}}{\mathrm{d}t}\, BenDIN_{srb} &= \mathcal{OXIC}_{srb}^{Ben\mathrm{N}} + \mathcal{ANOX}_{srb}^{Ben\mathrm{N}} \\
&- \Omega_{ben} \cdot (BenDIN_{srb} - DIN_{srb}) \\
&- \frac{\mathrm{N}_{mic}^{\mu}}{q_{mic}} \cdot Mic\mathrm{N} \qquad (2.83)
\end{aligned}$$

$$\begin{aligned}
\frac{\mathrm{d}}{\mathrm{d}t}\, BenDIC_{ns} &= \mathcal{OXIC}_{ns}^{Ben\mathrm{C}} + \mathcal{ANOX}_{ns}^{Ben\mathrm{C}} \\
&- \Omega_{ben} \cdot (BenDIC_{ns} - DIC_{ns}) \qquad (2.84) \\
\frac{\mathrm{d}}{\mathrm{d}t}\, BenDIC_{srb} &= \mathcal{OXIC}_{srb}^{Ben\mathrm{C}} + \mathcal{ANOX}_{srb}^{Ben\mathrm{C}} \\
&- \Omega_{ben} \cdot (BenDIC_{srb} - DIC_{srb}) + r_{zoo}(T_{srb}) \cdot Macro\mathrm{C} \\
&- (\mathrm{C}_{mic}^{\mu} - r_{phy}(T_{srb}) - \zeta \cdot \mathrm{N}_{mic}^{\mu}) \cdot Mic\mathrm{C} \qquad (2.85)
\end{aligned}$$

$$\begin{aligned}
\frac{\mathrm{d}}{\mathrm{d}t}\, BenALK_{ns} &= -\left(1 + \frac{1}{16}\right) \cdot (\mathcal{OXIC}_{ns}^{Ben\mathrm{N}} + \mathcal{ANOX}_{ns}^{Ben\mathrm{N}}) \\
&- \Omega_{ben} \cdot (BenALK_{ns} - ALK_{ns}) \qquad (2.86) \\
\frac{\mathrm{d}}{\mathrm{d}t}\, BenALK_{srb} &= -\left(1 + \frac{1}{16}\right) \cdot (\mathcal{OXIC}_{srb}^{Ben\mathrm{N}} + \mathcal{ANOX}_{srb}^{Ben\mathrm{N}}) \\
&- \Omega_{ben} \cdot (BenALK_{srb} - ALK_{srb}) \\
&- \left(1 + \frac{1}{16}\right) \cdot \frac{\mathrm{N}_{mic}^{\mu}}{q_{mic}} \cdot Mic\mathrm{N} \qquad (2.87)
\end{aligned}$$

Oxygen

The water column of the NS and the SRB are assumed to be 100% saturated with oxygen. Oxygen solubility in seawater is calculated after Garcia and Gordon (1992). Oxygen in the benthic layer is removed by oxic remineralization. The exchange of the porewaters with the water column resupplies oxygen to the benthic system.

$$\begin{aligned}
\frac{\mathrm{d}}{\mathrm{d}t}\, BenO2_{ns} &= \Omega_{ben} \cdot (O2_{ns} - BenO2_{ns}) - \mathcal{OXIC}_{ns}^{Ben\mathrm{C}} \qquad (2.88) \\
\frac{\mathrm{d}}{\mathrm{d}t}\, BenO2_{srb} &= \Omega_{ben} \cdot (O2_{srb} - BenO2_{srb}) - \mathcal{OXIC}_{srb}^{Ben\mathrm{C}} \qquad (2.89)
\end{aligned}$$

Microphytobenthos

Biomass of microphytobenthos is produced by nitrogen assimilation and photosynthesis. Respiration and grazing by macrozoobenthos decrease carbon biomass concentrations again.

$$\frac{\mathrm{d}}{\mathrm{d}t}\, Mic\mathrm{N} \;=\; \frac{\mathrm{N}^{\mu}_{mic}}{q_{mic}} \cdot Mic\mathrm{N} \;-\; gr_{mic} \cdot Macro\mathrm{N} \tag{2.90}$$

$$\begin{aligned}\frac{\mathrm{d}}{\mathrm{d}t}\, Mic\mathrm{C} \;&=\; (\mathrm{C}^{\mu}_{mic} \;-\; r_{phy}(T_{srb}) \;-\; \zeta \cdot \mathrm{N}^{\mu}_{mic}) \cdot Mic\mathrm{C} \\ &-\; \frac{gr_{mic}}{q_{mic}} \cdot Macro\mathrm{N}\end{aligned} \tag{2.91}$$

$$\frac{\mathrm{d}}{\mathrm{d}t}\, MicCHL \;=\; \left(\mathcal{S}^{chl} \;-\; \gamma_{chl}\right) \cdot MicCHL \;-\; gr_{mic} \cdot \theta^{\mathrm{N}}_{mic} \cdot Macro\mathrm{N} \tag{2.92}$$

Macrozoobenthos

Macrozoobenthos is assumed to graze on microphytobenthos only. Mortality of macrozoobenthic organisms is assumed to increase in winter.

$$\frac{\mathrm{d}}{\mathrm{d}t}\, Macro\mathrm{N} \;=\; gr_{mic} \cdot Macro\mathrm{N} \;-\; M_{mac} \cdot Macro\mathrm{N} \tag{2.93}$$

Macrozoobenthos carbon is also reduced by respiration.

$$\frac{\mathrm{d}}{\mathrm{d}t}\, Macro\mathrm{C} \;=\; \frac{gr_{mic}}{q_{mic}} \cdot Macro\mathrm{N} \;-\; M_{mac} \cdot Macro\mathrm{C} \;-\; r_{zoo}(T_{srb}) \cdot Macro\mathrm{C} \tag{2.94}$$

Chapter 3

A model of the carbon:nitrogen:silicon stoichiometry of diatoms based on metabolic processes

S. Hohn, C. Völker, D.A. Wolf-Gladrow

3.1 Introduction

Besides carbon, nitrogen, phosphorus and, in case of diatoms, silicon, iron is known to be an important element for algal growth (Geider and La Roche, 1994; Sunda and Huntsman, 1997). After Martin and Fitzwater (1988) proposed iron to be the limiting nutrient for phytoplankton growth in high-nutrient low-chlorophyll (HNLC) regions, research effort increased to investigate HNLC regions and the effects of iron concentrations on algal growth. Hutchins and Bruland (1998) and Takeda (1998) discovered strong effects of iron limitation on silicon to nitrogen (Si:N) ratios in diatom biomass, both, in coastal upwelling regimes and the open ocean. Diatoms grown under iron-limited conditions showed increased Si:N ratios of about 3 whereas diatoms grown under iron-replete conditions showed Si:N ratios of about 1 (Hutchins and Bruland, 1998; Takeda, 1998). The changing degree of silicification of diatoms with environmental iron concentrations may have strong effects on global distribution patterns of major nutrients and elemental export fluxes. The use of biogenic opal as a palaeoproxy for productivity may need to be revised as iron deficit seems to decouple the silicon cycle from the carbon and nitrogen cycles in biological production.

Ecosystem models that use one element only (usually C, N or P) as biomass unit while assuming constant C:N:P stoichiometry according to Redfield et al. (1963) for the assimilation of other elements are not able to reproduce observed systematic deviations from Redfield ratios depending on growth conditions. Primary production (in units of C) in nutrient-limited areas of the world oceans is often underestimated using constant C:N ratios as photosynthetic carbon fixation can still occur under nutrient limitations (Smetacek and Pollehne, 1986; Fasham et al., 1993; Fasham and Evans, 1995) and as a consequence C:N ratios may increase to 15 and above (Geider and La Roche, 2002). The model of Geider et al. (1996, 1998) for phytoplankton acclimation allows for the decoupling of nitrogen and carbon metabolism in algae. The Geider model or variants are currently used in several ecosystem models (Moore et al., 2002; Mongin et al., 2003; Schartau et al., 2007).

The discovery of Si:N variations in diatoms with iron concentration (Hutchins and Bruland, 1998; Takeda, 1998) gave rise to the need for further parameterizations in ecosystem models allowing

dynamic regulation of diatom metabolism by iron and a variable Si:N uptake ratio. The prescription of Si:N uptake ratios by either using literature values for different ocean regions (Pondaven et al., 1999) or making the Si:N or Si:C uptake ratio a function of iron concentrations (Lancelot et al., 2000) is an empirical method to simulate the effect of varying Si:N uptake ratios on global fluxes but does not explain the underlying mechanism leading to that phenomenon. Flynn and Martin-Jézéquel (2000) developed a very detailed model for diatom physiology that is based on the cell cycle and considers different modes of nutrient uptake at different stages of the cell cycle. Tracking the cell cycle of diatoms and dividing the pool of biogenic silica into valves, girdle bands, and setae appears much too complex to be included in a global ecosystem model. The intention of the current study is the development of a parameterization for the uptake of silicon, nitrogen and carbon in marine diatoms that can be explained by metabolic processes and be applied to improve the description of diatom growth in global ecosystem models.

3.2 Model description

The following model can be considered as an extension of the model by Geider et al. (1996, 1998) who simulated phytoplankton growth in units of C, N, and chlorophyll (Chl) but not Si and Fe, which are essential for regulating diatom growth.

3.2.1 Parameterization of algal physiology

In an ecosystem model implemented in a global general circulation model only the most important processes of diatom physiology can be considered. These key processes of the proposed model are photosynthetic fixation of carbon, respiration, assimilation of nitrogen, uptake of silicon, synthesis and degradation of chlorophyll and iron dependencies of diatom growth. Cellular uptake of iron is not described separately and no additional state variable is defined for the iron content of the cells to keep the number of state variables low. In this model, diatoms are assumed to react directly to ambient, extracellular iron concentrations. Luxury uptake and storage of iron in diatoms is not considered although this might occur in natural phytoplankton assemblages (Sunda and Huntsman, 1995; Twining et al., 2004).

Photosynthesis

Photoautotrophic organisms absorb light and convert it into chemically bound energy. Photopigments in the thylakoid membrane of the chloroplasts are excited by photons and drive a membrane-bound electron transport chain that produces reduction equivalents and ATP and induces the splitting of water and the production of oxygen (compare Kroon and Thoms (2006) for a detailed mathematical description). The produced ATP and reduction equivalents are needed to drive the Calvin Cycle where CO_2 is incorporated into biomass. In the electron transport chain and the Calvin Cycle, several proteins and enzymes are involved that contain iron as an important reaction center. Photosynthesis relies on the availability of light and on structural and functional components. Nitrogen starved cells are not able to maintain photosynthesis at normal rates. Iron starved cells show decreased contents of iron-containing proteins and a disturbed electron transport chain (Greene et al., 1992; Geider and La Roche, 1994).

Photosynthetic carbon fixation, C_{phot}, increases with irradiance levels as can be described by the PI-curve (Jassby and Platt, 1976; Falkowski et al., 1985), a relation between irradiance ($\mathcal{I}$) and primary production ($\mathcal{P}$). The PI-curve used here (Eq. 3.1) does not consider photoinhibition at very

high irradiance levels (Geider et al., 1998). The initial slope of the PI-curve, α_{Chl}, is regulated by the intracellular chlorophyll to carbon ratio, θ_{C}, which reflects the state of photoadaptation of the cells. High light intensities cause low chlorophyll to carbon ratios and low-light conditions induce an increase of chlorophyll per cell to increase the quantum yield. The maximum carbon fixation rate, μ_{C}^{max}, is known to vary with temperature and changes with the metabolic state of the cell and available iron (Greene et al., 1991, 1992; Geider et al., 1998). The temperature dependence of μ_{C}^{max} is accounted for by using an Arrhenius function, T_{func} (Eq. 3.7) (Eppley, 1972).

For co-limitation of iron, nitrogen or silicon, Liebig's law of the minimum (Eq. 3.3) is applied to decide which factor actually limits photosynthesis (Droop, 1973; De Baar, 1994). The extracellular iron concentration, [Fe], is considered for metabolic limitation of photosynthesis because a cellular iron quota has not been included in the model for the sake of simplicity. The uptake of iron can be assumed to follow Michaelis-Menten kinetics (Sunda and Huntsman, 1997) where K_{Fe} is the half-saturation constant.

The metabolic state of the cell is assumed to be represented by the intracellular N:C and Si:C ratios, q_{NC} and q_{SiC}, respectively. When nitrogen limited, the assimilation of nitrogen decreases at unchanged photosynthetic activity and the N:C ratio decreases. When the intracellular N:C ratio falls below a defined value, q_{NC}^{min}, photosynthetic activity is reduced. Silicon does not directly affect photosynthesis, but is needed to build new frustules. When diatoms are limited by the supply of silicon, they are known to arrest at a particular stage of their cell cycle just before cell division (Martin-Jézéquel et al., 2000; Ragueneau et al., 2000). To avoid unreasonably high cellular carbon contents at silicon limitation photosynthesis in the model is decreased at Si:C ratios lower than q_{SiC}^{min}. The values of the limiting functions used for regulation of the maximum carbon fixation rate range non-linearly between 0 and 1 (Eq. 3.4-3.6).

The assumptions behind the regulation term, $\mathcal{R}_{phot}$, in Eq. 3.4 are, (1) that the photosynthetic apparatus contains iron and does not work efficiently when iron is not available, (2) that photosynthesis requires proteins and enzymes that can also not be provided sufficiently during nitrogen limitation, and (3) that silicon limitation prevents diatoms from cell division so that diatom growth will halt until cellular silicon contents rise and cell division is enabled.

$$\mathrm{C}_{phot} = \mu_{\mathrm{C}} \times \left[1 - \exp\left(-\frac{\theta_{\mathrm{C}} \times \alpha_{Chl} \times \mathcal{I}}{\mu_{\mathrm{C}}}\right)\right] \tag{3.1}$$

$$\mu_{\mathrm{C}} = \mu_{\mathrm{C}}^{max} \times \mathcal{R}_{phot} \times T_{func} \tag{3.2}$$

$$\mathcal{R}_{phot} = min\left[L_{\mathrm{Fe}}, L_{q\mathrm{NC}}^{min}, L_{q\mathrm{SiC}}^{min}\right] \tag{3.3}$$

$$L_{\mathrm{Fe}} = \frac{[\mathrm{Fe}]}{[\mathrm{Fe}] + K_{\mathrm{Fe}}} \tag{3.4}$$

$$L_{q\mathrm{NC}}^{min} = 1 - \exp\left[\sigma_{gentle} \times \left(|q_{\mathrm{NC}}^{min} - q_{\mathrm{NC}}| - \left(q_{\mathrm{NC}}^{min} - q_{\mathrm{NC}}\right)\right)^2\right] \tag{3.5}$$

$$L_{q\mathrm{SiC}}^{min} = 1 - \exp\left[\sigma_{steep1} \times \left(|q_{\mathrm{SiC}}^{min} - q_{\mathrm{SiC}}| - \left(q_{\mathrm{SiC}}^{min} - q_{\mathrm{SiC}}\right)\right)^2\right] \tag{3.6}$$

$$T_{func} = exp\left[A_E\left(\frac{1}{T} - \frac{1}{T_{ref}}\right)\right] \tag{3.7}$$

Nitrogen assimilation

Nitrogen is a major nutrient for phytoplankton and a major component of biomass. The assimilation of nitrogen from the water column into the cell requires the transport of nitrate or ammonia through

the plasma membrane. The passage of charged ions through the lipophilic membrane is mediated by specific transport proteins or carriers that are located in the lipid bilayer. Transport mediated nutrient uptake into the cell has been shown to follow Michaelis-Menten kinetics (Morel, 1987). The half-saturation constant for nitrogen uptake, K_{DIN}, is proportional to the affinity of the transporters to the substrate and is assumed here to be a species specific constant, disregarding possible acclimatizations of the transport system. The maximum uptake rate depends on the translocation rate specific for the transporter and can be changed by the number of transport proteins located in the membrane. The uptake of nitrate is directly coupled to the reduction of nitrate to nitrite to ammonia by the enzyme nitrate reductase and exhibits diurnal periodicity (Eppley et al., 1971; Vergara et al., 1998). Nitrate reductase contains iron in its reaction center which leads to a strong dependency of nitrate assimilation on iron availability (Timmermans et al., 1994). The different chemical forms of nitrogen in seawater are summarized in the model as dissolved inorganic nitrogen (DIN) and uptake of DIN is treated as uptake of nitrate.

The uptake rate in the Michaelis-Menten kinetic (Eq. 3.8), $V_{\mathrm{C}}^{\mathrm{N}}$, is regulated in the same way as the actual photosynthetic rate, μ_{C}. Iron limitation leads to a decrease in nitrogen assimilation. At very low cellular Si:C ratios, e.g. at silicon starvation, nitrogen assimilation decreases together with photosynthesis until the silicon content of the cell is replenished. At very low N:C ratios the uptake of nitrogen is assumed to be limited by the availability of nitrogen itself as the amount of proteins and enzymes becomes too low to enable metabolic activity. At high N:C ratios exceeding q_{NC}^{max} nitrogen assimilation is downregulated (Eq. 3.9), e.g. when cellular carbon compounds are depleted and energy for nitrate reduction cannot be provided by photosynthesis or respiration. The maximum cellular N:C ratio, q_{NC}^{max}, is also used as the maximum N:C uptake ratio for conversion of the carbon specific nitrogen uptake into nitrogen units.

$$V_{\mathrm{C}}^{\mathrm{N}} = 0.7 \times \mu_{\mathrm{C}} \times q_{\mathrm{NC}}^{max} \times L_{q\mathrm{NC}}^{max} \times \frac{[\mathrm{DIN}]}{[\mathrm{DIN}] + K_{\mathrm{DIN}}} \tag{3.8}$$

$$L_{q\mathrm{NC}}^{max} = 1 - \exp\left[\sigma_{steep2} \times (|q_{\mathrm{NC}} - q_{\mathrm{NC}}^{max}| - (q_{\mathrm{NC}} - q_{\mathrm{NC}}^{max}))^2\right] \tag{3.9}$$

Silicon assimilation

The silicon metabolism in diatoms can be divided into uptake of Si, intracellular transport, storage of Si inside the cell, and formation of new frustules. Hildebrand et al. (1997) found genes encoding silicon transporters in several diatoms indicating a transport of silicon over the plasmamembrane into the cytoplasm. Silicon then would have to be transported over the silicalemma into the silicon deposit vesicle (SDV) or into other organelles that provide silicon to the SDV, as proposed by Schmid and Schulz (1979). This uptake mechanism has been described by a Michaelis-Menten equation (Paasche, 1973*b*,*a*; Del Amo and Brzezinski, 1999). It is assumed that the large amount of silicon that would have to pass the cytoplasm is bound to special organic molecules to prevent uncontrolled precipitation inside the cytoplasm (Martin-Jézéquel et al., 2000).

In the model, silicon uptake is described by Michaelis-Menten kinetics (Eq. 3.10) depending on the ambient silicon concentration, [Si], and the half-saturation constant for silicon uptake, K_{Si}, where the maximum uptake rate is multiplied by an Arrhenius function for temperature dependency and two limitation functions depending on the intracellular N:C (Eq. 3.5) and Si:C (Eq. 3.6) ratios. The maximum uptake rate for silicon is given by the maximum photosynthetic rate, μ_{C}^{max}, multiplied by the maximum Si:C uptake ratio, SiC_{upt}. Limitation by the intracellular N:C ratio occurs at very high

N:C ratios when energetic carbon rich compounds are depleted and energy for the silicon metabolism cannot be provided. At very slow growth rates due to iron or nitrogen limitation of photosynthesis, silicon uptake is reduced when intracellular Si:C ratios exceed the maximum cellular Si:C ratio, q_{SiC}^{max} (Eq. 3.11). This regulation attempts to describe a maximum amount of silicon that can be stored in a diatom cell.

Iron has been shown to have an impact on Si uptake kinetics (De La Rocha et al., 2000; Franck et al., 2000) but iron is not known to be involved in the cellular silicon metabolism. In the model, no iron dependencies appear in the equation for silicon uptake kinetics (Eq. 3.10). Iron shortage will therefore not limit silicon uptake directly. Iron limitation will affect the assimilation of nitrogen and carbon and thus change intracellular Si:N:C ratios. The metabolic state of the cell, that is simulated by the intracellular stoichiometry, then regulates the uptake of silicon ($L_{q\mathrm{NC}}^{max}$ and $L_{q\mathrm{SiC}}^{max}$) and causes an indirect feedback of ambient iron concentrations on silicon uptake kinetics.

Photosynthetic activity also has no direct influence on silicon assimilation (Martin-Jézéquel et al., 2000). The energy needed to maintain the silicon metabolism has been shown to be provided by respiration processes (Lewin, 1955).

$$V_{\mathrm{C}}^{\mathrm{Si}} = \mu_{\mathrm{C}}^{max} \times \mathrm{SiC}_{upt} \times T_{func} \times L_{q\mathrm{NC}}^{max} \times L_{q\mathrm{SiC}}^{max} \times \frac{[\mathrm{Si}]}{[\mathrm{Si}] + K_{\mathrm{Si}}} \tag{3.10}$$

$$L_{q\mathrm{SiC}}^{max} = 1 - \exp\left[\sigma_{steep3} \times (|q_{\mathrm{SiC}} - q_{\mathrm{SiC}}^{max}| - (q_{\mathrm{SiC}} - q_{\mathrm{SiC}}^{max}))^2\right] \tag{3.11}$$

Chlorophyll synthesis

Nitrogen is required for the synthesis of chlorophyll and light harvesting complexes. Geider et al. (1998) assumed the synthesis of chlorophyll, S_{Chl}, to be a linear function of nitrogen assimilation (Eq. 3.12) that is inversely proportional to the cellular chlorophyll to carbon ratio, θ_{C}. The slope of this function, $\mathcal{R}_{\mathrm{Chl}}$, is increased at low irradiance levels, $\mathcal{I}$, to improve photosynthetic yield by increasing chlorophyll concentrations inside the cell (Eq. 3.13).

$$S_{\mathrm{Chl}} = \frac{V_{\mathrm{C}}^{\mathrm{N}}}{\theta_{\mathrm{C}}} \times \mathcal{R}_{Chl} \tag{3.12}$$

$$\mathcal{R}_{Chl} = min\left[\theta_{\mathrm{N}}^{max}, \theta_{\mathrm{N}}^{max}\left(\frac{\mathrm{C}_{phot}}{\theta_{\mathrm{C}} \times \alpha_{Chl} \times \mathcal{I}}\right)\right] \tag{3.13}$$

Respiration

The transport of nutrients over a membrane against a concentration gradient consumes energy that is provided by respiration of energetic carbon compounds or directly by photosynthesis. This is realized in the model as a metabolic loss of carbon, r_{phy}, that is proportional to nutrient uptake. As the uptake of silicon is considered to be energetically cheaper than the uptake of nitrogen the metabolic costs, ζ, of silicon metabolism are assumed to be lower than of nitrogen assimilation (Martin-Jézéquel et al., 2000). For other metabolic processes a temperature dependent background respiration is assumed that adds to the metabolic costs of nutrient uptake.

$$r_{phy} \;=\; r_{\mathrm{C}} \times T_{func} \;+\; \zeta_{\mathrm{N}} \times V_{\mathrm{C}}^{\mathrm{N}} \;+\; \zeta_{\mathrm{Si}} \times V_{\mathrm{C}}^{\mathrm{Si}} \tag{3.14}$$

3.2.2 Integration of the physiological model; comparison with laboratory studies

Several authors have performed laboratory experiments that can be used to test the developed parameterization. As data from these experiments are usually derived from the exponential growth phases of batch-culture experiments, the parameterization is used to calculate exponential growth of diatoms under constant irradiance levels, temperature and nutrient concentrations to simulate diatom growth under different growth conditions. As temperature is kept constant, temperature effects are switched off in the model experiments. Nutrient concentrations are varied from replete to limiting. Four state variables that change over time are calculated for diatom biomass: diatom carbon ($dia\mathrm{C}$), diatom nitrogen ($dia\mathrm{N}$), diatom silicon ($dia\mathrm{Si}$), and diatom chlorophyll ($dia\mathrm{Chl}$). To account for excretion of polysaccharides and amino acids, a linear loss for C and N, γ_C and γ_N, is included into the growth equations. When internal silicon pools are high, diatoms are able to secrete excess silicon (Sullivan, 1976; Martin-Jézéquel et al., 2000). To account for this property a linear loss term with a constant rate for silicon excretion, γ_{Si}, has been added to the equations. The linear degradation rate of chlorophyll, γ_{Chl}, is needed to simulate turnover of photosynthetic pigments (Geider et al., 1998). Initial concentrations for diatom biomass are chosen to be 6.625 $\mathrm{mol\ C\ m^{-3}}$, 1 $\mathrm{mol\ N\ m^{-3}}$, 1 $\mathrm{mol\ Si\ m^{-3}}$ and 1.56 $\mathrm{mg\ Chl\ m^{-3}}$.

differential equations:

$$\frac{d}{dt}\, dia\mathrm{C} \;=\; (\mathrm{C}_{phot} - r_{phy} - \gamma_{\mathrm{C}}) \times dia\mathrm{C} \tag{3.15}$$

$$\frac{d}{dt}\, dia\mathrm{N} \;=\; V_{\mathrm{C}}^{\mathrm{N}} \times dia\mathrm{C} - \gamma_{\mathrm{N}} \times dia\mathrm{N} \tag{3.16}$$

$$\frac{d}{dt}\, dia\mathrm{Si} \;=\; V_{\mathrm{C}}^{\mathrm{Si}} \times dia\mathrm{C} - \gamma_{\mathrm{Si}} \times dia\mathrm{Si} \tag{3.17}$$

$$\frac{d}{dt}\, dia\mathrm{Chl} \;=\; (S_{\mathrm{Chl}} - \gamma_{\mathrm{Chl}}) \times dia\mathrm{Chl} \tag{3.18}$$

Model parameter values are compiled in tables 3.1 and 3.2.

Fe effects on diatom Si:N ratio - Experiment 1

Timmermans et al. (2004) investigated the response of four different Southern Ocean diatoms to iron limitation by growing them in Southern Ocean seawater medium with varying dissolved iron concentrations. The experiments showed species specific reactions of the Si:N biomass ratio to changing iron concentrations. To examine how the Si:N uptake ratio of the developed parameterization reacts to iron limitation, the experiments of Timmermans et al. (2004) shall be simulated here as model Experiment 1. Iron concentrations are varied in a defined range at constant [Si], [DIN] and light. The growth conditions are set to 10 $\mu\mathrm{mol\ L^{-1}}$ for [DIN] and [Si] at irradiance levels of 300 $\mathrm{W\ m^{-2}}$. Iron concentrations are varied from 0.01 to 1.0 $\mathrm{nmol\ L^{-1}}$ with an increment of 0.01 $\mathrm{nmol\ L^{-1}}$. For each iron concentration diatoms are allowed to grow until the intracellular composition of the diatoms is stable. The acclimation usually takes about 5 to 10 days in our experiments. For very low, growth-limiting nutrient concentrations, equilibration of diatom stoichiometry may take up to 100 days due to the very slow growth rates. We integrate for at least 500 days.

Table 3.1: Model parameters. Standard values.

Parameter	Standard value	Unit	Meaning
α_{Chl}	0.29	mmol C m^2 (mg Chl W d)$^{-1}$	initial slope of PI-curve
μ_{C}^{max}	13.1	d^{-1}	maximum carbon fixation rate
V_{fact}	0.7	dimensionless	scaling factor
K_{DIN}	0.55	mmol N m^{-3}	half-saturation constant
K_{Si}	4.0	mmol Si m^{-3}	half-saturation constant
K_{Fe}	0.12	μmol Fe m^{-3}	half-saturation constant
κ_{Si}	15.0	mmol Si m^{-3}	scaling factor
q_{NC}^{min}	0.05	mol N mol C^{-1}	minimum N:C ratio
q_{NC}^{max}	0.20	mol N mol C^{-1}	maximum N:C ratio
q_{SiC}^{min}	0.0408	mol Si mol C^{-1}	minimum Si:C ratio
SiC_{upt}	0.204	mol Si mol C^{-1}	maximum Si:C uptake ratio
q_{SiC}^{max}	0.5	mol Si mol C^{-1}	maximum Si:C biomass ratio
σ_{gentle}	50	dimensionless	regulation slope
σ_{steep1}	1000	dimensionless	regulation slope
σ_{steep2}	1000	dimensionless	regulation slope
σ_{steep3}	900	dimensionless	regulation slope
$\theta_{\mathrm{N}}^{max}$	6.0	dimensionless	maximum Chl:N ratio
r_{C}	0.025	d^{-1}	background respiration rate
ζ_{N}	2.0	mol C mol N^{-1}	costs of N uptake
ζ_{Si}	0.5	mol C mol Si^{-1}	costs of Si uptake
γ_{C}	0.2	d^{-1}	loss rate for C
γ_{N}	0.25	d^{-1}	loss rate for N
γ_{Si}	0.25	d^{-1}	loss rate for Si
γ_{Chl}	0.35	d^{-1}	chlorophyll degradation rate
A_E	4500.0	K	slope for Arrhenius function
T_{ref}	288.15	K	reference temperature

Fe effects on Si assimilation - Experiment 2

Experiments of comparable design to Experiment 1 have been performed by Leynaert et al. (2004) in artificial seawater. In this study diatoms were grown under six different inorganic iron concentrations using ethylenediaminetetraacetic acid (EDTA) to control iron speciation. The effect of iron on silicon uptake kinetics was determined by varying silicon concentrations for each level of iron concentrations. The experiments of Leynaert et al. (2004) result in a matrix of silicon uptake for changing iron and silicon concentrations showing a decrease in silicon uptake rates with decreasing iron concentrations. Michaelis-Menten kinetics are fitted to the data in order to derive maximum silicon uptake rates and half-saturation constants for each iron concentration level. For a set of fixed iron concentrations, we performed an experimental dilution series with respect to silicon concentrations. The design and time-span of the experiments was identical to experiment 1. For better comparison of uptake kinetics, iron concentrations are adopted from Leynaert et al. (2004) at 0.008, 0.023, 0.046, 0.076, 0.12 and 0.76 nmol L^{-1}. Irradiance levels are kept at 300 W m^{-2}, DIN is set to 10 μmol L^{-1}. Silicon concentrations are varied from 1 to 20 μmol L^{-1}.

Table 3.2: Adjustment of model parameters for experiment simulations. Ex1 refers to experiment 1 and so forth.

Variable	Ex1	Ex2	Ex3
K_{Si}	4.0	1.0	4.0
K_{Fe}	0.08	0.14	0.12
SiC_{upt}	0.45	0.29	0.04
q_{SiC}^{max}	1.2	0.64	0.125
σ_{steep2}	1000	500	1000

Varying Si:N ratio in the medium - Experiment 3

Kudo (2003) has observed variations of the Si:N ratio of diatom biomass with changing Si:N ratio in seawater. Diatoms were grown in batch cultures with different initial Si:N ratios in the growth medium. At the end of the experiment biomass and nutrient concentrations were measured to determine nutrient uptake ratios. To analyse the reaction of the modelled Si:N uptake ratio to varying Si:N ratios in the growth medium, DIN and Si concentrations are varied at constant [Fe], light and temperature. Irradiance levels are set to 300 $\mathrm{W\ m^{-2}}$, iron concentrations are kept constant at 0.76 $\mathrm{nmol\ L^{-1}}$ and silicon concentrations are then varied from 0.1 to 6 times the DIN concentrations. In order to fit the model solution to the measured data, DIN concentrations are varied logarithmically from 0.01 $\mu\mathrm{mol\ L^{-1}}$ to 10 $\mu\mathrm{mol\ L^{-1}}$. Si:N uptake ratios of diatoms are determined when diatom stoichiometry is stabilized.

Global model run

After validation, the physiological parameterization is implemented into a biogeochemical ecosystem model that is coupled to the ocean general circulation model of the Massachusetts Institute of Technology (Marshall et al., 1997; MITgcm Group, 2002) to study whether the proposed parameterization is able to reproduce the observed Si:N ratios in the ocean. The ecosystem model is based on the Carbon and Nitrogen Regulated Ecosystem Model (CN_REcoM, Schartau et al., 2007) which describes the dynamics of nutrients, phytoplankton, zooplankton, and detritus. In REcoM phytoplankton carbon, nitrogen, and chlorophyll are decoupled (variable stoichiometry). The phytoplankton compartment is replaced by the diatom parameterization described here. Other phytoplankton functional groups are absent. The global biogeochemical model is then used to simulate diatom growth in the ocean under various physical and chemical conditions.

The general circulation model includes a dynamic-thermodynamic sea ice model and is initialized with temperature and salinity data from Levitus and Boyer (1994*a*). The grid spacing is 2°×2°in the northern hemisphere and the Arctic Ocean is excluded north of 80°N to avoid the pole singularity. In the southern hemisphere the latitudinal (ϕ) spacing is scaled by $\cos\phi$ to ensure a locally isotropic grid with the convergence of the longitudes towards the pole. Climatological daily wind, air temperature and humidity, long and short wave radiation drive the physical model as external forcing using the CORE dataset (Large and Yeager, 2004). Irradiance is calculated by astronomical equations (Brock, 1981) and converted to photosynthetic available radiation (PAR) using a constant fraction of 0.43.

The biogeochemical model is initialized with nitrogen and silicon distributions, taken from Levitus et al. (1994*a*), and GLODAP data for initial DIC and alkalinity (Key et al., 2004). Iron concentrations are initialized using modelled distribution fields of the PISCES model (Aumont et al., 2003) that were

corrected towards lower iron concentrations in the Southern Ocean, especially in the deep sea. The correction was made on the basis of the observations by De Baar et al. (1999) and Boye et al. (2001). The biological tracers for C, N and Si biomass are initialized with a uniform distribution of 0.01 μmol N L^{-1}, assuming constant Si:N:C ratios of $1:1:6.625\ \mathrm{mol\ mol^{-1}}$ and a constant N:Chl ratio of $1:1.56\ \mathrm{mol\ mg^{-1}}$.

The model is integrated for three years. Two years are needed for model spin up in the surface ocean and the third model year is chosen for analysis. The standard parameter set (Table 3.1) is used in this model run. Silicon uptake kinetics are simulated assuming Michaelis-Menten kinetics (Eq. 3.10).

3.3 Results

3.3.1 Experiment 1

Intracellular Si:N ratios have been shown to increase with decreasing iron concentrations (Franck et al., 2000; Timmermans et al., 2004). The intensity of this increase as well as the Si:N ratio at replete iron concentrations strongly depends on diatom species (Fig.3.1). Our parameterization can reproduce this physiological behaviour and allows us to investigate what determines this physiological reaction. At low iron concentrations, nitrogen assimilation is reduced (Fig.3.2A, dashed line) as iron is needed for the enzyme nitrate reductase, assuming that DIN equals NO_3^-, which is true in the model and the experiment. The maximum uptake rate for nitrogen follows a Michaelis-Menten curve with varying iron concentrations as prescribed by the regulation term for μ_{C} (Eq. 3.4). Silicon assimilation slightly increases with decreasing iron concentrations and decreases at very low iron concentrations (Fig.3.2A, solid line). This regulation of the silicon uptake is derived only from the intracellular N:C and Si:C ratios. The effect of the intracellular Si:C ratio only affects silicon assimilation at very low iron concentrations when the intracellular Si:C ratio exceeds q_{SiC}^{max}. The differing response of the uptake rates for both nutrients leads to the variation in Si:N uptake ratios (Fig.3.2B). As the sink terms for nitrogen and silicon do not change with ambient iron concentrations the intracellular Si:N biomass ratio shows the same response to iron limitation as the uptake ratio.

The parameterization can be tuned to match the observed responses in the different diatom species considered by Timmermans et al. (2004) by changing the values of model parameters. The silicon to carbon uptake ratio, SiC_{upt}, determines Si:N ratios at replete iron concentrations and is thus different for highly silicifying Southern Ocean diatoms like *Fragilariopsis kerguelensis* or for other species with lower Si:N ratios. The maximum intracellular Si:C ratio, q_{SiC}^{max}, defines at which Si:N ratios the assimilation of silicon is reduced and thus determines maximum cellular Si:N ratios at iron limitation. The half-saturation constant for iron, K_{Fe}, affects the bending of the curve for increasing Si:N ratios at decreasing iron concentrations. Lowering K_{Fe} leads to a shifting of increasing Si:N ratios towards lower iron concentrations.

3.3.2 Experiment 2

Although iron is not known to be involved in the silicon metabolism of diatoms, iron limitation affects the maximum silicon uptake rate (Leynaert et al., 2004). Silicon uptake rates at highest Si concentrations in the experiments (20 $\mu\mathrm{mol\ L^{-1}}$) slightly increase with decreasing iron concentrations and decrease strongly at iron concentrations lower than K_{Fe} (Fig.3.3). This effect is reproduced in our parameterization by using the intracellular Si:C ratio as a variable for metabolic regulation of silicon uptake.

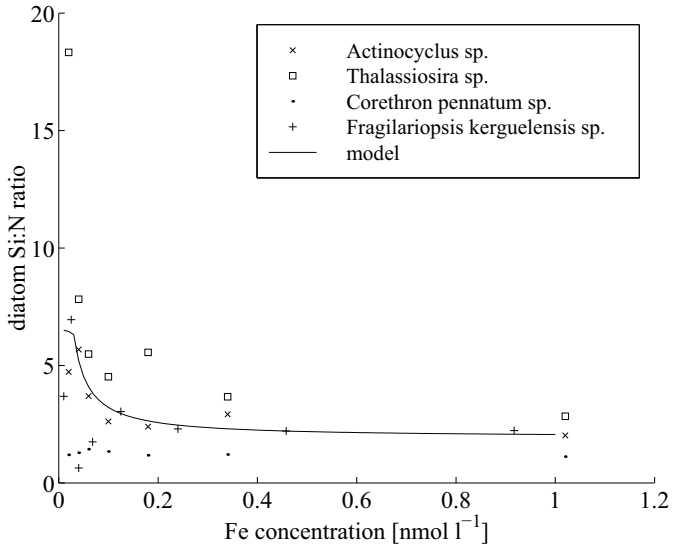

Figure 3.1: Si:N ratio in diatoms. The elemental ratio of silicon to nitrogen in diatom biomass varies with ambient iron concentrations. The plot shows model results together with data of four Southern Ocean diatoms (see Timmermans et al. (2004)).

The transporter mediated silicon uptake shows Michaelis-Menten kinetics with a strong influence of the ambient iron concentrations on maximum uptake rates for silicon (Fig.3.4) which is confirmed by the experiments of Leynaert et al. (2004). In their experiments, the half-saturation constants for silicon uptake also seemed to vary with different iron concentrations, which is not reproduced by our model.

The half-saturation constant of the Michaelis-Menten kinetics is assumed to represent the affinity of the transporter molecules. Increasing affinity of the uptake mechanism for its substrate would lead to a decrease of K_h as the maximum uptake would already be achieved at lower substrate concentrations. The expression of different transport systems is not regarded in the model and the half-saturation constant remains constant.

3.3.3 Experiment 3

The observations of Kudo (2003) show a well-defined linear increase of the Si:N uptake ratio with increasing Si:N ratio in the growth medium saturating at higher values of the Si:N ratio (Fig.3.5). The linear increase at lower Si:N ratios has a slope of about 1 and a y-axis intercept close to zero. Finding a set of model parameters such that the model can explain this physiological behaviour appears to be quite difficult. The modelled dependency of the diatom Si:N ratio on medium Si:N ratio does not only depend on the model parameter values, but also on the absolute nutrient concentrations in the medium. For DIN concentrations higher than 1 $\mu\mathrm{mol\,L}^{-1}$, the Si:N uptake ratio is rather constant (Fig.3.5) and does not change with Si:N in the medium. For very low DIN concentrations of 0.01 $\mu\mathrm{mol\,L}^{-1}$ a slight increase of the diatom Si:N ratio can be observed with increasing Si:N ratio in the medium, but this increase does not exhibit a saturating behaviour as can be seen in the data.

At DIN concentrations of 0.1 $\mu\mathrm{mol\,L}^{-1}$ and rather unrealistic parameter values the model produces a reasonable fit to the data (Fig.3.5).

This behaviour might be explained by a simple calculation: If one ignores all regulation effects on

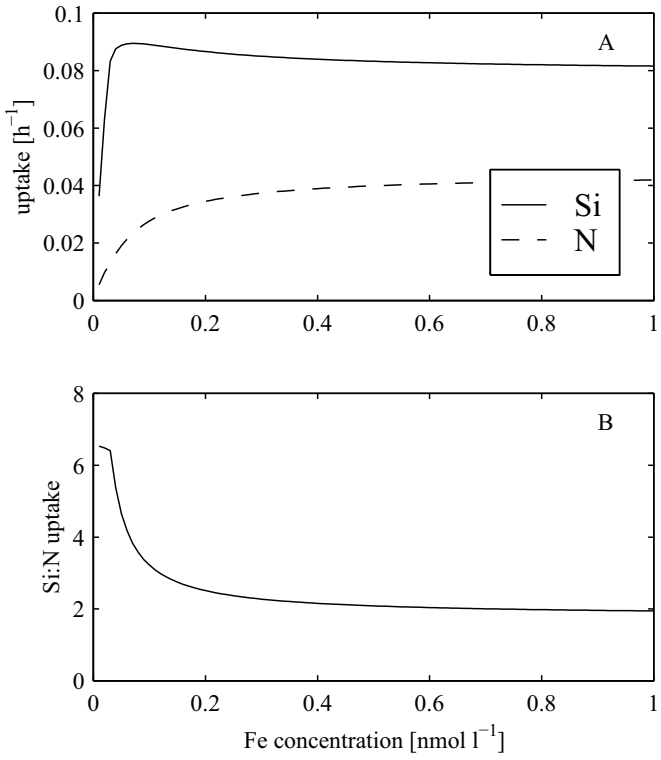

Figure 3.2: Silicon and nitrogen uptake as a function of ambient iron concentrations (panel A). The varying Si:N uptake ratio is produced by different responses of nutrient uptake kinetics to varying iron concentrations (panel B).

nitrogen and silicon assimilation other than extracellular Si and DIN concentrations, one obtains the Michaelis-Menten kinetics for nutrient uptake:

$$V^{\mathrm{Si}} = V^{\mathrm{Si}}_{max} \times \frac{[\mathrm{Si}]}{[\mathrm{Si}] + K_{\mathrm{Si}}} \tag{3.19}$$

$$V^{\mathrm{N}} = V^{\mathrm{N}}_{max} \times \frac{[\mathrm{DIN}]}{[\mathrm{DIN}] + K_{\mathrm{DIN}}} \tag{3.20}$$

The ratio of silicon uptake over nitrogen uptake, the Si:N uptake ratio, then reads:

$$\frac{V^{\mathrm{Si}}}{V^{\mathrm{N}}} = \frac{[\mathrm{Si}]}{[\mathrm{DIN}]} \times \frac{[\mathrm{DIN}] + K_{\mathrm{DIN}}}{[\mathrm{Si}] + K_{\mathrm{Si}}} \times \frac{V^{\mathrm{Si}}_{max}}{V^{\mathrm{N}}_{max}} \tag{3.21}$$

At high nutrient concentrations one can neglect the half-saturation constants and gets a constant Si:N uptake ratio that is only determined by the ratio of the maximum uptake rates. At silicon and nitrogen concentrations lower than the half-saturation constants the Si:N uptake ratio becomes a function of the ambient Si:N ratio in the medium, because silicon and DIN concentrations in the fraction can be neglected. The slope of this function, which is derived from the kinetic parameters determines the linear increase of the Si:N uptake ratio with increasing Si:N ratio in the medium.

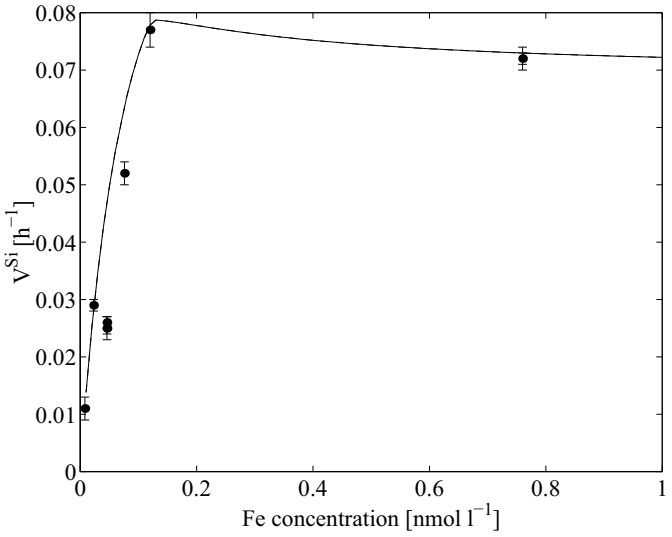

Figure 3.3: Silicon assimilation as a function of ambient iron concentrations compared to data from (Leynaert et al., 2004). Iron limitation decreases maximum silicon uptake rates at iron concentrations lower than the half-saturation constant for iron uptake.

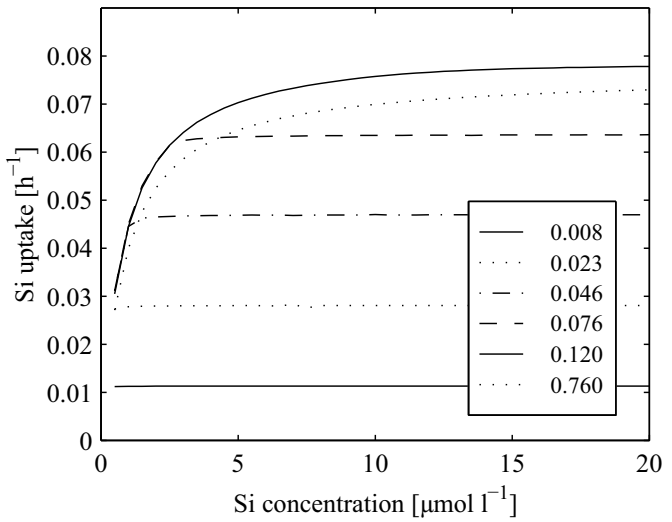

Figure 3.4: Silicon uptake kinetics for different iron concentrations. The diagram shows silicon uptake as a function of ambient silicon concentrations. Uptake kinetics are plotted for six different iron concentrations from 0.008 to 0.76 $\mathrm{nmol\ Fe\ L^{-1}}$.

The response to varying Si:N ratios in the growth medium that was observed by Kudo (2003) can best be fitted by the transporter mediated silicon uptake assuming very low DIN concentrations, but even then, the model strongly deviates from the observed data. At higher DIN concentrations, well above half-saturation constants, Si:N uptake ratios of diatoms are nearly constant (Fig.3.5) and cannot explain the response observed by Kudo (2003).

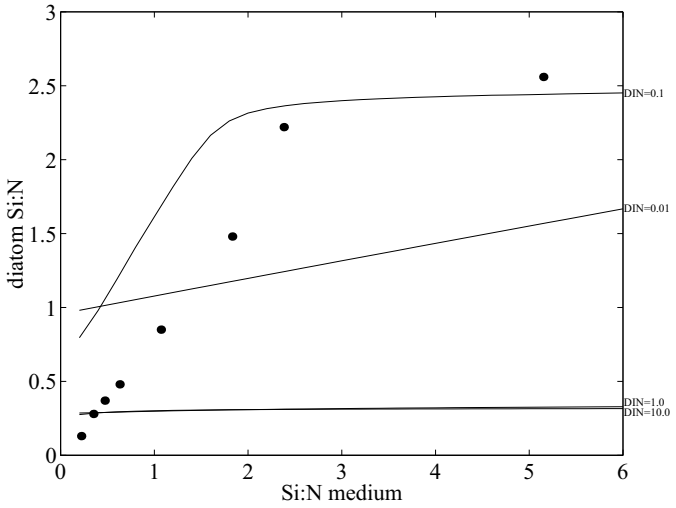

Figure 3.5: Si:N uptake ratio as a function of Si:N ratio in the medium. The Si:N uptake ratio of diatoms depends on the Si:N ratio in the surrounding water. The plot shows experimental data from Kudo (2003) and model runs for four different DIN concentrations. In order to present the sensitivity of this experiment to absolute nutrient concentrations, DIN concentrations are varied from 0.01 to 10 μmol DIN L^{-1}.

3.3.4 alternative Si uptake kinetics

Due to the difficulties in fitting the linear increase of the Si:N biomass ratio with increasing Si:N ratio in the growth medium in experiment 3, an alternative formulation of silicon uptake to Michaelis-Menten kinetics is tested. Thamatrakoln and Hildebrand (2008) recently discussed the existence of nonsaturable silicon uptake kinetics in diatoms and showed a transition between saturable and nonsaturable silicon uptake kinetics. We will not try to reproduce the observed transition but test the linear nonsaturable uptake as an alternative to Michaelis-Menten kinetics.

The nonsaturable silicon uptake could be modelled as follows:

$$V_C^{\mathrm{Si}} \quad = \quad \mu_{\mathrm{C}}^{max} \times \mathrm{SiC}_{upt} \times T_{func} \times L_{q\mathrm{NC}}^{max} \times L_{q\mathrm{SiC}}^{max} \times \frac{[\mathrm{Si}]}{\kappa_{\mathrm{Si}}} \tag{3.22}$$

The nonsaturable silicon uptake is described by an uptake rate that is linearly increasing with increasing silicon concentrations and regulated by temperature and the intracellular N:C and Si:C ratios as already described for the transporter mediated uptake. The constant maximum uptake rate is derived from the maximum photosynthetic carbon fixation rate multiplied with the maximum Si:C uptake ratio and scaled by a reference Si concentration, κ_{Si}. The latter three constants can be combined to a single model parameter.

The linear increase of the Si:N uptake ratio with increasing Si:N ratio in the medium can be reproduced with the nonsaturable silicon uptake (Fig.3.6). Standard values are used for all model parameters and κ_{Si} is set to 15 μmol Si L^{-1}. Silicon uptake linearly increases until intracellular Si:C ratios lead to a downregulation of silicon uptake. The response of the Si:N uptake ratio in the nonsaturable approach is not independent of the absolute nutrient concentrations but the parameterization can fit the data at normal absolute DIN concentrations of 10 μmol DIN L^{-1}.

For the experiments of Leynaert et al. (2004) the silicon uptake via Michaelis-Menten kinetics appears to be the most probable explanation as the results of the nonsaturable silicon uptake (Fig.3.7)

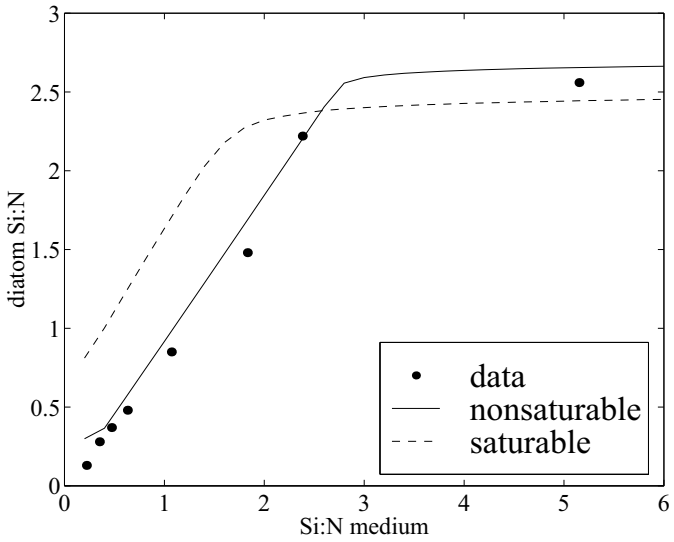

Figure 3.6: Si:N uptake ratio as a function of Si:N ratio in the medium. The results of model optimization for two different silicon uptake pathways are shown in this graph. To minimize deviations between model runs and data different absolute concentrations of DIN had to be assumed for both model runs. (10 μmol DIN L^{-1} for nonsaturable silicon uptake; 0.1 μmol DIN L^{-1} for the saturable uptake)

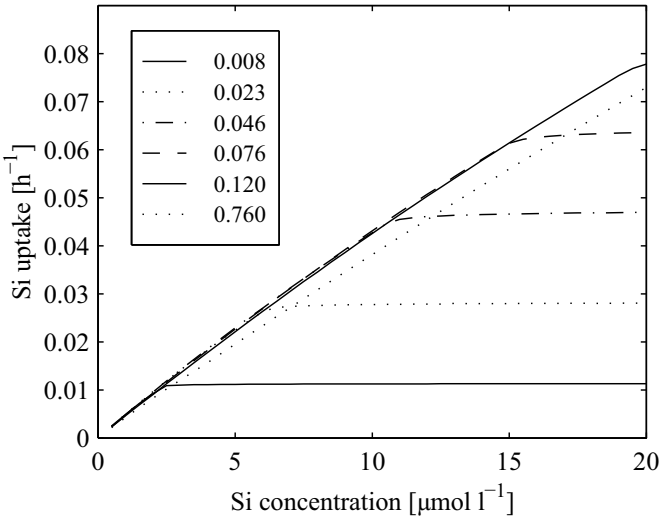

Figure 3.7: Iron dependent silicon uptake kinetics for the linear uptake approach. The diagram shows silicon uptake as a function of ambient silicon concentrations. Uptake kinetics are plotted for six different iron concentrations from 0.008 to 0.76 nmol Fe L^{-1}.

clearly differ from the observed kinetics. The response of the Si:N uptake ratio to varying Si:N ratios in the growth medium (Kudo, 2003) can best be explained with the linear silicon uptake.

The physiological response to iron limitation is independent of the assumed mechanism for silicon uptake. The parameterization shows the same results for the simulated experiments 1 and 2 for saturable and nonsaturable silicon uptake kinetics.

3.3.5 Global model run

In the ecosystem model the simulation of a global average diatom leads to a distribution pattern of diatom biomass. The model produces high chlorophyll concentrations in temperate and equatorial regions with a pronounced annual cycle of biomass production at higher latitudes. Very low biomass concentrations are observed in the subtropical gyres and ice-covered polar waters (data not shown). The distribution of diatoms strongly depends on the environmental conditions. After three years integration time absolute nutrient concentrations are still very close to initial concentrations and the ecosystem has evolved towards a cyclostationary state. Overlaid on this cyclostationary state there is a small trend, caused by the slow response of the nutrient distribution to the modelled vertical fluxes of organic matter and the adaptation of temperature and salinity to physical surface forcing. Diatom physiology, and thus diatom stoichiometry, quickly adapts to ambient growth conditions according to the distributions of light and nutrients. Although nutrient distributions have not yet run into equilibrium, the functional response of the developed parameterization can already be demonstrated in the relatively short time of model integration as the modelled response of diatom physiology acts on a much smaller time scale than the distribution of nutrients and biomass in the global ocean. The Si:N ratio in diatoms is of special interest because it varies with the availability of iron.

The distribution of the molar Si:N ratios in diatoms shows high values (larger than one) in the Southern Ocean (Fig.3.8A) and also in the northern Pacific (not shown). Iron concentrations, that are influenced by the dust deposition fields used in the model run, cause growth limitation of diatoms in the Antarctic Circumpolar Current (ACC; Fig.3.8B), leading to stronger silicification of diatoms in the surface waters. Elevated Si:N ratios correlate very well with iron limitation. North of the Antarctic Polar Front, low silicon concentrations lead to silicon limitation of diatom growth (Fig.3.8C), inhibiting elevated Si:N ratios despite iron limitation.

The North Atlantic Ocean and the whole subtropic and tropic ocean regions show normal to very low Si:N ratios. The very low Si:N ratios, lower than one, appear in those regions where diatom growth is strongly limited for silicon supply. Diatoms are not able to grow in these areas or only in very low numbers. In reality these regions are inhabited by other phytoplankton organisms than diatoms that are not incorporated in this model approach.

3.4 Discussion

The results of the simulated experiments 1 and 2 fit reasonably well with the literature data by Leynaert et al. (2004) and Timmermans et al. (2004). A decrease of ambient iron concentrations leads to a decrease of silicon uptake (Fig.3.2) although this is not explicitly requested by the parameterization. The parameterization simulates metabolic processes based on the current understanding of diatom physiology. It is assumed that the amount of silicon that can be taken up during diatom growth depends on the time diatoms spend in the G1 phase (the major nutrient uptake phase) of the cell cycle (Flynn and Martin-Jézéquel, 2000; Martin-Jézéquel et al., 2000; Ragueneau et al., 2000). Iron limitation leads to a decrease of diatom growth rates and the duration of G1 phase increases. This effect is reproduced by the model as silicon assimilation is not directly altered by iron availability while nitrogen assimilation decreases at low iron concentrations. The response of the silicon assimilation to iron limitation occurs indirectly via the intracellular Si:N:C ratio that feeds back to silicon uptake. Silicon assimilation thus reacts to iron induced changes in nitrogen or carbon contents of the cells rather than iron availability.

As the assimilation of nitrogen depends more strongly on environmental iron concentrations than the uptake of silicon, the decrease of nitrogen uptake is more pronounced than the decrease of silicon

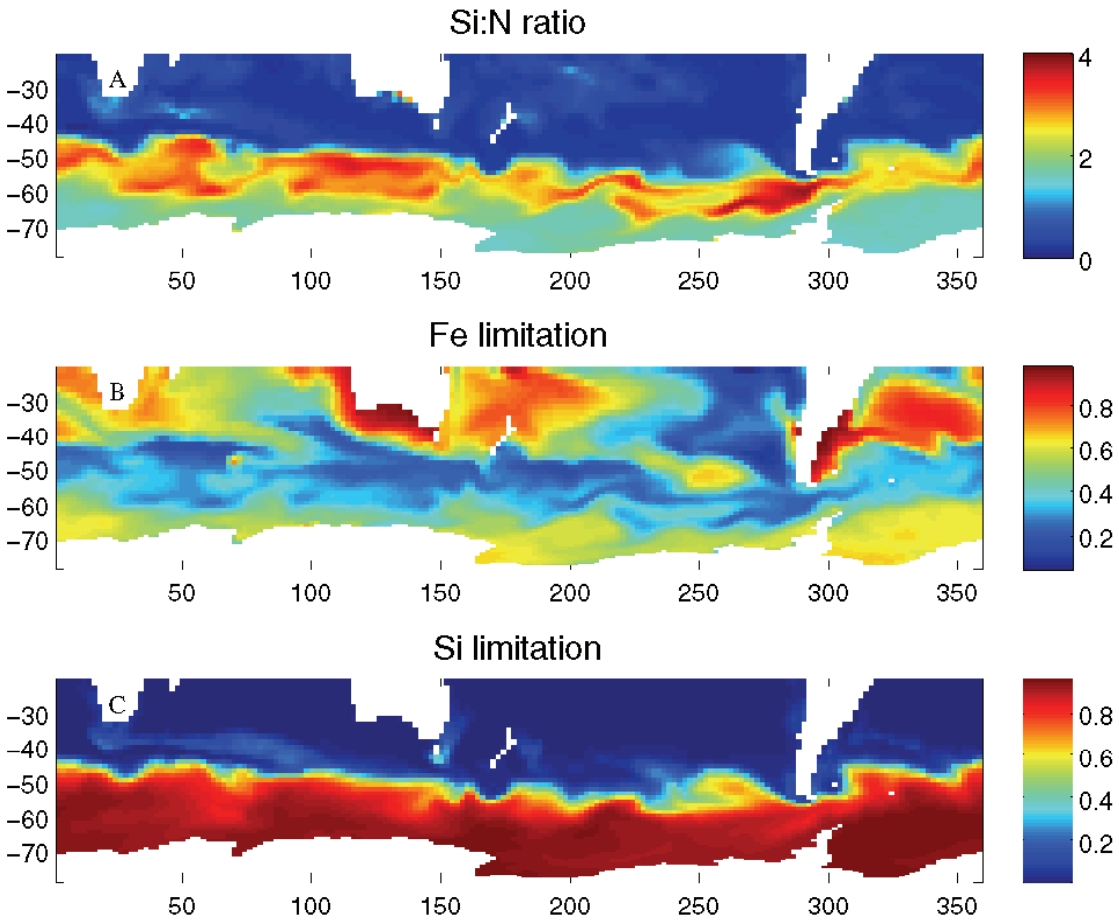

Figure 3.8: Global model run. Panel A shows molar Si:N ratios of diatom biomass in surface waters of the Southern Ocean. Panels B and C present the dimensionless value of the Michaelis Menten functions for iron and silicon, illustrating the limitation of diatom growth by the respective element. Elevated Si:N ratios can be observed in regions where diatom growth is limited by low iron concentrations. Silicon limitation north of the Antarctic Polar Front prevents elevated Si:N ratios in diatoms.

assimilation and thus the Si:N uptake ratio of diatoms increases (Fig.3.1 and 3.2). This increase of the Si:N ratio is limited at very low iron concentrations to a maximum Si:N ratio, which is prescribed by the maximum Si:C ratio, q_{SiC}^{max}, of the cells.

The iron-induced effects and metabolic regulations of diatom growth seem to be adequately represented in our model, with respect to the assumptions made for model development. Different diatoms were shown to react differently to iron limitation or other environmental forcing (Timmermans et al., 2004). The equations developed for this parameterization are able to reproduce these differing responses by changing the parameter values (Table 3.2) for the species or community that is to be simulated.

The silicon metabolism indeed seems to be strongly decoupled from other metabolic processes and does not show the same dependencies on iron as carbon fixation and nitrogen assimilation (Hildebrand, 2002). Downregulation of silicon assimilation at iron limitation may be explained by deterio-

rating metabolic conditions and not by a direct effect of iron on silicon metabolism. The decoupling of the silicon metabolism may be explained by either a different source of metabolic energy for the uptake of silicic acid or by a completely different pathway for silicon assimilation.

The silicon uptake mechanism in diatoms has not yet been identified (Martin-Jézéquel et al., 2000). However, the identification of the uptake mechanism is essential for the development of a parameterization of diatom physiology.

The studies of Paasche (1973*b*), Del Amo and Brzezinski (1999), and many others have shown a Michaelis-Menten like response of the silicon uptake to increasing silicon concentrations and Hildebrand et al. (1997) have identified genes encoding silicon transporters, indicating a transporter-mediated membrane passage of Si. But the observation of uptake kinetics that linearly increase with increasing silicon concentrations and the transition between nonsaturable and saturable silicon uptake kinetics (Thamatrakoln and Hildebrand, 2008) question the role of silicon transporters and would recommend an alternative pathway to the transporter-mediated silicon uptake.

Thamatrakoln and Hildebrand (2008) propose the uptake of silicic acid via simple diffusion over the plasmalemma. Vrieling et al. (2007) propose silicon uptake via pinocytosis, or fluid phase endocytosis. Both uptake mechanisms would be linearly dependent on extracellular silicon concentrations and could be regulated by intracellular mechanisms. Silicon uptake via diffusion could be regulated by the intracellular concentrations of silicic acid or silicon binding proteins as proposed by Thamatrakoln and Hildebrand (2008). Silicon uptake via endocytosis could be regulated by the amount of endocytotic vesicles produced and the intracellular vesicle transport and would be limited at an upper end of possible membrane turnover.

An uptake mechanism for silicon via endocytosis is not unthinkable in principle as all eukaryotes are able to carry out endocytosis. Endocytosis has been proven to occur in *Coscinodiscus wailesii* as the membrane impermeable dye used by Kühn and Brownlee (2005) can only have entered the observed vesicles via endocytotic constrictions in the plasmamembrane. However, the silicon transport vesicles proposed by Schmid and Schulz (1979) have never been proven to contain silicon. Besides the fate of solvents that are not needed by the cell but would be taken up by endocytotic vesicles, it also has to be questioned if this pathway is efficient enough to incorporate the amounts of silica that are needed to construct a new frustule and to explain the rapid incorporation of silicon observed by Hazelaar et al. (2005). However, if silicon can be shown to be taken up via endocytosis, it might explain the decoupling of the silicon metabolism from nitrogen and carbon metabolisms.

Furthermore, when diatoms first developed in the world ocean they experienced silicon concentrations up to 1000 $\mu\mathrm{mol\,Si\,L^{-1}}$ (Maliva et al., 1989; Siever, 1991). Silicon uptake experiments performed at silicon concentrations of up to 300 $\mu\mathrm{mol\,Si\,L^{-1}}$ showed unexpected silicon uptake kinetics in *Phaeodactylum tricornutum* (Del Amo and Brzezinski, 1999) that look similar to the kinetics of endocytotic uptake of a fluorescent probe in leaf protoplasts (Wright and Oparka, 1989). Even though *Phaeodactylum tricornutum* is not a typical diatom and may not be representative for other diatoms, future work on diatom physiology and silicon uptake kinetics should also consider higher silicon concentrations than can be found in the modern world ocean to really understand the silicon metabolism of diatoms.

The developed parameterization focuses on the biogeochemical fluxes and computes the C, N, Si, and Chl biomass of the whole diatom population.

Modelled chlorophyll concentrations in the Southern Ocean are close to SeaWiFs data (not shown). Low iron concentrations cause growth limitation of diatoms (Fig.3.8B) and thus alter the Si:N uptake ratio as described by the developed parameterization. The increased Si:N uptake ratio at iron

limitation is reflected in the Si:N biomass ratio (Fig.3.8A) and will also affect Si:N drawdown ratios in the ocean.

The advantage of the developed parameterization is that the Si:N uptake ratio of diatoms is not only indirectly dependent on ambient iron concentrations, but results from the metabolic history of the cells and external nutrient concentrations. This dynamic acclimation of diatom physiology leads to lower Si:N ratios north of the Antarctic Polar Front despite iron limitation. In these waters, diatom growth is limited by silicon supply. The developed parameterization of dynamic acclimation of diatom physiology to changing environmental conditions is based on the current understanding of metabolic processes and might be regarded as a reproduction rather than an empirical prescription of the Si:N uptake ratio on the basis of ambient iron concentrations (Pondaven et al., 1999; Lancelot et al., 2000).

Elevated Si:N biomass ratios of diatoms have been discussed in the context of increased silicification as the amount of silicon per cell increased under iron limitation (Takeda, 1998; De La Rocha et al., 2000; Leynaert et al., 2004). Marchetti and Harrison (2007) could show recently that pennate diatoms of the genus *Pseudo-nitzschia* did not increase the thickness of their frustules but changed the surface to volume ratio by changing the aspect ratio of their cell dimensions. Cell numbers or cell size effects are not regarded in this model. Generally, iron limitation leads to elevated Si:N ratios although this could not be confirmed for all diatom species (De La Rocha et al., 2000).

Increased silicification under non-favourable growth conditions will most probably cause a feedback on diatom mortality due to zooplankton grazing. The time needed to destroy the diatom frustule and to get access to the cytoplasm will increase with frustule thickness and the grazing rate on diatoms will decrease. This effect may have led to a coevolutionary development between diatoms and zooplankton grazers (Smetacek, 2001), especially in the Southern Ocean. But on shorter time scales, as considered in laboratory experiments, the physiological response appears to be independent on grazing pressure. The differences between diatom species may be explained by different evolutionary adaptations to grazing (Pondaven et al., 2007), but may also be explained by physiological adaptations to different environmental conditions.

The uptake of iron from the water column is an energy consuming process. In order to increase iron assimilation from the water column at very low concentrations (decreasing K_{Fe}) some algae possess high-affinity transporters and surface reductase that are even more energy consuming (Maldonado and Price, 2001). The energy needed for the uptake mechanism cannot be used for other metabolic processes. Diatoms adapted to low Fe concentrations will have lower half-saturation constants for Fe but lower maximum growth rates than diatoms adapted to high Fe concentrations because they spend more energy on iron uptake mechanisms. High-iron species grow out low-iron species at iron replete conditions because they spend less energy on the Fe uptake mechanism. Temperature and light dependencies of different species can be ignored in this respect because they outcompete each other in the same water bodies only depending on Fe concentrations. These adaptations will also affect the degree of silicification as species spending more energy on iron uptake will have slower growth rates and therefore stronger silicified shells, as silicification is less affected by metabolic regulations due to energy shortage.

The decoupling of the silicon metabolism from carbon and nitrogen metabolism may be the actual evolutionary adaptation to both, low nutrient concentrations and high grazing pressure. The stronger the bottom up control of nutrients, the grave the impact of top down control by grazers. Slowed growth rates cause stronger silicification lowering maximum grazing rates and thus decreasing grazing pressure at non-favourable growth conditions. To what extent ecological adaptations can be superimposed on the described physiological response , leading to increased silicification of diatoms in HNLC regions, remains an open question to be discussed.

The impact of the physiological response of diatoms and variable algal stoichiometry on global biogeochemical fluxes of Si, N, C and Fe will be adressed in another study, where the global model will be analysed in detail.

Chapter 4

Coupling and decoupling of silicon and nitrogen cycles in the Southern Ocean

S. Hohn, C. Völker, M. Losch, S. Loza, D.A. Wolf-Gladrow

4.1 Introduction

Diatoms are important primary producers in marine ecosystems and account for about 40 % of the global marine primary production (Nelson et al., 1995). Diatoms assimilate dissolved silicon, DSi, to form shells of amorphous hydrated silica, the frustules (Schmid and Schulz, 1979), that are thought to act as a defense mechanism against zooplankton grazing (Hamm et al., 2003). The densely compacted biogenic silica, BSi, in detritus sinks out of the water column towards the deep sea (Raven and Waite, 2004; Smetacek, 1985) and the export of biogenic silica is linked to the export of carbon (Ragueneau et al., 2002, 2006) and nitrogen (Pollard et al., 2006). While sinking, BSi is dissolved or remineralized and becomes silicic acid again. The transformation processes between BSi and DSi, production and remineralization, lead to a continuous cycling between two chemical forms of silicon. Both chemical forms are distributed via different predominating transport processes, as only BSi is targeted by sinking. The transformation processes are thus spatially separated from each other, production being bound to the euphotic zone and remineralization mainly occurring in deep waters (Ragueneau et al., 2000).

The phytoplankton community in the Southern Ocean is mainly dominated by diatoms (Assmy et al., 2007) and accumulation of opal in the sediments underlying the Antarctic Circumpolar Current (ACC), the so called opal belt, indicates high export of biogenic opal from surface waters (DeMaster, 1981). Diatom growth depletes dissolved silica in the euphotic zone, generating a vertical concentration gradient with low DSi concentrations at the ocean surface. Silicon is thus an important element regulating phytoplankton growth and therefore also primary production in the Southern Ocean. Dissolved silica is resupplied to surface waters via mixing with deep waters with high DSi concentrations.

The global distribution of dissolved silicon in the world ocean (Fig. 4.1) shows high accumulation of silicon in deep waters of the North Pacific, the Indian Ocean, and the Southern Ocean. Elevated concentrations in the deep ocean are typical for nutrients that are incorporated into biomass, as the gravitational attraction of the Earth draws the non-motile biomass into the deep sea where it gets remineralized.

Another feature of the global distribution of total silicon concentrations (Fig. 4.1) is a strong

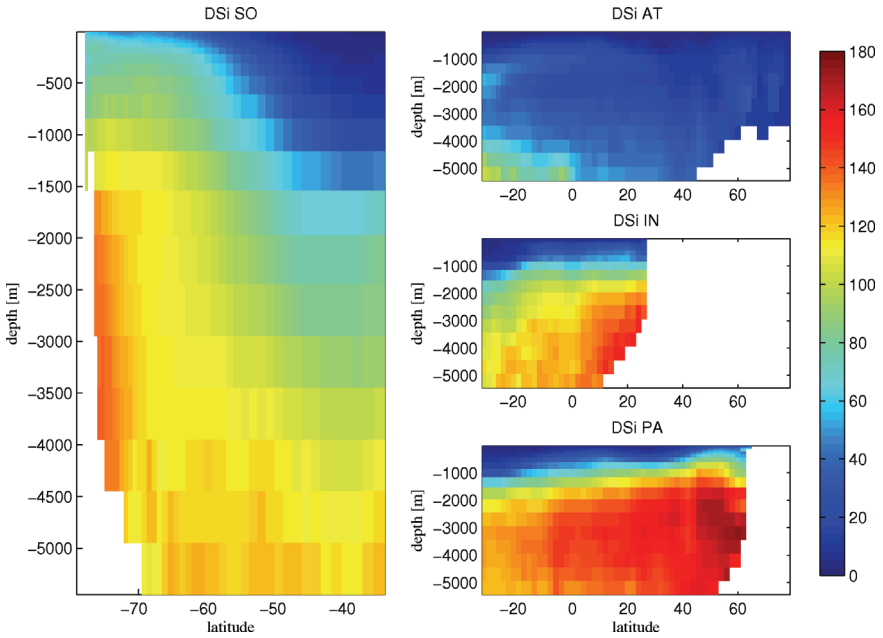

Figure 4.1: *Global distribution of zonally averaged dissolved silicon (DSi) concentrations for each ocean basin* $[\mathrm{mmol\ Si\ m^{-3}}]$ *from Conkright et al. (1994). Southern Ocean (left), Atlantic Ocean (upper right), Indian Ocean (middle right), Pacific Ocean (lower right).*

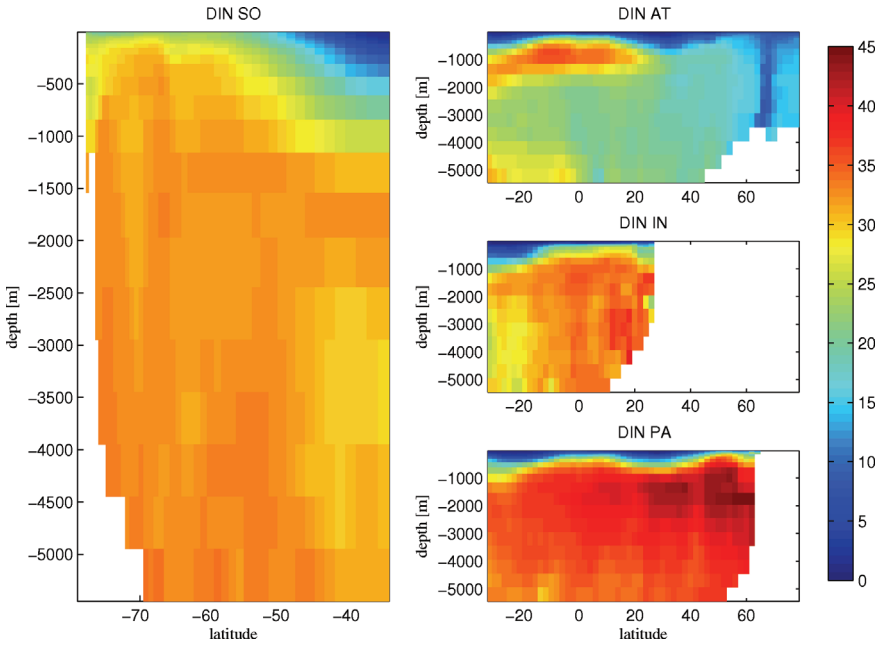

Figure 4.2: *Global distribution of zonally averaged dissolved inorganic nitrogen (DIN) concentrations for each ocean basin* $[\mathrm{mmol\ N\ m^{-3}}]$ *from Conkright et al. (1994). Southern Ocean (left), Atlantic Ocean (upper right), Indian Ocean (middle right), Pacific Ocean (lower right).*

silicon depletion in the Atlantic Ocean and very high concentrations in deep waters of the North Pacific. The concentrating mechanism of silicon towards the deep North Pacific Ocean is explained by the conveyor belt circulation (Broecker and Peng, 1982). Nutrients are depleted in the upper branch of the ocean conveyor during the passage from the North Pacific via the Indian Ocean to the North Atlantic and remineralization of sinking biomass concentrates the nutrients in the deep sea on its way from the deep North Atlantic to the deep North Pacific (Broecker and Peng, 1982). Only the Southern Ocean does not fit into this idealized scenario of the global ocean conveyor belt. Ekman transport towards the north causes strong upwelling and provides fresh nutrients to Southern Ocean surface waters (Sarmiento et al., 2004, 2007). Utilization of nutrients in northwards drifting surface waters and remineralization of sinking biomass in southwards flowing intermediate water leads to nutrient trapping in the Deacon cell and results in an upward shift of high silicon concentrations in the Southern Ocean.

The global distribution of dissolved inorganic nitrogen, DIN, also shows depletion in surface waters and accumulation towards the lower branch of the ocean conveyor belt in the deep North Pacific (Fig. 4.2). However, there are major differences between the global distribution patterns of nitrogen and silicon. Increased deep ocean concentrations of nitrogen reach higher towards the surface ocean than silicon concentrations and also maximum nitrogen concentrations in the North Pacific appear at shallower depths than concentrations of silicon (Figs. 4.1+4.2). Another important difference is the distribution of the two elements in the Atlantic Ocean. While the Atlantic Ocean is strongly depleted with respect to silicon, a tongue of nitrogen rich Antarctic Intermediate Water (AAIW) supplies nitrogen from the Southern Ocean to the main thermocline of the Atlantic Ocean (Fig. 4.2). Subantarctic Mode Water (SAMW) is formed in the Southern Ocean water ring between 40 and 55°S (Sarmiento et al., 2004) and becomes AAIW. Only low concentrations of silicon but high to moderate concentrations of nitrogen can be observed in surface waters of this ocean region and the stoichiometric signal of the SAMW is transmitted to the tracer composition of AAIW. Processes in Southern Ocean surface waters determine the nutrient concentrations in the SAMW formation zone and thus influence nutrient supply to the Atlantic Ocean (Sarmiento et al., 2007).

The Si:N uptake ratio by diatoms increases under iron-limitation (Hutchins and Bruland, 1998; Takeda, 1998; Franck et al., 2000; Leynaert et al., 2004) and the Southern Ocean is the largest iron-limited high-nutrient low-chlorophyll (HNLC) region in the world ocean (Martin et al., 1990). Preferable uptake of silicon over nitrogen by diatoms has therefore been proposed to generate the observed stoichiometric signal in the biogeochemical tracer composition in the SAMW formation zone (Sarmiento et al., 2004, 2007).

This study investigates whether increased Si:N uptake ratios due to iron-limitation can explain the stoichiometric signal in the SAMW and thus follows the hypothesis of Sarmiento et al. (2007). A biogeochemical ocean general circulation model is applied that allows for variable C:N:Si stoichiometry in phytoplankton biomass depending on ambient iron concentrations (Hohn et al., submitted) to investigate the coupling and decoupling of the nitrogen and silicon cycles in the Southern Ocean. Carbon, nitrogen, and silicon are partially decoupled during remineralization which leads to C:N:Si ratios in the exported biomass and the dissolved phase that differ from the Redfield ratios. The model is analysed for the biogeochemical implications of a variable stoichiometry in diatoms and its possible influence on the tracer composition of SAMW and thus nutrient supply to the Atlantic Ocean.

4.2 Model description

The global biogeochemical model consists of an ecosystem and biogeochemical model REcoM_SO (**R**egulated **Eco**system **M**odel for the **S**outhern **O**cean) that is coupled to the ocean general circulation model of the Massachusetts Institute of Technology (MITgcm). REcoM_SO is based on the model by Schartau et al. (2007), which has been extended by inclusion of the biological cycling of the elements Si and Fe (Hohn et al., submitted).

4.2.1 The general circulation model

The MITgcm is set up for the global ocean excluding the Arctic Ocean. The nominal horizontal resolution is 2°. In the northern hemisphere the grid spacing is constant at 2° and the domain is closed at 80°N in order to avoid any difficulties associated with the convergence of latitudes and the pole singularity. In the southern hemisphere, the grid spacing is locally isotropic, that is, the latitude (ϕ) spacing is scaled by $\cos\phi$, giving a resolution of 100 km near 60°S. In the vertical there are 23 layers with thicknesses of 10, 10, 15, 20, 20, 25, 35, 50, 75, 100, 150, 200, 275, 350, 415, 450, and 7×500 m.

Realistic topography is derived from a combination of GEBCO (British Oceanographic Data Center, 2003) and the Smith and Sandwell topography (Smith and Sandwell, 1997; Marks and Smith, 2006). The topography is represented by the model with the help of partial cells (Adcroft et al., 1997).

Horizontal mixing is parameterized following Gent and McWilliams (1990) with a variable diffusivity following Visbeck et al. (1996) with an imposed maximum of 600 $m^2\,s^{-1}$ and Large et al. (1997)'s slope clipping scheme; the horizontal viscosity for harmonic mixing of momentum is flow dependent according to a scheme by Leith (1996). Resulting maximum viscosities are on the order of 5×10^4 $m^2\,s^{-1}$ in western boundary currents and the Antarctic Circumpolar Current. In most parts of the ocean the viscosities are much lower. For vertical mixing, the KPP-scheme (Large et al., 1994) is used. Density is computed from a fully non-linear equation of state (McDougall et al., 2003). No surface restoring to climatology is applied.

A dynamic-thermodynamic sea ice model is coupled to the MITgcm and described in detail by Losch et al., (manuscript in preparation). It is based on the model used in Menemenlis et al. (2005), but involves a new discretization on a C-grid. Stress and buoyancy flux coupling to the ocean is standard.

The ocean model is initialized with temperature and salinity climatology (Levitus et al., 1994*b*; Levitus and Boyer, 1994*b*) and forced by daily wind, air temperature and humidity, downward long and short wave radiation fields, monthly precipitation fields and a constant river run-off field. All fields are part of the climatology ("normal year") of the Common Ocean-ice Reference Experiments (CORE) data set (Large and Yeager, 2004). Wind stress and buoyancy fluxes are computed from bulk formulae (Large and Pond, 1981, 1982; Large and Yeager, 2004).

4.2.2 REcoM_SO

The biogeochemical model calculates the concentrations of phytoplankton and zooplankton biomass, detritus, dissolved organic matter and nutrients in the water column. Phytoplankton biomass is divided into pools of carbon, nitrogen, silicon and chlorophyll (PhyC, PhyN, PhySi, and Chl, respectively). Detritus is also divided into pools of carbon, nitrogen, and silicon (DetC, DetN, DetSi). For zooplankton biomass and dissolved organic matter, only carbon and nitrogen pools (ZooC, ZooN, DOC, DON) are considered. Dissolved inorganic nutrients are divided into nitrogen, silicon and iron

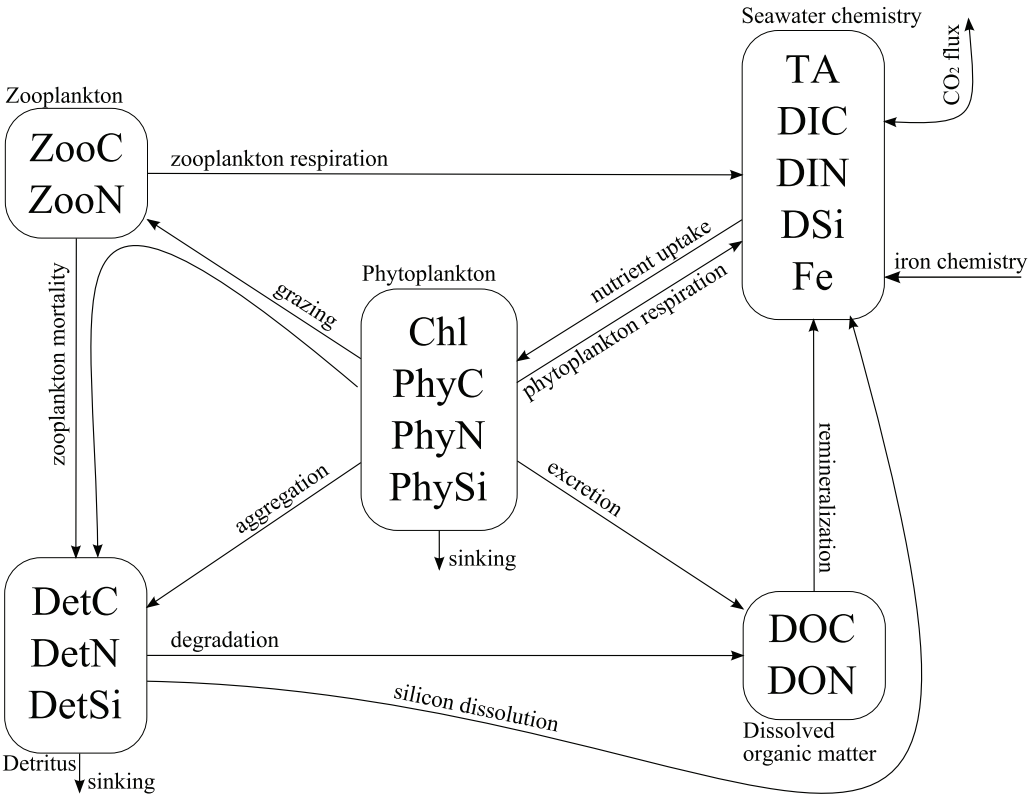

Figure 4.3: *Biogeochemical reservoirs and fluxes in REcoM_SO. Abbreviations are explained in the text.*

(DIN, DSi, Fe). Dissolved inorganic carbon, DIC, and total alkalinity, TA, are included for the caclulation of carbonate chemistry and the air-sea gas-exchange of CO_2. This model setup results in 16 different state variables (Fig. 4.3). All biogeochemical tracers are subject to advection and diffusion by the physical circulation. Additionally, detritus and phytoplankton are allowed to sink vertically in the water column, assuming constant sinking velocities, V_{det} and V_{phy}, respectively. The time development of the biogeochemical tracer concentrations can thus be written as:

$$\frac{\partial}{\partial t}C_x \quad = \quad \nabla \cdot (\kappa \nabla C_x) - \nabla \cdot (\vec{u} C_x) + SMS_x - V_x \frac{\partial C_x}{\partial z} \tag{4.1}$$

where C_x is the concentration of tracer x, $\nabla \cdot (\kappa \nabla C_x)$ stands for diffusion of tracer x, with κ representing the eddy diffusivity resulting from the mixing scheme, $\nabla \cdot (\vec{u} C_x)$ represents advection of tracer x by a three-dimensional velocity field $\vec{u}$, SMS_x are the source minus sink terms of biological processes that are described below, and $V_x \frac{\partial C_x}{\partial z}$ simulates the concentration changes of tracer x due to sinking with the sinking velocity V_x. Sinking velocities are assumed to be zero for all tracers that are not allowed to sink, eliminating the sinking term from the equations.

Seawater chemistry

Disregarding the different chemical properties of nitrate, nitrite, and ammonia, all different chemical forms of dissolved nitrogen are summarized as dissolved inorganic nitrogen, DIN. Nitrogen is one

of the major nutrients for algal growth and is assimilated by phytoplankton. The remineralization of dissolved organic nitrogen, DON, releases fresh DIN to the water column. As nitrate is supposed to be the dominant species, DIN is chemically treated as nitrate. The mass balance of nitrogen is closed in the modelled system. Denitrification, nitrification, and N_2-fixation are not considered as possible sources and sinks for nitrogen in this model approach. The variable V_C^{N} in Equation 4.2 represents the carbon specific nitrogen assimilation rate, ρ_{N} is the remineralization rate of DON.

$$SMS_{DIN} = \rho_{\mathrm{N}} \cdot DO\mathrm{N} - V_{\mathrm{C}}^{\mathrm{N}} \cdot Phy\mathrm{C} \tag{4.2}$$

CO_2 dissolves in seawater as carbonic acid that dissociates to bicarbonate and carbonate. The different chemical forms of carbon in this acid-base system are summarized as dissolved inorganic carbon, DIC. Respiration of phytoplankton and zooplankton releases DIC to the water column, photosynthetic carbon fixation of phytoplankton removes DIC. Remineralisation of dissolved organic carbon, DOC, adds to pelagic respiration. At the sea surface, the DIC pool is connected to the atmosphere via gas exchange of CO_2, $\mathcal{F}^{\mathrm{C}}$, assuming a constant atmospheric pCO_2 of 360 ppmv. The gas exchange attempts to establish equilibrium conditions for the carbonate system between the atmosphere and the surface ocean.

$$\begin{aligned} SMS_{DIC} &= (resp_{phy} - \mathrm{C}_{phot}) \cdot Phy\mathrm{C} + \rho_{\mathrm{C}} \cdot DO\mathrm{C} \\ &+ resp_{zoo} \cdot Zoo\mathrm{C} + \mathcal{F}^{\mathrm{C}} \end{aligned} \tag{4.3}$$

Respiration rates of phytoplankton and zooplankton are $resp_{phy}$ and $resp_{zoo}$, respectively. C_{phot} represents the rate of photosynthetic carbon fixation, ρ_{C} is the remineralization rate of DOC.

Total alkalinity, TA, is needed in the model to determine the speciation of carbon in the acid-base system, which is necessary to calculate the partial pressure of CO_2 in seawater. Total alkalinity is a conservative tracer (e.g. Wolf-Gladrow et al., 2007) and is thus also advected in the general circulation model. The consumption of anions like nitrate and phosphate increases alkalinity and the release decreases alkalinity. Although phosphorus is not regarded in the model, the effect of phosphorus uptake on alkalinity is included in the model, assuming a fixed Redfield ratio for uptake and degradation of N and P.

$$SMS_{TA} = \left(1 + \frac{1}{16}\right) \cdot \left(V_{\mathrm{C}}^{\mathrm{N}} \cdot Phy\mathrm{C} - \rho_{\mathrm{N}} \cdot DO\mathrm{N}\right) \tag{4.4}$$

Analogous to DIN, different chemical forms of silicon are summarized as dissolved silicon, DSi. DSi is released by dissolution of detritus silica and can be taken up by diatoms to build new frustules. $V_{\mathrm{C}}^{\mathrm{Si}}$ is the carbon specific uptake rate of silicon, ω_{Si} is the remineralization rate of detritus silica (see Eq. 4.5). The mass balance for silicon is closed within the modelled system.

$$SMS_{D\mathrm{Si}} = \omega_{\mathrm{Si}} \cdot Det\mathrm{Si} - V_{\mathrm{C}}^{\mathrm{Si}} \cdot Phy\mathrm{C} \tag{4.5}$$

Dissolved iron, Fe, is assumed to be consumed and released together with carbon at a constant Fe:C ratio, $f_{\mathrm{C}}^{\mathrm{Fe}}$. Due to the coupling with the carbon cycle, photosynthesis acts as a sink for iron. Respiration of phytoplankton and zooplankton, as well as remineralization of DOC, resupply iron to the water column. Additionally to biological consumption, iron can also be removed from the water column by adsorption to sinking particles (scavenging). Scavenging is parameterized to be linearly proportional to free iron concentrations, Fe', with a constant scavenging rate, k_{scav}. Organic complexation of iron is implicitly treated in the model following Parekh et al. (2004). Deposition of iron-containing dust, Fe_{dust}, provides new iron to oceanic surface waters.

$$\begin{aligned} SMS_{\mathrm{Fe}} &= f_{\mathrm{C}}^{\mathrm{Fe}} \cdot ((resp_{phy} - \mathrm{C}_{phot}) \cdot Phy\mathrm{C} + \rho_{\mathrm{C}} \cdot DO\mathrm{C} \\ &+ resp_{zoo} \cdot Zoo\mathrm{C}) - k_{scav} \cdot \mathrm{Fe}' + \mathrm{Fe}_{dust} \end{aligned} \tag{4.6}$$

Phytoplankton

Phytoplankton is the key component of the modelled ecosystem. As the phytoplankton community in the Southern Ocean is known to be dominated by diatoms, phytoplankton in the model is treated as diatoms, using the parameterization of Hohn et al. (submitted). The parameterization of diatom physiology is an extension to the model of (Geider et al., 1998) by inclusion of the elements Si and Fe. Phytoplankton biomass is described by seperate pools of carbon, nitrogen, silicon, and chlorophyll, allowing for variable stoichiometry and chlorophyll contents in diatom biomass. Photosynthesis, C_{phot}, nitrogen assimilation, $V_{\mathrm{C}}^{\mathrm{N}}$, and silicon uptake, $V_{\mathrm{C}}^{\mathrm{Si}}$, increase elemental biomass pools and are regulated via intracellular nutrient quotas and extracellular nutrient concentrations (Hohn et al., submitted). Nutrient uptake ratios are thus depending on environmental nutrient concentrations and cellular history. Synthesis of chlorophyll, $\mathcal{S}_{Chl}$, is proportional to the assimilation of nitrogen according to Geider et al. (1998). Degradation, γ_{Chl}, steadily reduces chlorophyll concentrations and simulates the turnover of chlorophyll.

Zooplankton grazing and aggregation with other diatoms and detritus are the major sinks for diatom biomass. The grazing rate and aggregation rate are noted as gr and agg, respectively. Phytoplankton carbon and nitrogen are reduced by excretion of organic molecules, γ_{N} and γ_{C}, that enter the pools of dissolved organic nitrogen and carbon, DON and DOC, respectively. Phytoplankton carbon is additionally reduced by phytoplankton respiration, $resp_{phy}$.

$$SMS_{Phy\mathrm{N}} = V_{\mathrm{C}}^{\mathrm{N}} \cdot Phy\mathrm{C} - (\gamma_{\mathrm{N}} \cdot L_{q\mathrm{NC}}^{min} + agg + gr) \cdot Phy\mathrm{N} \quad (4.7)$$

$$SMS_{Phy\mathrm{C}} = \left(\mathrm{C}_{phot} - resp_{phy} - \gamma_{\mathrm{C}} \cdot L_{q\mathrm{NC}}^{min} - agg - gr\right) \cdot Phy\mathrm{C} \quad (4.8)$$

$$SMS_{Chl} = (\mathcal{S}_{Chl} - \gamma_{Chl} - agg - gr) \cdot Chl \quad (4.9)$$

$$SMS_{Phy\mathrm{Si}} = V_{\mathrm{C}}^{\mathrm{Si}} \cdot Phy\mathrm{C} - (\gamma_{\mathrm{Si}} \cdot L_{q\mathrm{NC}}^{min} + agg + gr) \cdot Phy\mathrm{Si} \quad (4.10)$$

At very low intracellular N:C ratios, we assume metabolic activity of diatoms to be reduced due to the lack of protein. Excretion rates for carbon, nitrogen and silicon are thus multiplied by a regulation factor, $L_{q\mathrm{NC}}^{min}$ (description see below).

Zooplankton

Zooplankton biomass is fed via zooplankton grazing. Secondary production in this model is only based on carbon and nitrogen while phytoplankton silicon, that is ingested via zooplankton grazing, is directly transferred to the detritus pool by production of fecal pellets or sloppy feeding. Sloppy feeding means that only a fraction, g_{eff}, of the grazed phytoplankton is ingested and incorporated into zooplankton biomass. The remaining phytoplankton biomass, $1 - g_{eff}$, is directly transferred to detritus. Zooplankton respiration, $resp_{zoo}$, reduces zooplankton carbon pools and adds to DIC. A quadratic closure term with a constant mortality rate, γ_{zoo}, simulates grazing of higher trophic levels on zooplankton. This simulated zooplankton mortality is a sink for zooplankton biomass and a source of detritus carbon and nitrogen. The life cycle of zooplankton is not considered in this model and zooplankton biomass is assumed to directly respond to biomass uptake via grazing and not to exhibit a time-lag due to reproduction processes.

$$SMS_{Zoo\mathrm{N}} = gr \cdot g_{eff} \cdot Phy\mathrm{N} - \gamma_{zoo} \cdot Zoo\mathrm{N}^2 \quad (4.11)$$

$$SMS_{Zoo\mathrm{C}} = gr \cdot g_{eff} \cdot Phy\mathrm{C} - \gamma_{zoo} \cdot Zoo\mathrm{N} \cdot Zoo\mathrm{C} - resp_{zoo} \cdot Zoo\mathrm{C} \quad (4.12)$$

Detritus

Detritus carbon and nitrogen, DetC and DetN, are produced by aggregation of phytoplankton, with an aggregation rate, agg, zooplankton mortality, and zooplankton grazing (sloppy feeding). Degradation with a constant degradation rate, ω, which is assumed to differ for carbon and nitrogen, converts detritus carbon and nitrogen into the more labile forms of dissolved organic carbon and nitrogen. The silica pool of detritus, DetSi, is exposed to silica dissolution. The sources of detritus silica are zooplankton grazing and aggregation.

$$\begin{aligned} SMS_{Det\mathrm{N}} &= (agg + gr \cdot (1 - g_{eff})) \cdot Phy\mathrm{N} \; + \; \gamma_{zoo} \cdot Zoo\mathrm{N}^2 \\ &- \; \omega_{\mathrm{N}} \cdot Det\mathrm{N} \end{aligned} \tag{4.13}$$

$$\begin{aligned} SMS_{Det\mathrm{C}} &= (agg + gr \cdot (1 - g_{eff})) \cdot Phy\mathrm{C} \; + \; \gamma_{zoo} \cdot Zoo\mathrm{N} \cdot Zoo\mathrm{C} \\ &- \; \omega_{\mathrm{C}} \cdot Det\mathrm{C} \end{aligned} \tag{4.14}$$

$$SMS_{Det\mathrm{Si}} = (agg + gr) \cdot Phy\mathrm{Si} \; - \; \omega_{\mathrm{Si}} \cdot Det\mathrm{Si} \tag{4.15}$$

Dissolved organic matter

Dissolved organic carbon and nitrogen represent labile forms of organic molecules that can be accessed by bacteria. Besides the formation of DOM via degradation of detritus, DOC and DON can also be produced by excretion of organic compounds by diatoms. Bacterial remineralization of dissolved organic matter (DOM) delivers fresh nutrients to the dissolved inorganic pools of DIC, DIN. As iron is assumed to be coupled to the fluxes of carbon with a fixed Fe:C ratio, remineralization of DOC also acts as a source of Fe to the water column. Background concentrations of refractory DOC are not considered in this model. The release of DOC and DON during grazing is also not considered in the model.

$$SMS_{DO\mathrm{N}} = \gamma_{\mathrm{N}} \cdot L_{q\mathrm{NC}}^{min} \cdot Phy\mathrm{N} \; + \; \omega_{\mathrm{N}} \cdot Det\mathrm{N} \; - \; \rho_{\mathrm{N}} \cdot DO\mathrm{N} \tag{4.16}$$

$$SMS_{DO\mathrm{C}} = \gamma_{\mathrm{C}} \cdot L_{q\mathrm{NC}}^{min} \cdot Phy\mathrm{C} \; + \; \omega_{\mathrm{C}} \cdot Det\mathrm{C} \; - \; \rho_{\mathrm{C}} \cdot DO\mathrm{C} \tag{4.17}$$

4.2.3 Processes

The description of the SMS terms contains a number of processes and rates that are themselves functions of other model state variables. The following section describes how the processes, leading to the concentration changes of the modelled biogeochemical tracers as depicted by the arrows in the sketch of the model setup (Fig. 4.3), are parameterized.

Phytoplankton

Phytoplankton related processes, such as nutrient uptake kinetics and metabolic regulations, are described in detail by Hohn et al. (submitted) and will not be recapitulated here completely. Photosynthetic carbon fixation, C_{phot}, is regulated by an Arrhenius function, T_{func}, for temperature dependence (Eppley, 1972), where ambient temperature, T, and reference temperature, T_{ref}, are given in Kelvin. For simplicity, the same temperature dependence is used to regulate respiration and

remineralization rates for carbon and nitrogen, effectively assuming the same metabolic temperature dependency for bacteria and zooplankton.

$$T_{func} = e^{A_E\left(\frac{1}{T}-\frac{1}{T_{ref}}\right)} \tag{4.18}$$

Diatoms release carbon and nitrogen rich organic molecules that accumulate in the water column as dissolved organic matter. Leakage of silicon can also occur when intracellular silicon pools are high. Excretion is parameterized as a linear function of phytoplankton biomass with constant excretion or loss rates, γ, for carbon, nitrogen, and silicon. As each loss rate is multiplied by the respective elemental pool of diatom biomass, excretion of carbon, nitrogen and silicon is directly coupled to internal stoichiometric composition. The excess silicon that is secreted by diatoms again enters the pool of dissolved silicon, $D\mathrm{Si}$. All loss processes are assumed to be regulated by the intracellular N:C ratio, via a function $L^{min}_{q\mathrm{NC}}$, decreasing metabolic activity and thus excretion at very low N:C ratios.

$$L^{min}_{q\mathrm{NC}} = 1 - \exp\left[\sigma \times \left(|q^{min}_{\mathrm{NC}} - q_{\mathrm{NC}}| - \left(q^{min}_{\mathrm{NC}} - q_{\mathrm{NC}}\right)\right)^2\right] \tag{4.19}$$

When organic particles like detritus and phytoplankton cells collide they may stay attached to each other due to surface bound organic molecules, mostly polysaccharides, that act like glue (Mopper et al., 1995). Aggregation of these organic particles can produce very large aggregates that sink out of the water column as marine snow (Engel et al., 2004) and contribute largely to the export flux of organic carbon from surface waters to the deep sea. The higher the concentrations of either detritus or phytoplankton, the more likely these particles collide and the formation of aggregates increases. The aggregation rate is implemented to be linearly dependent on phytoplankton and detritus nitrogen concentrations. The aggregation parameters, Φ_P and Φ_D, represent values for the stickiness of either component which determine the likeliness of aggregation.

$$agg = \Phi_P \cdot Phy\mathrm{N} + \Phi_D \cdot Det\mathrm{N} \tag{4.20}$$

Zooplankton

Predation is a density dependent process (Begon et al., 1998). The consumption of phytoplankton by zooplankton steadily increases with phytoplankton density until a maximum grazing rate is reached (Gentleman et al., 2003). This saturating response can be described by Michaelis-Menten kinetics, or in the context of grazing, the disc equation after Holling (1959). In some cases, when zooplankton organisms decrease their hunting activity at decreasing prey densities or when they switch prey preferences, the grazing rate shows a sigmoidal response to phytoplankton concentrations (Begon et al., 1998). This functional response is assumed in the model and implemented as a Holling type 3 function (Gentleman et al., 2003). It is further assumed that zooplankton organisms do not transfer all ingested biomass into own biomass pools and that only a fraction of the captured prey is ingested during the feeding process (sloppy feeding). This is accounted for by using a factor, g_{eff}, to channel a percentage of the removed phytoplankton biomass between adding to detritus and incorporation of zooplankton biomass.

$$gr = \frac{g_{max} \cdot Phy\mathrm{N}^2}{\varepsilon^2 + Phy\mathrm{N}^2} \cdot Zoo\mathrm{N} \tag{4.21}$$

Mortality of zooplankton can either be caused by natural death or grazing by higher trophic levels on zooplankton. As the ecosystem in this model is supposed to be rather simple, trophic levels higher than first order secondary producers are not considered and the food chain is closed at herbivorous zooplankton. To account for the loss of zooplankton to higher trophic levels, a closure term is implemented that is supposed to simulate grazing pressure by higher trophic predators. The removed zooplankton biomass is transferred to detritus. The mathematical form of the closure term strongly affects the model solution (Edwards and Yool, 2000). Here, a quadratic form is used that is assumed to represent the most realistic form (Edwards and Yool, 2000).

Zooplankton respiration, $resp_{zoo}$, is a loss of zooplankton carbon to DIC. When the C:N ratio of zooplankton biomass exceeds 6.625 $\mathrm{mol\,mol^{-1}}$, zooplankton respiration is assumed to restore the C:N ratio to Redfield by increasing the respiratory loss of carbon. When the zooplankton C:N ratio is lower than Redfield, respiration is simply a temperature dependent constant, r_{zoo}. The temperature dependence is assumed to be the same Arrhenius function, T_{func}, as is used to regulate photosynthetic carbon uptake (Eppley, 1972; Hohn et al., submitted).

$$resp_{zoo} = max\left(r_{zoo} \cdot \left(\frac{Zoo\mathrm{C}}{Zoo\mathrm{N}} - 6.625\right), r_{zoo}\right) \cdot T_{func} \tag{4.22}$$

Detritus

While detritus sinks through the water column, it is decomposed by bacteria and other marine organisms. This process may be called remineralisation when fresh nutrients (minerals) are produced. In this model it is assumed that remineralization of detritus carbon and nitrogen proceeds via an intermediate step, the production of dissolved organic carbon and nitrogen, DOC and DON. Detritus is broken up by larger animals and DON and DOC is released. This process is hereafter called degradation, or decomposition as in terrestrial soil ecology. Degradation of detritus carbon and nitrogen is implemented as a temperature dependent linear function of detritus concentrations assuming that this process only depends on substrate availability and that the abundance of the decomposing organisms linearly increases with detritus concentrations with a constant degradation rate, ω. The decomposition activity of detritus carbon and nitrogen is assumed to increase with temperature using the same temperature dependence as for temperature regulation of photosynthesis and respiration (Eppley, 1972).

Silica directly dissolves from detritus and becomes DSi. Dissolution of silica in seawater has a temperature dependence different from biological remineralization processes of carbon and nitrogen (Erez et al., 1982; Kamatani, 1982) and is parameterized after Gnanadesikan (1999).

$$\omega_{\mathrm{Si}}(T) = 1.32 \cdot 10^{16} \cdot e^{\left(\frac{-11481}{T}\right)} \tag{4.23}$$

Dissolved organic matter

In this model it is assumed that bacteria access DON and DOC and fresh nutrients are released by remineralisation of DON and DOC. Bacterial remineralization is implemented as a linear function analogue to degradation of detritus. Constant remineralization rates for carbon and nitrogen are assumed that are regulated by an Arrhenius function for temperature dependence. Bacterial activity is thus implicitly assumed to be linearly correlating with DOC and DON availability.

Iron chemistry

Iron chemistry in seawater is very complex and a detailed modelling as in Weber et al. (2007) is out of scope for the present model. In this model, iron can either be complexed or freely dissolved. Complexation of iron is caused by strong organic ligands, siderophores, that may be produced by algae or bacteria. Organically complexed iron is here described as $\mathrm{Fe}L$. Inorganic ligands such as OH^-create rather weak complexes, therefore, inorganically complexed iron is combined with freely dissolved iron and treated as free iron, Fe'. Dissolved free iron can adsorb to particles and thus become unavailable for biological consumption. This process is termed scavenging. Complexation by organic ligands prevents scavenging and keeps dissolved iron bioavailable.

Iron chemistry is parameterized after Parekh et al. (2004). Knowing the total iron concentration, Fe, the total ligand concentration, L (which is assumed to be constant), and the stability constant of the $\mathrm{Fe}L$ complex, $K_{\mathrm{Fe}L}$, a quadratic equation can be solved to derive the concentration of freely dissolved iron, Fe'. The net iron sink due to scavenging is then calculated by multiplying Fe' by a constant scavenging rate, k_{scav} (Eq. 4.6).

$$\mathrm{Fe} = \mathrm{Fe}' + \mathrm{Fe}L \tag{4.24}$$

$$L = L' + \mathrm{Fe}L \tag{4.25}$$

$$K_{\mathrm{Fe}L} = \frac{\mathrm{Fe}L}{\mathrm{Fe}' \cdot L'} \tag{4.26}$$

Carbonate chemistry

In the surface layer, atmosphere-ocean gas-exchange of CO_2, $\mathcal{F}^{\mathrm{C}}$, is calculated following Wanninkhof (1992). The pCO_2 in surface waters is determined after Millero (1995), using data of Mehrbach et al. (1973) as refitted by Dickson and Millero (1987). DIC and TA are calculated in the model. The solubility of CO_2 in seawater is calulated according to Weiss and Price (1980). Atmospheric partial pressure of CO_2 is set to 360 μatm as an average value for the time period corresponding to the initial DIC field, neglecting spatial or temporal variability.

4.2.4 Forcing and initialization

Radiation at the ocean surface, $\mathcal{I}_{surf}$, is calculated from long and short wave radiation fields that already consider variable cloud cover. Average photosynthetic available radiation in the water column, PAR_{ave}, is determined by the integral of surface irradiance minus extinction over water depth. The extinction coefficient, κ, is assumed to depend linearly on chlorophyll concentrations in the water column.

$$\kappa = \kappa_w + \kappa_{chl} \cdot CHL \tag{4.27}$$

Total alkalinity and DIC concentrations are initialized from GLODAP (Key et al., 2004). Initial fields of DIN and DSi are taken from the World Ocean Atlas 1994 (Conkright et al., 1994). Biological tracers are initialized with very low concentrations assuming Redfield ratios (Redfield et al., 1963) for the initial stoichiometric composition. Monthly dust deposition fields are taken from the transport model by Tegen and Fung (1994) as a source of iron.

Iron concentrations are initialized with output of the PISCES model (Aumont et al., 2003). Southern Ocean iron concentrations in the first model integrations appeared to be way too high and no iron-limitation of phytoplankton growth appeared in the Southern Ocean. Comparison of iron distribution fields with in situ measurements by De Baar et al. (1999) revealed strong overestimation of Fe concentrations in Southern Ocean deep waters. The PISCES data is therefore corrected towards lower concentrations in the Southern Ocean.

The model is integrated over a period of 10 years to allow for the spin up of the geostrophic and wind driven circulation and to establish a quasi-stable seasonal cycle of the biogeochemical tracers. After 10 years of spinup with a formerly chosen ad-hoc reference parameter set, the fully coupled model is integrated with a new parameter set of the biogeochemical model over a period of 3 years with an internal time step of 30 minutes and a biological time step of 15 minutes. Biogeochemical tracers adapt to the new parameter set and monthly average tracer concentrations and fluxes are analysed for the third year of integration time.

4.2.5 Model parameters

The ecosystem model REcoM_SO contains 45 parameters that have to be defined (Tab. 4.1). Parameters like bacterial remineralization rates or silicon dissolution seem to have some general values and adjust to different ecosystems due to their temperature dependence. Biological model parameters represent the traits of organisms that are adapted to a certain environment and may therefore vary between different ocean regions (Losa et al., 2004). As this study is intended to concentrate on Southern Ocean biogeochemistry, growth parameters of phytoplankton are chosen to represent the traits of organisms that are adapted to the Southern Ocean, as far as information is available.

The parameter values used in the reference run are compiled in Table 4.1. For parameter values of the physical model see Losch et al. (in prep.).

Export

The use of a constant sinking velocity of detritus and a constant degradation rate results in an exponential decrease of the flux of particulate organic carbon, FC, with depth. A typical depth profile of the change of carbon flux with depth has been determined by using data of sediment traps which can be fitted by assuming a power law distribution, the Martin curve (Martin et al., 1987). To derive a typical profile as proposed by Martin et al. (1987) in the model, the sinking velocity or the degradation rate, or both, have to be assumed to change with depth (Eqs. 4.28+4.29). Equations 4.28 and 4.29 are derived from equating the Martin curve and an exponential profile for export production and solving the equation for the sinking velocity of detritus, V_{det}, or the degradation rate, ω_{C}, respectively. Changing sinking velocities with depth have already been observed by Berelson (2002), whereas Ploug et al. (2008) report remarkably constant bacterial remineralization rates. Assuming constant sinking velocities and remineralization rates in the model will lead to deviations between modelled and observed nutrient concentrations, but as the difference between the exponential profile and the Martin curve will mainly affect the carbon flux in the deep sea, and thus the distribution of

nutrients in the deep ocean, the effect will be small in simulations of nutrient distributions in surface waters on decadal time scales. Kriest and Oschlies (2008) also state that applying a constant sinking velocity may still be suitable for decadal model simulations.

$$V_{det} = \frac{\omega_{\mathrm{C}} \cdot z}{ln(100^b) - b \cdot ln(z)} \tag{4.28}$$

$$\omega_{\mathrm{C}} = \frac{-V_{det}}{z} \cdot \big(ln(100^b) - b \cdot ln(z)\big) \tag{4.29}$$

Assuming a constant carbon remineralization rate of $0.15\ \mathrm{d}^{-1}$ (Ploug et al., 2008), Equation 4.28 is used to calculate a sinking velocity of about $50\ \mathrm{m\ d}^{-1}$ at the bottom of the euphotic zone. A particle sinking speed of $50\ \mathrm{m\ d}^{-1}$ has also been proposed by Honjo and Manganini (1993) in the North Atlantic and is therefore considered a reasonable estimate of this parameter.

The degradation rate of nitrogen can be determined by using profiles of C:N ratios in export fluxes. The change of the C:N ratio in sinking detritus indicates different time scales for carbon and nitrogen remineralization. Remineralization of nitrogen is always about 10% faster than remineralization of carbon.

Dissolution of biogenic silica is parameterized after Gnanadesikan (1999) following Equation 4.23. This parameterization results in silicon dissolution rates between 0.01 d^{-1} and 0.25 d^{-1} (at temperatures of 0 and 25°C) and confirms differences in time scales between the remineralization of carbon and silicon as discussed by Ragueneau et al. (2002).

Biomass Production

The model is most sensitive to changes of parameters that directly affect phytoplankton biomass. These parameters are manually tuned to reproduce chlorophyll concentrations at JGOFS station KERFIX (as discussed below). The timing of the bloom development depends on the light sensitivity of diatom growth and is tuned by the parameter α_{Chl}. The work by Bracher et al. (1999) indicates very low values for α_{Chl} in the Southern Ocean. Maximum and minimum chlorophyll concentrations can be adjusted by changing the maximum carbon fixation rate, P_{cm}, and the maximum grazing rate of zooplankton, g_{max}. The parameter γ_{zoo}, that determines zooplankton mortality in the zooplankton closure term, also determines background concentrations of zooplankton and thus absolute biomass of phytoplankton in the model.

4.3 Results

4.3.1 Parameter studies

More than a hundred model runs have been performed to find a set of parameter values with which the model reasonably reproduces surface chlorophyll concentrations as estimated by SeaWiFS (Yoder and Kennelly, 2003) and in-situ measured chlorophyll concentrations at JGOFS station KERFIX (Kleypas and Doney, 2001). Taylor diagrams (Taylor, 2001) are produced to visually compare model results with observations. For this purpose, the standard deviations of the modelled signals and the reference dataset, as well as the correlations and root mean squared deviations (RMSD) between model runs and reference data are calculated as described in Taylor (2001).

The Taylor diagrams (Figs. 4.4-4.8) show standard deviation of the datasets on the x and y axis. The correlation between reference data and model output is given by the angle with the x axis (in

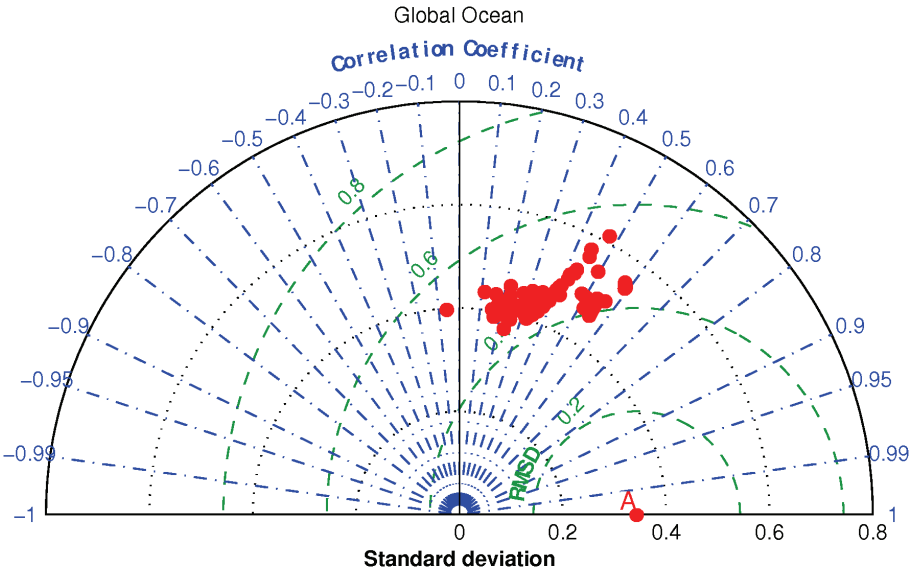

Figure 4.4: *Taylor diagram for 82 model runs with different parameter sets. Reference data (A) in this diagram is the spatial and temporal distribution of surface chlorophyll in the global ocean according to SeaWiFS.*

blue). The root mean squared deviation (RMSD) between the model output and reference data (A) is given by the distance to the reference data (in green).

The agreement of model results with observations strongly depends on the set of data that is considered as reference. Model results are compared to four different sets of reference data. In Figure 4.4, the reference data for model comparison is a monthly climatology of SeaWiFS data of the years 1994-2004 (Yoder and Kennelly, 2003), which has been interpolated to the applied model

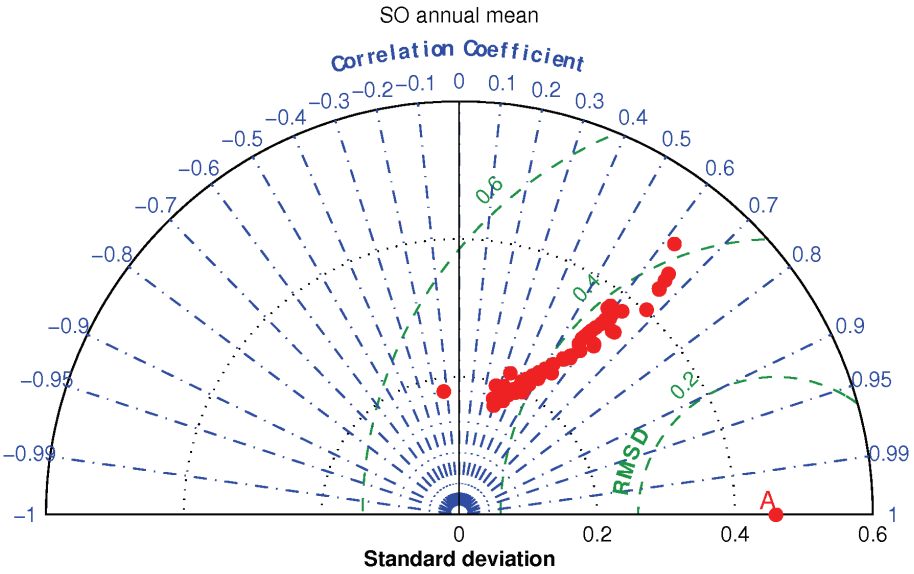

Figure 4.5: *Taylor diagram for 82 model runs with different parameter sets. Reference data (A) is the geographical distribution of annual average surface chlorophyll in the Southern Ocean according to SeaWiFS.*

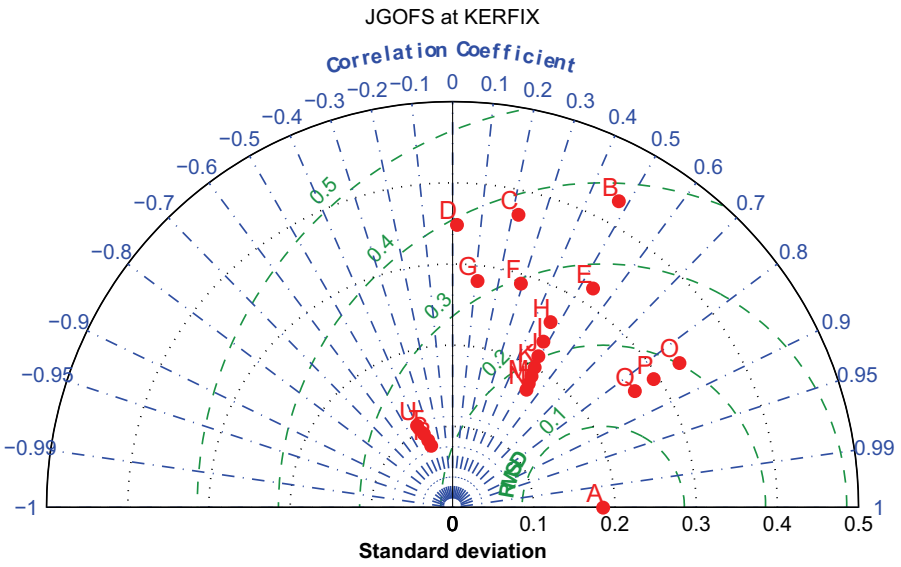

Figure 4.6: *Taylor plot for a collection of 20 model runs with different parameter sets (Table 4.2). Reference data (A) in this diagram are surface chlorophyll concentrations as observed at JGOFS station KERFIX (Fig. 4.9 upper left).*

grid. The data is geographically distributed over the global ocean and includes the time development of the geographically distributed signal. As chlorophyll is logarithmically distributed over the ocean (Campbell, 1995), reference and model data are log-transformed before calculation of statistics.

Model results of all performed model runs reach maximum correlation with the global SeaWiFS climatology of about 0.6 but can even exhibit negative correlation (Fig. 4.4). The model run showing negative correlation with the global SeaWiFS climatology has used parameter values as applied for large phytoplankton in the model by Moore et al. (2004). Standard deviations of modelled chlorophyll concentrations in the global ocean are in general higher than in the SeaWiFS data.

Figure 4.5 uses the same dataset as reference as in Figure 4.4 but cut at 45°S to exclude every data except in the Southern Ocean. The data is then averaged over the annual cycle to account for the geographical distribution only and again log-transformed. The arrangement of model runs in the diagram seems to follow a linear or slightly curved progression. Correlation of model results with the Southern Ocean annual mean chlorophyll distribution is slightly better than with the global dataset and modelled chlorophyll concentrations also show smaller RMSD values than in the global ocean (Fig. 4.5).

In Figure 4.6, in-situ measured chlorophyll concentrations at JGOFS station KERFIX are taken as reference data. The JGOFS data has been converted to a monthly climatology. Chlorophyll concentrations of the model runs are taken from the surface layer of the grid cell that is closest to the KERFIX station (50.4°S, 68.25°E). Model and reference data are compared without further transformation.

Model runs show much larger scatter in the Taylor diagram when only the annual signal of chlorophyll concentrations at JGOFS station KERFIX is taken for comparison. A collection of 20 model runs is chosen in the next Taylor diagrams to document the sensitivity of the model agreement to the data for linear changes of some important parameters and to identify a model run that is chosen as reference run and taken for further analysis. Variations in parameter values of the chosen model runs

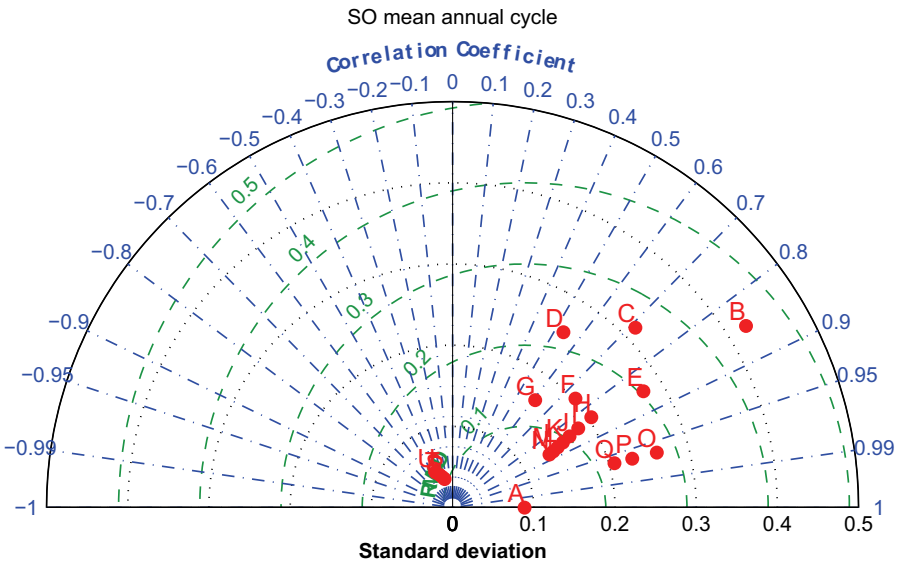

Figure 4.7: *Taylor plot for a collection of 20 model runs with different parameter sets (Table 4.2). The annual cycle of the geographically averaged surface chlorophyll in the Southern Ocean as presented in the lower right panel of Figure 4.9 is taken as reference data (A) in this diagram.*

are compiled in Table 4.2.

In the series B-D and E-G the parameter α_{Chl} has been changed in linear intervals. The positions of the model runs in the Taylor diagram indicate that decreasing α_{Chl} improves the correlation between

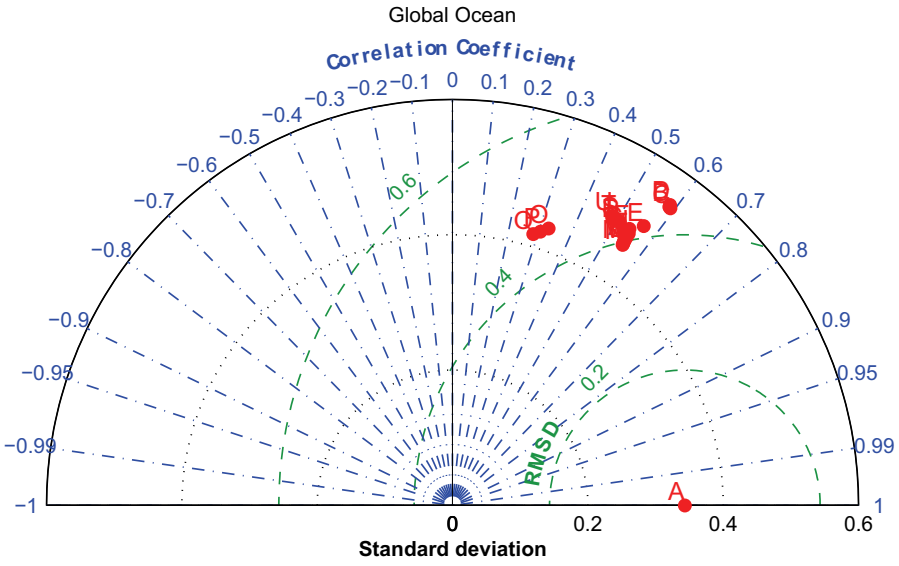

Figure 4.8: *Taylor plot for a collection of 20 model runs with different parameter sets (Table 4.2). Reference data (A) in this diagram is the spatial and temporal distribution of surface chlorophyll in the global ocean according to SeaWiFS.*

model results and KERFIX chlorophyll and also increase the standard deviation in the modelled signal. The timing of the beginning of the phytoplankton bloom depends on the parameter value of α_{Chl} as it determines the light intensity at which photosynthesis exceeds carbon losses. Higher values of α_{Chl} lead to very early phytoplankton growth and even to an anticorrelation with the observed signal when the bloom period already starts in winter at very low irradiance levels and ends due to nutrient depletion and increased zooplankton grazing. From the interpretion of the model response to changes in α_{Chl}, relatively low values have to be chosen to adequately represent the time development of chlorophyll concentrations in the Southern Ocean as has also been proposed by Bracher et al. (1999).

Changes in the maximum grazing rate, g_{max}, in series H-M and O-Q depict improvements of the RMSD values with increasing grazing pressure due to higher g_{max}. In most model runs, chlorophyll concentrations are higher than in the observations. Increasing the grazing pressure on phytoplankton leads to a lower amplitude of the chlorophyll signal and almost no changes in the correlation with the observations (Fig. 4.6). The response of the model solution to changes in the maximum grazing rate indicates that very high values for g_{max} are favoured in the Southern Ocean.

In the series of models runs R-U, the half-saturation constant for iron-limitation, K_{Fe}, was changed to test whether the anticorrelation of model runs R with the observations were caused by too little response to changes in ambient iron concentrations. An increase in K_{Fe} lead to even stronger anticorrelation and an increase in the annual amplitude, just the opposite of the expected. The anticorrelation in these model runs was in fact caused by the high value for α_{Chl} that lead to a very early beginning of the diatom bloom and the increasing anticorrelation is explained by an early breakdown of diatom biomass due to earlier limitation by low iron concentrations.

In Figure 4.7, the climatology of SeaWiFS data as is used in Figure 4.4 is again cut at 45°S to consider only data from the Southern Ocean. The data is then geographically averaged to exclude the geographical information of the chlorophyll distribution and derive a time development only of the Southern Ocean average chlorophyll signal. Again, the temporal signals are compared between reference and model without log-transformation. In this Taylor diagram (Fig. 4.7) the reference data shows lower standard deviation and thus a lower amplitude in the annual chlorophyll signal. The model runs show better correlations with the Southern Ocean mean annual chlorophyll cycle than with the KERFIX data. The response to changes in the parameter values remains the same.

Figures 4.4 and 4.5 have already indicated that there are differences between comparing the model to global chlorophyll distributions and chlorophyll patterns in the Southern Ocean. Figure 4.8 again uses the global chlorophyll climatology as in Figure 4.4 but shows the chosen 20 model runs as in Figures 4.6 and 4.7. The model runs O-Q that had best correlations with KERFIX data and the SO mean annual cycle exhibit lowest correlations with the global chlorophyll pattern. This phenomenon has been observed several times during the analysis of more than hundered model runs, in which parameter sets that lead to good correlation in the Southern Ocean showed even lower correlation with the global pattern. From this response one could argue for two different or independent model solutions for the Southern Ocean ecosystems and the rest of the ocean that differ at least in the parameter value of α_{Chl} for the light sensitivity of photosynthesis.

4.3.2 Reference run

The model run M is chosen as reference run for further model analysis. Even though the modelled chlorophyll signal in this model run does not correlate too well with the in-situ data at station KERFIX (Fig. 4.6), it correlates well with the mean annual cycle in the geographically averaged Southern Ocean and shows lowest RMSD values when compared to the SO annual mean chlorophyll signal

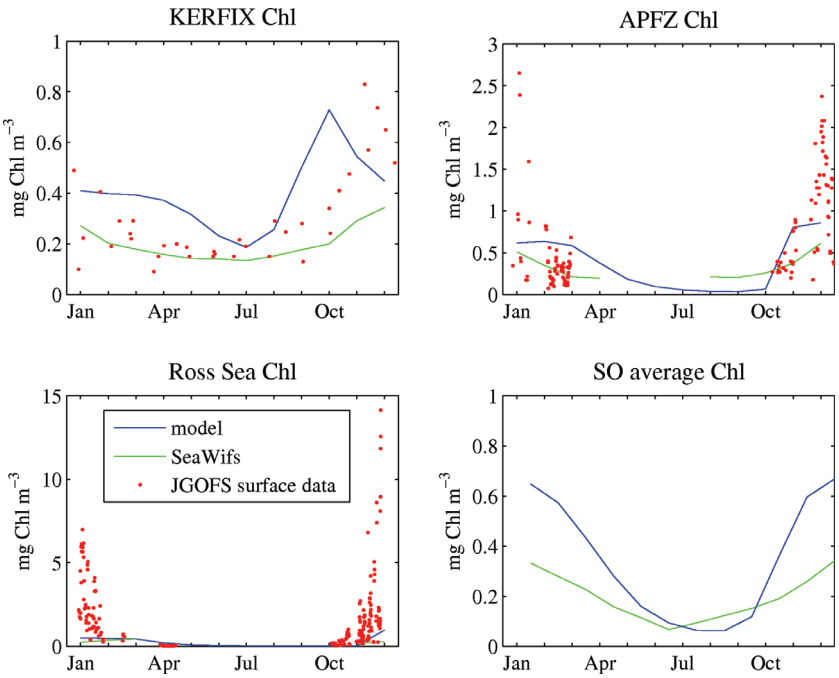

Figure 4.9: *Surface chlorophyll concentrations at JGOFS Station KERFIX (50.4°S, 68.25°E), in the Antarctic Polar Front Zone (APFZ, 60-70°S, 165-175°W), in the Ross Sea (70-76°S, 168°E-175°W), and geographically averaged over the whole Southern Ocean (south of 45°S). Green=SeaWiFS chlorophyll, red=JGOFS data, blue=model simulation.*

(Fig. 4.7).

The time development of surface chlorophyll concentrations at three Southern Ocean JGOFS stations is shown in Figure 4.9 (upper left and right and lower left panels) and for the whole geographically averaged Southern Ocean south of 45°S (lower right panel). Surface chlorophyll concentrations from the in-situ JGOFS data are plotted as red dots, model results and SeaWiFS estimates of the nearest grid cell to the in-situ data are drawn as blue and green lines, respectively. The lower right panel shows only model results and SeaWiFS data.

The beginning of the spring bloom at KERFIX appears too early in the model run and maximum chlorophyll concentrations are reached about one month earlier than observed in the in-situ data. The amplitude of the chlorophyll signal is in good agreement with the observations but much higher than what is derived from SeaWiFS data. The deviation between the JGOFS and SeaWiFS data indicates a general underestimation of chlorophyll concentrations by the remote sensing estimates in the Southern Ocean. The decrease of chlorophyll concentrations at the end of the spring bloom is not as steep in the reference run as in the JGOFS data, leading to an overestimation of chlorophyll at KERFIX in the period around April. Modelled winter chlorophyll concentrations descend to 0.2 $\mathrm{mg\ Chl\ m^{-3}}$ and agree well with the observations.

The data of the Antarctic Polar Frontal Zone (APFZ) in the JGOFS dataset comprises a region from 60 to 70°S and 165 to 175 °W. For comparison of the in-situ data with SeaWiFS and model results, surface chlorophyll concentrations in the grid cell nearest to 65°S and 170°W are chosen. The JGOFS data at the APFZ and in the Ross Sea only comprises chlorophyll concentrations during the blooming period. SeaWiFS data lack winter chlorophyll concentrations due to clouds, polar night or ice cover in austral winter. The model seems to underestimate winter chlorophyll concentrations at

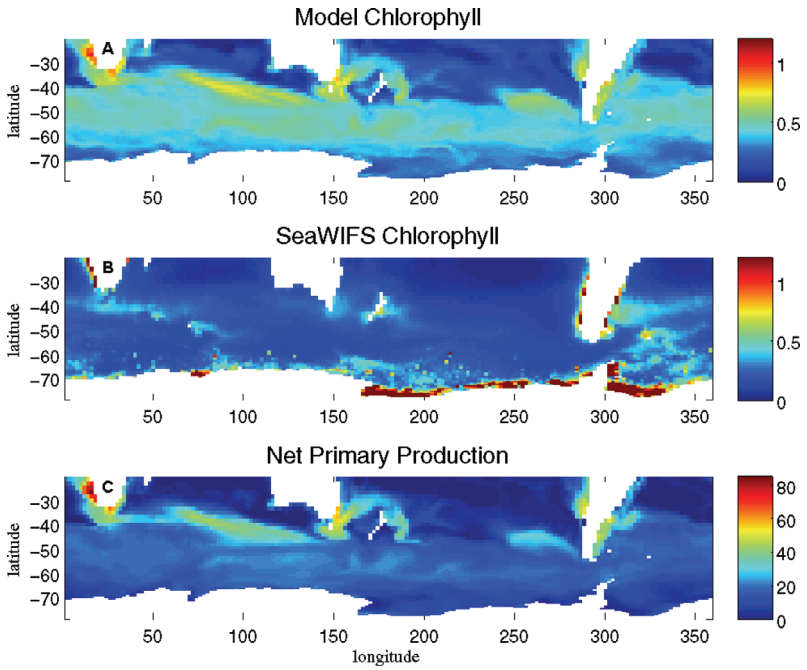

Figure 4.10: **A** *Annually averaged upper layer modelled chlorophyll distribution in* $[\mathrm{mg\ Chl\ m^{-3}}]$. **B** *Annually averaged SeaWIFS chlorophyll distribution in* $[\mathrm{mg\ Chl\ m^{-3}}]$. **C** *Annually averaged modelled Net Primary Production in* $[\mathrm{g\ C\ m^{-2}\ d^{-1}}]$.

the APFZ but captures the beginning of the phytoplankton bloom (Fig. 4.9 upper right). The JGOFS data shows very large scatter in the data and also very large maximum chlorophyll concentrations which are most probably caused by spatial variation over a larger ocean region.

In the Ross Sea (Fig. 4.9 lower left panel), model results and SeaWiFS data underestimate the high chlorophyll concentrations during the short growth period after the retreat of the sea ice, as measured during the JGOFS project. In the model, the Ross Sea exhibits relatively strong ice cover (not shown) which may explain the underestimation of chlorophyll in this region.

When surface chlorophyll concentrations are averaged over the complete Southern Ocean south of 45°S, the time development of average surface chlorophyll shows very good correlation between the reference run and SeaWiFS data (Fig. 4.9 lower right panel). However, the model overestimates surface chlorophyll concentrations with respect to SeaWiFS during the growth period as already shown in the other panels of Figure 4.9.

The distribution pattern of the annual average surface chlorophyll concentrations in Southern Ocean waters again shows relatively high chlorophyll concentrations in the model run (Fig. 4.10A) with respect to the SeaWiFS data (Fig. 4.10B). The annual average chlorophyll distribution in the SeaWiFS data (Fig. 4.10B) is strongly biased towards the little available data in the marginal ice zone in austral summer and highlights the high chlorophyll concentrations after the retreat of the sea ice. The model also captures the development of these ice edge blooms but the high chlorophyll concentrations in the marginal ice zone are averaged out by the low chlorophyll concentrations underneath the sea ice in austral winter.

The model develops increased chlorophyll concentrations around South Africa, in the Agulhas return current, south of Australia and around New Zealand, and around South America (Fig. 4.10A).

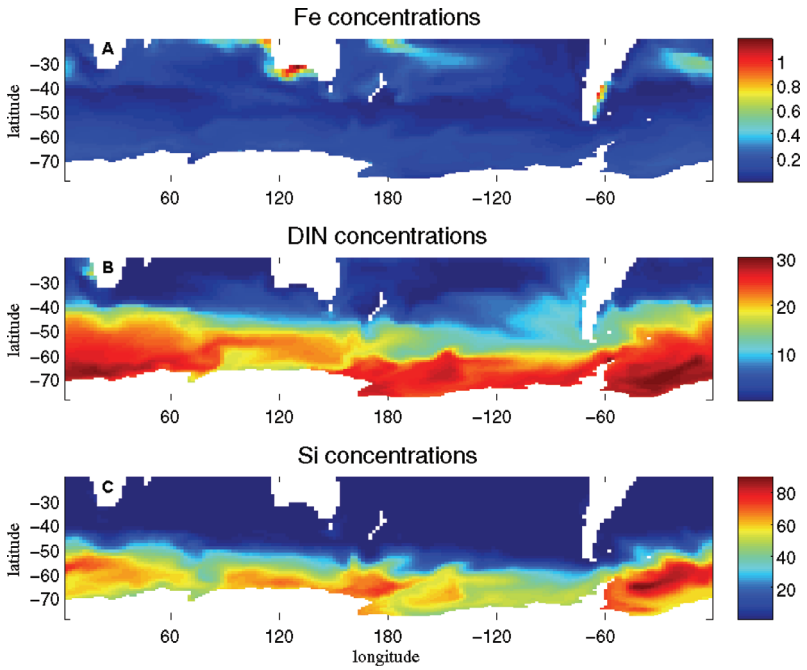

Figure 4.11: *Surface distribution of annual mean nutrient concentrations.* **A** *Fe in* $[\mu\mathrm{mol\ m^{-3}}]$. **B** *DIN in* $[\mathrm{mmol\ m^{-3}}]$. **C** *DSi in* $[\mathrm{mmol\ m^{-3}}]$.

These regions also show increased chlorophyll concentrations in the SeaWiFS data (Fig. 4.10B) but the model (strongly) overestimates chlorophyll concentrations, especially in the open ocean regions in the Antarctic circumpolar current (ACC). Despite overestimating surface chlorophyll concentrations, the reference run exhibits rather low rates of primary production, in the Southern Ocean and also in the rest of the global ocean. As the model considers only one phytoplankton group and this group depends on the availability of silicon for growth, it is not expected that the model reaches net primary production rates of 35-70 $\mathrm{Pg\ C\ a^{-1}}$ as proposed for the whole phytoplankton of the global ocean (Carr et al., 2006). Anyway, global gross primary production in the reference run is only 13.4 $\mathrm{Pg\ C\ a^{-1}}$ which is lower than what is assumed for the contribution of diatoms to global primary production of at least 15-26 $\mathrm{Pg\ C\ a^{-1}}$ (Raven and Waite, 2004). Southern Ocean gross primary production (south of 50°S) is 1.17 $\mathrm{Pg\ C\ a^{-1}}$ in the model run, compared to an estimate of 1.1 $\mathrm{Pg\ C\ a^{-1}}$ new production (Pollard et al., 2006).

Figure 4.11A shows the geographical distribution of annual average surface iron concentrations in the Southern Ocean in $\mu\mathrm{mol\ Fe\ m^{-3}}$. Panels B and C in Figure 4.11 show the annual average surface concentrations of DIN and DSI in $\mathrm{mmol\ N\ m^{-3}}$ and $\mathrm{mmol\ Si\ m^{-3}}$, respectively. After three years of model integration, modelled nutrient concentrations are still relatively close to initial conditions. High iron concentrations occur around Australia and east of South America due to input of iron containing dust (Fig. 4.11A). The rest of the Southern Ocean, especially in the open ocean, shows only low iron concentrations.

DIN concentrations exhibit a strong gradient at the 8°isotherm and reach up to 30 $\mathrm{mmol\ DIN\ m^{-3}}$ in the Weddel Sea and in the Ross Sea (Fig. 4.11B). Dissolved silicon concentrations are also highest in the Weddel Sea and exceed 80 $\mathrm{mmol\ DSi\ m^{-3}}$ (Fig. 4.11C). Dissolved silicon concentrations decrease towards the north with a strong gradient at the 2°C isotherm. On a 2×2°resolution, no

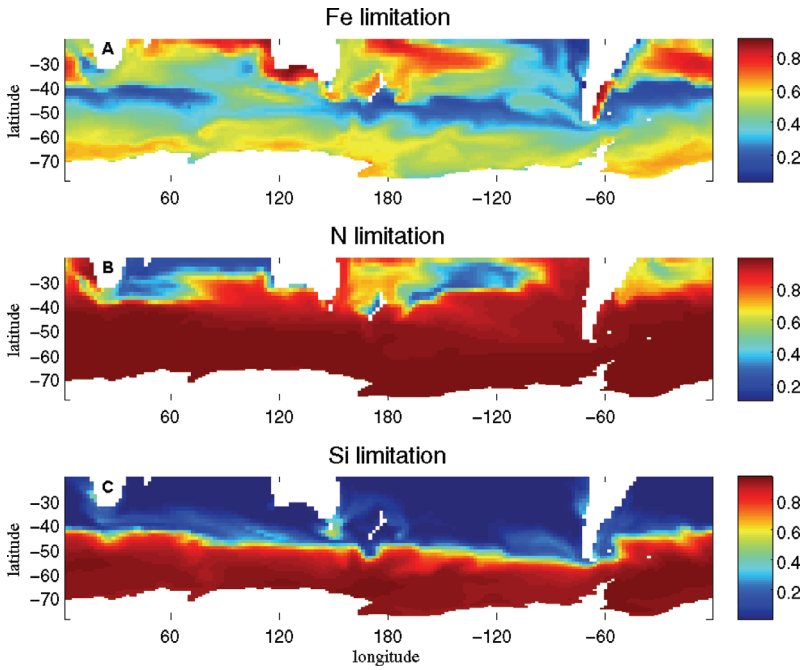

Figure 4.12: *Nutrient limitation of diatom growth.* **A** *Fe limitation.* **B** *N limitation.* **C** *Si limitation. A value of 1 means no limitation at all, a value of 0 indicates nutrient-limitation. All values are annual mean.*

sharp frontal systems are expected to develop. Nevertheless, we will hereafter refer to the 2°and 8°C isotherms as the Polar Front and Subtropical Front, respectively.

The distribution of nutrients strongly affects the growth of diatoms in the Southern Ocean. Figure 4.12 shows the geographical distribution of the value of the limitation term of nutrient uptake for iron, nitrogen and silicon. Limitation of nutrient uptake is defined here as a normalized Michaelis-Menten term $\frac{[X]}{K_X+[X]}$, with K_X representing the half-saturation constant for nutrient uptake and $[X]$ the concentration of the nutrient X. A value of 0 indicates absolute limitation of nutrient uptake, a value of 1 signifies non-limited uptake.

North of the subtropical front, the algae are limited by the supply of nitrogen. South of this front, enough nitrogen is available to promote algal growth (Fig. 4.12B). The subantarctic front divides the Southern Ocean into a silicon limited region, north of the front, and an area with high silicon concentrations that support diatom growth in the south (Fig. 4.12C). The distribution of silicon and nitrogen concentrations divides the Southern Ocean into three biogeochemical regimes: 1. nitrogen-limited and silicon-limited, 2. nitrogen-limited but not silicon-limited, and 3. neither limited by nitrogen or silicon.

In addition to the limitation by nitrogen or silicon supply, the supply of iron to the Southern Ocean via dust input and upwelling and the resulting iron concentrations in surface waters (see Fig. 4.11A) also lead to promotion or limitation of diatom growth, which is shown in Figure 4.12A. The waters around Australia and at the south-east tip of South America can be shown to be not limited by low iron concentrations in the reference run, as well as the waters close to the Antarcic continent. In the ACC, a zonal band of iron-limitation can be recognized whose position that corresponds well with the transition between silicon-limited and silicon replete waters.

Figure 4.13 shows the annual average molar C:N:Si ratios in diatom biomass in Southern Ocean surface waters. Limitation of diatom growth by different nutrients affects the stoichiometric compo-

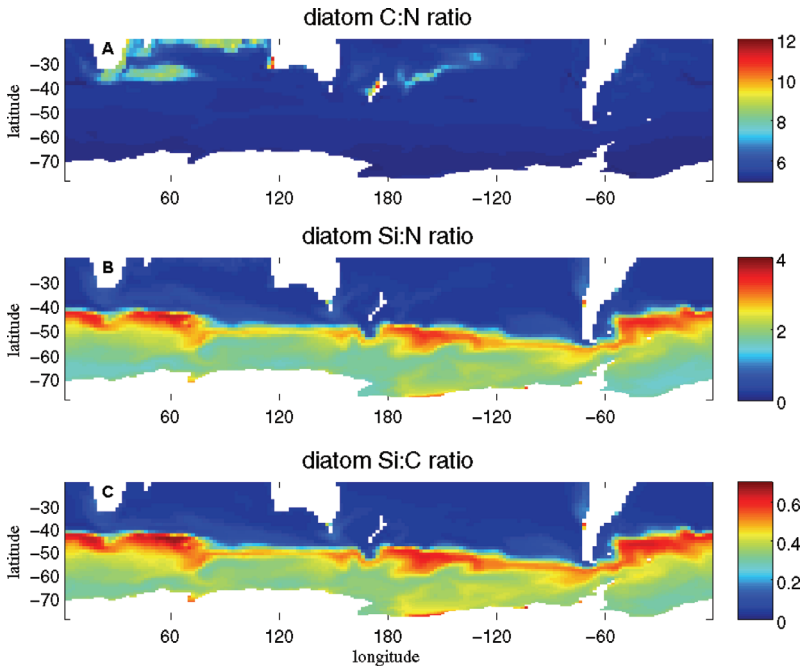

Figure 4.13: *Annual average molar ratios of C:N:Si in diatom biomass.* **A** *C:N.* **B** *Si:N.* **C** *Si:C.*

sition of the diatom cells. In the applied parameterization of diatom growth (Hohn et al., submitted), only the iron-limitation term directly limits diatom growth. The Michaelis-Menten term for nitrogen or silicon only limits the uptake of the respective nutrient and diatom growth is then indirectly affected by changes the intracellular stoichiometric composition.

When diatoms are limited for the uptake of nitrogen, they exhibit increased carbon to nitrogen (C:N) ratios as the uptake of nitrogen is suppressed but photosynthetic carbon fixation can still occur (Geider et al., 1998; Schartau et al., 2007). Increased C:N ratios only occur in nitrogen-limited subtropical waters in the Indian Ocean and in the Pacific. In the remaining Southern Ocean waters, C:N ratios in phytoplankton biomass are rather low at about 5.5 $\mathrm{mol\ C\ (mol\ N)^{-1}}$.

At iron limitation, photosynthetic carbon fixation and nitrogen assimilations decrease as iron is needed in the photosynthetic apparatus and in the enzyme nitrate reductase. As iron is not directly involved in the silicon metabolism, the silicon to carbon and silicon to nitrogen uptake ratios increase. Increased Si:N and Si:C biomass ratio in diatoms can be observed in the iron-limited zonal band in the ACC (Fig. 4.13B+C). Elevated Si:N and Si:C uptake ratios in the iron-limited regions north of the subtropical front are prevented by silicon-limitation (see Fig. 4.12C).

Figure 4.14 shows the geographical pattern of DIN and DSi drawdown in the Southern Ocean (Fig.4.14A+B) and also the resulting Si:N drawdown ratio (Fig. 4.14C). The modelled pattern of the Si:N drawdown ratio in the Southern Ocean (Fig. 4.14C) is much more heterogeneous than the distribution of the Si:N ratio in diatom biomass and also exhibits a higher amplitude. Drawdown of DIN and DSi is defined in the model as maximum concentrations minus minimum concentrations during an annual cycle. The drawdown of silicon and nitrogen (Fig. 4.14A+B) thus also reflects concentration changes due to physical reasons rather than only the biological nutrient uptake by diatoms.

The stoichiometric composition of diatom biomass in the surface ocean is also transmitted into the

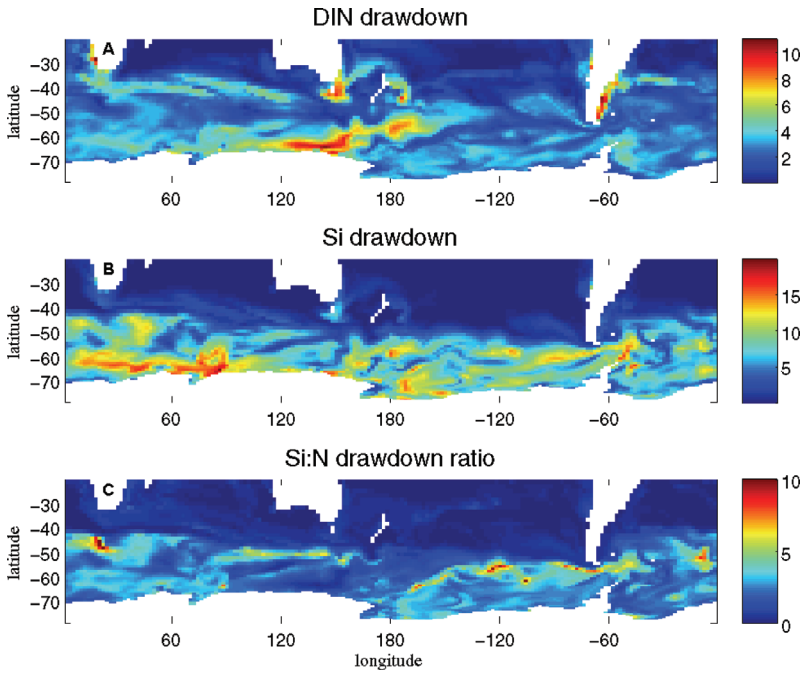

Figure 4.14: *Nutrient drawdown.* **A** *DIN drawdown in* [mmol DIN m^{-3}]. **B** *DSi drawdown in* [mmol DSi m^{-3}]. **C** *Molar Si:N drawdown ratio in* [mol Si mol DIN^{-1}].

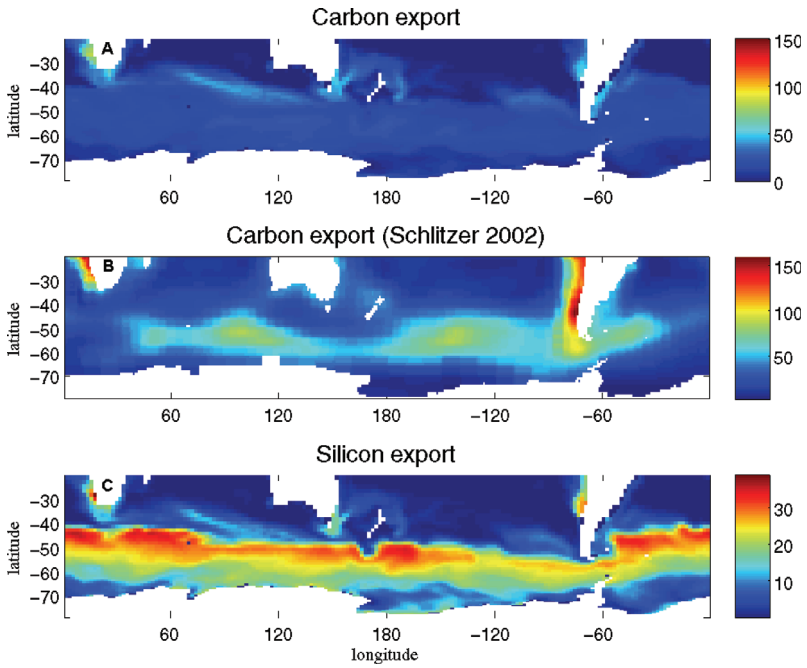

Figure 4.15: *Export production.* **A** *Modelled Carbon export in* [g C m^{-2} a^{-1}]. **B** *Carbon export in* [g C m^{-2} a^{-1}] *according to Schlitzer (2002).* **C** *Modelled Silicon export in* [g Si m^{-2} a^{-1}].

export of organic matter into the deep ocean (not shown). Pollard et al. (2006) calculate the export of nitrogen in Southern Ocean waters south of 50°S to be about 14 $\mathrm{Tmol\ N\ a^{-1}}$ and silicon export of about 51 $\mathrm{Tmol\ Si\ a^{-1}}$. These values also indicate increased Si:N ratios of about 3.6 on average in Southern Ocean export. Assuming the Redfield ratio for C:N ratios, Pollard et al. (2006) estimate carbon export to be about 1.1 $\mathrm{Pg\ C\ a^{-1}}$ in the Southern Ocean south of 50°S, which agrees well with the estimate of 1.0 $\mathrm{Pg\ C\ a^{-1}}$ by Schlitzer (2002). In our reference run, Southern Ocean export production only reaches 0.61 $\mathrm{Pg\ C\ a^{-1}}$ and also global export production of about 5.5 $\mathrm{Pg\ C\ a^{-1}}$ is much lower than what other estimates propose (Schlitzer, 2002).

In general, modelled carbon export production shows a similar geographical pattern as modelled Primary Production (Fig. 4.10C). The pattern of carbon export at about 100 m depth exhibits areas with slightly increased export in open ocean regions between Africa and Australia, in the South Pacific, and downstream of South America (Fig. 4.15A).

The model generates a closed belt of strong opal export around Antarctica and also increased silicon export at the South American and African West coast. The zonal band of increased opal export is congruent with the region that also exhibits iron-limitation of diatom growth (Fig. 4.12A) and thus increased Si:C and Si:N ratios in diatom biomass (Fig. 4.13B+C).

Opal export in the model run is about 23.5 $\mathrm{Tmol\ Si\ a^{-1}}$ in the Southern Ocean, which is only half of what is proposed by Pollard et al. (2006). Modelled nitrogen export of 9.2 $\mathrm{Tmol\ N\ a^{-1}}$ is also lower than estimated by Pollard et al. (2006) and the average Si:N export ratio in the Southern Ocean results in 2.5 $\mathrm{mol\ mol^{-1}}$.

4.3.3 Decoupling of silicon and nitrogen cycles

The molar ratio of total silicon over total nitrogen can be shown to increase from the surface ocean to the deep (Fig. 4.16). This increase is primarily caused by different time scales of silicon and nitrogen remineralization. The different temperature dependence of silicon dissolution and nitrogen remineralization causes slower dissolution of silicon compared to nitrogen remineralization in deep ocean waters and deeper penetration of biogenic silica into the deep ocean (compare Figs. 4.1 and 4.2). The global distribution of the Si:N ratio shows a pattern similar to dissolved silicon concentrations, increasing towards the deep North Pacific and an upward shift of constant Si:N isolines in the Southern Ocean (Fig. 4.16). Also in the North Pacific Ocean, a slight upward shift of Si:N isolines can be recognized. The high concentrations of silicon in Southern Ocean surface waters can be explained by the combination of production of biogenic silica in surface waters, remineralization of sinking BSi, and upwelling of silicon rich waters, leading to an accumulating mechanism for total silicon and other nutrients in the Southern Ocean. As the utilization of Si and N by diatoms normally appears at a molar ratio of about 1 (Brzezinski, 1985), the accumulating mechanism for nutrients cannot explain the increased Si:N ratios in the Southern Ocean surface waters. The upward shift in Si:N isolines is most likely the result of the increased Si:N uptake ratios in iron-limited Southern Ocean surface waters, that have been shown in the last section.

To unravel the effect of iron concentrations on silicon and nitrogen fluxes, two model runs are compared. The first run (Run1) is the reference run as presented before, that has a variable Si:N ratio, changing with the degree of iron-limitation. In the second run (Run2), the parameter q_{SiC}^{max} is set to 0.204 $\mathrm{mol\ Si\ mol\ C^{-1}}$, leading to a maximum Si:N uptake ratio of about 1, which is not affected by iron concentrations at all. The difference of the Si:N ratio in the exported biomass between both model runs is shown in Figure 4.17. The model generates increased Si:N biomass ratios in iron-limited surface waters of the Southern Ocean and the North Pacific (Fig. 4.17). Si:N ratios in the exported biomass exhibit elevated values in the Deacon cell and in the upwelling region in the

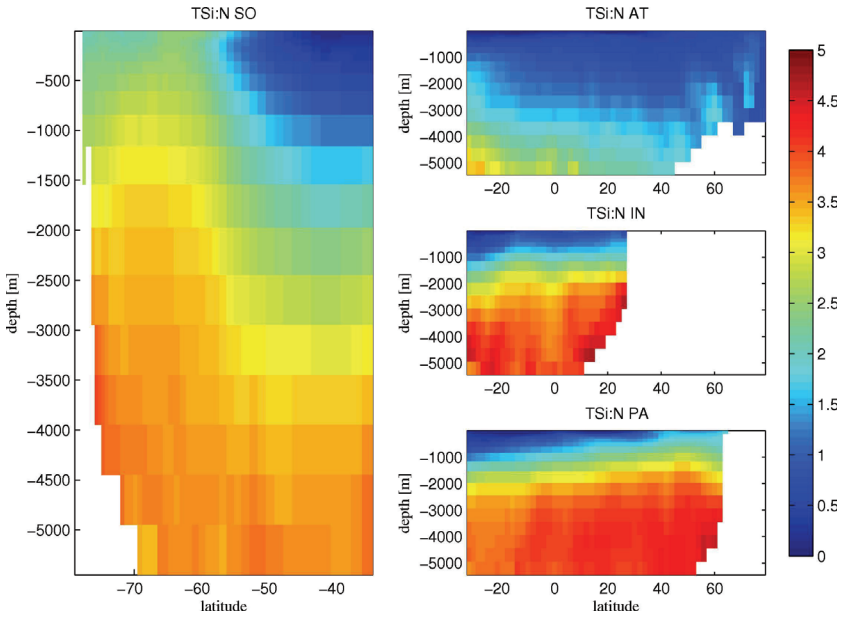

Figure 4.16: *Molar ratio of total Si over total N in the Southern Ocean (left), the Atlantic Ocean (upper right), the Indian Ocean (middle right), and the Pacific Ocean (lower right). The ratio of total silicon to total nitrogen is calculated first and then zonally averaged. The absolute concentrations of silicon and nitrogen in the water column are dominated by the concentrations of the inorganically dissolved tracers.*

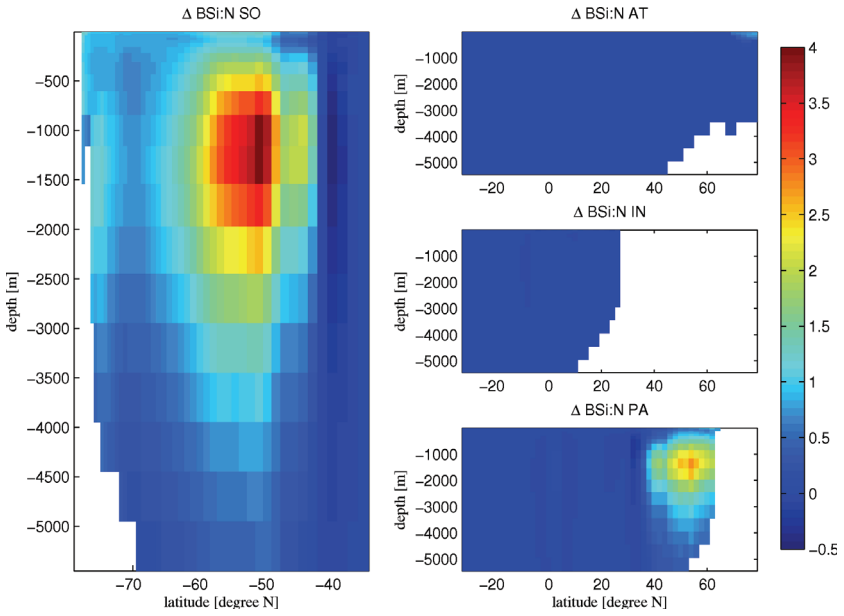

Figure 4.17: *Difference in molar Si:N ratios of biogenic Silicon and Nitrogen between two model runs (SiN in Run1-SiN in Run2). Run1 with variable Si:N ratio, Run2 with fixed Si:N ratio of about 1. Southern Ocean (left), Atlantic Ocean (upper right), Indian Ocean (middle right), Pacific Ocean (lower right).*

North Pacific. Already after three years of model integration the effect of variable Si:N ratios due to

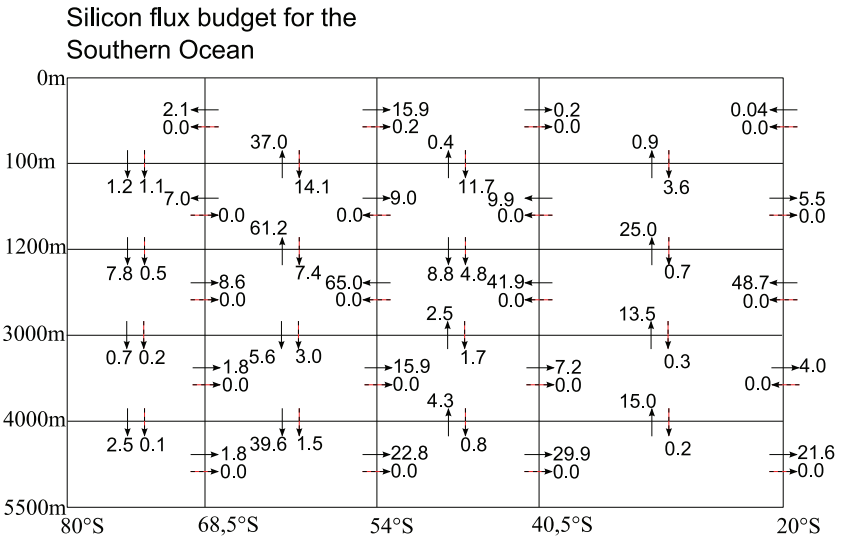

Figure 4.18: *Silicon flux budget in the Southern Ocean. Advective and diffusive fluxes of dissolved silica, DSi, over four horizontal layers and four latitudinal and vertical layers are summarized and presented by solid arrows. The sum of advective, diffusive and sinking fluxes of biogenic silica, BSi, over these layers is given by the dashed arrows. Fluxes are given in* $\mathrm{Tmol\ Si\ a^{-1}}$.

iron-limitation can be noticed to penetrate into the deep Southern Ocean.

In order to investigate the absolute fluxes of silicon and nitrogen, we calculate a transport budget for silicon and nitrogen over four defined vertical and horizontal layers in the Southern Ocean (Figs. 4.18+4.19). The advectice and diffusive fluxes and the Gent-McWilliams fluxes of silicon and nitrogen in vertical and longitudinal direction and the sinking fluxes of BSi and particulate organic nitrogen, PON, are zonally integrated and then integrated over the defined surfaces at 100 m, 1200 m, 3000 m, and 4000 m water depth and at 68.5°S, 54°S, 40.5°S, and 20°S, . The transport fluxes of dissolved silicon and nitrogen are depicted by the solid arrows, fluxes of particulate silicon and nitrogen are shown by dashed arrows.

The arrows of the transport fluxes of the dissolved tracers depict the zonally integrated circulation pattern in the Southern Ocean interior. Two anticlockwise and clockwise circulating apparent convection cells are centered at 68.5 and 54°S at about 1200 m depth. Deep Water enters the Southern Ocean from the north between 1200 and 3000 m depth, and Antarctic Bottom Water flows northwards at the sea floor.

Strong westerly winds lead to northwards directed Ekman transport over the ACC. The emerging divergence of water masses leads to upwelling of nutrient rich water mainly between the two apparent convection cells at 68.5°S and 54 °S. A fraction of the upwelling water is transported near the surface towards the antarctic continent, where it sinks down again and contributes to the formation of Antarctic Bottom Water. The increased Si:N uptake ratio of iron-limited diatoms indeed leads to very strong depletion of silicon in northwards drifting surface waters in the Southern Ocean, but only moderate depletion of DIN. The transport budget of silicon and nitrogen over 40.5°S in the upper 100 m of the water column shows a northwards directed nitrogen flux of 3.6 $\mathrm{Tmol\ N\ a^{-1}}$ and a silicon flux of only 0.2 $\mathrm{Tmol\ Si\ a^{-1}}$. The molar Si:N ratio in the transport flux over this surface is thus only 0.04 $\mathrm{mol\ mol^{-1}}$. Between 100 and 1200 m water depth at 40.5°S, a southwards directed net silicon

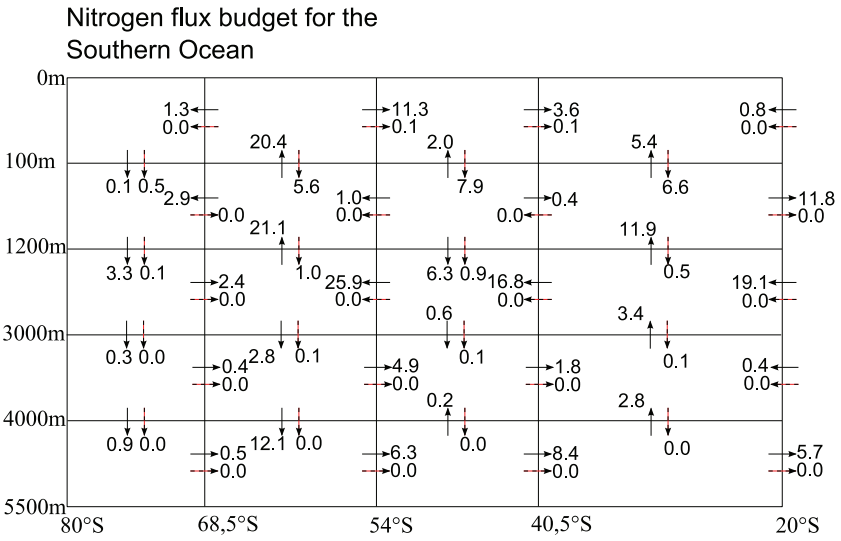

Figure 4.19: *Nitrogen flux budget in the Southern Ocean. Advective and diffusive fluxes of dissolved inorganic nitrogen, DIN, over four horizontal layers and four latitudinal and vertical layers are summarized and presented by solid arrows. The sum of advective, diffusive and sinking fluxes of particulate organic nitrogen (here defined as phytoplankton nitrogen+detritus nitrogen) over these layers is given by the dashed arrows. Fluxes are given in* $\mathrm{Tmol\ N\ a^{-1}}$.

flux can be seen in Figure 4.18 and a northwards directed nitrogen flux in Figure 4.19. The Si:N flux ratio over this surface would thus have a negative value, indicating that the coupling of silicon and nitrogen may not only vary for a certain degree but can also be strongly decoupled in the direction of the net transport fluxes.

4.4 Discussion

Analysis of the model runs with different sets of parameter values indicate strong differences between parameter sets that lead to good reproduction of global chlorophyll patterns and parameter sets that lead to good correlations with chlorophyll distributions in the Southern Ocean. Low values of the parameter α_{Chl} for the light-sensitivity of photosynthesis lead to better correlations with the annual signal of surface chlorophyll in the Southern Ocean, while leading to low correlation with the global distribution of surface chlorophyll. The differences between the parameter values for α_{Chl} for the Southern Ocean and the global ocean might be interpreted as adaptation of phytoplankton to deep vertical mixing in the Southern Ocean. However, low values of α_{Chl} signify little response to changes in irradiance levels and not necessarily an improved photosynthetic yield. Nevertheless, systematic differences between growth parameters in the Southern Ocean and the rest of the global ocean seem to exist.

Correlation coefficients between model results and the observed geographical pattern of Southern Ocean surface chlorophyll are always lower than 0.7. However, the model does reproduce chlorophyll signals on a local scale (Fig. 4.9). This characteristic can be explained by the chosen model setup. An ecosystem model with only one group of algae and one group of zooplankton organisms (N1P1ZD) is not capable of simulating all ecosystems in the global ocean. Different species are known to have different growth rates, nutrient dependencies, grazing rates, etc., and the mod-

elled system represents an ecosystem where a global average diatom is eaten by a global average zooplankton grazer that produces detritus with an average sinking velocity. Regional differences in ecosystem structures and thus regional differences of biological parameter values are not accounted for in this model setup. The proposed model therefore has to be understood as a regional ecosystem model, that is run in a global setup.

The model produces a belt of increased opal export around Antarctica (Fig. 4.15C) that is present in all model runs, even without strong iron-limitation in the Southern Ocean. The belt of opal export occurs at the steep gradient of dissolved silicon concentrations in surface waters of the ACC. Towards the north, diatoms become limited by low silicon concentrations and towards the south they become limited by light. Diatoms thus grow in the ACC where enough light and DSi are provided. Phytoplankton growth then leads to depletion of iron and the increased Si:N uptake rates in iron-limited waters further increases the export of opal in the ACC.

The applied parameterization of variable Si:N ratios in diatoms seems to be very robust. Elevated Si:N uptake ratios appear in iron-limited waters in the Southern Ocean and in the North Pacific. The parameterization is strongly dependent on ambient iron concentrations and is thus mainly affected by phytoplankton productivity, that depletes iron from the water column, and resupply of iron via upwelling of iron rich waters or dust input. As the major source of iron in the Southern Ocean is assumed to be due to upwelling (Meskhidze et al., 2007), accurate iron distribution fields are required for model initialization. Unfortunately, only few measurements of deep iron concentrations are available in the Southern Ocean and the iron concentrations as provided by the PISCES model (Aumont et al., 2003) are way too high when compared to the observations (De Baar et al., 1999).

The introduction of silicon and iron to the model as additional nutrients also introduces additional species specific parameters. The parameterization automatically excludes all phytoplankton organisms that do not depend on the availability of silicon but on the other side improves the description of diatom growth in the Southern Ocean. The growth dependency on iron concentrations is important to simulate primary productivity and the coupling of biogeochemical cycles in the Southern Ocean. But, modelling multinutrient interactions in phytoplankton growth rather leads to a specialization than generalization of the model.

The underestimation of global primary production is one artefact of this specialization. The global primary production is estimated from satellite data to be about 40-50 $\mathrm{Gt\ C\ a^{-1}}$ (Carr et al., 2006). The reference run results in a global gross primary production of 13.4 $\mathrm{Gt\ C\ a^{-1}}$. As the model excludes all other primary producers than diatoms, it can be expected to underestimate the global primary production of 40-50 $\mathrm{Gt\ C\ a^{-1}}$, but the contribution of diatoms to global primary production is assumed to at least 15 $\mathrm{Gt\ C\ a^{-1}}$ (Raven and Waite, 2004) or even as high as 26 $\mathrm{Gt\ C\ a^{-1}}$ (Nelson et al., 1995), which is still larger than what results from the model. Several model parameters can be changed to increase overall primary productivity, but all model runs giving primary production values of about 26 $\mathrm{Gt\ C\ a^{-1}}$ show strong overestimation of chlorophyll concentrations in the Southern Ocean.

The coupling of chlorophyll synthesis to nitrogen assimilation in the Geider model (Geider et al., 1998) may lead to overestimations of chlorophyll in the Southern Ocean and thus a methodological deviation between chlorophyll concentrations and carbon fluxes in the model. The resulting Chl:C ratios in the model output will be investigated next to clarify the reasons of this disagreement. The model further produces C:N ratios in the phytoplankton of the Southern Ocean of about 5.5 $\mathrm{mol\ mol^{-1}}$ which is lower than the Redfield ratio. As many studies assume the Redfield ratio to calculate carbon export from nitrogen fluxes (Schlitzer, 2002; Pollard et al., 2006), these estimates may also tend to overestimate carbon export in the Southern Ocean if light-limited phytoplankton exhibits

lower C:N ratios than assumed. Comparisons of observed and modelled C:N ratios in the Southern Ocean are required to validate model performance with respect to C:N deviations from Redfield.

One important model parameter that affects modelled primary production is the sinking velocity of detritus. As the sinking velocity can be supposed to increase with depth (Berelson, 2002), a sinking velocity of $50\ \mathrm{m\ d^{-1}}$ at $100\ \mathrm{m}$ water depth will most probably overestimate export in surface waters and underestimate export in the deep ocean. An underestimation of remineralization in surface waters due to overestimating sinking affects nutrient distributions in the surface ocean and leads to lower primary production in the euphotic zone. To overcome this problem, slower sinking velocities and remineralization rates are usually applied in ecosystem models changing the remineralization length scales and also the representation of export production below the euphotic zone. But usually these models also tend to overestimate chlorophyll concentrations in the Southern Ocean.

The sinking velocity of $50\ \mathrm{m\ d^{-1}}$ is derived from Equation 4.28, assuming a carbon specific remineralization rate of 0.15 $\mathrm{d^{-1}}$ and an exponent, b, of 0.86 in the Martin curve. Accounting for the temperature dependence of the remineralization processes would lead to a decrease of sinking velocities in cold waters after Equation 4.28. (Berelson, 2001) has shown the exponent of the Martin curve to vary between different ocean basins. But nevertheless, it is very likely that the sinking velocity of detritus depends on the composition of species that are responsible for detritus formation. Ballasting materials like biogenic silica may be a reason of increasing detritus sinking velocities in temperate and polar waters.

The influence of the coupling of Si and N cycles on the distribution of nitrogen and silicon in the global ocean indirectly affects the global carbon cycle and the biogeographical distribution of different plankton functional groups. At the Subtropical front in the South Atlantic, Southern Ocean surface water is subducted and forms a tongue of Subantarctic Mode Water (SAMW) that penetrates the water column of the Atlantic towards the north. The biogeochemical signature of this water mass is characterized by processes that occur in surface waters of the ACC. Elevated Si:N uptake ratios of iron limited diatoms deplete ACC surface waters with respect to silicon and leave excess DIN that is subducted as preformed nutrient. The Subantarctic Mode Water is therefore rich in nitrogen but depleted of silicon (Sarmiento et al., 2007). Changes in dust deposition fields on glacial-interglacial timescales or due to recent climate change may affect the biogeochemical signature of SAMW and thus the nutrient supply to the North Atlantic Ocean.

The accumulation of silicon in the deep waters of the North Pacific may be explained by a concentrating mechanism via the conveyor belt circulation and the gravitational attraction of particulate matter by the Earth. Accumulation of silicon in the Southern Ocean may be explained by nutrient trapping due to local upwelling of DSi and sinking of biogenic silica in the Deacon cell. Increased Si:N uptake ratios due to iron-limitation would then increase the nutrient trapping mechanism by a factor of three to four.

The long-term development of nutrient distributions can unfortunately not be investigated with the model as the model neglects the activity of other organisms that are important for the cycling of carbon and nitrogen in the global ocean. The resulting differences between the nitrogen and carbon cycle in the real ocean and the model will mostly affect nutrient distributions in other regions than the Southern Ocean which is dominated by diatoms. But on longer time-scales, these differences will influence the biogeochemistry of the Southern Ocean.

Nevertheless, the model connects the carbon cycle to the cycles of nitrogen, silicon, and iron and may help to improve predictions of climate induced feedback mechanisms of the carbon cycle in the Southern Ocean. The proposed model calculates stoichiometric variations in biomass and export

production in the Southern Ocean. To create a real global biogeochemical model, the ecological resolution of the model has to be improved, i.e. other plankton groups than diatoms will have to be included in order to improve regional fluxes and tracer distributions. The representation of zooplankton is still of great uncertainty. As modelled phytoplankton abundances are very sensitive to zooplankton grazing, the parameterization of higher trophic levels and the model closure should also be improved in the future. To improve the description of export production and stoichiometric variations in exported matter, the model requires at least a second size class of detritus with a slower sinking velocity, that could be fueled by picoplankton.

Future studies should also adress the effect increased Si:N ratios in diatoms might have on zooplankton grazing or sinking velocities of phytoplankton and detritus, to investigate whether the stoichiometric response of diatom growth to iron limitation has direct effects on the global carbon cycle.

Table 4.1: Model parameters. Units and description of model parameters and parameter values as used in the reference run are presented in this Table.

Parameter	Value	Unit	Description
α_{Chl}	0.03	mmol C m^2 (mg Chl W d)$^{-1}$	initial slope of PI-curve
μ_{C}^{max}	3.0	d^{-1}	maximum carbon fixation rate
r_{C}	0.01	d^{-1}	background respiration rate phytoplankton
V_{fact}	0.7	dimensionless	scaling factor
K_{N}	0.55	mmol N m^{-3}	half saturation constant N
K_{Si}	4.0	mmol Si m^{-3}	half saturation constant Si
K_{Fe}	0.12	μmol Fe m^{-3}	half saturation constant Fe
γ_{C}	0.1	d^{-1}	excretion rate of EOC
γ_{N}	0.05	d^{-1}	excretion rate of EON
γ_{Chl}	0.01	d^{-1}	degradation rate of chlorophyll
$\theta_{\mathrm{N}}^{max}$	4.9	mg Chl (mmol N)$^{-1}$	maximum Chl:N ratio
ζ	2.0	mmol C (mmol N)$^{-1}$	biosynthetic costs chlorophyll production
ζ_{N}	2.0	mol C mol N^{-1}	costs of N uptake
ζ_{Si}	0.0	mol C mol Si^{-1}	costs of Si uptake
q_{NC}^{min}	0.04	mol N mol C^{-1}	minimum N:C ratio
q_{NC}^{max}	0.20	mol N mol C^{-1}	maximum N:C ratio
NC_{upt}	0.20	mol N mol C^{-1}	maximum N:C uptake ratio
q_{SiC}^{min}	0.0408	mol Si mol C^{-1}	minimum Si:C ratio
q_{SiC}^{max}	0.8	mol Si mol C^{-1}	maximum Si:C biomass ratio
SiC_{upt}	0.204	mol Si mol C^{-1}	maximum Si:C uptake ratio
σ_{Nmin}	50	dimensionless	regulation slope
σ_{Nmax}	1000	dimensionless	regulation slope
σ_{Simin}	1000	dimensionless	regulation slope
σ_{Simax}	1000	dimensionless	regulation slope
g_{max}	10.5	d^{-1}	maximum grazing rate
ε	0.9	mmol N m^{-3}	half saturation constant of grazing
g_{eff}	0.1	dimensionless	grazing efficiency
r_{zoo}	1.0	d^{-1}	zooplankton respiration rate
γ_{zoo}	0.3	m^3 (mmol N d)$^{-1}$	mortality rate of zooplankton
Φ_P	0.02	(mmol N d)$^{-1}$	aggregation parameter
Φ_D	0.22	(mmol N d)$^{-1}$	aggregation parameter
V_{det}	40.0	m d^{-1}	detritus sinking velocity
V_{phy}	0.0	m d^{-1}	phytoplankton sinking velocity
ρ_{C}	0.1	d^{-1}	EOC remineralization rate
ρ_{N}	0.11	d^{-1}	EON remineralization rate
ω_{C}	0.15	d^{-1}	detritus C remineralization rate
ω_{N}	0.165	d^{-1}	detritus N remineralization rate
κ_w	0.04	m^{-1}	attenuation coefficient of water
κ_{chl}	0.03	m^{-1} (mg Chl)$^{-1}$	chlorophyll specific attenuation coefficient
A_E	4500.0	K	slope for Arrhenius function
$Tref$	288.15	K	reference temperature
k_{scav}	0.001	a^{-1}	scavenging rate
L	1.0	μmol m^{-3}	total ligand concentration
$K_{\mathrm{Fe}L}$	100.0	m^3 μmol^{-1}	ligand stability constant
$f_{\mathrm{C}}^{\mathrm{Fe}}$	0.005	molmol^{-1}	iron to carbon ratio

Table 4.2: Parameter changes in the collection of model runs in Figures 4.6-4.8 with respect to the reference parameter set. For a description of parameter symbols and units, see Table 4.1.

	Parameters						
Model run	α_{Chl}	γ_{zoo}	ε	g_{eff}	g_{max}	V_{det}	K_{Fe}
B	0.03	0.3	0.9	1.0	0.35	50	0.12
C	0.04	0.3	0.9	1.0	0.35	50	0.12
D	0.05	0.3	0.9	1.0	0.35	50	0.12
E	0.03	0.3	0.9	0.1	3.50	40	0.12
F	0.02	0.3	0.9	0.1	3.50	40	0.12
G	0.01	0.3	0.9	0.1	3.50	40	0.12
H	0.03	0.3	0.9	0.1	4.50	40	0.12
I	0.03	0.3	0.9	0.1	5.50	40	0.12
J	0.03	0.3	0.9	0.1	6.50	40	0.12
K	0.03	0.3	0.9	0.1	7.50	40	0.12
L	0.03	0.3	0.9	0.1	8.50	40	0.12
M	0.03	0.3	0.9	0.1	9.50	40	0.12
N	0.03	0.3	0.9	0.1	10.50	40	0.12
O	0.01	0.3	0.9	0.1	8.50	50	0.12
P	0.01	0.3	0.9	0.1	10.50	50	0.12
Q	0.01	0.3	0.9	0.1	12.50	50	0.12
R	0.14	0.05	0.35	0.3	2.40	50	0.10
S	0.14	0.05	0.35	0.3	2.40	50	0.08
T	0.14	0.05	0.35	0.3	2.40	50	0.06
U	0.14	0.05	0.35	0.3	2.40	50	0.04

Chapter 5

High resolution modelling

M. Losch, M. Schröder, S. Hohn, C. Völker

5.1 Introduction

The marine biology, especially the phytoplankton (suspended microscopic algae and photosynthesizing bacteria), is tightly involved in the geochemical cycling of many elements, especially of carbon, but also compound substances that may have climatic impacts, such as dimethylsulfide or organohalogens. The ocean contains approximately 50 times as much carbon as the atmosphere, and over time-scales longer than a few decades the CO_2 partial pressure of the atmosphere is tightly coupled to the distribution of carbon within the oceans. An important process in regulating this distribution is the so-called 'biological pump', the fixation of carbon through photo-synthesis close to the ocean surface, and the subsequent sinking and decomposition of parts of the produced biological material in the deep ocean. Changes in the growth, mortality and sinking of phytoplankton therefore have the potential to act as a strong feedback on the change in climate that is induced by the anthropogenic accumulation of greenhouse gases in the atmosphere (Maier-Reimer et al., 1996; Cox et al., 2000; Friedlingstein et al., 2003).

The Southern Ocean is a place of extremely strong exchange fluxes between ocean and atmosphere and plays an important role also for the global carbon cycle (Orr et al., 2001). At the same time, it is also a place where strong changes in the ocean circulation are expected under global warming, e.g. a southward shift and strengthening of the Antarctic Circumpolar Current (ACC) (Fyfe and Saenko, 2006), a reduction in sea ice cover (Flato, 2004) and a warming of the water column (Gille, 2002).

A good understanding of the feedbacks in this system can only be gained by the use of computer models that allow to predict the physical background that the biology operates in, i.e. the ocean circulation and other external factors that influence phytoplankton growth (nutrients, light), but also the internal regulations within the planktonic ecosystem. Owing to their often large number of advected tracers (and therefore memory requirements) and the longer integration times required, coupled physical-biogeochemical models of the ocean are still often relatively coarsely resolved (on the order of 100-200 km spatial resolution in the horizontal), i.e. they are unable to represent the action of the energetic mesoscale eddy field that has lengths scales on the order of the Rossby radius of deformation (10-40 km). The mesoscale eddies have been shown to exert a strong influence of the mean circulation, especially in the Southern Ocean (Olbers et al., 2004). Model predictions of atmosphere-ocean carbon fluxes differ most between different models in the Southern Ocean, owing to a poor representation of the physics there in coarse-resolution models (Orr et al., 2001). It

is therefore desirable to run coupled physical-biogeochemical ocean models at the state-of-the-art spatial resolution that is used in purely physical modelling.

There are also new challenges for the biogeochemical and ecosystem part of the coupled models. Marine ecosystem models have traditionally worked on the assumptions of a single limiting nutrient, usually nitrogen, for phytoplankton growth, and a constant carbon:nitrogen ratio in biomass (Six and Maier-Reimer, 1996; Fennel et al., 2001). However, over the last decade it has become clearer that (i) different phytoplankton functional groups (diatoms, coccolithophorids) have different effects on the carbon flux through the system, (ii) that other nutrients, such as iron and silicate are important regulators of ecosystem structure and functioning, and (iii) that there is some plasticity in phytoplankton physiology, allowing the cells to adapt to different light/nutrient conditions and resulting in variable elemental stoichiometry. We have developed an ecosystem model that focuses mainly on the two last challenges, by implementing a model for diatoms with variable C:N:Si:chlorophyll ratio that depends on the availability of the nutrients N, Si, and Fe. Here we show some results from implementing this model into both a coarser-resolution and a high-resolution global circulation model that have been run on the IBM system *JUMP* at NIC.

5.2 The Model

5.2.1 Biogeochemical model

The ecosystem model is based on the physiological model for the adaptation of algal cells to light, nutrient and temperature by Geider et al. (1998) that describes the variation of the cells C:N:chlorophyll ratios with varying conditions assuming balanced growth. This model has been somewhat extended and implemented into a full marine ecosystem model, which describes also the mortality of phytoplankton from zooplankton grazing, the formation of detritus (also through the excretion and aggregation of transparent exopolymeric particles), and other processes by Schartau et al. (2007).

We have extended this Regulated Ecosystem Model (REcoM) (Schartau et al., 2007) to a model for diatom growth that also includes limitations by silica and iron availability. The parameterization for the uptake of silica and the dependence of growth on the silica quota is based on physiological observations. It results in increased Si:N ratios in the cells under iron-limiting conditions without prescribing this effect explicitly (Hohn et al., in preparation).

5.2.2 Physical model and CS510 configuration

The simulation of the ocean circulation is done using the Massachusetts Institute of Technology general circulation model (MITgcm) (Marshall et al., 1997; MITgcm Group, 2002) which solves the time-dependent, Boussinesq-approximated Navier-Stokes equations with or without hydrostatic approximation, and conservation equations for salinity and energy (in the form of an equation for potential temperature). Turbulent diffusion and viscosity are parameterized following the scale-dependent Smagorinsky approach. For the vertical mixing in the surface layer, the KPP model by Large et al. (1994) is used.

The equations are discretized using a finite-volume method on an orthogonal grid. To avoid the singularity of a latitude-longitude grid at the poles and to ensure an approximately homogeneous spatial resolution, we have used the 'cubed sphere' grid configuration provided my the MITgcm, which is obtained by mapping a regular grid on the surface of a cube onto a sphere. The high-resolution runs were performed with a horizontal resolution of 510×510 grid points on each of the 6 sides of the cube.

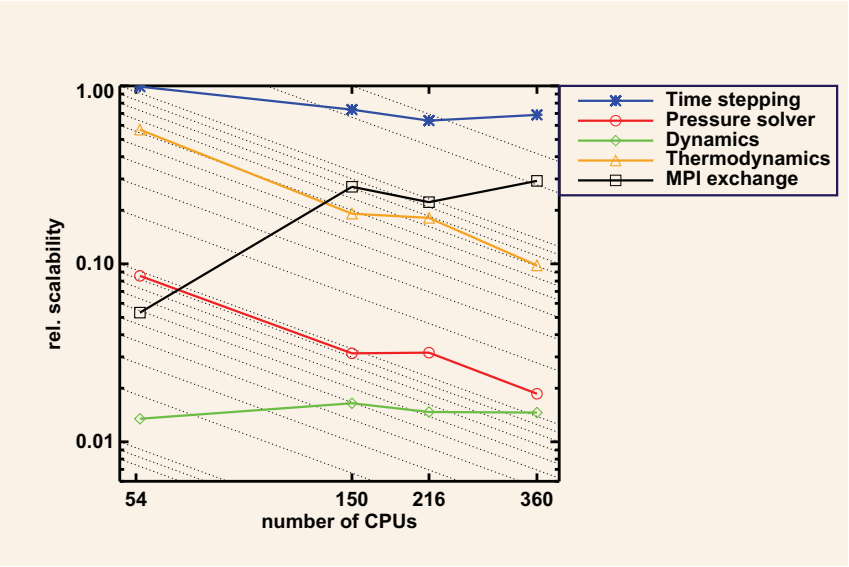

Figure 5.1: Relative execution times for certain/different parts of the MITgcm model. Here the biogeochemistry module (including 16 tracers) has been switched on. The diagonal lines show an ideal scaling behaviour (computing time inversely proportional to the number of CPUs)

5.3 Scalability

The MITgcm model has been chosen among other reasons, because of its known good multi-processor scalability over a large range of processor numbers and computer architectures. However, contrary to our previous experiences, the coupled system MITgcm + REcoM shows a bad scaling behaviour on the IBM system *JUMP* with increasing number of processors used. The wall-clock time only weakly decreases with increasing processor number, and even slightly increases in the simulation with 360 processors, compared to a 216-processor configuration. An analysis of the execution times for individual parts of the program (Figure 5.1) shows the reason for this scaling behaviour. While the main parts of the model (dynamical, thermodynamical and biogeochemical) scale approximately linearly, the required computing time for MPI interprocessor exchange increases with increasing number of processors used. The fact that the execution time for the pressure solver also does not decrease linearly with processor number does not influence the overall execution time significantly, as it is only a small fraction of the total.

A comparison to test without the biogeochemical module (Figure 5.2) shows that it is the MPI-communication for the 16 passive tracers that is responsible for the bad scaling behaviour of the model. Without the additional biogeochemical tracers the MPI exchange (and therefore the model as a whole) scales reasonably linear.

This showed that the MPI communication for the advection of the passive tracers had to be optimized. Instead of sending the data packages for the advection of each tracer over the halo boundaries of each model time individually, a new communication scheme was implemented that is adapted to the properties of the network, where the data for all passive tracers is exchanged jointly with one MPI_SEND/MPI_RECV statement. As Figure 5.3 shows, this decreased the time for the MPI exchange in the target model configuration with 216 processors significantly (by about 60%), which also resulted in an overall gain in efficiency.

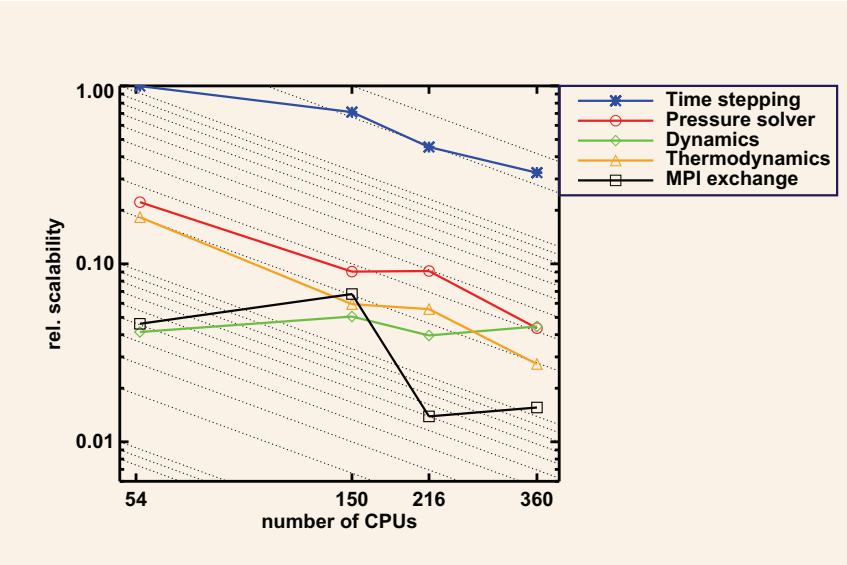

Figure 5.2: Same as Figure 5.1, but the biogeochemistry module has been switched off (no passive tracers).

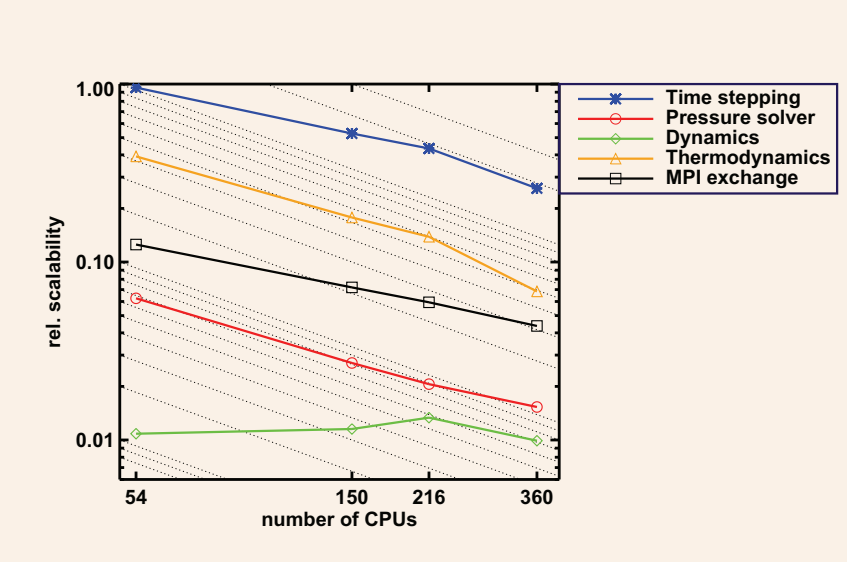

Figure 5.3: Same as Figure 5.1, but now including the biogeochemistry module and an optimized passive tracer communication.

5.4 Results

Our main goal, a high-resolution run of the coupled physical-biogeochemical model over a decade, has not been reached during the first phase of the project due to the described scaling problems. We therefore just briefly demonstrate the potential of the model with some results from a coarse-resolution run and from the spinup phase of a high-resolution run.

The coarse-resolution model runs show that the representation of phytoplankton physiology in the model and the resulting decoupling of the elemental cycles of Si, C and N lead to new insights. In the

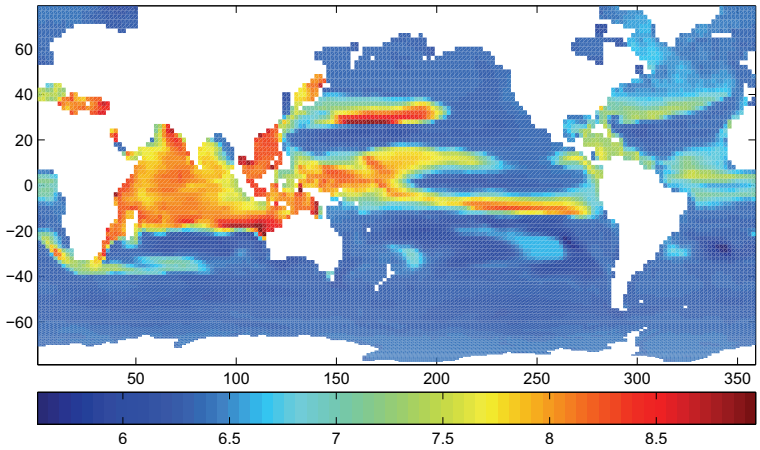

Figure 5.4: Modeled ratio between carbon and nitrogen (mol:mol) in the biomass within the oceanic surface mixed layer. At a sufficient supply of light and nutrients, phytoplankton cells tend toward a C.N ratio of around 6.6. The elevated values in the subtropical gyres are a consequence of strong nutrient limitation.

subtropical gyres, which are biological 'deserts' due to the scarcity of nutrients, significantly elevated C:N ratios are modelled in the biomass (Figure 5.4). This would imply that these regions would contribute more that hitherto assumed to the vertical export of carbon into the deep ocean, given a fixed N and Si supply. This has consequences for the strength of the feedback between climate change and the marine carbon cycle through changes in stratification and therefore nutrient supply. The model also is able to reproduce the so-called 'opal-belt', a region of high deposition of diatom silica in the sediment around Antarctica, a feature that is usually not found in fixed-composition models (not shown).

At the same time, Figure 5.4 clearly shows deficits in the representation of the ocean circulation, such as an overestimate of nutrient upwelling along the equator. It will be very interesting to see whether the better reproduction in the high-resolution model of sharp fronts between nutrient-rich and nutrient-poor waters, e.g. in the ACC, will lead to an enhanced export of high C:N biomass into the deep ocean.

Model results from the high-resolution run (Figure 5.5) are not yet in equilibrium. However, they clearly show that the activity of eddies is reflected in the distribution of chlorophyll, especially along the ACC, and that the overly strong primary production around upwelling regions in the coarse-resolution run has been reduced and is much more in line with satellite-based estimates.

5.5 Concluding Remarks and Outlook

In spite of initial problems with scalability, the coupled MITgcm-REcoM model shown here shows some promise regarding the model-based description of the decoupling between the elemental cycles of carbon, nitrogen, silica and iron in a high-resolution model setup. Further model experiments will start from an optimized set of ecosystem parameter values that has been obtained by tuning the coarse-resolution model to observations of chlorophyll and export production, and will increasingly

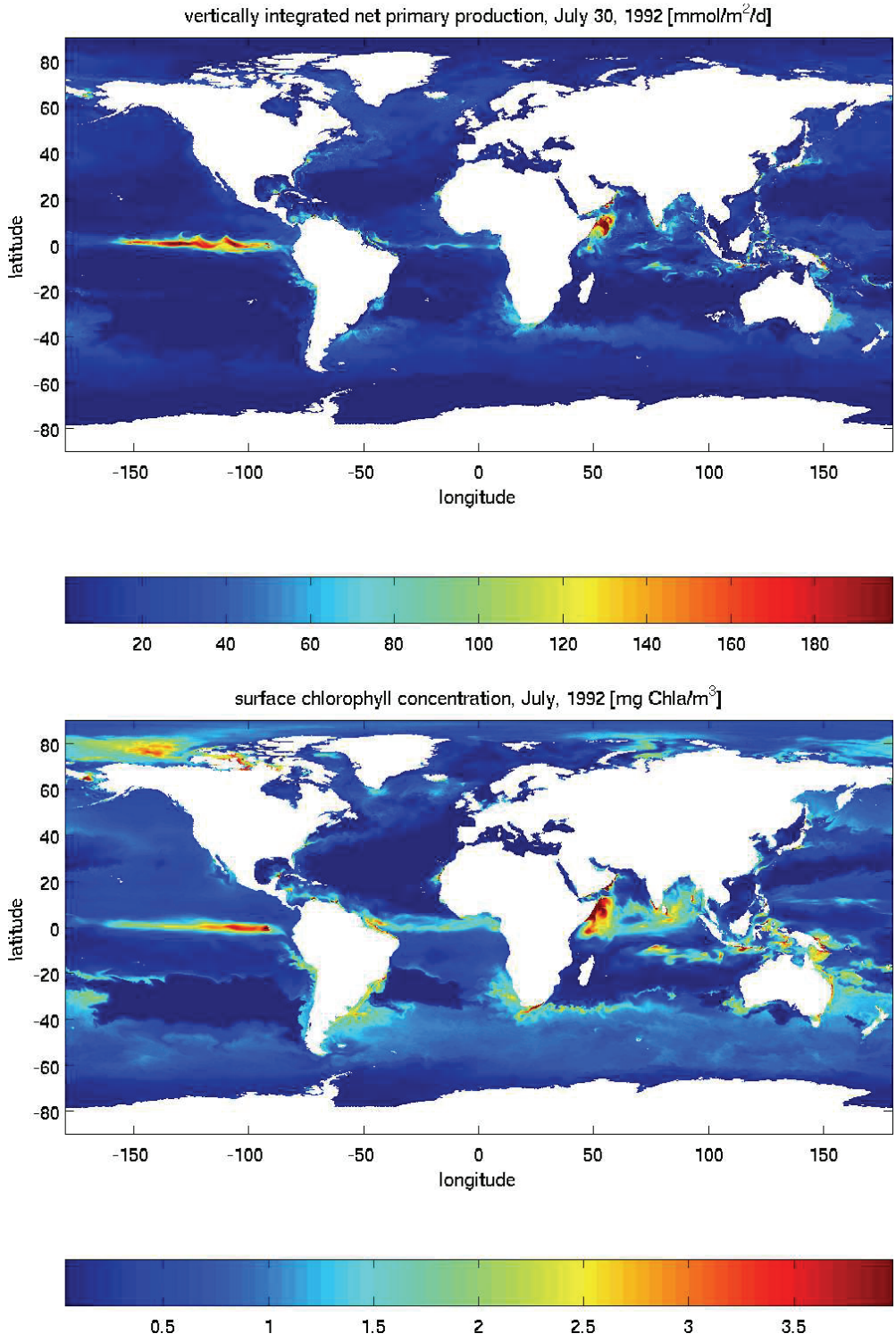

Figure 5.5: Results from a high-resolution run after 7 months of integration. Above: vertically integrated primary production on July 30, 1992. Below: mean concentration of chlorophyll-a at the sea surface for July, 1992.

focus on the role of inter-annual variability on biogeochemical fluxes.

Acknowledgements

Markus Schartau (GKSS research centre, Geesthacht) has contributed much to the development of the biological model code. Sönke Hohn and Christoph Völker are supported by a EU grant within the EU FP6 program CarboOcean, contract number 511176 (GOCE). The benchmark computations were performed with a grant of computer time provided by the Research Centre Jülich.

Chapter 6

General Discussion

The biogeochemical cycles of biologically important elements are coupled to each other via the production of organic molecules and compartimentation in cellular structures and the production of biominerals. This coupling is based on the stoichiometric composition of biomass that is often assumed to have a general stoichiometric structure (Redfield et al., 1963). However, the stoichiometric composition of biomass may deviate from Redfield ratios under certain growth conditions and with different species. These systematic deviations are often referred to as 'decoupling' of elemental cycles although 'variable coupling' might be a more appropriate term.

The studies presented in this thesis investigated the coupling of the elements carbon, nitrogen, and silicon in phytoplankton biomass and the role of iron, using mathematical models that were applied on different spatial scales. In the following section, the biogeochemical implications of a variable Si:N:C stoichiometry in phytoplankton biomass on large scale biogeochemical fluxes are discussed. The second section discusses the importance of the applied parameterizations and chosen parameter values for realistic representation of biogeochemical processes in marine ecosystem models. Suggestions for future research are given on the background of the findings of my thesis.

6.1 Coupling of elemental cycles

The application of the Geider model (Geider et al., 1998) in an ecosystem box model for the North Sea and the Wadden Sea (study 1) allows for variations in the C:N ratio of the modelled phytoplankton compartment. The ratio between carbon and nitrogen exchange of phytplankton biomass between the North Sea and the Wadden Sea shows interannual variations and even a negative sign in the year 2000 (Tab. 2.3), indicating that the annual transport of phytoplankton carbon and nitrogen can occur in opposite directions. In the Wadden Sea, growth conditions for phytoplankton alternate between light-limitation in winter and nitrogen-limitation in summer (Colijn and Cadée, 2003). The molar C:N ratios in the modelled phytoplankton biomass are shown in Figure 6.1 in the North Sea (blue) and the Sylt-Rømø tidal basin (green) for the years 2000 and 2003. Modelled C:N ratios exhibit increased values during summer and low values due to light-limitation in winter. The growth period in the Sylt-Rømø tidal basin was about one month longer in the year 2003 than in 2000 and the simulated phytoplankton shows slightly higher C:N ratios in the summer of 2003 than in the summer of 2000.

If phytoplankton used carbon and nitrogen in a fixed ratio, as is assumed in many other model studies, carbon and nitrogen biomass would always be transported and exchanged between different water parcels with a constant stoichiometry. However, the difference between phytoplankton C:N

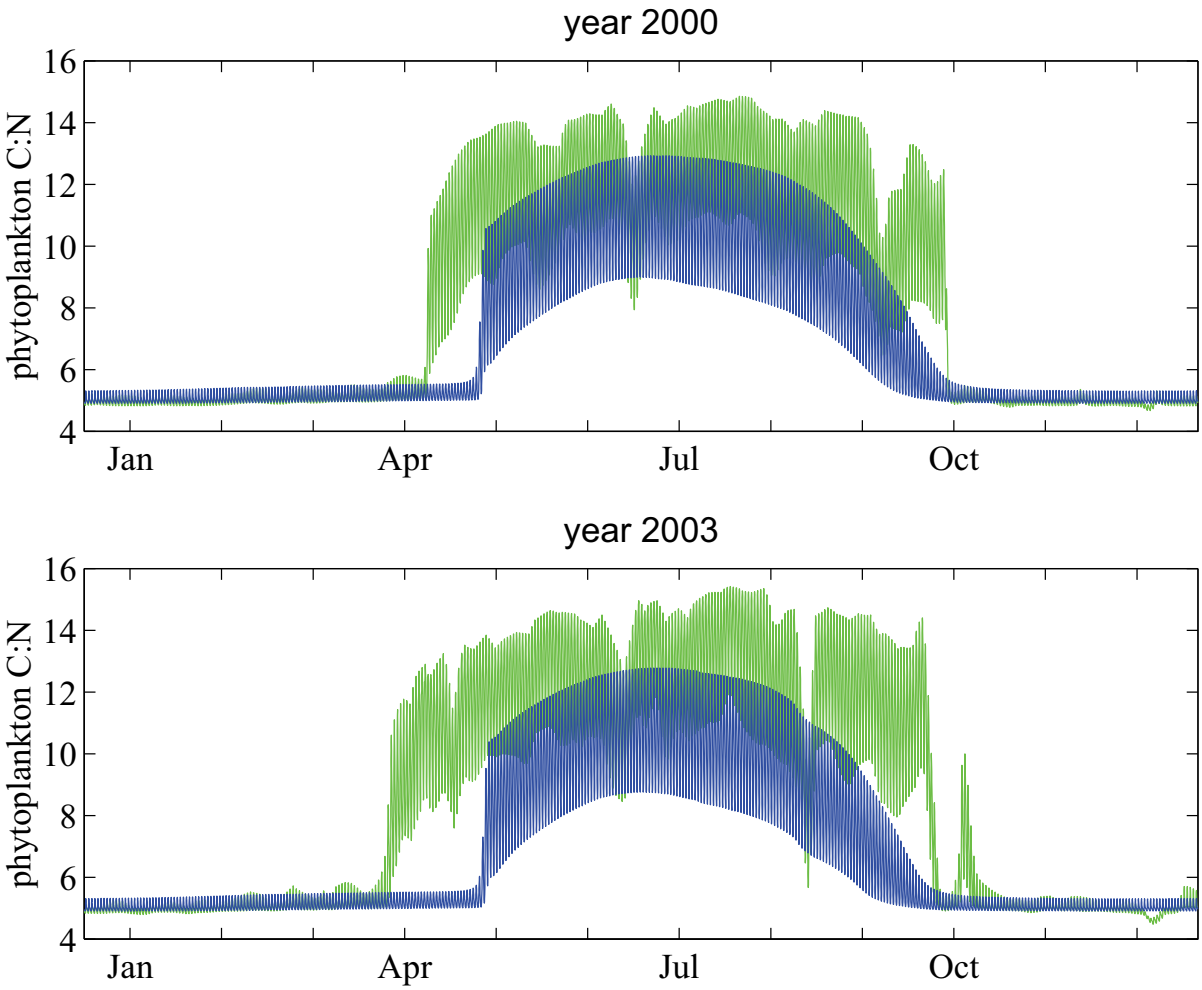

Figure 6.1: *Simulated C:N ratios (*$\mathrm{mol\,mol^{-1}}$*) in phytoplankton biomass in the North Sea (blue) and the Sylt-Rømø tidal basin (green) for the years 2000 and 2003.*

ratios in the North Sea and in the Sylt-Rømø bight as presented in Figure 6.1 does not explain the differences in the transport budgets between the years 2000 and 2003 as the exchange of biomass between two water boxes depends on the absolute concentration differences of total biomass and not on the ratios. In general, phytoplankton concentrations during the growth period are higher in the Wadden Sea than in the North Sea. On the other hand, phytoplankton concentrations are higher in the North Sea during winter (see Figure 2.5). The exchange of phytoplankton biomass thus changes its direction between summer and winter and the duration of the different phases determines the absolute transport of biomass. Phytoplankton nitrogen concentrations in the SRB are higher during the growth period in the year 2000, leading to lower C:N ratios in the bight in summer. But as the growth period in the year 2000 is shorter than in the year 2003, less phytoplankton nitrogen is exported into the North Sea in the year 2000 than in 2003. The export of phytoplankton nitrogen in the year 2000 is also less than the amounts of phytoplankton nitrogen that are imported from the North Sea after the growth period in the bight has ended. Variations in phytoplankton C:N ratios in the North Sea and in the Wadden Sea during different times of the year can thus lead to opposite directions in the

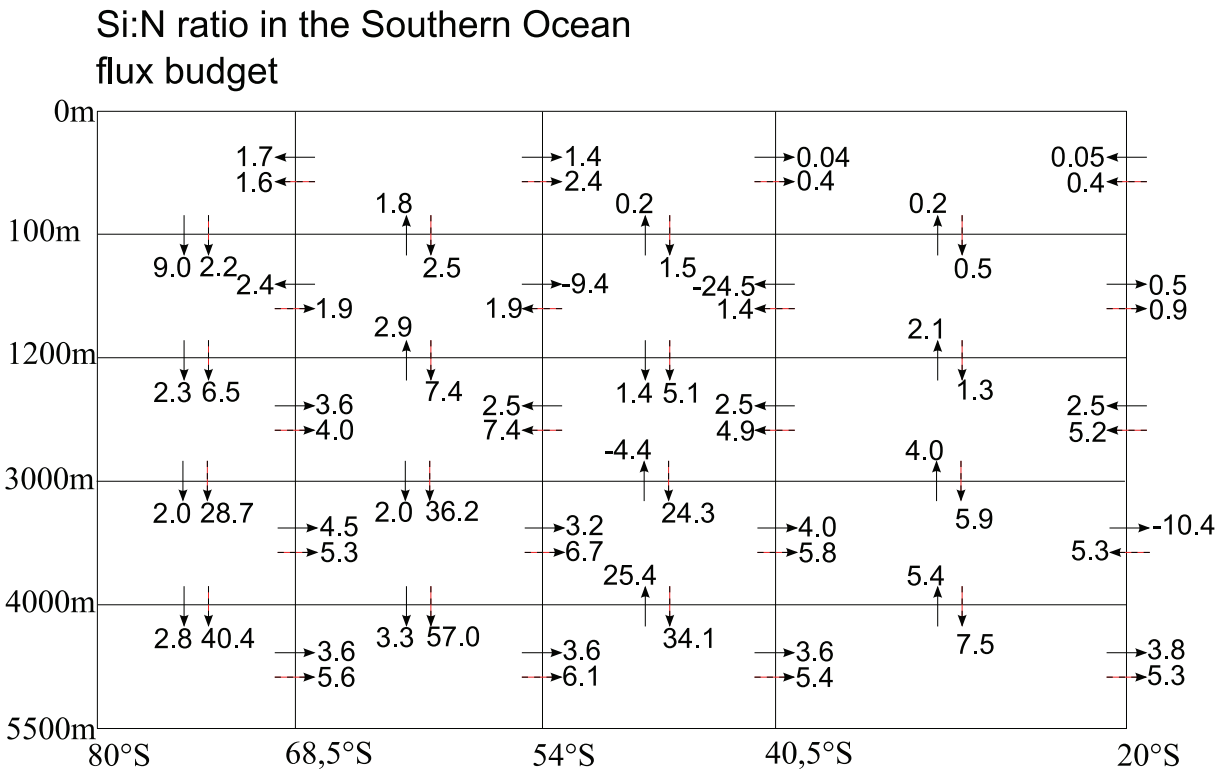

Figure 6.2: *Advection, diffusion and sinking fluxes of all silicon and nitrogen tracers are summarized to determine the total vertical and horizontal fluxes of silicon and nitrogen. The picture presents the molar Si:N ratios of the total fluxes of silicon and nitrogen over three horizontal and four vertical layers in the Southern Ocean. Solid arrows stand for the transport of dissolved tracers, dashed arrows represent fluxes of particulate silicon and nitrogen.*

net annual transport budget and a true decoupling of carbon and nitrogen fluxes.

In the biogeochemical general circulation model (study 3), advection, diffusion, and sinking of all simulated forms of silicon and nitrogen are used to track the elements in the three-dimensional circulation pattern and to determine the processes that lead to the observed distribution patterns in the global ocean. The molar ratios of silicon to nitrogen fluxes over four horizontal and four vertical layers in the Southern Ocean are shown in Figure 6.2. The layer at 100 m has been chosen to highlight fluxes at the ocean surface. The other layers have been chosen to investigate fluxes in the ocean interior. The arrows depict the direction of the silicon fluxes and the numbers give the molar Si:N flux ratios. Some important features in this picture are highlighted in the following.

In general, Si:N ratios of particulate and dissolved tracers increase with depth because of different remineralization length scales of silicon and nitrogen. Simulated upwelling of Antarctic Bottom Water across the layer at 4000 m depth between 54°S and 40.5°S occurs with a Si:N ratio of more than 25 $\mathrm{mol\ mol^{-1}}$. The assumption of a constant sinking velocity of detritus in the model in combination with the different remineralization rates for silicon and nitrogen leads to an overestimation of Si:N export ratios in the deep ocean and may also cause an overestimation of DSi:DIN ratios in Antarctic Bottom Water.

Between the two apparent convection cells at 68.5 and 54°S at 1200 m, upwelling of Circumpolar

Deep Water supplies nutrients to the euphotic zone with a molar Si:N ratio of 1.8 (Fig. 6.2). The increased Si:N uptake ratio by iron-limited diatoms leads to stronger depletion of DSi with respect to DIN in the northwards flowing surface waters, which can be seen in the decreasing Si:N ratios in the dissolved tracers. When averaged over a layer from 100 to 1200 m, the Si:N flux ratio at 40.5°S exhibits a negative value (Fig. 6.2). That means that silicon is transported southwards and nitrogen is transported northwards in this region which agrees with the formation of relatively nitrogen rich and silicon poor Subantarctic Mode Water that becomes Antarctic Intermediate Water and penetrates the Atlantic Ocean water column.

A negative value in the flux ratio is a combination of the circulation and tracer concentrations. Tracer concentrations are positive numbers and as the transport of two tracers with the ocean currents usually happens in the same direction, the flux ratio of these tracers is also positive. A negative value of the flux ratio can only occur if the direction of the transport changes in combination with the ratio of both tracers, leading to opposite directed net transport fluxes.

In the Sylt-Rømø tidal basin, different flux ratios of phytoplankton carbon to phytoplankton nitrogen over the year 2000 lead to a decoupling of the transport fluxes in the annual budget. As transport fluxes can also exhibit regional differences, e.g. in different ocean basins of ocean depths, integrating over a geographical distribution can also lead to the decoupling of transport fluxes due to spatial differences in the flux ratios. The latter effect can be recognized in Figure 6.2 at 20°S between 3000 and 4000 m depth. Here, silicon rich waters are transported to the north and nitrogen rich waters flow from north to south.

The global distribution of total silicon shows an accumulation of silicon in the North Pacific and also in the Southern Ocean (Fig. 4.1). Biological processes like production and remineralization of biomass have a strong influence on nutrient concentrations and the distribution of nutrients in the global ocean. As upwelling regions are very productive due to the supply of nutrients from the deep ocean, trapping of nutrients mainly occurs in these regions due to large amounts of produced biomass that vertically sink through the water column and become remineralized in the water masses that are upwelled again. Remineralization of biomass releases all elements that were incorporated into biomass, also iron. As scavenging by sinking particles is a sink of iron in the water column (Bergquist and Boyle, 2006), the nutrient rich deep water is depleted in iron and upwelling of deep water resupplies less iron than would be required to use up the other nutrients. The North Pacific and the Southern Ocean are subject to upwelling of "old" water and are known to exhibit iron-limitation in surface waters (Martin and Fitzwater, 1988; Martin et al., 1990). Iron is supplied to the ocean via input of dust to surface waters (Tegen and Fung, 1994), but due to the distribution of land masses in the southern hemisphere, the major source of iron to the euphotic zone of the Southern Ocean is currently upwelling of nutrient rich waters (Meskhidze et al., 2007). As diatoms exhibit elevated Si:N uptake ratios under iron-limitation, the increased incorporation of silicon into biomass increases the accumulating mechanism for silicon compared to nitrogen in iron-limited ocean regions. Accumulation of silicon over nitrogen in iron-limited ocean regions improves growth conditions for diatoms, so that diatoms could be regarded as ecosystem engineers, changing their environment in their own favour.

6.2 Parameter values and parameterizations

As phytoplankton productivity depends on the availability of nutrients and light, the modelling of nutrient dynamics is fundamental for the modelling of carbon fluxes in the ocean. This thesis provides

a new parameterization of variable Si:N uptake ratios of diatoms as a function of iron concentrations in the growth medium and the application of the parameterization in a biogeochemical general circulation model. The parameterization of elevated Si:N uptake ratios in iron-limited diatoms appears to be relatively robust and can easily be adjusted to simulate the physiological behaviour of different diatom species by changing the parameter values of the maximum silicon uptake rate, SiC_{upt}, and the maximum Si:C cell quota, q_{SiC}^{max}. The simulation of variable Si:N and Si:C uptake ratios by diatoms and their dependence on iron concentrations provides further insight in the interplay of different biogeochemical elements and the emergence of nutrient distributions and their feedbacks with biological processes.

Multi-nutrient modelling of phytoplankton growth requires knowledge of phytoplankton physiology and intracellular regulations of different metabolic processes. Nutrient uptake mechanisms and photosynthetic carbon fixation can be parameterized to be regulated via intracellular stoichiometric ratios (quotas) that are assumed to represent the metabolic condition of the cell (Geider et al., 1998; Mongin et al., 2003; Hohn et al., submitted). Unfortunately, little is known about the regulation processes in the cells and the mathematical forms of the required regulation functions remain uncertain.

The application of Liebig's Law of the Minimum for the regulation of phytosynthesis in the proposed parameterization (Eq.3.3) results in direct influence of ambient iron concentrations to phytoplankton growth. When applied to model the iron fertilization experiment EisenEx in the Southern Ocean, phytoplankton growth exhibits an immediate response to the addition of iron and no lag-phase as can be observed in the data (Martin Losch, pers. comm.). The Geider model (Geider et al., 1998) does not capture the lag phase of phytoplankton growth after addition of nutrients as acclimation of cellular components and pools of energy due to environmental changes are not adequately represented by the Geider model. This leads to an immediate increase in phytoplankton chlorophyll after fertilization.

Inclusion of an iron quota in the modelled phytoplankton compartment and iron dependencies of the synthesis of chlorophyll might improve the behaviour of the model and lead to a delay in phytoplankton growth due to replenishment of the cellular iron content before increasing metabolic activity. However, the inclusion of an iron quota would require further regulation functions via the cellular iron content and would increase the number of unknown parameters and equations.

The high DIN concentrations in the Southern Ocean may be responsible for the high chlorophyll concentrations produced by the model. The coupling of nitrogen assimilation and chlorophyll synthesis could explain the overestimation of modelled chlorophyll concentrations while underestimating carbon fluxes in the Southern Ocean. Anyway, the underestimation of primary production and export production in the Southern Ocean can also be caused by the low C:N ratios of modelled Southern Ocean phytoplankton. Applying the model by Pahlow (2005) may lead to an improvement of modelled chlorophyll concentrations in the Southern Ocean as this model makes more realistic assumptions concerning the synthesis of chlorophyll and its coupling to C and N metabolism in phytoplankton cells.

Overestimation of Southern Ocean chlorophyll and underestimation of carbon fluxes might indicate a general mismatch in Chl:C ratios in the model. This mismatch could also be explained by too low productivity and too low grazing and phytoplankton mortality in the model. Model solutions with increased phytoplankton growth and merely no zooplankton mortality lead to very high primary production but also to very large pools of zooplankton biomass, that were much larger than the amounts of phytoplankton biomass. In general, there is a systematic error in the Geider model as the synthesis of chlorophyll is directly coupled to the assimilation of nitrogen. Uptake of nitrogen thus produces chlorophyll.

In the Wadden Sea, the environment changes between light-limitation and nitrogen-limitation. Strong variations may therefore be expected in the phytoplankton C:N ratio as are produced by the model (study 1). In the Southern Ocean, strong vertical mixing leads to rather low irradiance levels in the deep mixed layers and the model produces low C:N ratios in the phytoplankton biomass of about 5.5 $\mathrm{mol\ mol^{-1}}$. As primary production and export production are often estimated on a nitrogen basis assuming the Redfield ratio for C:N (Schlitzer, 2002; Pollard et al., 2006), the low C:N ratios in the model also contribute to the discrepancies between the simulated carbon fluxes (study 3) and the estimates by Schlitzer (2002) and Pollard et al. (2006).

In the proposed model, Michaelis-Menten kinetics are applied to simulate concentration dependencies of nutrient uptake. The silicon metabolism in diatoms is still not completely understood (for a review, see Martin-Jézéquel et al. (2000)). Even though genes have been found to encode silicon transport molecules in diatoms (Hildebrand et al., 1997), silicon uptake kinetics can exhibit unusual responses to concentration changes (Del Amo and Brzezinski, 1999; Thamatrakoln and Hildebrand, 2008) that might indicate an alternative pathway of silicon uptake to a transporter-mediated membrane passage (Thamatrakoln and Hildebrand, 2008; Vrieling et al., 2007). The identification of the uptake mechanism is essential for the development of the parameterization. The applied Michaelis-Menten kinetics cannot explain all features of silicon and nitrogen uptake as observed by Kudo (2003) and Leynaert et al. (2004). Maybe the model by Aksnes and Egge (1991) can improve the description of nutrient assimilation in the parameterization.

The consideration of different elemental pools in biogeochemical ocean models and separation of the assimilation of different nutrients by phytoplankton can improve simulations of nutrient distributions in the global ocean and multi-nutrient regulations of phytoplankton growth can explain biogeographical distributions of the modelled plankton groups. As the applied model considers only one phytoplankton group that depends on the availability of silicon, it is not capable of simulating biogeochemical fluxes in ocean regions that are not dominated by diatoms. Deviations in the modelled nutrient distributions will emerge in ocean regions whose phytoplankton community cannot be represented by the applied model. Also the parameterization of export into the deep ocean will lead to deviations of deep ocean nutrient concentrations as the sinking speed of particles may not be assumed to be constant in the ocean (Berelson, 2002; Kriest and Oschlies, 2008). But these deviations in deep ocean nutrient concentrations will affect surface ocean biogeochemistry only on time scales of several hundreds of years. The addition of phytoplankton compartments that do not require silicon for growth will improve the simulations of surface chlorophyll concentrations and biogeochemical fluxes in the model. However, introducing further phytoplankton groups into the model, requires the setting of parameter values that are often not known and finding a set of parameter values with which the model reasonably reproduces the observations may become even more complicated. Nevertheless, optimization of a model often assumes that the model is able to fit the data and the best fitting solution can be found by systematically changing the parameter values.

Neglecting the elements silicon and phosphorus in a model for the Sylt-Rømø tidal basin leads to a mismatch in the ending of the modelled phytoplankton bloom with observations as the spring bloom ends simultaneously with the depletion of silicon and phosphorus concentrations in the Wadden Sea (Loebl et al., 2007). Depletion of nitrogen occurs after a second chlorophyll peak due to a succeeding bloom of *Phaeocystis globosa*. The choice of model equations to describe the pelagic ecosystem restricts the model solution and thus sets the minimum achievable deviation between model results and observations.

In the global model, the consideration of one phytoplankton group only neglects biogeographical variations in the phytoplankton community and the introduction of silicon dependencies of phyto-

plankton growth leads to specialization of the model to the functional group of diatoms. The model can be used to investigate the cycling of silicon in the ocean. For the simulation of the cycles of carbon and nitrogen, other important functional groups such as calcifying organisms and nitrogen fixing cyanobacteria are missing. Nevertheless, the model provides a good possibility to investigate the coupling of the nitrogen and silicon cycle.

As the biogeochemical tracers are distributed via the ocean current system, a good representation of ocean physics is required for the simulation of biogeochemistry and transport fluxes in marine ecosystems. In the model study of the Sylt-Rømø tidal basin, the assumption of two homogeneously mixed water boxes and implicit assumption of instantaneous mixing of the tracers that are exchanged with the tidal currents leads to difficulties in the interpretation of the mixing rate that results from the optimization of the salinity model as other model approaches propose a much higher exchange efficiency than our box model.

The representation of the ocean circulation strongly depends on the resolution of the applied model grid. In the global biogeochemical circulation model in study 3, the applied model grid has a resolution of $2\times2°$in the northern hemisphere and a resolution of $2\times cos(\phi)°$in the southern hemisphere. The model is not eddy resolving and mixing processes have to be parameterized on a subgrid scale. The still rather coarse resolution leads to nutrient trapping in the Equatorial Pacific and prevents the development of a well defined frontal system in the Southern Ocean. Increasing the resolution of the model grid to derive an eddy resolving high resolution model strongly improves ocean physics and the spatial patterns of surface chlorophyll concentrations (Fig. 5.5). However, increasing the model resolution also inreases computing time and memory requirements and the analysis of the large files of model output takes up a great deal of time. The biogeochemical general circulation model should therefore be improved further to derive a real global ocean carbon cycle model and then be applied on a high resolution model grid to improve the representation of ocean biogeochemical fluxes.

6.3 Proposal for future research

The studies presented in this thesis provide an ecosystem model for the Sylt-Rømø tidal basin and the adjacent North Sea, parameterization of variable incorporation of silicon and nitrogen in diatoms depending on ambient iron concentrations and a biogeochemical general circulation model that allows for variable Si:N:C:Chl ratios in phytoplankton biomass and considers the global cycles of carbon, nitrogen, silicon, and iron.

The ecosystem model for the Sylt-Rømø bight only considers the elements carbon and nitrogen and only one compartment of phytoplankton to describe the development of chlorophyll concentrations in the pelagic of the bight and the North Sea. In the observations, the diatom spring bloom ends when silicon and phosphorus become depleted and a bloom of *Phaeocystis globosa* follows until the remaining nitrogen is used up. Inclusion of phosphorus and silicon and inclusion of a second phytoplankton compartment for *Phaeocystis* could improve the representation of modelled chlorophyll concentrations and the biogeochemical fluxes of carbon during the summer period as *Phaeocystis* is known to contribute largely to carbon fixation in summer (Loebl et al., 2007). Also the parameterization of benthic filterfeeders and benthic remineralization processes may be extended to improve the description of zoobenthos biomass and the fate of carbon and nitrogen in the benthic compartment. To overcome the dicrepancies of the proposed exchange efficiencies of the tidal currents between the North Sea and the bight, the dynamic biogeochemical model could be coupled to a three-dimensional circulation model, to improve the representation of model physics.

For a better representation of phytoplankton physiology in ecosystem models, development of further parameterizations and identification of intracellular regulation mechanisms are required to derive the mathematical form of the regulation functions in quota models. The Si:N uptake ratio is currently only implemented to affect the distribution of nutrients in the ocean water column and may thus indirectly affect the fluxes of carbon, but increased Si:N ratios in diatom biomass may also be expected to directly affect carbon cycling via implications for diatom sinking or zooplankton grazing. The frustules of diatoms are assumed to function as a defense mechanism against zooplankton grazing (Hamm et al., 2003) by increasing the stability of the cell wall. Incorporation of larger amounts of silicon can be assumed to lead to even stronger cell walls and thus even better defense against grazing. Grazing experiments with iron-limited and non-limited diatoms that exhibit different degrees of silicified frustules could provide answers to these speculations and help to develop a parameterization for the dependency of grazing pressure on the degree of silicification.

Simulation of growth experiments with diatoms under different environmental conditions, i.e. different nutrient-limitations, may provide further insight into phytoplankton physiology and the regulation of metabolic processes via intracellular stoichiometric ratios. On the basis of these experiments, the parameterizations that are applied to large scale biogeochemical models can be improved. However, these experiments are only valuable for the development of multi-nutrient parameterizations when all particulate and dissolved tracers are measured.

The global biogeochemical model can be regarded as a silicon cycle model as it currently considers only diatoms as the single group of phytoplankton. To make it a real carbon cycle model, at least one group of non-silicifying phytoplankton should be included to improve the simulation of chlorophyll and nutrient concentrations in ocean regions that are not dominated by diatoms. Other important functional goups like cyanobacteria and coccolithophores may be included in the model to account for the effects of calcification on total alkalinity and nitrogen fixation as an additional source of reactive nitrogen in nitrogen-limited surface waters. But before adding phytoplankton groups to the model, the parameterization of C:N ratios and Chl:C ratios should be analysed for eventual systematic deviations of Chl:C ratios in the Southern Ocean to eventually solve the systematic underestimation of carbon fluxes while overestimating chlorophyll concentrations in the Southern Ocea.. Also the sinking parameterization in the model needs further improvement as it will lead to deviations in deep water nutrient concentrations and maybe also in upwelling regions in long-term model runs.

With these improvements, the model will be suitable to investigate the ocean's response to variations in the physical forcing in climate change model scenarios and to simulate biogeochemical fluxes on a larger scale than a few decades.

References

Adcroft, A., C. Hill, and J. Marshall. 1997. Representation of topography by shaved cells in a height coordinate ocean model. Monthly Weather Review **125**: 2293–2315.

Aksnes, D. and J. Egge. 1991. A theoretical model for nutrient uptake in phytoplankton. Marine Ecology Progress Series **70**: 65–72.

Armstrong, R. 1999. Stable model structures for representing biogeochemical diversity and size spectra in plankton communities. Journal of Plankton Research **21**: 445–464.

Asmus, H. and R. Asmus. 1998*a*. The role of macrobenthic communities for sediment-water material exchange in the sylt-rømø tidal basin. Senckenbergiana maritima **29**: 111–119.

Asmus, H., R. Asmus, and W. Hickel. 1998*a*. Biogenic Exchange and Transformation Processes in the Sylt-Rømø Wadden Sea: An Overview. *In* C. Gätje and K. Reise [eds.] , Ökosystem Wattenmeer: Austausch-, Transport- und Stoffumwandlungsprozesse, p. 215–217. Springer-Verlag, Berlin Heidelberg.

Asmus, R. and H. Asmus. 1998*b*. The Role of Benthic Communities for the Material Exchange in the Sylt-Rømø Wadden Sea. *In* C. Gätje and K. Reise [eds.] , Ökosystem Wattenmeer: Austausch-, Transport- und Stoffumwandlungsprozesse, p. 257–302. Springer-Verlag, Berlin Heidelberg.

Asmus, R., M. Jensen, D. Murphy, and R. Doerffer. 1998*b*. Primary Production of Microphytobenthos, Phytoplankton and the Annual Yield of Macrophytic Biomass in the Sylt-Rømø Wadden Sea. *In* C. Gätje and K. Reise [eds.] , Ökosystem Wattenmeer: Austausch-, Transport- und Stoffumwandlungsprozesse, p. 367–391. Springer-Verlag, Berlin Heidelberg.

Asmus, R. M. and H. Asmus. 1991. Mussel beds: limiting or promoting phytoplankton? Journal of Experimental Marine Biology and Ecology **148**: 215–232.

Assmy, P., J. Henjes, C. Klaas, and V. Smetacek. 2007. Mechanisms determining species dimonance in a phytoplankton bloom induced by the iron fertilization experiment EisenEx in the Southern Ocean. Deep Sea Research I **54**: 340–362.

Aumont, O., E. Maier-Reimer, S. Blain, and P. Monfray. 2003. An ecosystem model of the global ocean including Fe, Si, P colimitations. Global Biogeochemical Cycles **17**: doi:10.1029/2001GB001745.

Backhaus, J., D. Hartke, U. Hübner, H. Lohse, and A. Müller. 1998. Hydrographie und Klima im Lister Tidebecken. *In* C. Gätje and K. Reise [eds.] , Ökosystem Wattenmeer - Austausch-, Transport- und Stoffumwandlungsprozesse, p. 367–391. Springer-Verlag, Heidelberg, Berlin.

Baird, D., H. Asmus, and R. Asmus. 2004. Energy flow of a boreal intertidal ecosystem, the sylt-rømø bight. Marine Ecology Progress Series **279**: 45–61.

Baker, K. and R. Smith. 1982. Bio-optical classification and model of natural waters. 2. Limnology and Oceanography **27**: 500–509.

Banse, K. 1996. Low seasonality of low concentrations of surface chlorophyll in the Subantarctic water ring: underwater irradiance, iron, or grazing? Progress in Oceanography **37**: 241–291.

Baretta, J., W. Ebenhöh, and P. Ruardij. 1995. The european regional seas ecosystem model, a complex marine ecosystem model. Netherlands Journal of Sea Research **33**: 233–246.

Beddington, J. and R. May. 1977. Harvesting natural populations in a randomly fluctuating environment. Science **197**: 463–465.

Begon, M., J. Harper, and C. Townsend. 1998. Ökologie. Spektrum Akademischer Verlag GmbH, Heidelberg, Berlin.

Berelson, W. 2001. The Flux of Particulate Organic Carbon Into the Ocean Interior: A Comparison of Four U.S. JGOFS Regional Studies. Oceanography **14**: 59–67.

Berelson, W. 2002. Particle settling rates increase with depth in the ocean. Deep-Sea Research II **49**: 237–251.

Bergquist, B. and E. Boyle. 2006. Dissolved iron in the tropical and subtropical Atlantic Ocean. Global Biogeochemical Cycles **20**: doi:10.1029/2005GB002505.

Beukema, J. and R. Dekker. 2005. Decline of recruitment success in cockles and other bivalves in the Wadden Sea: possible role of climate change, predation on postlarvae and Fisheries. Marine Ecology Progress Series **287**: 149–167.

Boye, M., C. Van Den Berg, J. De Jong, H. Leach, P. Croot, and H. De Baar. 2001. Organic complexation of iron in the Southern Ocean. Oceanographic Research Papers **48**: 1477–1497.

Bracher, A., B. Kroon, and M. Lucas. 1999. Primary production, physiological state and composition of phytoplankton in the Atlantic Sector of the Southern Ocean. Marine Ecology Progress Series **190**: 1–16.

Bricaud, A. and A. Morel. 1986. Light attenuation and scattering by phytoplanktonic cells: a theoretical modeling. Applied Optics **25**: 571–580.

British Oceanographic Data Center. 2003. Centenary edition of the GEBCO digital atlas [CD-ROM]. Liverpool, UK: Published on behalf of the Intergovernmental Oceanographic Commission and the International Hydrographic Organization.

Brock, T. D. 1981. Calculating solar radiation for ecological studies. Ecological Modelling **14**: 1–19.

Broecker, W. and T.-H. Peng. 1982. Tracers in the Sea. Eldigio Press.

Bruns, R. and L.-A. Meyer-Reil. 1998. Benthic Nitrogen Turnover and Implications for the Budget of Dissolved Inorganic Nitrogen Compounds in the Sylt-Rømø Wadden Sea. *In* C. Gätje and K. Reise [eds.] , Ökosystem Wattenmeer: Austausch-, Transport- und Stoffumwandlungsprozesse, p. 219–232. Springer-Verlag, Berlin Heidelberg.

Brzezinski, M. 1985. The Si:C:N ratio of marine diatoms: interspecific variability and the effect of some environmental variables. Journal of Phycology **21**: 347–357.

Burchard, H., G. Flöder, J. Staneva, T. Badewien, and R. Riethmüller. 2008. Impact of Density Gradients on Net Sediment Transport into the Wadden Sea. Journal of Physical Oceanography **38**: 566–587.

Büttger, H., H. Asmus, R. Asmus, C. Buschmann, S. Dittmann, and G. Nehls. 2008. Community dynamics of intertidal soft-bottom mussel beds over two decades. Helgoland Marine Research **62**: 23–36.

Campbell, J. 1995. The lognormal distribution as a model for bio-optical variability in the sea. Journal of Geophysical Research **100**: 13,237–13,254.

Carr, M.-E., M. Friedrichs, M. Schmeltz, M. Noguchi Aita, D. Antoine, K. Arrigo, I. Asanuma, O. Aumont, R. Barber, M. Behrenfeld, R. Bidigare, E. Buitenhuis, J. Campbell, A. Ciotti, H. Dierssen, M. Dowell, J. Dunne, W. Esaias, B. Gentili, W. Gregg, S. Groom, N. Hoepffner, J. Ishizaka, T. Kameda, C. Le Quéré, S. Lohrenz, J. Marra, F. Mélin, K. Moore, A. Morel, T. Reddy, J. Ryan, M. Scardi, T. Smyth, K. Turpie, G. Tilstone, K. Waters, and Y. Yamanaka. 2006. A comparison of global estimates of marine primary production from ocean color. Deep-Sea Research II **53**: 741–770.

Colijn, F. and G. C. Cadée. 2003. Is phytoplankton growth in the wadden sea light or nitrogen limited? Journal of Sea Research **49**: 83–93.

Conkright, M., S. Levitus, and T. Boyer. 1994. World Ocean Atlas 1994. Volume 1: Nutrients. NOAA Atlas NEDSIS 1, NOAA, Washington D.C.

Cooper, P. 1969. The absorption of solar radiation in solar stills. Solar Energy **12**: 333–346.

Cox, P. M., R. A. Betts, C. D. Jones, S. A. Spall, and I. J. Totterdell. 2000. Acceleration of global warming due to carbon-cycle feedbacks in a coupled climate model. Nature **408**: 184–187.

De Baar, H. 1994. von Liebig's Law of the Minimum and plankton ecology (1899-1991). Progress in Oceanography **33**: 347–386.

De Baar, H., J. De Jong, R. Nolting, K. Timmermans, M. Van Leeuwe, U. Bathmann, M. Rutgers Van Der Loeff, and J. Sildam. 1999. Low dissolved Fe and the absence of diatom blooms in remote Pacific waters of the Southern Ocean. Marine Chemistry **66**: 1–34.

De La Rocha, C., D. Hutchins, M. Brzezinski, and Y. Zhang. 2000. Effects of iron and zinc deficiency on elemental composition and silica production by diatoms. Marine Ecology Progress Series **195**: 71–79.

Del Amo, Y. and M. Brzezinski. 1999. The chemical form of dissolved Si taken up by marine diatoms. Journal of Phycology **35**: 1162–1170.

DeMaster, D. 1981. The supply and accumulation of silica in the marine environment. Geochimica et Cosmochimica Acta **45**: 1715–1732.

Denman, K. and M. Peña. 2002. The response of two coupled 1-D mixed layer / planktonic ecosystem models to climate change in the NE Subarctic Pacific Ocean. Deep-Sea Research II **49**: 5739–5757.

Denman, K. L. 2003. Modelling planktonic ecosystems: parameterizing complexity. Progress In Oceanography **57**: 429–452.

Dick, S. and W. Schönfeld. 1996. Water transport and mixing in the north frisian wadden sea - results of numerical investigations. German Journal of Hydrography **48**: 27–48.

Dickson, A. and F. Millero. 1987. A comparison of the equilibrium constants for the dissociation of carbonic acid in seawater media. Deep-Sea Research **34**: 1733–1743.

Diederich, S., G. Nehls, J. van Beusekom, and K. Reise. 2005. Introduced Pacific oysters (*Crassostrea gigas*) in the northern Wadden Sea: invasion accelerated by warm summers? Helgoland Marine Research **59**: 97–106.

Droop, M. 1973. Some thoughts on nutrient limitations in algae. Journal of Phycology **9**: 264–272.

Edwards, A. M. and A. Yool. 2000. The role of higher predation in plankton population models. Journal of Plankton Research **22**: 1085–1112.

Engel, A., S. Thoms, U. Riebesell, E. Rochelle-Newall, and I. Zondervan. 2004. Polysaccharide aggregation as a potential sink of marine dissolved organic carbon. Nature **428**: 929–932.

Eppley, R. 1972. Temperature and Phytoplankton Growth in the Sea. Fishery Bulletin **70**: 1063–1085.

Eppley, R., J. Rogers, J. McCarthy, and A. Sournia. 1971. Light/dark periodicity in nitrogen assimilation of the marine phytoplankters *Skeletonema costatum* and *Coccolithus huxleyi* in N-limited culture. Journal of Phycology **7**: 150–154.

Erez, J., K. Takahashi, and S. Honjo. 1982. In-situ dissolution experiment of Radiolaria in the central North Pacific Ocean. Earth and Planetary Science Letters **59**: 245–254.

Falkowski, P. 2000. Rationalizing elemental ratios in unicellular algae. Journal of Phycology **36**: 3–6.

Falkowski, P., Z. Dubinsky, and K. Wyman. 1985. Growth-irradiance relationships in phytoplankton. Limnology and Oceanography **30**: 311–321.

Fasham, M., H. Ducklow, and S. McKelvie. 1990. A nitrogen-based model of plankton dynamics in the ocean mixed layer. Journal of Marine Research **48**: 591–639.

Fasham, M. and G. Evans. 1995. The use of optimization techniques to model marine ecosystem dynamics at the JGOFS station at 47°N 20°W. Philosophical Transactions of the Royal Society of London **B348**: 203–209.

Fasham, M., J. Sarmiento, R. Slater, H. Ducklow, and R. Williams. 1993. Ecosystem behaviour at Bermuda Station ”S” and Ocean Weather Station ”INDIA”: A general circulation model and observational analysis. Global Biogeochemical Cycles **7**: 379–415.

Fast, T., A. Müller, and A. Wilhelm. 1999. The sylt-rømø bight ecosystem model (srb model) - an introduction. Technical Report 99/E/28, GKSS.

Fennel, K., M. Losch, J. Schröter, and M. Venzel. 2001. Testing a marine ecosystem model:Sensitivity analysis and parameter optimization. Journal of Marine Systems **28**: 45–63.

Flato, G. 2004. Sea-ice and its response to CO2 forcing as simulated by global climate models. Climate Dynamics **23**: 229–241.

Flynn, K. 2003. Modelling multi-nutrient interactions in phytoplankton; balancing simplicity and realism. Progress in Oceanography **56**: 249–279.

Flynn, K. and V. Martin-Jézéquel. 2000. Modelling Si-N-limited growth of diatoms. Journal of Plankton Research **22**: 447–472.

Franck, V., M. Brzezinski, K. Coale, and D. Nelson. 2000. Iron and silicic acid concentrations regulate Si uptake north and south of the Polar Frontal Zone in the Pacific Sector of the Southern Ocean. Deep-Sea Research Part II **47**: 3315–3338.

Franks, P. J. S. 2002. NPZ Models of Plankton Dynamics: Their Construction, Coupling to Physics, and Application. Journal of Oceanography **58**: 379–387.

Friedlingstein, P., J.-L. Dufresne, P. M. Cox, and P. Rayner. 2003. How positive is the feedback between climate change and the carbon cycle? Tellus **55B**: 692–700.

Fyfe, J. and O. Saenko. 2006. Simulated changes in the extratropical Southern Hemisphere winds and currents. Geophysical Research Letters **33**: doi:10.1029/2005GL025332.

Garcia, H. E. and L. I. Gordon. 1992. Oxygen solubility in seawater: Better fitting equations. Limnology and Oceanography **37**: 1307–1312.

Gätje, C. and K. Reise. 1998. Ökosystem Wattenmeer, Austausch-, Transport- und Stoffumwandlungsprozesse. Springer Verlag, Berlin, Heidelberg.

Geider, R. and J. La Roche. 1994. The role of iron in phytoplankton photosynthesis, and the potential for iron-limitation of primary productivity in the sea. Photosynthesis Research **39**: 275–301.

Geider, R. and J. La Roche. 2002. Redfield revisited: variability of C:N:P in marine microalgae and its biochemical basis. European Journal of Phycology **37**: 1–17.

Geider, R. J., H. L. MacIntyre, and T. M. Kana. 1996. A dynamic model of photoadaptation in phytoplankton. Limnology and Oceanography **41**: 1–15.

Geider, R. J., H. L. MacIntyre, and T. M. Kana. 1998. A dynamic regulatory model of phytoplanktonic acclimation to light, nutrients, and temperature. Limnology and Oceanography **43**: 679–694.

Gent, P. R. and J. C. McWilliams. 1990. Isopycnal mixing in ocean circulation models. Journal of Physical Oceanography **20**: 150–155.

Gentleman, W. 2002. A chronology of plankton dynamics *in silico*: how computer models have been used to study marine ecosystems. Hydrobiologia **480**: 69–85.

Gentleman, W., A. Leising, S. Strom, and J. Murray. 2003. Functional responses for zooplankton feeding on multiple ressources: a review of assumptions and biological dynamics. Deep-Sea Research II **50**: 2847–2875.

Gille, S. 2002. Warming of the Southern Ocean since the 1950s. Science **295**: 1275–1277.

Gnanadesikan, A. 1999. A global model of silicon cycling: Sensitivity to eddy parameterization and dissolution. Global Biogeochemical Cycles **13**: 199–220.

Greene, R., R. Geider, and P. Falkowski. 1991. Effect of iron limitation on photosynthesis in a marine diatom. Limnology and Oceanography **36**: 1772–1782.

Greene, R., R. Geider, Z. Kolber, and P. Falkowski. 1992. Iron-Induced Changes in Light Harvesting and Photochemical Energy Conversion Processes in Eukaryotic Marine Algae. Plant Physiology **100**: 565–575.

Grimm, V. 1999. Ten years of individual-based modelling in ecology: what have we learned and what could we learn in the future? Ecological Modelling **115**: 129–148.

Grimm, V., K. Frank, F. Jeltsch, R. Brandl, J. Uchmański, and C. Wissel. 1996. Pattern-oriented modelling in population ecology. The Science of the Total Environment **183**: 151–166.

Hamm, C., R. Merkel, O. Springer, P. Jurkojc, C. Maier, K. Prechtel, and V. Smetacek. 2003. Architecture and material properties of diatom shells provide effective mechanical protection. Nature **421**: 841–843.

Hazelaar, S., H. van der Strate, W. Gieskes, and E. Vrieling. 2005. Monitoring rapid valve formation in the pennate diatom *Navicula salinarum* (Bacillariophyceae). Journal of Phycology **41**: 354–358.

Hedtkamp, S. 2005. Shallow subtidal sand: Permeability, nutrient dynamics, microphytobenthos and organic matter. Ph.D. thesis, Christian-Albrechts-Universität, Kiel.

Heip, C. H. R., N. K. Goosen, P. M. J. Herman, J. Kromkamp, J. J. Middelburg, and K. Soetaert. 1995. Production and consumption of biological particles in temperate tidal estuaries. Oceanography and Marine Biology: an Annual Review **33**: 1–149.

Hickel, W. 1980. The influence of elbe river water on the wadden sea of sylt (german bight, north sea). German Journal of Hydrography **33**: 43–52.

Hildebrand, M. 2002. Lack of coupling between silicon and other elemental metabolisms in diatoms. Journal of Phycology **38**: 841–843.

Hildebrand, M., B. Volcani, W. Gassmann, and J. Schroeder. 1997. A gene family of silicon transporters. Nature **385**: 688–689.

Hohn, S., C. Völker, and D. Wolf-Gladrow. submitted. A model of the carbon:nitrogen:silicon stoichiometry of diatoms based on metabolic processes. submitted to MEPS .

Holling, C. 1959. Some characteristics of simple types of predation and parasitism. Canadian Entomologist **91**: 385–398.

Honjo, S. and S. Manganini. 1993. Annual biogenic particle fluxes to the interior of the North Atlantic Ocean; studied at 34°N 21°W and 48°N 21°W. Deep-Sea Research I **40**: 587–607.

Hutchins, D. and K. Bruland. 1998. Iron-limited diatom growth and Si:N uptake ratios in a coastal upwelling regime. Nature **393**: 561–564.

IPCC. 2007. Working group 1 report 'the physical science basis'. Technical report, Intergovernmental Panel on Climate Change. URL `http://ipcc-wg1.ucar.edu/wg1/wg1-report.html`.

Jassby, A. D. and T. Platt. 1976. Mathematical formulation of the relationship between photosynthesis and light for phytoplankton. Limnology and Oceanography **21**: 540–547.

Kamatani, A. 1982. Dissolution Rates of Silica from Diatoms Decomposing at Various Temperatures. Marine Biology **68**: 91–96.

Key, R., A. Kozyr, C. Sabine, K. Lee, R. Wanninkhof, J. Bullister, R. Feely, F. Millero, C. Mordy, and T.-H. Peng. 2004. A global ocean carbon climatology: Results from Global Data Analysis Project (GLODAP). Global Biogeochemical Cycles **18**: 1–23.

Kleypas, J. and S. Doney. 2001. Nutrients, Chlorophyll, Primary Production and Related Biogeochemical Properties in the Ocean Mixed Layer - A Compilation of Data Collected at Nine JGOFS Sites. Technical Report TN-447+STR, National Center for Atmospheric Research. 55pp.

Kriest, I. and A. Oschlies. 2008. On the treatment of particulate organic matter sinking in large-scale models of marine biogeochemical cycles. Biogeosciences **5**: 55–72.

Kroon, B. and S. Thoms. 2006. From electron to biomass: a mechanistic model to describe phytoplankton photosynthesis and steady-state growth rates. Journal of Phycology **42**: 593–609.

Kudo, I. 2003. Change in the uptake and cellular Si:N ratio in diatoms responding to the ambient Si:N ratio and growth phase. Marine Biology **143**: 39–46.

Kühn, S. and C. Brownlee. 2005. Membrane organisation and dynamics in the marine diatom *Coscinodiscus wailesii* (Bacillariophyceae). Botanica Marina **48**: 297–305.

Lancelot, C., E. Hannon, S. Becquevort, C. Veth, and H. De Baar. 2000. Modeling phytoplankton blooms and carbon export production in the Southern Ocean: dominant controls by light and iron in the Atlantic sector in Austral spring 1992. Deep-Sea Research I **47**: 1621–1662.

Large, W. G., G. Danabasoglu, S. C. Doney, and J. C. McWilliams. 1997. Sensitivity of surface forcing and boundary layer mixing in a global ocean model: Annual-mean climatology. Journal of Physical Oceanography **27**: 2418–2447.

Large, W. G., J. C. McWilliams, and S. C. Doney. 1994. Oceanic vertical mixing: A review and a model with a nonlocal boundary layer parameterization. Review of Geophysics **32**: 363–404.

Large, W. G. and S. Pond. 1981. Open ocean momentum flux measurements in moderate to strong winds. Journal of Physical Oceanography **11**: 324–336.

Large, W. G. and S. Pond. 1982. Sensible and latent heat flux measurements over the ocean. Journal of Physical Oceanography **12**: 464–482.

Large, W. G. and S. Yeager. 2004. Diurnal to decadal global forcing for ocean and sea-ice models: the data sets and flux climatologies. Technical Report NCAR/TN-460+STR, CGD Division of the National Center for Atmospheric Research.

Le Quéré, C., S. Harrison, I. Prentice, E. Buitenhuis, O. Aumont, L. Bopp, H. Claustre, L. Cotrim da Cunha, R. Geider, X. Giraud, C. Klaas, K. Kohlfeld, L. Legendre, M. Manizza, T. Platt, R. Rivkin, S. Sathyendranath, J. Uitz, A. Watson, and D. Wolf-Gladrow. 2005. Ecosystem dynamics based on plankton functional types for global ocean biogeochemistry models. Global Change Biology **11**: 2016–2040.

Leith, C. E. 1996. Stochastic models of chaotic systems. Physica D: Nonlinear Phenomena **98**: 481–491.

Lenton, T. and A. Watson. 2000. Redfield revisited 1. Regulation of nitrate, phosphate, and oxygen in the ocean. Global Biogeochemical Cycles **14**: 225–248.

Levitus, S. and T. Boyer. 1994*a*. World Ocean Atlas 1994. Technical report, NOAA.

Levitus, S. and T. Boyer. 1994*b*. World Ocean Atlas 1994. Volume 4: Temperature. NOAA Atlas NEDSIS 4, NOAA, Washington D.C.

Levitus, S., R. Burgett, and T. Boyer. 1994*a*. World Ocean Atlas 1994. NOAA Atlas NEDSIS 3, NOAA, Washington D.C.

Levitus, S., R. Burgett, and T. Boyer. 1994*b*. World Ocean Atlas 1994. Volume 3: Salinity. NOAA Atlas NEDSIS 3, NOAA, Washington D.C.

Lewin, J. 1955. Silicon metabolism in diatoms III. Respiration and Silicon Uptake in *Navicula pelliculosa*. Journal of General Physiology **39**: 1–10.

Leynaert, A., E. Bucciarelli, P. Claquin, R. Dugdale, V. Martin-Jézéquel, P. Pondaven, and O. Ragueneau. 2004. Effect of iron deficiency on diatom cell size and silicic acid uptake kinetics. Limnology and Oceanography **49**: 1134–1143.

Loebl, M., T. Dolch, and J. van Beusekom. 2007. Annual dynamics of pelagic primary production and respiration in a shallow coastal basin. Journal of Sea Research **58**: 269–282.

Longhurst, A. 1998. Ecological geography of the sea. Academic Press.

Loreau, M. 1995. Consumers as maximizers of matter and energy flow in ecosystems. The American Naturalist **145**: 22–42.

Losa, S., G. Kivman, and V. Ryabchenko. 2004. Weak constraint parameter estimation for a simple ocean ecosystem model: what can we learn about the model and data? Journal of Marine Systems **45**: 1–20.

MacIntyre, H. L., R. J. Geider, and D. C. Miller. 1996. Microphytobenthos: The ecological role of the ”secret garden” of unvegetated, shallow-water marine habitats. i. distribution, abundance and primary production. Estuaries **19**: 186–201.

Maier-Reimer, E., U. Mikolajewicz, and A. Winguth. 1996. Future ocean uptake of CO_2: interaction between ocean circulation and biology. Climate Dynamics **12**: 711–721.

Maldonado, M. and N. Price. 2001. Reduction and transport of organically bound iron by *Thalassiosira oceanica* (Bacillariophyceae). Journal of Phycology **37**: 298–309.

Maliva, R., A. Knoll, and R. Siever. 1989. Secular change in chert distribution: a reflection of evolving biological participation in the silica cycle. Palaios **4**: 519–532.

Marchetti, A. and P. J. Harrison. 2007. Coupled changes in the cell morphology and the elemental (C, N, and Si) composition of the pennate diatom *Pseudo-nitzschia* due to iron deficiency. Limnology and Oceanography **52**: 2270–2284.

Marks, K. M. and W. H. F. Smith. 2006. An evaluation of publicly available global bathymetry grids. Marine Geophysical Researches **27**: 19–34.

Marshall, J., C. Hill, L. Perelman, and A. Adcroft. 1997. Hydrostatic, quasi-hydrostatic, and nonhydrostatic ocean modeling. Journal of Geophysical Research **102**: 5733–5752.

Martin, J. and S. Fitzwater. 1988. Iron deficiency limits phytoplankton growth in the north-east Pacific subarctic. Nature **331**: 341–343.

Martin, J., S. Fitzwater, and R. Gordon. 1990. Iron deficiency limits phytoplankton growth in Antarctic waters. Global Biochemical Cycles **4**: 5–12.

Martin, J., G. Knauer, D. Karl, and W. Broenkow. 1987. VERTEX: carbon cycling in the northeast Pacific. Deep Sea Research **34**: 267–285.

Martin-Jézéquel, V., M. Hildebrand, and M. Brzezinski. 2000. Silicon metabolism in diatoms: Implications for growth. Journal of Phycology **36**: 821–840.

McDougall, T. J., D. R. Jackett, D. G. Wright, and R. Feistel. 2003. Accurate and computationally efficient algorithms for potential temperature and density of seawater. Journal of Atmospheric and Oceanographic Technology **20**: 730–741.

Mehrbach, C., C. Culberson, J. Hawley, and R. Pytkowicz. 1973. Measurement of the apparent dissociation constants of carbonic acid in seawater at atmospheric pressure. Limnology and Oceanography **18**: 897–907.

Menemenlis, D., C. Hill, A. Adcroft, J.-M. Campin, B. Cheng, B. Ciotti, I. Fukumori, A. Koehl, P. Heimbach, C. Henze, T. Lee, D. Stammer, J. Taft, and J. Zhang. 2005. Nasa supercomputer improves prospects for ocean climate research. Eos, Transactions, American Geophysical Union **86**: 89, 95–96.

Meskhidze, N., A. Nenes, W. Chameides, C. Luo, and N. Mahowald. 2007. Atlantic Southern Ocean productivity: Fertilization from above or below? Global Biogeochemical Cycles **21**: doi:10.1029/2006GB002711.

Michal, G. 1999. Biochemical Pathways. Spektrum Akademischer Verlag, Heidelberg.

Milankovitch, M. 1930. Mathematische Klimalehre und Astronomische Theorie der Klimaschwankungen. *In* Handbuch der Klimatologie, page 298. Gebrüder Bornträger, Berlin.

Millero, F. 1995. Thermodynamics of the carbon dioxide system in the oceans. Geochimica et Cosmochimica Acta **59**: 661–677.

MITgcm Group. 2002. MITgcm Release 1 Manual. Online documentation, MIT/EAPS, Cambridge, MA 02139, USA. `http://mitgcm.org/sealion/online_documents/manual.html`.

Moll, A. 1998. Regional distribution of primary production in the north sea simulated by a three-dimensional model. Journal of Marine Systems **16**: 151–170.

Mongin, M., D. Nelson, P. Pondaven, M. Brzezinski, and P. Tréguer. 2003. Simulation of upper-ocean biogeochemistry with a flexible-composition phytoplankton model: C, N and Si cycling in the western Sargasso Sea. Deep-Sea Research I **50**: 1445–1480.

Moore, J., S. Doney, and K. Lindsay. 2004. Upper ocean ecosystem dynamics and iron cycling in a global three-dimensional model. Global Biogeochemical Cycles **18**: doi:10.1029/2004GB002220.

Moore, K., S. Doney, J. Kleypas, D. Glover, and I. Fung. 2002. An intermediate complexity marine ecosystem model for the global domain. Deep-Sea Research II **49**: 403–462.

Mopper, K., J. Zhou, K. Ramana, U. Passow, H. Dam, and D. Drapeau. 1995. The role of surface-active carbohydrates in the flocculation of a diatom bloom in a mesocosm. Deep Sea Research II **42**: 47–73.

Morel, F. 1987. Kinetics of nutrient uptake and growth in phytoplankton. Journal of Phycology **23**: 137–150.

Nelson, D., P. Tréguer, M. Brzezinski, A. Leynaert, and B. Quéguiner. 1995. Production and dissolution of biogenic silica in the ocean: Revised global estimates, comparison with regional data and relationship to biogenic sedimentation. Global Biogeochemical Cycle **9**: 359–372.

Nixdorf, B., A. Fyson, and H. Krumbeck. 2001. Review: plant life in extremely acidic waters. Environmental and Experimental Botany **46**: 203–211.

NOAA. 1988. Data Announcement 88-MGG-02, Digital relief of the Surface of the Earth. Technical report, National Geophysical Data Center, Boulder, Colorado.

Olbers, D., D. Borowski, C. Völker, and J.-O. Wolff. 2004. The dynamical balance, transport and circulation of the Antarctic Circumpolar Current. Antarctic science **16**: 439–470.

Orr, J., E. Maier-Reimer, U. Mikolajewicz, P. Monfray, J. Sarmiento, J. Toggweiler, N. Taylor, J. Palmer, N. Gruber, C. Sabine, C. Le Quéré, R. Key, and J. Boutin. 2001. Estimates of anthropogenic carbon uptake from four three-dimensional global ocean models. Global Biogeochemical Cycles **15**: 43–60.

Orsi, A., T. Whitworth, and W. Nowlin Jr. 1995. On the meridional extent and fronts of the Antarctic Circumpolar Current. Deep Sea Research **42**: 641–673.

Oschlies, A. and V. Garcon. 1999. An eddy-permitting coupled physical-biological model of the North Atlantic 1. Sensitivity to advection numerics and mixed layer physics. Global Biogeochemical Cycles **13**: 135–160.

Paasche, E. 1973*a*. Silicon and the Ecology of Marine Plankton Diatoms. I. *Thalassiosira pseudonana (Cyclotella nana)* Grown in a Chemostat with Silicate as Limiting Nutrient. Marine Biology **19**: 117–126.

Paasche, E. 1973*b*. Silicon and the Ecology of Marine Plankton Diatoms. II. Silicate-Uptake Kinetics in Five Diatom Species. Marine Biology **19**: 262–269.

Pahlow, M. 2005. Linking chlorophyll-nutrient dynamics to the Redfield N:C ratio with a model of optimal phytoplankton growth. Marine Ecology Progress Series **287**: 33–43.

Parekh, P., M. Follows, and E. Boyle. 2004. Modelling the global iron cycle. Global Biogeochemical Cycles **18**: doi:10.1029/2003GB002061.

Pasciak, W. and J. Gavis. 1974. Transport limitation of nutrient uptake in phytoplankton. Limnology and Oceanography **19**: 881–888.

Pätsch, J. and H.-J. Lenhart. 2004. Daily Loads of Nutrients, Total Aklalinity, Dissolved Inorganic Carbon and Dissolved Organic Carbon of the European Continental Rivers for the Years 1977-2002. Reihe B: Ozeanographie 48, Zentrum für Meeres- und Klimaforschung, Universität Hamburg.

Ploug, H., M. Iversen, M. Koski, and E. Buitenhuis. 2008. Production, oxygen respiration rates, and sinking velocity of copepod fecal pellets: Direct measurements of ballasting by opal and calcite. Limnology and Oceanography **53**: 469–476.

Pollard, R., P. Tréeguer, and J. Read. 2006. Quantifying nutrient supply to the Southern Ocean. Journal of Geophysical Research **111**: doi:10.1029/2005JC003076.

Pondaven, P., M. Gallinari, S. Chollet, E. Buciarelli, G. Sarthou, S. Schultes, and F. Jean. 2007. Grazing-induced Changes in Cell Wall Silicification in a Marine Diatom. Protist **158**: 21–28.

Pondaven, P., D. Ruiz-Pino, J. N. Druon, C. Fravalo, and P. Tréguer. 1999. Factors controlling silicon and nitrogen biogeochemical cycles in high nutrient, low chlorophyll systems (the Southern Ocean and the North Pacific): Comparison with a mesotrophic system (the North Atlantic). Deep-Sea Research II **46**: 1923–1968.

Postma, H. 1981. Exchange of materials between the north sea and the wadden sea. Marine Geology **40**: 199–215.

Radach, G. and J. Pätsch. 1997. Climatological annual cycles of nutrients and chlorophyll in the north sea. Journal of Sea Research **38**: 231–248.

Ragueneau, O., N. Dittert, P. Pondaven, P. Tréguer, and L. Corrin. 2002. Si/C decoupling in the world ocean: Is the Southern Ocean different? Deep-Sea Research Part II: Topical Studies in Oceanography **49**: 3127–3154.

Ragueneau, O., S. Schultes, K. Bidle, P. Claquin, and B. Moriceau. 2006. Si and C interactions in the world ocean: Importance of ecological processes and implications for the role of diatoms in the biological pump. Global Biogeochemical Cycles **20**: doi:10.1029/2006GB002688.

Ragueneau, O., P. Tréguer, A. Leynaert, R. Anderson, M. Brzezinski, D. DeMaster, R. Dugdale, J. Dymond, G. Fischer, R. Francois, C. Heinze, E. Maier-Reimer, V. Martin-Jézéquel, D. Nelson, and B. Quéguiner. 2000. A review of the Si cycle in the modern ocean: Recent progress and missing gaps in the application of biogenic opal as a paleoproductivity proxy. Global and Planetary Change **26**: 317–365.

Raven, J. and A. Waite. 2004. The evolution of silicification in diatoms: Inescapable sinking and sinking as escape? New Phytologist **162**: 45–61.

Redfield, A. 1958. The biological control of chemical factors in the environment. American Scientist **46**: 205–221.

Redfield, A., B. Ketchum, and F. Richards. 1963. The influence of organisms on the composition of seawater. In: The Sea. Vol. 2, M. N. Hill (edit.), Interscience, New York, p. 1-34.

Reed, R. 1977. On estimating innsolation over the ocean. Journal of Physical Oceanography **7**: 482–485.

Reise, K. 2005. Coast of change: habitat loss and transformations in the Wadden Sea. Helgoland Marine Research **59**: 9–21.

Risovic, D. 1993. Two component model of sea particle size distribution. Deep Sea Research **40**: 1459–1473.

Rusch, A. and M. Huettel. 2000. Advective particle transport into permeable sediments - evidence from experiments in an intertidal sandflat. Limnology and Oceanography **45**: 525–533.

Sarmiento, J., J. Simeon, A. Gnanadesikan, N. Gruber, R. Key, and R. Schlitzer. 2007. Deep ocean biogeochemistry of silicic acid and nitrate. Global Biogeochemical Cycles **21**: doi:10.1029/2006GB002720.

Sarmiento, J., R. Slater, R. Barber, L. Bopp, S. Doney, A. Hirst, J. Kleypas, R. Matear, U. Mikolajewicz, P. Monfray, V. Soldatov, S. Spall, and R. Stouffer. 2004. Response of ocean ecosystems to climate warming. Global Biogeochemical Cycles **18**: doi:10.1029/2003GB002134.

Sarmiento, J., R. Slater, M. Fasham, H. Ducklow, J. Toggweiler, and G. Evans. 1993. A seasonal three-dimensional ecosystem model of nitrogen cycling in the North Atlantic euphotic zone. Global Biogeochemical Cycles **7**: 417–450.

Schartau, M., A. Engel, J. Schröter, S. Thoms, C. Völker, and D. Wolf-Gladrow. 2007. Modelling carbon overconsumption and the formation of extracellular particulate organic carbon. Biogeosciences **4**: 433–454.

Scheffer, M., J. M. Baveco, D. L. DeAngelis, K. A. Rose, and E. H. van Nes. 1995. Super-individuals a simple solution for modelling large populations on an individual basis. Ecological Modelling **80**: 161–170.

Schlitzer, R. 2002. Carbon export fluxes in the Southern Ocean: results from inverse modelling and comparison with satellite-based estimates. Deep Sea Research II **49**: 1623–1644.

Schmid, A.-M. and D. Schulz. 1979. Wall Morphogenesis in Diatoms: Deposition of Silica by Cytoplasmic Vesicles. Protoplasma **100**: 267–288.

Siever, R. 1991. Silica in the oceans: biological-geochemical interplay, p. 287–295. *In* S. Schneider and P. Boston [eds.] , Scientists on Gaia. MIT Press.

Six, K. and E. Maier-Reimer. 1996. Effects of plankton dynamics on seasonal carbon fluxes in an ocean general circulation model. Global Biogeochemical Cycles **10**: 559–583.

Skogen, M. D. and A. Moll. 2000. Interannual variability of the north sea primary production: comparison from two model studies. Continental Shelf Research **20**: 129–151.

Smetacek, V. 1985. Role of sinking in diatom life-history cycles: ecological, evolutionary and geological significance. Marine Biology **84**: 239–251.

Smetacek, V. 2001. A watery arms race. Nature **411**: 745.

Smetacek, V. and F. Pollehne. 1986. Nutrient cycling in pelagic systems: a reappraisal of the conceptual framework. Ophelia **26**: 401–428.

Smith, W. H. F. and D. T. Sandwell. 1997. Global seafloor topography from satellite altimetry and ship depth soundings. Science **277**: 1957–1962.

Steele, J. 1958. Plant production in the northern North Sea. Scottish Home Department. Marine Research **7**: 1–36.

Sterner, R. and J. Elser. 2002. Ecological Stoichiometry, The Biology of Elements from Molecules to the Biosphere. Princeton University Press, Princeton and Oxford.

Sullivan, C. 1976. Diatom mineralization of silicic acid. I. $Si(OH)_4$ transport characteristics in *Navicula pelliculosa*. Journal of Phycology **12**: 390–396.

Sunda, W. and S. Huntsman. 1995. Iron uptake and growth limitation in oceanic and coastal phytoplankton. Marine Chemistry **50**: 189–206.

Sunda, W. and S. Huntsman. 1997. Interrelated influence of iron, light and cell size on marine phytoplankton growth. Nature **390**: 389–392.

Takahashi, T. 2004. The Fate of Industrial Carbon Dioxide. Science **305**: 352–353.

Takeda, S. 1998. Influence of iron availability on nutrient consumption ratio of diatoms in oceanic waters. Nature **393**: 774–777.

Taylor, K. 2001. Summarizing multiple aspects of model performance in a single diagram. Journal of Geophysical Research **106**: 7183–7192.

Tegen, I. and I. Fung. 1994. Modeling of mineral dust in the atmosphere: Sources, transport, and optical thickness. Journal of Geophysical Research **99**: 22,897–22,914.

Thamatrakoln, K. and M. Hildebrand. 2008. Silicon Uptake in Diatoms Revisited: A Model for Saturable and Nonsaturable Uptake Kinetics and the Role of Silicon Transporters. Plant Physiology **146**: 1397–1407.

Thieltges, D., M. Strasser, J. van Beusekom, and K. Reise. 2004. Too cold to prosper - Winter mortality prevents population increase of the introduced american slipper limpet *Crepidula fornicata* in northern europe. Journal of Experimental Marine Biology and Ecology **311**: 375–391.

Thomas, H., Y. Bozec, K. Elkalay, and H. J. W. de Baar. 2004. Enhanced open ocean storage of co_2 from shelf sea pumping. Science **304**: 1005–1008.

Timmermans, K., W. Stolte, and H. de Baar. 1994. Iron-mediated effects on nitrate reductase in marine phytoplankton. Marine Biology **121**: 389–396.

Timmermans, K., B. Van Der Wagt, and H. De Baar. 2004. Growth rates, half-saturation constants, and silicate, nitrate, and phosphate depletion in relation to iron availability of four large, open-ocean diatoms from the Southern Ocean. Limnology and Oceanography **49**: 2141–2151.

Turpin, D. 1991. Effects of inorganic N availability on algal photosynthesis and carbon metabolism. Journal of phycology **27**: 14–20.

Twining, B., S. Baines, and N. Fisher. 2004. Element stoichiometries of individual plankton cells collected during the Southern Ocean Iron Experiment (SOFeX). Limnology and Oceanography **49**: 2115–2128.

Tyrrell, T. 1999. The relative influences of nitrogen and phosphorus on oceanic primary production. Nature **400**: 525–531.

van Beusekom, J. 2005. A historic perspective on Wadden Sea eutrophication. Helgoland Marine Research **59**: 45–54.

van Beusekom, J., M. Loebl, and P. Martens. 2008*a*. Distant riverine nutrient supply and local temperature drive the long-term phytoplankton development in a temperate coastal basin. Journal of Sea Research In press.

van Beusekom, J., S. Weigelt-Krenz, and P. Martens. 2008*b*. Long-term variability of winter nitrate concentrations in the Northern Wadden Sea driven by freshwater discharge, decreasing riverine loads and denitrification. Helgoland Marine Research **62**: 49–57.

van Beusekom, J. E. E., U. H. Brockmann, K.-J. Hesse, W. Hickel, K. Poremba, and U. Tillmann. 1999. The importance of sediment in the transformation and turnover of nutrients and organic matter in the wadder sea and german bight. German Journal of Hydrography **51**: 245–266.

van Boeckel, W. 1991. Ability of *Phaeocystis* sp. to grow on organic phosphates: direct measurement and prediction with the use of an inhibition constant. Journal of Plankton Research **13**: 959–970.

Vergara, J., J. Berges, and P. Falkowski. 1998. Diel periodicity of nitrate reductase activity and protein levels in the marine diatom *Thalassiosira weissflogii* (Bacillariophyceae). Journal of Phycology **34**: 952–961.

Visbeck, M., J. Marshall, and H. Jones. 1996. Dynamics of isolated convective regions in the ocean. Journal of Physical Oceanography **26**: 1721–1734.

Vrieling, E., Q. Sun, M. Tian, P. Kooyman, W. Gieskes, R. van Santen, and N. Sommerdijk. 2007. Salinity-dependent diatom biosilicification implies an important role of external ionic strength. Proceedings of the National Academy of Sciences **104**: 10441–10446.

Wanninkhof, R. 1992. Relationship Between Wind Speed and Gas Exchange Over the Ocean. Journal of Geophysical Research **97**: 7373–7382.

Watson, A. and J. Orr. 2003. Carbon dioxide fluxes in the global ocean. *In* M. Fasham [ed.] , Ocean Biogeochemistry: The Role of the Ocean Carbon Cycle in Climate Change, page 123..144. Springer-Verlag, New York.

Weber, L., C. Völker, A. Oschlies, and H. Burchard. 2007. Iron profiles and speciation of the upper water column at the Bermuda Atlantic time-series Study site: a model based sensitivity study. Biogeosciences **4**: 689–706.

Weiss, R. and B. Price. 1980. Nitrous oxide solubility in water and seawater. Marine Chemistry **8**: 347.

Winter, J. E. 1973. The filtration rate of *mytilus edulis* and its dependence on algal concentration, measured by a continuous automatic recording apparatus. Marine Biology **22**: 317–328.

Wolf-Gladrow, D., R. Zeebe, C. Klaas, A. Körtzinger, and A. Dickson. 2007. Total alkalinity: The explicit conservative expression and its application to biogeochemical processes. Marine Chemistry **106**: 287–300.

Woods, J. 2005. The Lagrangian Ensemble metamodel for simulating plankton ecosystems. Progress in Oceanography **67**: 84–159.

Woods, J. and W. Barkmann. 1994. Simulating plankton ecosystems by the Lagrangian Ensemble method. Philosophical Transactions of the Royal Society B **343**: 27–31.

Woods, J., A. Perilli, and W. Barkmann. 2005. Stability and predictability of a virtual plankton ecosystem created with an individual-based model. Progress in Oceanography **67**: 43–83.

Wright, K. and K. Oparka. 1989. Uptake of Lucifer Yellow CH into plant-cell protoplasts: a quantitative assessment of fluid-phase endocytosis. Planta **179**: 257–264.

Yoder, J. and M. Kennelly. 2003. Seasonal and ENSO variability in global ocean phytoplankton chlorophyll derived from 4 years of SeaWiFS measurements. Global Biogeochemical Cycles **17**: doi:10.1029/2002GB001492.

Zusammenfassung

Diese Doktorarbeit untersucht die Kopplung wichtiger biogeochemischer Elemente in der Produktion von Biomasse und die Auswirkungen variabler Stöchiometrie in Algenzellen auf großräumige, biogeochemische Transportflüsse. Das Hauptaugenmerk liegt hierbei auf den Elementen Kohlenstoff, Stickstoff, Silizium und Eisen. Obwohl auch Phosphor bekanntlicherweise eine wichtige Rolle in biologischen Prozessen spielt, wird Phosphor in dieser Arbeit nicht betrachtet.

In dieser Doktorarbeit werden ausschließlich mathematische Modelle angewandt, um die zu untersuchenden biogeochemischen Prozesse zu simulieren. In der ersten Studie wird ein Ökosystemmodell für die Gezeitenbucht zwischen den Inseln Sylt und Rømø im deutsch-dänischen Wattenmeer und der angrenzenden Nordsee entwickelt und analysiert. Das Modul für Phytoplanktonphysiologie basiert auf dem Modell von Geider et al. (1998) und ermöglicht eine variable Stöchiometrie von C und N in der berechneten Phytoplanktonbiomasse, aufgrund der Entkopplung von Kohlenstoffixierung und Stickstoffassimilation in den mathematischen Gleichungen. Das Modell wird einerseits in Hinsicht auf die Auswirkungen der variablen Kopplung von Kohlenstoff und Stickstoff in Phytoplanktonbiomasse auf die Transportflüsse zwischen dem Wattenmeer und der offenen Nordsee untersucht, liefert jedoch noch weitere Erkenntnisse zu der Rolle des physikalischen Gezeitenaustausches und der bentho-pelagischen Kopplung in den flachen Schelfgewässern. Die Darstellung des physikalischen Austausches zwischen der Nordsee und der Sylt-Rømø Bucht durch die Gezeitenströme ist besonders wichtig für die Erstellung der biogeochemischen Transportbudgets und die einfache Beschreibung der Wasserkörper durch die Annahme zweier homogen durchmischter Boxen führt zu wesentlich geringeren modellierten Austauscheffizienzen der Gezeitenströme als bisher in der Literatur angenommen. Nach dem ermittelten Transportbudget für Kohlenstoff und Stickstoff kann das Wattenmeer als Senke für organischen Kohlenstoff bestätigt werden. Die Flüsse von organischem Kohlenstoff teilen sich jedoch auf unterschiedliche Komponenten auf. Während Detritus und gelöster, organischer Kohlenstoff in die Bucht importiert werden, werden Phytoplankton und Zooplankton Kohlenstoff aus der Bucht in die Nordsee exportiert. Der geringe Wert für die Austauscheffizienz der Gezeitantransporte führt jedoch zu einer Unterschätzung der bisher angenommenen Kohlenstoffflüsse zwischen der Nordsee und der Sylt-Rømø Bucht.

Desweiteren wird die Frage untersucht, ob benthische Filtrierer im Wattenmeer durch das Herausfiltern von Phytoplankton aus der Wassersäule eine limitierende oder durch die Sekretion von anorganisch gelöstem Stickstoff in das Wasser eine unterstützende Wirkung auf die Gesamtprimärproduktion im Wattenmeer haben (Asmus and Asmus, 1991). Durch Variation der Kohlenstoffaufnahme der benthischen Filtrierer im Modell kann bei den derzeit geschätzten Filtrationsleistungen ein unterstützender Effekt auf die Primärproduktion in der Wattenmeerbucht ermittelt werden.

In der zweiten Studie wird die in der ersten Studie verwendete Parametrisierung der Phytoplanktonphysiologie von Geider et al. (1998) um die Wachstumsabhängigkeiten von Kieselalgen von Si-

lizium und Eisen erweitert. Die entwickelte Parametrisierung für die Beschreibung von Diatomeenwachstum wird dann angewendet, um den zeitlichen Verlauf von Laborexperimenten mit Diatomeen-Batch-Kulturen zu simulieren. Die ausgewählten Laborexperimente betrachten die Variabilität der Si:N Verhältnisse unter variierenden Eisenkonzentrationen und Si:N Verhältnissen in den gelösten Nährstoffkonzentrationen im Wachstumsmedium. Die entwickelte Parametrisierung gibt die physiologische Antwort der Aufnahme von Silizium und Stickstoff in die Zellen unter Eisenlimitierung wieder. Stickstoffaufnahme und Siliziumaufnahme sinken unter Eisenlimitierung. Da jedoch die Aufnahme von Stickstoff in die Zellen direkt von der Verfügbarkeit von Eisen für den Zellstoffwechsel abhängig ist, ist die Reduzierung der Stickstoffaufnahme stärker als die Reduzierung der Siliziumaufnahme, die nicht direkt von Eisenverfügbarkeit, dafür aber von intrazellulären Kohlenstoff- und Stickstoffpools abhängt. Die unterschiedliche Regulierung der Aufnahmeraten von Silizium und Stickstoff in die Zelle führt zu einem erhöhten Si:N Aufnahmeverhältnis von eisenlimitierten Diatomeen.

Der lineare Anstieg der Si:N Aufnahmeverhältnisse mit steigenden Si:N Verhältnissen im Wachstumsmedium kann nicht eindeutig durch die Parametrisierung wiedergegeben werden, was in der mangelnden Erkenntnis über den Silikatstoffwechsel in Diatomeen begründet sein kann. Der genaue Aufnahmemechanismus von Silizium in die Zelle ist noch nicht vollständig verstanden. Die Beobachtungen linearer Aufnahmekinetiken für Silizium sprechen gegen die Aufnahme durch Transporter-Moleküle, da dieser Transportmechanismus eine sättigende Kinetik zeigen würde. Eventuell sind die Unzulänglichkeiten der Siliziumaufnahmekinetiken aber auch in der gewählten Michalis-Menten-Kinetik zu begründen und die Verwendung des Modells von Aksnes and Egge (1991) könnte bereits zu einer deutlichen Verbesserung führen. Die Abhängigkeit des Si:N Aufnahmeverhältnisses von den Eisenkonzentrationen wird jedoch sehr gut durch die Parametrisierung wiedergegeben.

Die neu entwickelte Parametrisierung wird in der dritten Studie in ein globales, biogeochemisches Ozean-Zirkulationsmodell implementiert und auf die Auswirkungen der variablen Stöchiometrie von Silizium und Stickstoff unter Eisenlimitierung auf die großskaligen biogeochemischen Flüsse und die resultierenden Nährstoffverteilungen im globalen Ozean untersucht. Der erste und langwierigste Schritt in der globalen Modellierung ist die Identifikation der richtigen Parameterwerte für das globale Modell und der Vergleich der simulierten Konzentrationen und Flüsse mit Beobachtungen. Weit über hundert Modelläufe wurden durchgeführt, um sich einer Modellösung anzunähern, die die Beobachtungen weitestgehend wiederzugeben vermag. Die vielen unterschiedlichen Parametersätze werden zur Analyse der Sensitivität des Modells gegenüber Veränderungen der Parameterwerte herangezogen. Ein Vergleich der vielen Modellösungen mit unterschiedlichen Referenzdaten führt zu unterschiedlichen Bewertungen der Parametersätze. Vor allem die Auswahl der zu verwendenden Wachstumsparameter für Phytoplankton und der maximalen Grazingraten hängt stark von dem zu simulierenden Ozeangebiet ab. Um die Oberflächenchlorophyllverteilungen im Südlichen Ozean zu simulieren, werden sehr geringe Werte für die Lichtsensitivität und hohe Grazingraten favorisiert, die im gesamten globalen Ozean eher zu einer Verschlechterung der Wiedergabe von Oberflächenchlorophyll nach SeaWiFS führen. Es lässt sich daraus ableiten, daß die Modellierung biologischer Prozesse im Südlichen Ozean anscheinend einen anderen Satz von Parameterwerten erfordert, als für die Simulation biogeochemischer Prozesse im restlichen Ozean anzuwenden ist. Dieses Ergebnis spricht für die Trennung von Phytoplankton und Zooplankton in dem Modell in unterschiedliche Gruppen, die eine biogeographische Verteilung im simulierten Ozean mit unterschiedlich angepassten Eigenschaften ermöglichen.

Die Wiedergabe der Diatomeenverteilung im Südlichen Ozean durch das Modell ist akzeptabel. Das Modell überschätzt die Chlrophyllkonzentrationen im Südlichen Ozean etwas, verglichen mit

SeaWiFS Daten, gibt die Amplitude der Chlorophyllkonzentrationen in in-situ gemessenen Chlorophyllkonzentrationen bei KERFIX jedoch sehr gut wieder. Im Antarktischen Zirkumpolarstrom erzeugt das Modell einen Gürtel mit erhöhtem Export von biogenem Silikat in den tiefen Ozean. Diese Gewässer liegen über den silikatreichen Sedimenten im Südlichen Ozean, die als Opalgürtel bekannt sind. Die Regionen mit erhöhtem Silikatexport korrelieren sehr gut mit den Gebieten, in denen Eisenlimitierung des Phytoplankton auftritt. Der verstärkte Opalexport tritt jedoch auch in Modellösungen auf, in denen keine deutliche Eisenlimitierung entsteht. Dennoch führt Eisenlimitierung in dem Modell zu erhöhten Si:N Aufnahmeverhältnissen und damit zu einer Verstärkung des Opalexports in eisenlimitierten Gebieten.

Die verstärkte Aufnahme von Silizium gegenüber Sticktoff führt zu einer stärkeren Zehrung von gelöstem Silizium im durch Ekman-Drift nordwärts fließenden Oberflächenwasser des Südlichen Ozean. Das Wasser, das in etwa zwischen 40 und 50°S als Subantarctic Mode Water absinkt, ist dadurch sehr arm an gelöstem Silizium, enthält aber immer noch größere Mengen an gelöstem Stickstoff. Dieses Stöchiometrische Signal, das sich in das Antarktische Zwischenwasser fortpflanzt, das den Atlantischen Ozean mit Nährstoffen versorgt, ist somit durch Oberflächenprozesse im Südlichen Ozean entstanden und direkt abhängig von den Eisenkonzentrationen und der Nachlieferung von Eisen im Oberflächenwasser des Südlichen Ozean.

Die variable Kopplung von Kohlenstoff, Stickstoff und Silizium in Phytoplanktonbiomasse ermöglicht Variationen in den stöchiometrischen Verhältnissen in den Transportflüssen und die zeitliche oder räumliche Integration dieser Transporte kann zu einer tatsächlichen Entkopplung und unterschiedlich gerichteten Transportflüssen verschiedener Elemente führen. Die Berücksichtigung variabler Stöchiometrie kann also eine wichtige Rolle für die Entwicklung realistischer Nährstoffverteilungen in biogeochemischen Ozeanzirkulationsmodellen spielen und die Modellösungen auf größeren Zeitskalen maßgeblich beeinflussen. Das entwickelte Modell stellt eine gute Grundlage dar, um, aufbauend auf diesen Studien, ein Modell für den globalen Kohlenstoffkreislauf zu entwickeln, das realistische Nährstoffverteilungen erzeugt und somit auch realistische Angaben zu den globalen Kohlenstoffflüssen und deren Veränderungen unter Klimawandelszenarien machen kann. Das Modell ist außerdem implementiert auf einem hoch aufgelösten Modellgitter, das eine wesentlich realistischere Darstellung der Ozeanzirkulation und damit auch der Verteilungen der biogeochemischen Tracer ermöglicht.

Danksagung

In erster Linie möchte ich Christoph Völker für die erstklassige Betreuung während meiner Doktorandenzeit am AWI danken. Du hast Dir immer viel Zeit für mich genommen und hattest immer ein offenes Ohr. Vielen Dank für die tolle Unterstützung.

Ohne Dieter Wolf-Gladrow wäre diese Arbeit nicht zustande gekommen. Dir danke ich für Dein Vertrauen, das Du in mich gesetzt hast, und für Deine Kommentare, die hoffentlich geholfen haben, aus dieser Arbeit eine runde Sache zu machen.

Andreas Oschlies danke ich dafür, daß er sich als Gutachter für diese Arbeit zur Verfügung gestellt hat.

Martin Losch danke ich für seine Hilfsbereitschaft und die Lösung diverser technischer Probleme.

Weiterer Dank geht in jedem Falle an meine Koautoren, Markus Schartau und Justus van Beusekom, für viele anregende Diskussionen und Verbesserungsvorschläge für das Sylt-Rømø Bucht Modell.

Sören möchte ich für die unverhoffte Möglichkeit danken, an der Polarsternfahrt ANT23/2 teilgenommen und den Südlichen Ozean erlebt zu haben. Außerdem nochmal vielen Dank für diverse Grillfackeln und Dokoabende mit Claudette und Miss F. Schweinchen.

Das legendäre DokTeam sei hier auch noch einmal erwähnt. Ihr habt mich zwar etwas von der Arbeit abgehalten, aber es war ja für einen guten Zweck.

Die Arbeitsatmosphäre in der Sektion Biogeosciences war einfach großartig. Vielen Dank hiermit an Euch alle für jede Menge Kuchen, Kaffee und anregender Diskussionen. Und nebenbei hat mir die allmittägliche Essensrunde sehr geholfen, auf dem Boden der nicht ganz so wissenschaftlichen Tatsachen zu bleiben.

Sehr dankbar bin ich vor allem meiner Familie, die mich in allen Lebenslagen nach Kräften unterstützt hat. Aber ganz besonders, und am allermeisten, danke ich meiner Süßen für einen starken Rücken und für ein Leben, wie ich mir kein schöneres vorstellen kann.

Erklärung

Hiermit erkläre ich, daß ich die Arbeit mit dem Titel:

'Coupling and decoupling of biogeochemical cycles in marine ecosystems'

selbständig verfasst und geschrieben habe und außer den angegebenen Quellen keine weiteren Hilfsmittel verwendet habe.

Ebenfalls erkläre ich hiermit eidesstattlich, daß es sich bei den von mir vorgelegten Arbeiten um 3 identische Exemplare handelt.

.....
Unterschrift